Health and pollution impacts in avoided and future worlds according to Earth system models

Wareing, Nicola

This dissertation is submitted for the degree of Doctor of Philosophy

July 2021

Lancaster Environment Centre

For Indigo, a rebel girl

"Essentially, all models are wrong, but some are useful."

(Box and Draper, 1987)

Declaration

This thesis has not been submitted in support of an application for another degree at this or any other university. It is the result of my own work and includes nothing that is the outcome of work done in collaboration except where specifically indicated. Many of the ideas in this thesis were the product of discussion with my supervisor Paul J. Young.

Abstract

Air pollution has an adverse effect on human health and, in the absence of air quality legislation, climate change may exacerbate poor air quality. The Paris Agreement global mean surface temperature change (ΔGMST) goals of 1.5 °C and 2 °C above pre-industrial levels were proposed to avoid dangerous levels of climate change.

Climate change increases the frequency of warm days and heat waves, as well as increasing average temperature. Daily maximum surface temperature is highly correlated with surface ozone in many regions and the frequency of heatwaves is expected to increase with GMST. To illustrate the success of European emission controls, I compare air pollution during the European 2003 heatwave with and without air quality policy and advances in technology. If the 2003 heatwave had occurred in 2030, future emission scenarios would have further reduced air pollution and associated excess mortality, even with a higher population, highlighting the potential to reduce the health impact of future heatwaves.

When projecting heat-related mortality due to climate change, studies must consider an optimum temperature for human health, above which there is an increase in mortality rate. I use a linear regression model to estimate the percentile corresponding to the optimum temperature. I project the number of days above this temperature (warm days) for climates where ΔGMST is 1.5, 2, 3, and 4 °C. Exposure and vulnerability to warm days is higher in tropical countries and differences in impacts between regions may be underestimated by using a constant percentile globally to define an optimum temperature. This method is useful for projecting mortality in regions where there is a lack of epidemiological research.

Acknowledgements

Firstly, I would like to thank the Engineering and Physical Science Research Council (EPSRC), without which I would not have been able to pursue a PhD.

Thank you to the Environmental Modellers group who gave me invaluable feedback on various figures, posters, oral presentations, and experimental methods throughout the PhD. Especially Nando, who was very generous with his time and Python-related advice. Thank you to my second supervisor, Dr Andrew Jarvis, for discussions on various aspects of the thesis. I extend my thanks to Drs Vaishali Naik, Fernando Iglesias-Suarez, Simone Tildes, and others for helping with model simulations needed for Chapter 3.

Thank you to Dr Kirsti Ashworth and Dr Alex Archibald, my viva examiners, for your helpful comments, suggestions, and patience.

I would not have got this far without the support of my supervisor, Dr Paul J. Young, who showed a great deal of patience and optimism throughout my PhD, even when shipping emissions hit the fan.

I would like to thank my friends and family for their emotional and practical support, including Dr Miriam Sturdee, who was an indispensable source of support during the PhD.

Finally, I am deeply indebted to Beau, who supported me throughout the PhD in various ways.

Contents

List of Tables

List of Figures

List of Abbreviations and Acronyms

ACCMIP	Atmospheric Chemistry and Climate Model Intercomparison project
AR	Assessment report
CI	Confidence interval
CMIP5	Coupled Model Intercomparison Project Phase 5
CTM	Chemical transport model
ΔGMST	Change in global mean surface temperature
ERA	European Centre for Medium-Range Weather Forecasts (ECMWF) Re-Analysis
GCM	General circulation model
GMST	Global mean surface temperature
IPCC	Intergovernmental Panel on Climate Change
MMP	Minimum mortality temperature
mx2t	Daily maximum temperature at 2 m
NAM	Northern Annular Mode
NMVOC	Non-methane volatile organic compound

NO$_x$ Nitrogen oxides

PM$_{2.5}$ Particulate matter with diameter < 2.5 μm

PM$_{10}$ Particulate matter with diameter < 10 μm

PPE   Perturbed physics ensemble

RCP   Representative Concentration Pathway

RMSD   Root mean squared deviation

TOAR   Tropospheric Ozone Assessment Report

VOC   Volatile organic compound

UNFCCC   United Nations Framework Convention on Climate Change

1 Introduction and background

The Intergovernmental Panel on Climate Change (IPCC) project that the global mean surface temperature change (ΔGMST) is likely to reach between 2.6 and 4.8 °C by the end of the century under a high-emissions scenario (Collins et al., 2013) – the so-called RCP8.5 scenario, discussed below. Several aspects of the climate system are projected to change, such as atmospheric circulation (Coumou et al., 2015; Hardiman et al., 2014; Ma and Xie, 2013), the water cycle (Huang et al., 2013; O'Gorman and Muller, 2010; Trenberth et al., 2014), and the cryosphere (Brutel-Vuilmet et al., 2013; Derksen and Brown, 2012; Wang and Overland, 2012). In turn, climate changes will impact economies and human health, through increases in heat-related mortality (Gasparrini et al., 2017; World Health Organization, 2014), decreases in worker productivity due to heat stress (Dunne et al., 2013; Niemelä et al., 2002; Seppänen et al., 2006; Zander et al., 2015), and reductions in crop yield (Asseng et al., 2015; Chen et al., 2018; Deryng et al., 2014; Lobell and Field, 2007; Schlenker and Lobell, 2010), for example.

In 2015, there was an international agreement, The Paris Agreement, between UNFCCC countries aimed at keeping ΔGMST from pre-industrial levels well below 2 °C and to

pursue efforts towards a 1.5 °C warmer limit. Although the 0.5 °C difference between these two targets may sound insignificant, the difference in regional impacts between these two targets may be substantial (Mba et al., 2018; Schleussner et al., 2016). Between 1991-2010 and 1960-1979, there was a warming of around 0.5 °C, and according to reanalysis data (the result of using data assimilation to estimate gridded meteorological variables using observations and a weather forecast model) over a quarter of the land experienced an intensification in hot extremes by over 1 °C (Schleussner et al., 2017). Schleussner et al. (2017) found that the historical 0.5 °C increase showed similar changes in heat and precipitation extremes as those shown by CMIP5 models (discussed in section 1.3 and used throughout the thesis) between future +1.5 and 2 °C climates. However, they note that at higher levels of warming the risks associated with human health and crop production impacts are likely to scale non-linearly. Other studies have also noted that average temperatures and extreme precipitation, defined as the maximum annual daily precipitation accumulation each year (Pendergrass et al., 2015), scale with ΔGMST in most models.

Alongside the problem of climate change, decision-makers must also address the issues of air quality, which may be worsened by climate change. In 2010, there were around 3 million deaths globally due to outdoor air pollution (Lelieveld et al., 2015; Lim et al., 2012), increasing to over 4 million deaths in 2015 (Cohen et al., 2017), and if no new air pollution legislation is introduced there may be around 6.6 million deaths in 2050 (Lelieveld et al., 2015). Poor ambient air quality may impact worker productivity, for example in the agricultural sector (Zivin and Neidell, 2012). Exposure of a foetus or child to air pollutants may impact their future school performance (Bharadwaj et al., 2017; Sanders, 2012) and earnings in adulthood (Isen et al., 2017). Potentially, these

impacts could exacerbate socioeconomic and health inequality as pollutants may be higher in more deprived areas (Fecht et al., 2015).

1.1   Climate change and extreme events

The World Health Organization (WHO) concluded that there will be approximately 250,000 additional deaths per year between 2030 and 2050 from a range of causes including around 38,000 more heat-related deaths in the elderly population (World Health Organization, 2014).

The immediate danger to human health is, perhaps, not the gradual change in surface temperature, but the increase in "extreme events" like heatwaves and floods. If warm days are defined as days where the temperature is above the 90th percentile for a present-day climate, for example, and the mean of the temperature distribution increases then we will see an increase in the frequency of warm days. Likewise, if we define cool days as the 10th percentile of a present-day climate, increasing the mean will see a decrease in the number of cool days. By increasing the variance of present-day daily temperatures, there will be an equal increase in frequency of cool and warm days, assuming a Gaussian distribution. A change in the skewness towards warm temperatures would see an increase in warm days. Simultaneously increasing the mean and the variance of daily temperatures as well as increasing the skew towards warm temperatures could lead to a larger increase in warm day frequency than the decrease in frequency of cool days. The latter temperature distribution change would be most disadvantageous to human health and the economy. However, it is still uncertain whether or not observed climate extremes are related to changes in the variance (Rhines and Huybers, 2013) and future temperature variance and skewness are spatially heterogeneous (Donat and Alexander, 2012; Lewis and King, 2017).

There is a projected increase in the intensity and duration of heatwaves, for which there is no universal quantitative definition, but are usually defined by sustained periods of high temperatures (Collins et al., 2013; Meehl and Tebaldi, 2004; Perkins-Kirkpatrick and Gibson, 2017). Heatwaves can be defined by exceedances of absolute temperatures and relative thresholds. For example, an absolute definition used for the USA may be two consecutive days where the daily minimum temperature is greater or equal to 26.7 °C and/or the daily maximum temperature is greater or equal to 40.6 °C (Robinson, 2001). In contrast, Dosio (2017) used a threshold of the 90th percentile of daily maximum temperatures centred round a 31-day window.

Similarly, there is no universal definition of a warm spell. In Chapter 4, a warm spell is defined by consecutive days where the daily mean temperature exceeded an optimal temperature for human health (the temperature where mortality is lowest and above that temperature there is an increase in mortality), which is defined by a percentile, rather than an absolute temperature due to varying climatic conditions across the world. For warmer regions in particular, these temperatures would not traditionally be considered extreme (unlike temperatures during a heatwave) because the health impacts start as relatively low percentiles.

There have been efforts to implement heatwave adaptation measures in Europe after the 2003 heatwave, which resulted in less heat-related mortality than expected in France during a heatwave in 2006 (Fouillet et al., 2008). Unfortunately, there is a limit to physiological human heat tolerance and the ability to adapt differs between regions. Plus, not all regions have equal capacity to adapt to higher temperatures. Therefore in Chapter 4, I explore a "worst case scenario" with no adaptation to higher temperatures.

Many heatwaves are associated with anticyclonic synoptic conditions (Trenberth and Fasullo, 2012; Zittis et al., 2016), such as the European heatwave in 2003 (Black et al., 2004; Fink et al., 2004). However, a climate with an increase in heatwaves does not necessarily mean that there will be an increase in the large-scale meteorology associated with them (Palipane and Grotjahn, 2018).

The stagnant conditions associated with heatwaves can lead to a build-up of air pollution (Jacob and Winner, 2009). However, the air stagnation index (ASI) itself – defined by Wang and Angell (1999) – is commonly not the strongest predictor of bad air quality (Kerr and Waugh, 2018). An increase in air pollutants, dry weather and high temperatures affects plant and human health, meaning that, heatwaves are often accompanied by various negative economic impacts and an increase in human mortality and morbidity (Anderson and Bell, 2010; Cheng et al., 2018; García-Herrera et al., 2010; Knowlton et al., 2011).

1.2   Climate change and air pollutants

Heatwave conditions are ideal for the formation of tropospheric ozone, a secondary pollutant. Around 90% of the atmosphere's ozone is in the stratosphere, where it absorbs incoming solar ultraviolet radiation: most UVC (<280 nm) and around 90% of UVB (280-315 nm), protecting life at the surface. In contrast, ozone in the troposphere is a greenhouse gas and it is detrimental to human health near the surface.

Breathing in ozone allows it to react chemically with internal body tissues, such as the lungs, where it can cause inflammation of lung lining. As a result, short-term exposure to ozone can affect lung function, even in healthy young adults (Kim et al., 2011) and non-asthmatic children (Chen et al., 2015). There may also be adverse effects on the

cardiovascular system, for instance, a higher level of ozone was associated with an increase in out-of-hospital coronary deaths in Italy (Nuvolone et al., 2013). Evidence of chronic effects of ozone are less conclusive than acute effects, but long-term exposure to ozone has been linked to development of asthma in non-smoking adult males (McDonnell et al., 1999).

Anthropogenic emissions of volatile organic compounds (VOCs) and NO_x affect levels of surface ozone. Higher temperatures are associated with increases in biogenic emissions of ozone precursors and faster decomposition-rate of peroxyacetyl nitrate (PAN; a reservoir for NO_2). Temperature increase is associated with an increase of surface ozone over land, particularly over Europe, which may be more sensitive to biogenic VOCs than other regions (M. J. Kim et al., 2015).

Clearer skies (higher solar radiation) increase rates of photolysis, but climate change does not necessarily mean less cloudy days in the future. Decreases in cloud cover have been observed in the UK (Athanassiadou et al., 2010) and over the tropics (Cess and Udelhofen, 2003). On the other hand, increases in total cloud cover have been observed over the USA (Dai et al., 2006). Models project decreases in cloud cover over parts of western Europe (Katragkou et al., 2011) and north-east USA (Kunkel et al., 2008).

The sequence of reactions leading to ozone formation is usually initiated by the reaction of CO or a VOC with the OH radical, which produces RO_2 or HO_2 radicals. Through a reaction with the RO_2 or HO_2 radicals, NO is converted into NO_2. The photolysis of NO_2 produces NO and the ground electronic state oxygen atom ($O(^3P)$) that is responsible for the formation of ozone through:

$$O(^3P) + O_2 \rightarrow O_3 \tag{1.1}$$

NO may be converted to NO_2 via the following:

$$O_3 + NO_2 \rightarrow NO + O_2 \qquad (1.2)$$
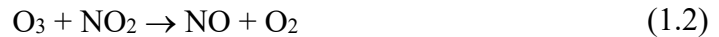
which removes ozone. The relationship between NO_x, VOCs, and ozone is non-linear (Lin et al., 1988), as demonstrated by Figure 1.1. When ozone levels are reduced at high levels of NO_x through processes such as 1.2 it is referred to as NO_x titration. Regions with a high NO_x/VOC ratio are associated with VOC-sensitive (or NO_x-saturated regimes), where increases in VOC emissions will increase the rate of reaction of VOC and CO with OH, which will determine the rate of ozone formation. NO_x/VOC ratios are associated with the instantaneous production rate of ozone, not necessarily the ambient mixing ratio of ozone, which will depend upon transport.
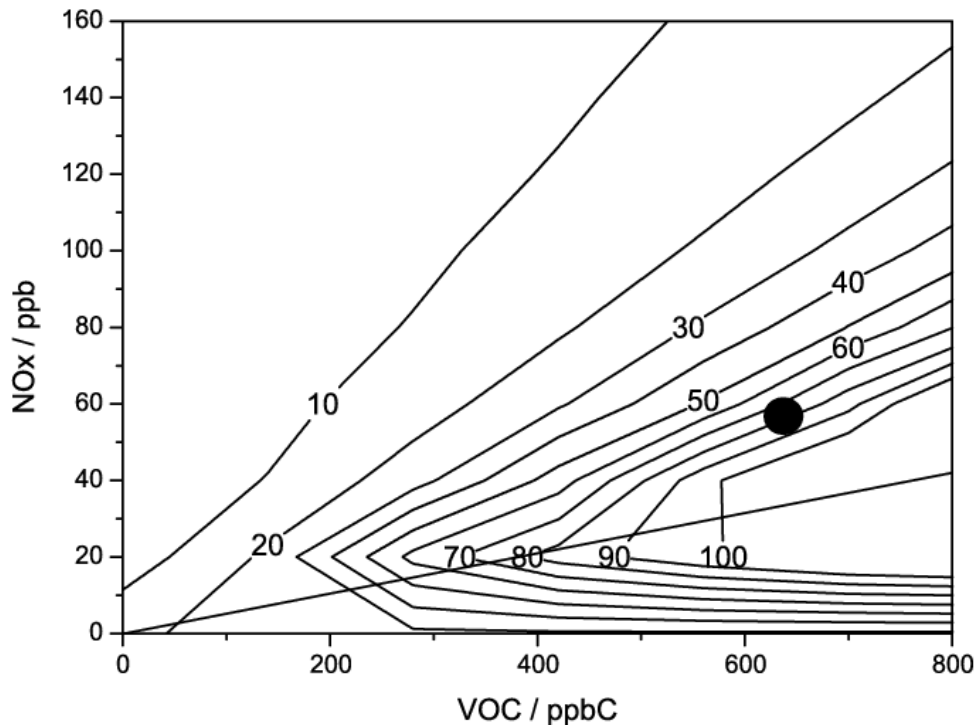
Figure 1.1: An example of an ozone isopleth plot, from Martins et al. (2015), licensed under CC BY 4.0, showing the relationship between NO_x, VOC, and ozone concentrations in the city Rio de Janeiro.

Ground-level ozone is detrimental to human health and increases in ozone levels are associated with increased human morbidity (Zu et al., 2017) and mortality (Vicedo-Cabrera et al., 2020). For example, the short-term effect of elevated ozone had a significant effect on Mortality during the European heatwave of 2003. In Toulouse, the relative contribution of ozone to mortality due to ozone and temperature combined was 83%, whereas, in Bordeaux, the relative contribution of ozone was only 2.5% (i.e., temperature was a much larger factor) (Filleul et al., 2006).

In addition, there are studies on premature mortality attributable to long-term exposure to surface ozone. For example, Lelieveld *et al.* (2015) estimated that there were around 142,000 premature deaths from chronic obstructive pulmonary disease in 2010 due to long-term exposure to ozone, using relative-risk estimates from an 18-year follow up study (Jerrett et al., 2009). Turner et al. (2016) found that, with longer follow-up studies and improved exposure models, estimated relative risk of death from respiratory causes increased from 1.040 (95% confidence interval; CI, 1.010-1.067) to 1.12 (95% CI; 1.08-1.16) per 10 ppb increment in ozone concentration. Using updated relative risk estimates and exposure parameters, Malley *et al.* (2017) estimated 1.04-1.23 million excess respiratory deaths due to surface ozone in 2010.

When estimating deaths attributable to ozone in the future, choices in future population projection, climate model and emission scenario, and air quality model, as well as concentration-response function impact the results. Post *et al.* (2012) found that, in the United States, changes in ozone-related mortality from 2000 to 2050 ranged from around 600 avoided deaths to 2500 deaths attributable to climate change and that the largest source of uncertainty was the choice of model.

Particulate matter (PM) is also a concern for public-health, with around 3.2 million premature deaths associated with PM2.5 in 2010 (Apte et al., 2015), much larger than the number of estimated ozone-related excess deaths. PM is usually characterised by size, where coarse particles (PM10) have a diameter between 2.5 and 10 μm, fine particles (PM2.5) have a diameter of 2.5 μm or less, and ultra-fine particles have a diameter of less than 0.1 μm. Particles larger than 10 μm are not easily lifted by the wind and have shorter atmospheric lifetimes due to their high sedimentation rate. Ultra-fine particles are produced via the clustering of precursor gases (nucleation), which grow rapidly into 0.01-1 μm size range as particles coalesce, and through condensation of gases. After reaching 1 μm growth slows down, and particulates tend to accumulate; they are removed from the atmosphere via scavenging by cloud droplets (followed by rainout) or direct scavenging by raindrops. Course particles are removed via rainout and sedimentation. Most PM resides in the lower troposphere, which reflects its short lifetime. Natural primary sources of PM include volcanic and sea-spray emissions and anthropogenic sources include fossil-fuel combustion and industrial processes.

Particles also have a radiative effect on the atmosphere, but this varies between components and is dependent on the single scattering albedo. One major component of PM2.5 is the sulphate aerosol (SO_4^{2-}), which has a cooling effect on the Earth via backscattering incoming solar radiation. Whereas other particulate components, such as black carbon, have a warming effect, as a result of absorbing solar and thermal-IR radiation.

1.3   Earth system modelling

Global warming occurs when there is an increase in emissions of greenhouse gases, such as carbon dioxide, which causes the global mean temperature to increase. Knowing that the global mean surface temperature is increasing does not reveal any information about changes in meteorology and atmospheric chemistry. As a result, policy makers are not informed about what change in global mean surface temperature since pre-industrial levels (referred to as ΔGMST through the thesis) they should aim for or what anthropogenic emissions are necessary to meet climate targets.

Complex Earth system models are used to project future climate change, which simulate many processes of the climate system. They can also be used for filling in observational gaps, making them useful for interpreting past and present-day interactions between climate, meteorology, and atmospheric chemistry.

It is impossible for even the most complex models to include all processes that go on in the Earth system. Not all processes are fully understood, they interact with one another, creating feedbacks which would be computationally expensive to calculate, and there are uncertainties in the observations used as boundary conditions in the models (McGuffie and Henderson-Sellers, 2005). For example, some general circulation models (GCMs) are run without interactive ocean and sea-ice components and are run with prescribed sea surface temperatures and sea ice concentrations or they are run with offline chemistry, so they may have prescribed ozone or methane values. The chemistry in Chemistry GCMs is affected by climate change, but those changes in radiative gases and aerosols do not impact climate in the model. The most complex models are the chemistry-climate models (CCMs), where atmospheric composition is coupled with climate.

Different research groups prioritise different processes in the Earth system and run their models at different spatial resolutions. To create consistency between models there are model intercomparison projects, which are collaborations between research groups to improve understanding of climate and atmospheric chemistry as well as explore structured uncertainty. The Coupled Model Intercomparison Project (CMIP), coordinated by the World Climate Research Project and is conducted in support of the IPCC and climate science in general, is a multi-model ensemble of GCMs that couple the ocean and the atmosphere.

It is important to note that models in a multi-model ensemble, such as those contributed to CMIP5, make up an 'ensemble of opportunity' so the models are not independent of one another, they share ideas and code (Knutti et al., 2013), and these ensembles were not designed to cover the full range of uncertainty and behaviour of the climate system. Therefore, robust model predictions, when most models agree on an outcome, do not necessarily mean that they capture the "truth" (Parker, 2011). However, model performance for capturing large-scale temperature and precipitation patterns as well as periodic internal variability (e.g., El Niño) has improved over time (Flato et al., 2014; Reichler and Kim, 2008), and models have predicted phenomenon that had not otherwise been detected. Though multi-model ensembles are unlikely to represent the full range of uncertainty in future climate, it is worth noting that our current understanding of climate change is not exclusively based on models and that they are useful for quantifying and supporting a broader picture of the effects of climate change (Hargreaves and Annan, 2014).

Single models can be used to create a 'single-model ensemble' (or 'perturbed physics ensemble'; PPE), which are constructed by varying parameters of a single model and

can be used to quantify and explore the effects of parameter uncertainties (Lambert et al., 2013; Rougier et al., 2009). However, PPEs do not explore structural uncertainty, and multi-model ensembles have been shown to be more reliable at representing a present-day climate, with PPEs tending to over- or under-estimate observations (Flato et al., 2014; Yokohata et al., 2013).

There are various techniques used to evaluate model performance. The method chosen to evaluate model skill depends on the application and the available observations (Young et al., 2018). To assess how well a model simulates the seasonal cycle or spatial distribution of a variable, standard statistical metrics are calculated, such as the mean bias, the root mean square deviation (RMSD), and the spatial/temporal correlation co-efficient. These methods can also be used to evaluate higher frequency output (hourly or daily) and long-term trends. In addition, relationships between different chemical species and their relationship with meteorological parameters can be compared to those found using observations. Areas with larger model bias in surface temperatures tend to be places with inconsistency between reanalysis datasets (usually areas with sparse observations) (Flato et al., 2014), reflecting how observations have informed climate models.

In this thesis, I exploited models from CMIP Phase 5 (CMIP5), which supported the IPCC Fifth Assessment Report (AR5). I calculated an unweighted multi-model mean result from all models and to show model uncertainty I indicate areas where less than 80% models agree in the change of direction, which is similar to the IPCC's approach to illustrating model agreement (Kirtman et al., 2013).

When making climate projections there are other sources of uncertainty in addition to model uncertainty: internal variability of the climate system and emission scenario

uncertainty. When projecting decadal mean GMST, the dominant contributions of uncertainty for lead times of the next few decades are model uncertainty and natural fluctuations in the climate system (Hawkins and Sutton, 2009). Later on, the biggest uncertainty for global projections will be emissions scenario. Fractional uncertainty will vary between regions, for example scenario uncertainty does not become the dominant uncertainty for surface temperature for the British Isles until much later than it does considering global mean (Hawkins and Sutton, 2009).

It is understandable why future anthropogenic emissions of greenhouse gases and air pollutants would provide such a large uncertainty; they depend on future technology, economic development, demographic change, land use change and policy decisions. Therefore, anthropogenic emissions in climate models are characterised by Representative Concentrations Pathways (RCPs), which are named for their radiative forcing target level for the year 2100.

RCP8.5 is the worst case scenario, sometimes referred to as the "business-as-usual" scenario, where greenhouse gas emissions increase over time and the radiative forcing reaches 8.5 W m^{-2} ($\sim$1370 ppm CO_2) by 2100 (van Vuuren et al., 2011). However, emissions of air pollutants are expected to decrease as income and environmental awareness increases (Riahi et al., 2011). This world assumes a regionally "heterogeneous" world with a global population increasing to 12 billion by 2100. There is slow economic development and low energy efficiency improvements, leading to high energy demands (Riahi et al., 2007). This is the main emissions scenario used in my thesis as I will be looking at the implications of a +1.5 and +2 °C world and most models will reach these targets before 2100 using this scenario.

RCP6.0 is a policy intervention scenario, whereby policies are used to prevent radiative forcing from exceeding 6.0 W m^{-2}. Emissions peak around 2060 and decline due to reductions in GHG emissions. There is rapid economic growth in China, which is responsible for over 60% of global CO_2 emissions in 2100. Both economic and population growth mean an increase in food and energy demands, so to mitigate carbon emissions more energy is provided by oil, gas, and renewable energy rather than coal (Masui et al., 2011).

RCP4.5 aims to achieve a stable radiative forcing of 4.5 W m^{-2} by 2100, but with emissions and GHG concentrations varying. While GDP continues to grow until 2100, population starts to decline in the late 21st Century (Thomson et al., 2011).

RCP2.6 is an aggressive mitigation scenario that aims to keep the ΔGMST below 2 °C (with a 66% chance of meeting this goal). To achieve this target requires substantial changes in energy use and emissions of non-CO_2 gases. GDP is assumed to grow faster in poorer countries than richer countries (van Vuuren et al., 2011).

The four RCP scenarios are a result of independent efforts by four individual modelling groups, therefore differences between results from each scenario cannot be linked to individual differences in climate policy nor socio-economic developments. They should not be seen as policy forecasts or boundaries for possible development (van Vuuren et al., 2011). However, they provide consistent input for climate modelling and impact assessment meaning that results can be based on multiple-model output.

Moreover, the RCP scenarios were not designed to characterize a pathway towards ΔGMST targets (e.g., +1.5 and +2 °C climates). Therefore, to assess the regional impacts of these targets, it is necessary to extract specific models, scenarios, or time

periods from GCMs that reflect the desired ΔGMST. James et al. (2017) suggests the following approaches to characterise the 0.5 °C difference between 1.5 and 2 °C ΔGMST:

Emission scenario approach may mean that a time slice is taken from each scenario, usually at the end of the century so that RCP2.6, for example, corresponds to an approximate ΔGMST between 1.5 and 2 °C. The variance in ΔGMST between the models for each RCP scenario means that it is difficult to measure impacts of a small difference in ΔGMST like 0.5 °C using different scenarios. Characterising a larger ΔGMST difference is less problematic, for example, Fortems-Cheiney et al. (2017) compared the impacts of +3 °C (2040-2069 under RCP8.5) and +4 °C (2028-2057 under RCP45) climates.

The alternative is to design new mitigation scenarios that aim for specific ΔGMST of interest (e.g., experiments comparing scenarios that aim for +1.5 and +2 °C climates for 2106-2115 (Mitchell et al., 2017)). This would provide the full response of the climate system, but it is computationally expensive to run new experiments, particularly if there is a large MME involved.

Sub-selecting models involves selecting model runs from a large ensemble based on their global temperature response. For example, Clark et al. (2010) sub-selected members of a PPE based on the ΔGMST, which were grouped into 2, 3, and 4 °C ± 0.5 °C climates to compare impacts. This method means it is difficult to explore inter-model variability since each ΔGMST has a different sub-set of models rather than the whole ensemble.

Pattern scaling involves extracting changes associated with one ∆GMST (e.g., +2 °C world) and multiply these changes to get changes for other ∆GMST (e.g., +4 °C). This was used method was used by Zelazowski et al. (2011) to explore a +4°C climate for models that did not reach that global temperature by the end of the simulation. However, this method is only valid where there is a linear relationship between GMST and the regional climate variable. This method is computationally cheap, but it does not consider the impacts of emission pathway.

Time sampling means that time periods are extracted from each model that corresponds to the ∆GMST of interest. This is computationally cheaper than running new experiments and it does not assume that there is a linear relationship between local change and ∆GMST like pattern scaling.

I extracted time periods from specific scenarios in Chapters 2 and 4 to look at the impacts of different ∆GMST scenarios. I used scenario RCP8.5 because it includes the most models and all the models reach a ∆GMST of 2 °C before the end of the century since it is the "worst case" scenario. This method does not consider the impact of path dependency on physical climate change. The reason for only using one scenario for the majority of analysis was limits on space and the quantity of data that would need to be processed and stored.

1.4   Aims and structure of this thesis

The core aim of this research is to explore the implications of policy-relevant climate change on atmospheric chemistry and human health using CMIP5 data (comprised of atmosphere-ocean global climate models and Earth System Models) and climate-chemistry models (CCMs). Specific objectives are to explore the impacts of the Paris

Agreement temperature goals on surface ozone and warm spells, as well as the impacts of past air quality legislation and future emission scenarios on European air quality during a heatwave. The next three chapters of this thesis are the results chapters, which are summarised below and have self-contained literature reviews. They are followed by a conclusions and summary, which explains how this research has contributed to the field.

Chapter 2: This chapter explores the possible impacts of a 1.5 and 2 °C ΔGMST on meteorology relevant to average and extreme values of surface ozone. The following questions will be addressed:

1. Is there a clear relationship between ΔGMST and surface ozone in atmospheric chemistry models?

2. What chemistry-relevant changes in climate will there be as a result of +1.5 and +2 °C climates?

3. Where is there a significant present-day relationship between meteorology and surface ozone?

Chapter 3: This chapter investigates how air quality policy impacted air pollution during the 2003 European heatwave. As well as considering the impacts of possible future policy decisions (or lack thereof), I ask what could have happened without air quality policy in place (i.e., a "world-avoided" scenario). Previous studies have asked what the ozone hole could look like without the Montreal Protocol and its amendments (Newman et al., 2008; Prather et al., 1996). Decision-makers already know what a world looks like with the policy in place, so to assess the success of a policy it is useful to look at what may have happened without it - what impacts were avoided? It is also possible

to look at what difference future policies would make on a present-day climate; would some impacts have been avoided?

Chapter 4: Climate change is expected to increase the number of extreme weather events globally. However, weather events and their subsequent impacts are not projected to increase equally for every region. Moreover, each region is differently adapted to extreme weather events, and has a different capacity to manage their impacts. The main objectives are to:

1. Find an appropriate threshold to define warm days and spells: is it appropriate to define them by a constant percentile globally when considering human health impacts?

2. Project the frequency of warm days and duration of warm spells for ΔGMST temperature targets

3. Project which regions are the most vulnerable when considering temperature-related mortality

2 Chemistry-climate interactions as a function of global mean surface temperature change

2.1 Introduction

The United Nations Framework Convention on Climate Change (UNFCCC) agreed that their ultimate objective was to "prevent dangerous anthropogenic interference with the climate system" (United Nations, 1992), which was recently refined in the Paris Agreement as well below 2 °C global mean surface temperature change (ΔGMST) above pre-industrial GMST (UNFCCC, 2015). As well as impacting physical climate change, global warming will affect atmospheric chemistry and transport of short-lived climate forcers. Changes in distribution of air pollutants and their precursors are particularly important in terms of air quality and climate feedbacks. This chapter focuses on changes in climate that will influence surface ozone and its precursors. While other studies have explored future changes in atmospheric chemistry, these have typically been as a function of time (e.g., what are the changes and impacts simulated for 2080-2100) for each model under a particular emissions scenario (V. Eyring et al., 2013; Fang et al., 2013; Y.-M. Kim et al., 2015; Pommier et al., 2017; Revell et al., 2015; Sicard et al., 2017; Stevenson et al., 2013; Young et al., 2013). However, the climate policy landscape calls for assessing risks and impacts as a function of ΔGMST. There is a need to inform policy makers of the likely impacts of reaching or not reaching ΔGMST-related goals, which is an approach focused on mitigation and solutions (Lee,

2015) rather than mapping out impacts over time following several different emission scenarios.

There are various studies that have looked at changes in climate, extreme weather, and impacts as a function of ΔGMST (Barcikowska et al., 2018; Dosio and Fischer, 2018; Guo et al., 2017, 2016; Andrew D. King and Karoly, 2017; C. Li et al., 2018; W. Liu et al., 2017; Sanderson et al., 2017; Schleussner et al., 2016; Weber et al., 2018; Whan et al., 2015) and there are studies that have explored changes in atmospheric chemistry in Europe for a +2 °C climate (with RCP4.5 scenario) using a four-model ensemble (Lacressonnière et al., 2017, 2016; Watson et al., 2016). Watson et al. (2016) found that the warmer climate would have a small impact on surface ozone and would not hinder air quality emission reduction efforts. This chapter considers changes in surface ozone due to climate change globally rather than focusing on Europe.

In the troposphere, ozone is a secondary pollutant with a relatively short lifetime, ranging from hours in polluted regions to several weeks in the free troposphere – about 22 days on average (Stevenson et al., 2006). It is the product of oxidation of CO and hydrocarbons in the presence of NO_x. Another source of ozone is the stratosphere, and a future climate may increase stratosphere-troposphere exchange (STE) (Collins, 2003; Sudo et al., 2003). Near the surface, it is a threat to human health and an estimated 8.0% deaths from chronic obstructive pulmonary disease in 2015 were due to ozone exposure (Cohen et al., 2017). It is detrimental to plant health too, and ozone-related plant damage reduces the uptake of carbon into the biosphere increasing its impact on climate (Sitch et al., 2007). Changes in humidity, precipitation and temperature are likely to have an impact, affecting biogenic emissions (e.g., isoprene) and deposition of

ozone (stomatal uptake), the production of the hydroxyl radical (OH), and the lifetime of the peroxyacetyl nitrate (PAN), an important reservoir of NO_x.

I explore changes to tropospheric ozone using a future climate and year 2000 emissions using model output from the Atmospheric Chemistry and Climate Model Intercomparison Project (ACCMIP) (Lamarque et al., 2013) to determine whether there is a relationship between ΔGMST and ozone in these models. Furthermore, I analyse chemistry-relevant changes in climate using physical climate output from the fifrth Coupled Model Intercomparison Project (CMIP5) models as a function of ΔGMST.

2.2   Model data and ΔGMST calculation

This study utilises ACCMIP and CMIP5 model output. ACCMIP output consists of chemistry-climate model simulations, including for sensitivity studies where anthropogenic precursor emissions vary and the climate is held constant. Analysis of these simulations can further our understanding of chemistry-climate links. On the other hand, CMIP5 is mainly focused on physical climate change: exploring climate sensitivity, historical climate, and projecting future climate. Chemical output is limited, and unlike ACCMIP output there are no simulations exploring the impact of precursor emissions and climate change on future atmospheric chemistry separately. However, CMIP5 output does allow an exploration of *potential* chemical change as a function of ΔGMST, using the physical model output in combination with offline reasoning to suggest the magnitude of the potential climate-composition impacts.

The ACCMIP output consisted of time slices, where representative conditions for a fixed period in time (e.g., 1850, 1980, 2000, and different scenarios for 2030 and 2100) were run for several years in order to estimate a climatology. Therefore, it is not possible

to explore atmospheric chemistry as a function of ΔGMST using ACCMIP output. The number of years each time slice was run varied between models (typically 3-7 years; see Lamarque *et al.* (2013)). For this study, sensitivity simulations were used, where ozone precursor emissions were fixed at their 2000 level, but with RCP8.5 climates for the year 2000, 2030 (Em2000Cl2030), and 2100 (Em2000Cl2100). The constant precursor emissions meant that changes in atmospheric chemistry and composition are driven by climate change rather than anthropogenic emission changes.

Future scenario projections for CMIP5 were continuous, unlike ACCMIP, where the historical simulations were ran from 1850 to 2005 and all future simulations were ran from 2006 to 2100 (Taylor et al., 2012a). I applied methods developed by Vautard et al. (2014) to calculate GMST changes above pre-industrial levels (ΔGMST). The first 30-year period where the average GMST exceeds the temperature target is defined as the +1.5/2 °C world. According to observational datasets, the ΔGMST from pre-industrial (1881 – 1910) to "present-day" (1971 – 2000) is +0.46 °C (Jacob et al., 2018; Vautard et al., 2014), therefore changes from present-day are 1.04 °C and 1.54 °C for targets 1.5 °C and 2 °C respectively. Two of the global observational datasets used to assess warming between the pre-industrial period and present day start at 1880 (GISSTEMP Team, 2018; NOAA NCDC, n.d.) so this is the earliest pre-industrial period I could use to follow this method.

I mainly used the RCP8.5 scenario to analyse future climate using CMIP5 output because it has the highest number of model simulations out of all the future RCP scenarios. However, I also used RCP4.5 output too, to compare results from two different emission scenarios. To calculate the multi-model mean without bias towards models with more ensemble members, the average value for all ensemble members was

calculated for each model then the multi-model mean was calculated from these values. Monthly mean CMIP5 data were interpolated onto a 1.9 ° latitude × 2.5 ° longitude grid and daily mean data were interpolated onto the same 2 ° × 2 ° grid as the ERA-Interim data (discussed below).

Model disagreement between CMIP5 models was defined as less than 80% of models agreeing with the direction of change in parameter from a present-day climate.

ERA-Interim data were used with gridded Tropospheric Ozone Assessment Report (TOAR) data (Schultz et al., 2017) to explore the relationship between historical surface ozone and climate indices.

2.3 Ground-level ozone in a warming climate using ACCMIP models

The impact of climate change on tropospheric ozone was quantified by comparing the present-day (ALL2000) scenario against two sensitivity scenarios that used fixed present-day (2000) anthropogenic precursor emissions but with changed climate (RCP8.5 scenario) to drive different natural emissions and meteorology (Em2000Cl2030 and Em2000Cl2100 for a 2030 and 2100 climate respectively). ACCMIP simulations were focussed on the scenario, rather than a particular ΔGMST target, meaning that it was not possible to find time periods where the ΔGMST since pre-industrial times was equal to 1.5 or 2 °C. Therefore, GMST was calculated for 2000, 2030, and 2100 for each model ozone change could be considered as a function of GMST, even if particular ΔGMST targets could not be considered. The analysis in this

section explores and quantifies the possibility of a linear relationship between surface

ozone and ΔGSMT, both for global mean ozone and for ozone by grid square.
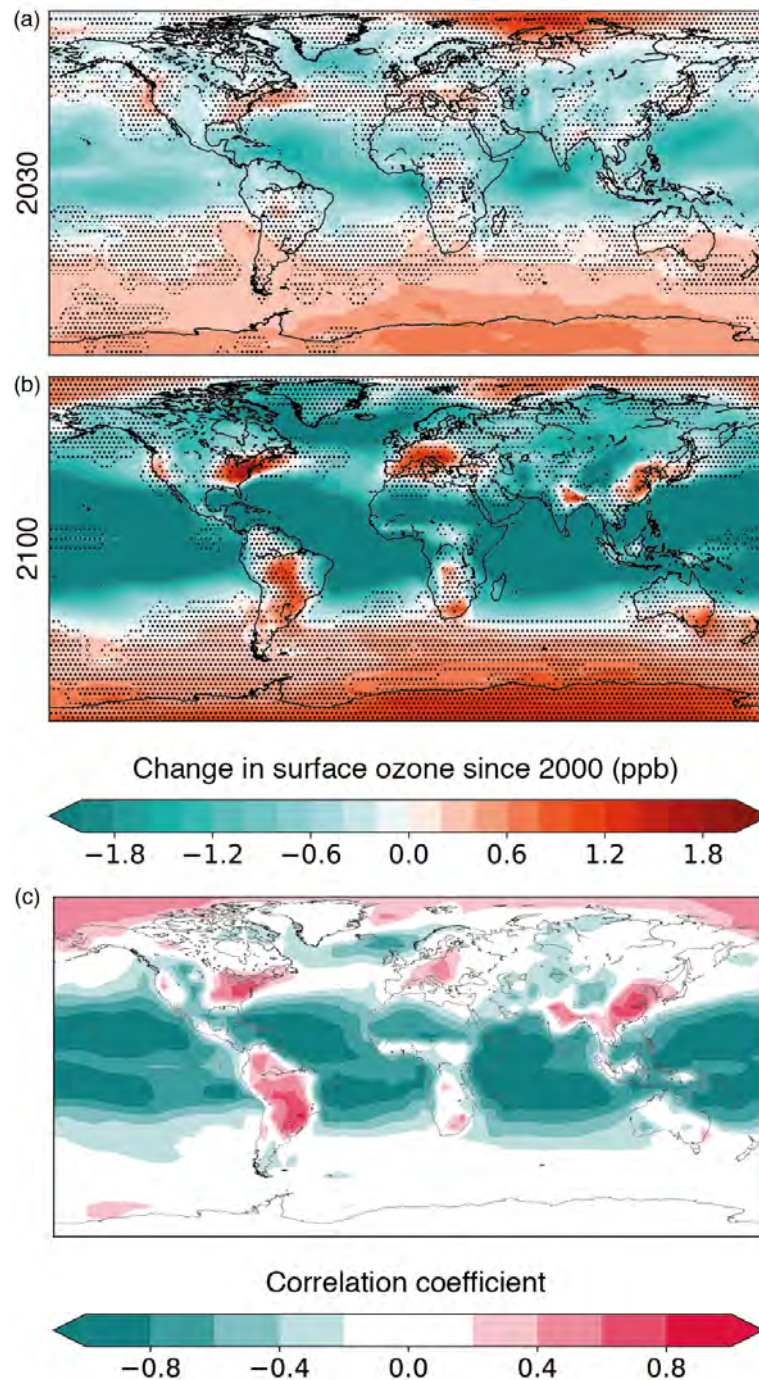
Figure 2.1: The multi-model mean change in surface ozone concentration since 2000 using ACCMIP models for (a) Em2000Cl2030 and (b) Em2000Cl2100. The ΔGMST for 2030 and 2100 were 0.85 ± 0.32 and 3.53 ± 1.36 respectively. Areas with dotted grid cells show where less than 80% of models agree on direction of change. (c) Correlation coefficient between ΔGMST and change in yearly average surface ozone for each grid square (using ACCMIP scenarios: ALL2000, Em2000Cl2030, and Em2000Cl2100).

Figure 2.1 shows the change in yearly-mean surface ozone since present-day. Over 80% of models agree that there will be a decrease in average ozone over the oceans in the tropics. Some models suggest an increase over eastern USA, parts of South America, parts of Europe, South Africa, and parts of South and East Asia at the end of the century. Similarly, Murazaki and Hess (2006) found that average summer ozone increased by around 5 ppb over eastern USA between 1990-2000 and 2090-2100 only taking climate change into account. Some of these regions are also regions with high anthropogenic ozone precursor emissions.

There is a negative correlation between global average annual mean surface ozone and global mean surface temperature change. This is in agreement with previous work and – at this scale – most likely reflects an increase in water vapour, which increases the ozone loss rate via the $O(^1D) + H_2O$ reaction (e.g., Johnson et al. 1999).

However, global mean values do not provide insight about how ΔGMST may affect ozone levels (and air quality) locally. To address this, Figure 2.1(c) shows the correlation coefficient between average surface ozone and ΔGMST for each grid square using present-day and the two sensitivity scenarios. There is a clear negative relationship between ΔGMST and change in surface ozone over the tropical oceans, where climate-driven increases in specific humidity will increase ozone loss. There is a positive relationship between ΔGMST and surface ozone over some areas of land, notably eastern USA, parts of South America, and parts of South and East Asia, which could impact air quality in those regions.

2.4 Surface ozone in a warming climate using CMIP5 models

Unlike ACCMIP, the CMIP5 experiment did not include sensitivity simulations that that isolate the impact of climate change on atmospheric composition. Therefore, changes in surface ozone as a function of ΔGMST will depend on the time a model reaches a given ΔGMST threshold because emissions and land changes will vary with time.

Figure 2.2 shows the multi-model mean change in surface ozone using only the CMIP5 models with interactive tropospheric ozone chemistry – i.e. not including models that used prescribed ozone or semi-online chemistry (see Eyring *et al.* (2013)). Still noting the caveats described above, there is a decrease in surface ozone from present-day to a warmer +1.5/2 °C climate for the majority of the globe using both RCP4.5 and RCP8.5 scenarios. Using RCP8.5, ozone is actually higher for a +1.5 °C than a +2 °C for the places that show a decrease from present-day, apart from eastern USA, which shows a decrease in ozone with ΔGMST for both RCP4.5 and RCP8.5. This decrease for a +2 °C world is larger in magnitude than the increase shown over the eastern USA for a 2100 climate and 2000 emissions shown in Figure 2.1. This suggests that the emission reductions for both these scenarios will have more of an effect on annual mean surface ozone than climate change. Over parts of eastern China, using RCP8.5, surface ozone increases from present-day to a +1.5 ° climate, but surface ozone is lower for a +2 °C climate than a +1.5 °C climate. This reflects the initial increase in atmospheric air pollutant emissions before peaking and decreasing in many regions for RCP8.5 (Riahi et al., 2011). Over India, surface ozone increases with ΔGMST, which would reflect more modest air quality controls for a RCP8.5 scenario.

Using RCP4.5, ozone decreases with ΔGMST for most of the northern hemisphere (i.e. many of the places that saw a decrease in surface ozone from present-day to 1.5/2 °C, also have lower ozone for a +1.5 °C climate compared to a +2 °C climate). This reflects the decrease in atmospheric pollutant emissions with time for RCP4.5.

The difference between the two scenarios illustrates the importance of emissions scenario in determining future surface ozone concentration as well as demonstrating the need for simulations with constant anthropogenic emissions and changing climate to assess the climate's impact on atmospheric chemistry.
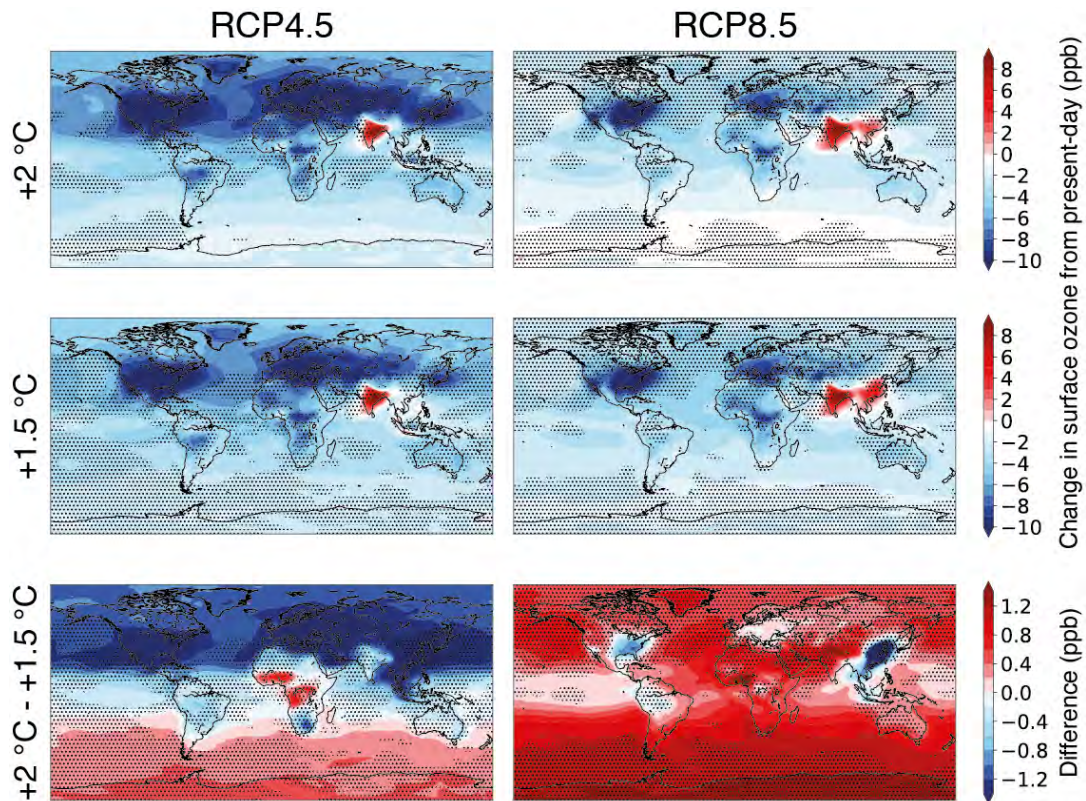
Figure 2.2: The multi-model mean change in surface ozone from present-day and the difference between +2 °C and +1.5 °C climates using only CMIP5 models with interactive tropospheric ozone chemistry (i.e. no models with prescribed or semi-online chemistry) for RCP4.5 and RCP8.5 scenarios. Areas with dotted grid cells show areas with model disagreement (where less than 80% of models agree on direction of change).

Figure 2.3 shows the difference in surface ozone between RCP4.5 and RCP8.5 for a ΔGMST of 1.5 and 2 °C. RCP8.5 generally has higher average surface ozone than RCP4.5, which could be attributed to the decrease in methane for the RCP4.5 scenario and the large increase for the RCP8.5 scenario (methane burden in 2100 is more than double in 2000; Young *et al.*, (2013)).
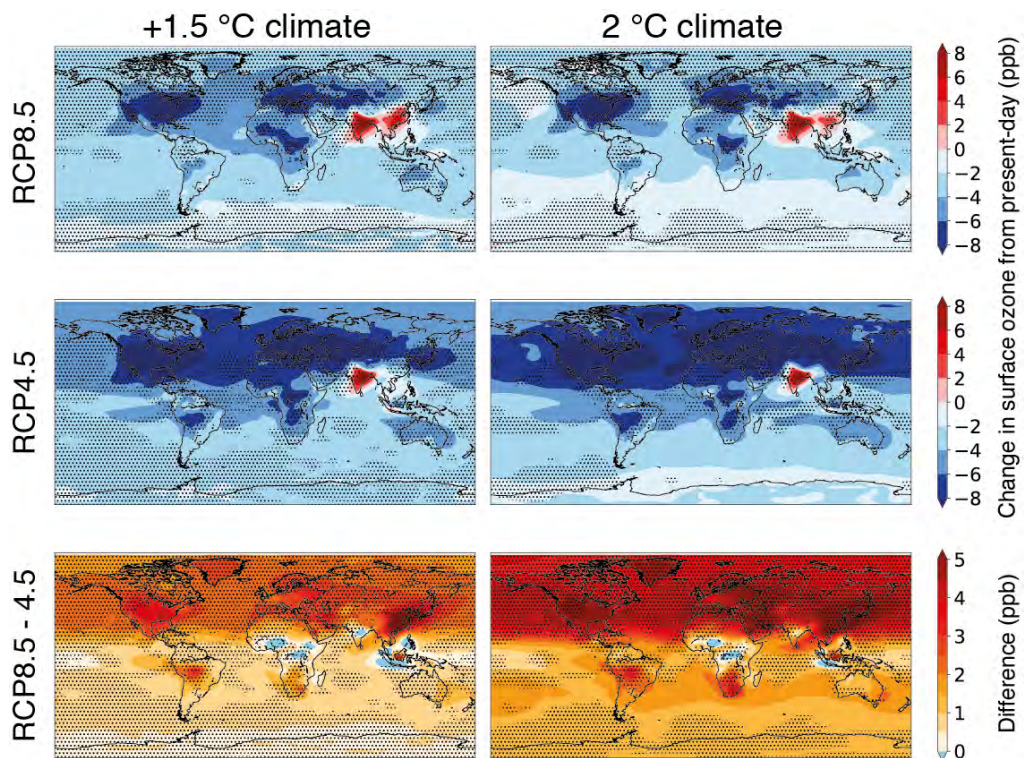
Figure 2.3: The multi-model mean change in surface ozone between present-day and a +1.5 °C climate using scenarios RCP4.5 and RCP8.5 and the difference between the two scenarios, only using CMIP5 models with interactive chemistry. Areas with dotted grid cells show areas with model disagreement (where less than 80% of models agree on direction of change).

The differences in surface ozone concentration between the two RCP scenarios for a +2 °C climate were generally much larger than the 0.5 °C ΔGMST difference for either scenario. Despite the fact that precursor emissions were not held constant in these

experiments, this overall result is consistent with previous research by Watson et al. (2016) that found that a ΔGMST of 2 °C alone would only lead to a modest increase in surface ozone over Europe and that future air quality would be more dependent on emission reductions.

Figure 2.4 shows the inter-model standard deviation for models with interactive tropospheric ozone chemistry for surface ozone. The standard deviation is generally larger than the multi-model mean ozone, which was not the case for Em2000Cl2030, where the multi-model mean for ozone in 2030 was either similar to the standard deviation or much less. Therefore, there is high model uncertainty once you take into account changes in anthropogenic emissions. Unexpectedly, considering emissions vary with time rather than ΔGMST, the standard deviation between models was greater using a common time period, rather than ΔGMST, using RCP8.5. Though the difference between the standard deviation for a +1.5 °C world and corresponding time period was generally much less than the inter-model standard deviation.

RCP4.5, on the other hand, has a higher inter-model standard deviation using a common ΔGMST for most places other than the Southern Ocean and Antarctica (where emissions are low). This may be because, using only CMIP5 models with interactive tropospheric ozone chemistry, the standard deviation in time to reach a ΔGMST of 1.5 °C is more than 7 years for RCP4.5 and less than 5 years for RCP8.5 – meaning that the model differences in anthropogenic emissions may be larger for RCP4.5 than RCP8.5 for a +1.5 °C world.
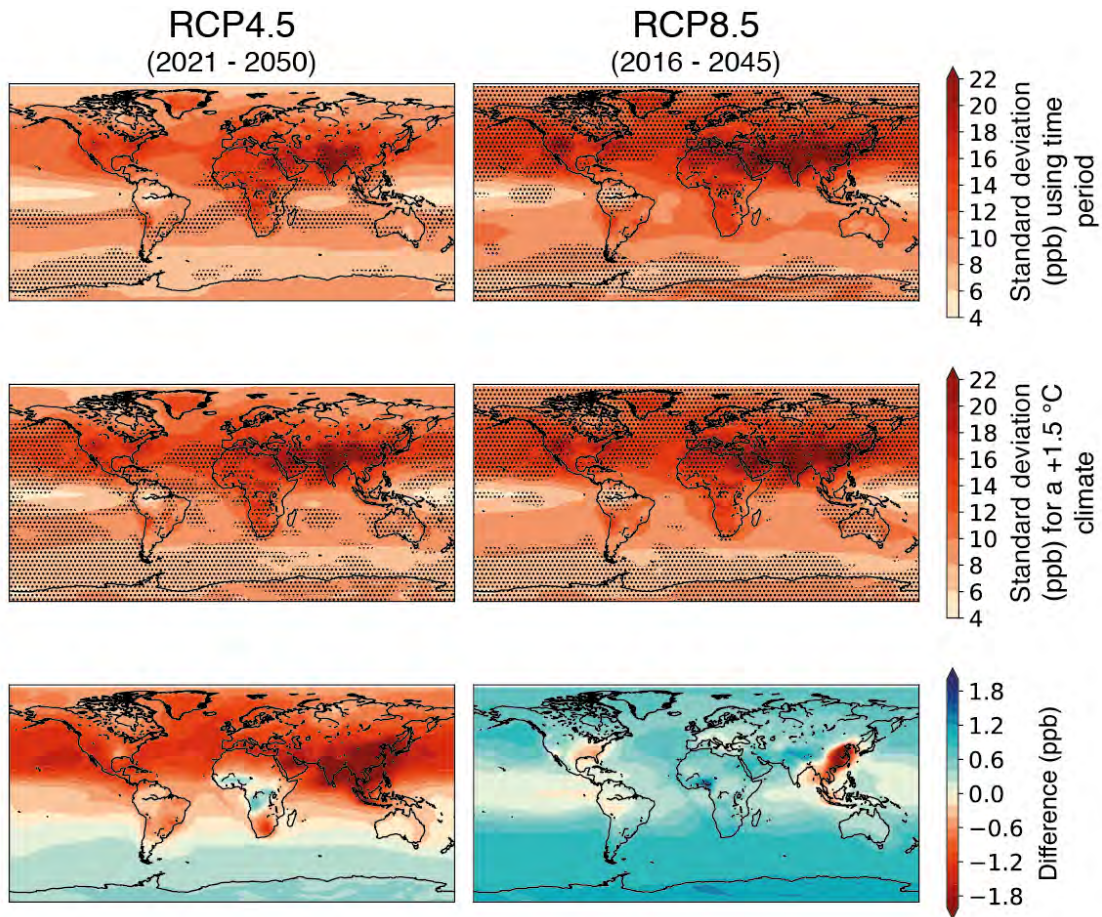
Figure 2.4: The standard deviation between CMIP5 models that have interactive tropospheric chemistry for surface ozone for scenarios RCP4.5 and RCP8.5. The first column shows the standard deviation for average surface ozone for 2021 – 2050 (medium time period where models reach +1.5 °C climate) and 2016 – 2045 (medium time period where models reach +1.5 °C climate). The middle column shows standard deviation for average surface ozone for a +1.5 °C climate (so that each model has passed 1.5 °C ΔGMST, but not usually the same time period). The bottom column shows the difference between the two standard deviations.

2.5   Chemistry-relevant physical climate change as a function of ΔGMST

This results section exploits the CMIP5 physical climate output to quantify the potential impacts on a selection of processes relevant for the production and transport of surface ozone.

2.5.1 Changes in 30-year mean values

Temperature

Changes in surface temperatures can have an impact on ground-level ozone. Temperature-dependent mechanisms that could affect ozone levels include the emission rates of biogenic VOCs and soil NO_x, lifetime of peroxyacyl nitrate, and stomatal resistance. Temperature and surface ozone levels are positively correlated over eastern USA in May using observations (Rasmussen et al., 2012) and temperature has the highest positive correlation with seasonal-mean (summer) ozone using a global chemical transport model (M. J. Kim et al., 2015). Given its relationship to surface ozone, I explored changes in surface temperature as a function of ΔGMST.

Global mean surface temperature change is the manifestation of regionally heterogeneous changes. Figure 2.5 shows the spatial pattern of the 30-year mean surface temperature change since present-day for a ΔGMST of 1.5 and 2 °C, using CMIP5 output for both the RCP4.5 and RCP8.5 scenarios. Temperature increases the most in the Arctic and the least over the oceans and there is model uncertainty over the subpolar North Atlantic ocean because while most models project warming in this region, some project abrupt cooling, mainly those that project reliable present-day stratification (Sgubin et al., 2017). Multi-model mean surface temperature change is higher using RCP8.5 than RCP4.5 because I defined the ΔGMST as 1.5/2 °C as the first 30-year mean temperature to cross the threshold, which will not be 1.5/2 °C exactly. For example, for a +2 °C climate, the multi-model mean ΔGMST using RCP8.5 was 2.16 °C, whereas it was 2.15 °C using RCP4.5. The spatial correlation coefficient between RCP4.5 and RCP8.5 for multi-model mean 30-year mean surface temperature was 0.998, for both +1.5 and +2 °C worlds.
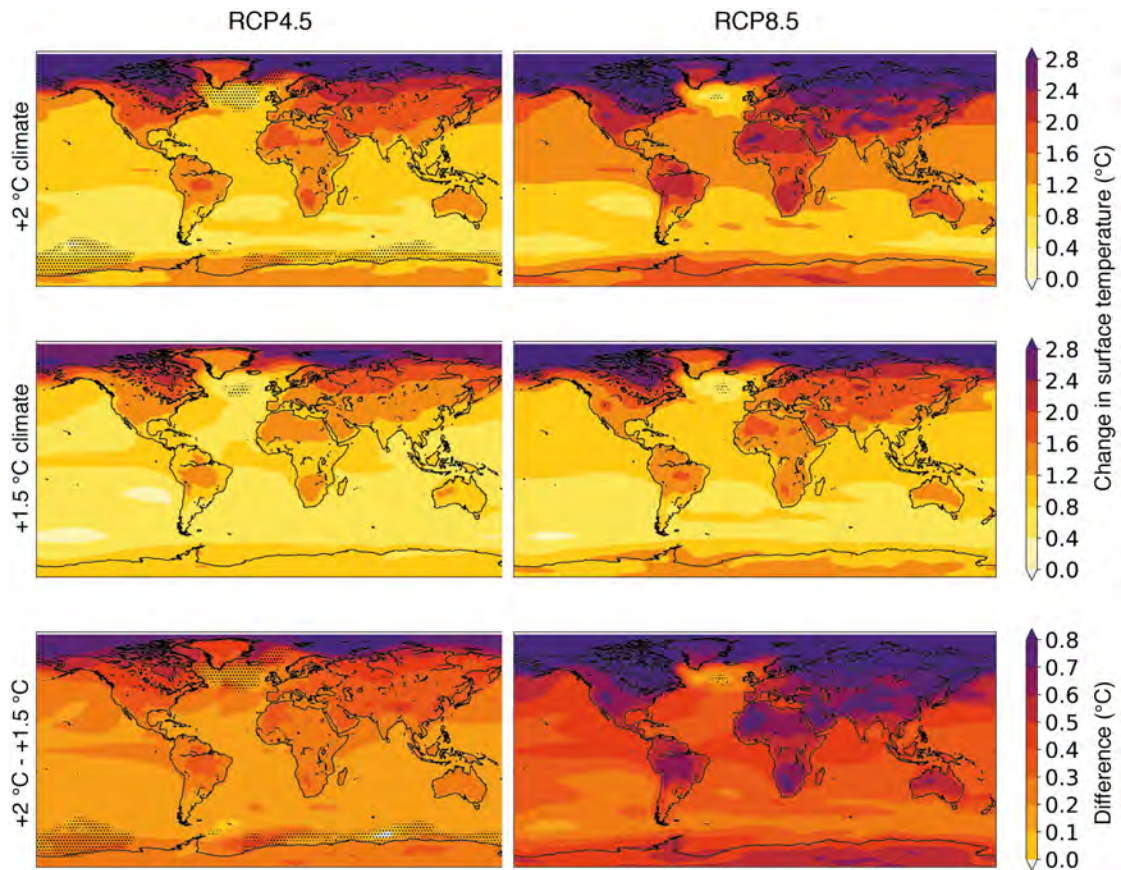
Figure 2.5: 30-year mean surface temperature for 2 and 1.5 °C ΔGMST and the difference between the two climates for scenarios RCP4.5 and RCP8.5. The bottom row shows the surface temperature in a +2 °C minus the surface temperature in a +1.5 °C climate. The dotted areas show where less than 80% of models agree with the direction of change in the mean surface temperature change.

From a chemical point of view, the increase in surface temperature will affect biogenic VOCs from plants (Guenther et al., 1995; Peñuelas and Llusià, 2001) and NO_x (Schindlbacher, 2004; Williams and Fehsenfeld, 1991) emissions from soil microorganisms, correspondingly.
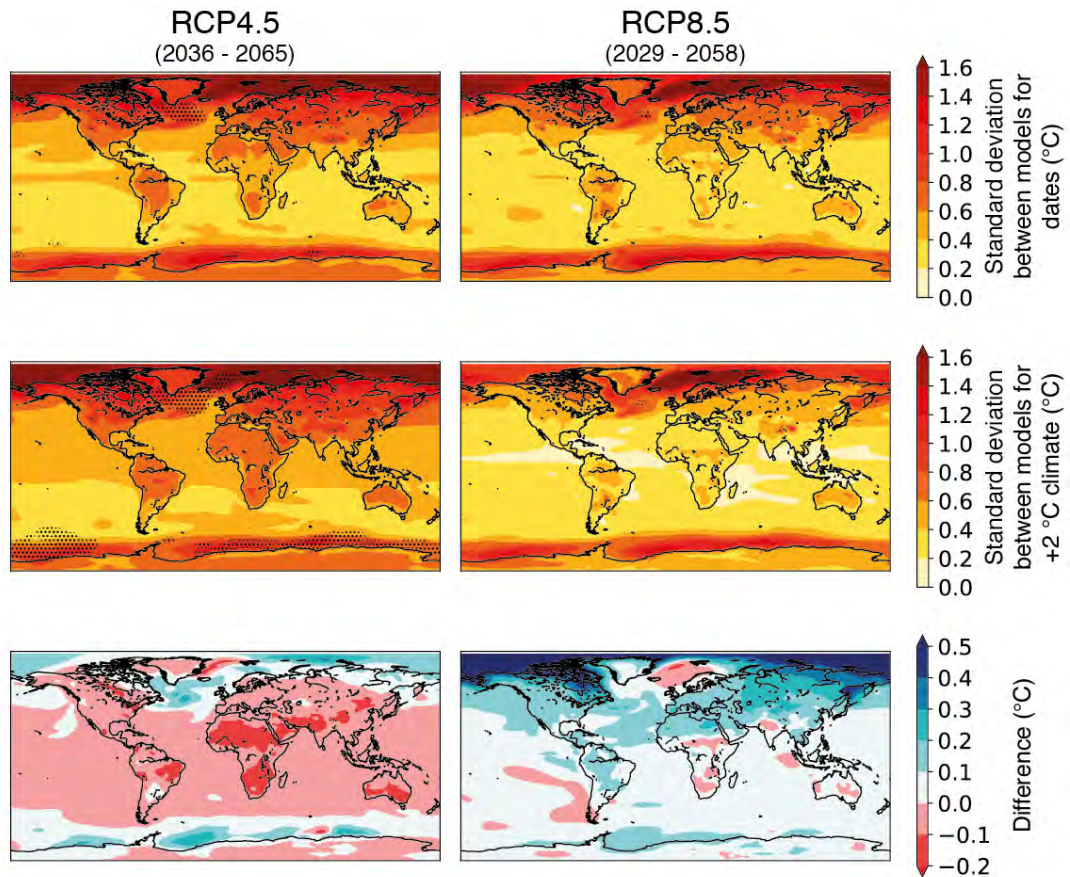
Figure 2.6: The standard deviation between models using a 30-year period corresponding to a ΔGMST of 2 °C (middle row) and the standard deviation where all models cover the same time period (median dates where models reach +2 °C; top row). The dotted areas show where less than 80% of models agree with the direction of change in the mean surface temperature change. For the bottom row, positive values (blue) show areas where standard deviation is higher. The difference between the two standard deviation values (bottom row) for RCP4.5 (σ(2036 - 2065) - σ(+2 °C)) and RCP8.5 (σ(2029 - 2058) - σ(+2 °C)).

One reason to examine variables as a function of ΔGMST rather than time would be the possibility of reducing the disagreement between models: i.e., in terms of spatial patterns, is there more model agreement when they are normalised by ΔGMST rather than by time? Figure 2.6 shows the difference in standard deviation between models for surface temperature change as a function of ΔGMST and time. The dates used to compare standard deviation to a +2 °C climate were 2036 – 2065 and 2029 – 2058, which represent the median time period that models cross these thresholds for scenarios

RCP4.5 and RCP8.5 respectively. There is a reduction in standard deviation between models using different time periods and a similar ΔGMST for the majority of the Earth for RCP8.5 for both +1.5 and +2 °C worlds. This is not the case for RCP4.5, which sees a reduction in standard deviation using ΔGMST for most of the Earth for a +1.5 °C climate, but not for a +2 °C climate. There is less model agreement on when RCP8.5 will cross the 2 °C threshold than RCP4.5

The correlation coefficient between the spatial distribution for both thresholds between RCP4.5 and RCP8.5 is 0.998 using a common time period, similar to using a common ΔGMST threshold and the correlation between results between using a common time period and a common threshold is high (>0.998) for all scenarios and thresholds. So whichever scenario or method you choose the spatial distribution of surface temperature change remains about the same.

Figure 2.7 shows the correlation between CMIP5 surface temperature and ozone using each model and 30-year period (present-day, and +1.5 °C and +2 °C climates using RCP4.5 and RCP8.5). There is a negative correlation between gridded surface temperature and ozone over most of North America, Europe, and Australia. This is most likely due to the decrease in pollutant emissions (they decrease in both RCP4.5 and RCP8.5) rather than a negative correlation with surface temperature. For example, there is a negative correlation over eastern USA using CMIP5 data, but using ACCMIP Em2000Cl2030 and Em2000Cl2100 there is a positive correlation between surface ozone and GMST and there is an increase in surface ozone with time using Em2000Cl2100 (Figure 2.1). Both CMIP5 scenarios show a positive correlation between ozone and temperature over the Southern Ocean (a correlation coefficient of over 0.9 in some areas), likewise ACCMIP Em2000Cl2030 and Em2000Cl2100

showed an increase in ozone with time over this area (Figure 2.1). Most of the places with a correlation coefficient over 0.9 were over the ocean, possibly due to the fact ozone in these areas are less affected by reduction in anthropogenic emissions and more affected by climate change than over the land. North Africa shows a small positive correlation, despite showing a negative correlation in Figure 2.1(c), so changes in anthropogenic precursor emissions are increasing ozone where climate would have decreased ozone. Similarly, there is a stronger positive correlation over southern India, where there was not with constant emissions using ACCMIP data.
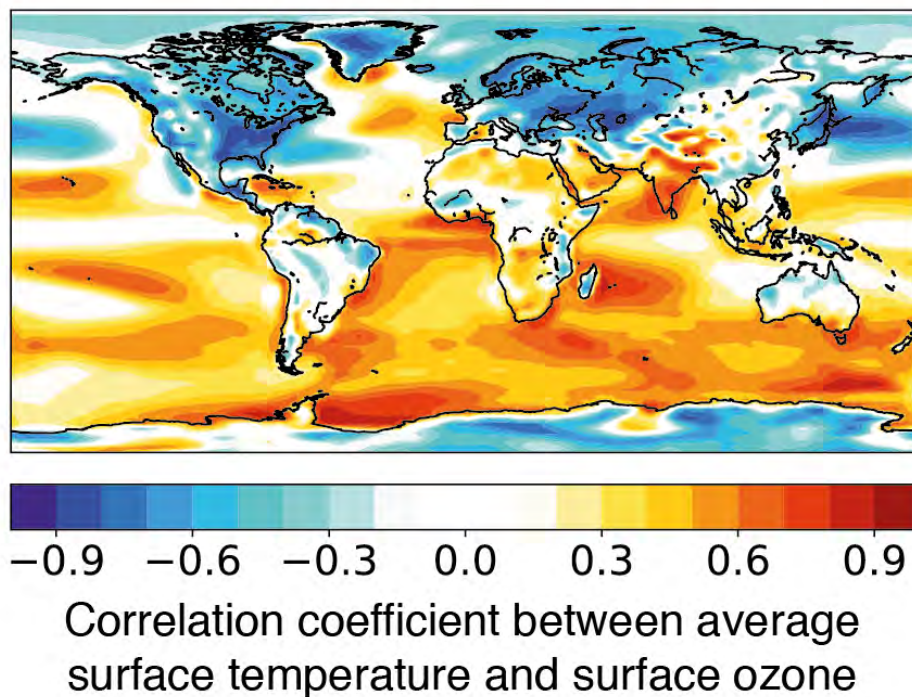
Figure 2.7: The correlation coefficient between the CMIP5 30-year mean surface temperature and 30-year mean surface ozone using present-day and both RCP4.5 and RCP8.5 scenarios.

Specific humidity

Water vapour is the main sink of ozone over the oceans, through the following simultaneous processes:

$$O_3 + h\nu \rightarrow O(^1D) + O_2 \qquad (2.1)$$

$$O(^1D) + H_2O \rightarrow 2OH \qquad (2.2)$$

reaction (2.2) is competing with N_2 or O_2 absorbing energy shown in 2.1, which would stabilise $O(^1D)$ to ground-state atom $O(^3P)$, which would react with O_2 to form ozone. Therefore, in absence of other effects, an increase in water vapour would lead to a decrease in ozone production.

Under polluted conditions there are additional effects: the OH radicals produced by 2.2 react with VOCs and CO to produce peroxy radicals that can result in ozone production, or they can convert NO_2 to nitric acid, which supresses ozone formation. Therefore, under polluted conditions model studies found that the sensitivity of ozone to water vapour is weak (Dawson et al., 2007; Jacob and Winner, 2009). Therefore, as was evident from the ACCMIP analysis in Figure 2.1, in some areas yearly-mean surface ozone may decrease with climate change, whereas peak surface ozone concentrations may increase with climate change, during extreme pollution events. To meet air quality standards there will need to be stricter emissions controls, as ozone extremes will increase with climate change in already polluted regions, this is referred to as the 'climate penalty' (Jacob and Winner, 2009; Rasmussen et al., 2013; Wu et al., 2008).

Figure 2.8 shows that for most regions there is an increase in specific humidity with ΔGMST, the biggest increase and model agreement being in the tropics over the oceans. This increase in humidity with GMST should lead to a decrease in surface ozone over

the oceans, which is consistent with the negative correlation between GMST and surface

ozone using ACCMIP models (Figure 2.1).
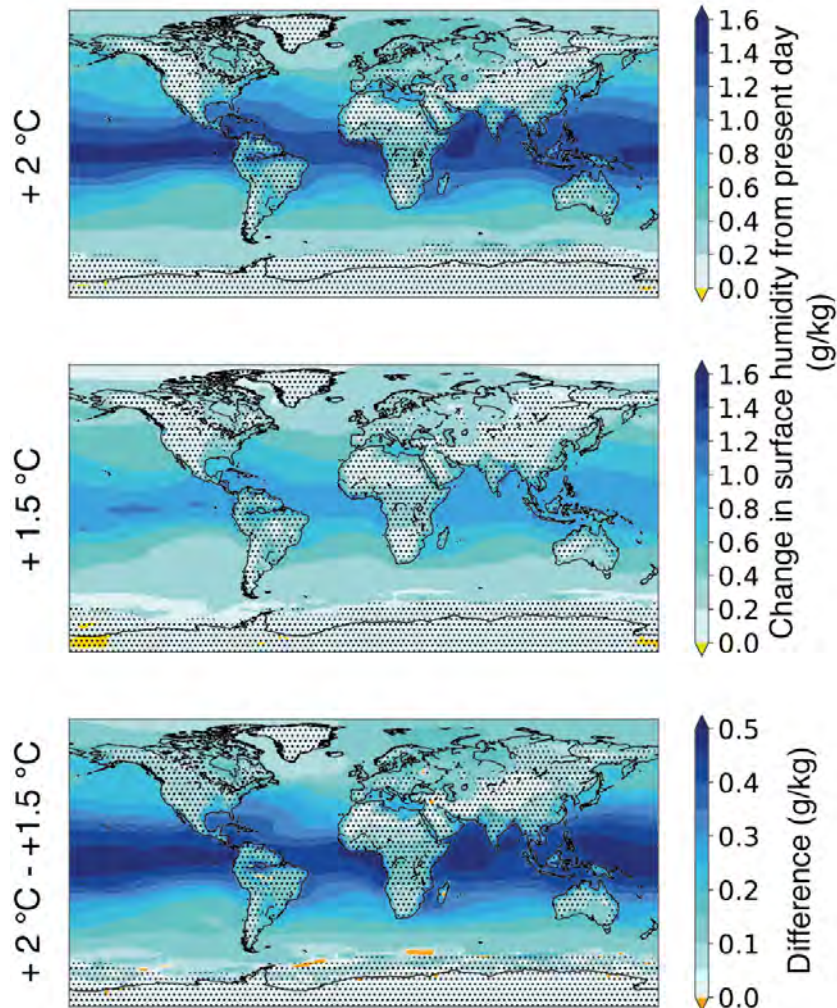
Figure 2.8: 30-year mean surface specific humidity change from present-day (1971-2000) for a ΔGMST of (a) 1.5 °C and (b) 2 °C, where (c) is (a) – (b). The dotted areas show where less than 80% of the models agree with direction of change.

2.5.2 Natural examples of ozone precursors and ΔGMST

Biogenic emissions

Changes in surface temperature will affect biogenic ozone precursor emissions. A large proportion of biogenic NMVOC global total emissions are isoprene emissions, which are also affected by changes in water availability, land cover, and CO_2 concentration. Isoprene is highly reactive and in NO_x-limited areas it will react directly with ozone and ozone concentration will decrease. On the other hand, oxidation of isoprene results in peroxy radicals (RO_2), which react with NO_x to form ozone. Isoprene also contributes to PAN formation.

Due to its important role in ozone formation, I assessed the impact of changes in ΔGMST on isoprene formation. One model for isoprene emission was described by Guenther et al. (2006), who described the net isoprene emission rate (E) by:

$$E = [\varepsilon][\gamma][\rho], \qquad (2.3)$$

where ε is the emission factor, which represents isoprene emissions at standard conditions, γ is a normalised ratio that accounts for changes in emissions due to deviations from standard conditions, and ρ is a normalised ratio that accounts for production and loss within the canopy.

I assumed that landcover does not change because I estimated biogenic emissions as a function of ΔGMST rather than time and any anthropogenic land use change will change with time rather than ΔGMST. Therefore, the calculation assumed that ε stays constant.

γ accounts for emission response to light, temperature, leaf age, soil moisture, leaf area index, and CO_2 inhibition (Guenther et al., 2012). In this section, I focus on changes in CO_2 and temperature, and ignore changes in light, leaf age, soil moisture, and leaf area index in response to climate change.

E was estimated for present-day and future temperature CMIP5 output and CO_2 projections using:

$$E = \frac{E_{2000}\gamma_T\gamma_C}{\gamma_{T_{2000}}\gamma_{C_{2000}}} \tag{2.4}$$

where E_{2000} is the emission rate for the year 2000, γ_T and γ_C are the model temperature and CO_2 emission activity factors respectively and $\gamma_{T_{2000}}$ and $\gamma_{C_{2000}}$ are the temperature and CO_2 emission activity factors for the year 2000.

The activity factor for CO_2 response (γ_C) was estimated by:

$$\gamma_C = I_{Smax} - \left[\frac{I_{Smax}(0.7C_a)^h}{(C*)^h + (0.7C_a)^h}\right], \tag{2.5}$$

where I_{Smax} (=1.344), h (=1.4614), and $C*$ (=585) are emperically determined co-efficients and C_a is the ambient CO_2 concentration (Heald et al., 2009). The temperature-dependant activity factor (γ_T) was estimated as follows:

$$\gamma_T = E_{Opt} \cdot \left[\frac{C_{T2}e^{C_{T1}\cdot x}}{C_{T2} - C_{T1} \cdot (1 - e^{C_{T2}\cdot x})}\right], \tag{2.6}$$

where $x = \left[(1/T_{Opt}) - (1/T)\right]/0.00831$, T is leaf temperature (assumed to be the same as air temperature), and empirical coefficients C_{T1} and C_{T2} are 95 and 230 respectively (Guenther et al., 2006). Empirical coefficients E_{Opt} and T_{Opt} were assumed to be 1.9 and 312.5 respectively (Guenther et al., 1999). I did not calculate leaf temperature from air temperature because it would require various other variables, such as humidity, which would have meant processing and storing large amounts of data.

I used MEGAN emissions of isoprene flux for the year 2000 (E_{2000}), and calculated the γ_T using mean 2000 ERA-Interim 2m temperature, mean CMIP5 present-day surface temperatures, and mean CMIP5 future surface temperatures. To calculate isoprene emissions for present-day I multiply E_{2000} by CMIP5 present-day γ_T and divide by $\gamma_{T_{2000}}$ and follow the same method to estimate future isoprene flux using future CMIP5 temperature projections.

Future atmospheric concentrations for CO_2 for a particular ΔGMST were different for each model because I used the average CO_2 concentration for the 30-year period where the model reaches the GMST target. Whereas, $\gamma_{C_{2000}}$ using dates would be the same for each model. Therefore, I also estimated changes in total isoprene emissions just due to projected temperature changes.
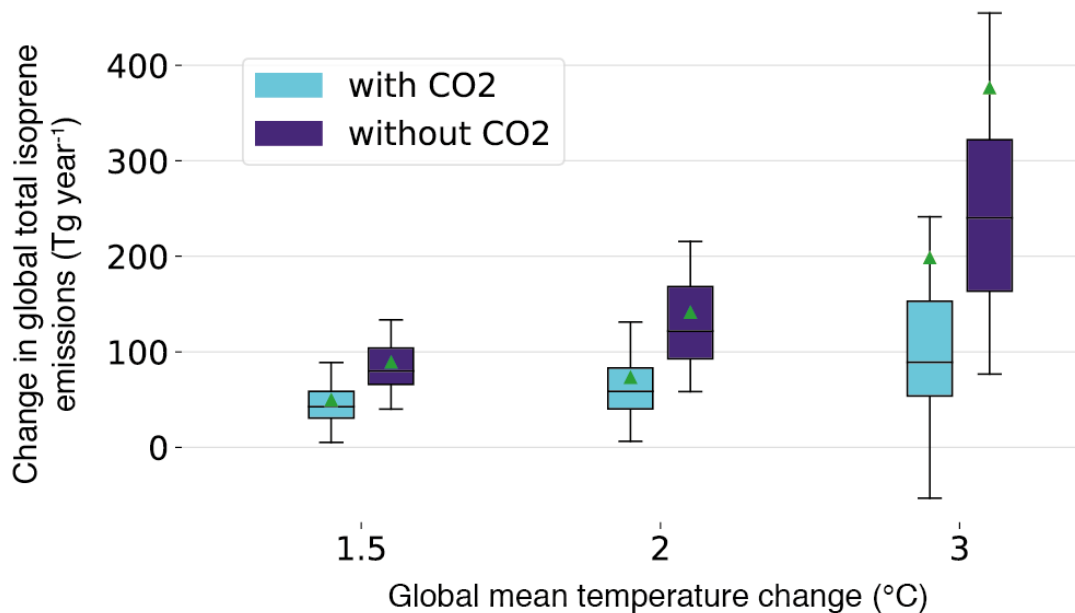
Figure 2.9: Global total isoprene emission change from present-day (1971-2000) for different ΔGMST, where cyan box plots on the left take into account the average change in CO_2 and the purple plots on the right do not. The black line and green triangles indicate the median and mean model values respectively.

Figure 2.9 shows the model spread for the estimated change in global total isoprene emissions from the projected change in temperature with and without the projected change in CO_2. At higher ΔGMST some models show a decrease in total isoprene emissions for a +3 °C climate when considering future CO_2 emissions, which has been found in previous work for the late 21st Century (Arneth et al., 2007; Heald et al., 2009; Young et al., 2009).
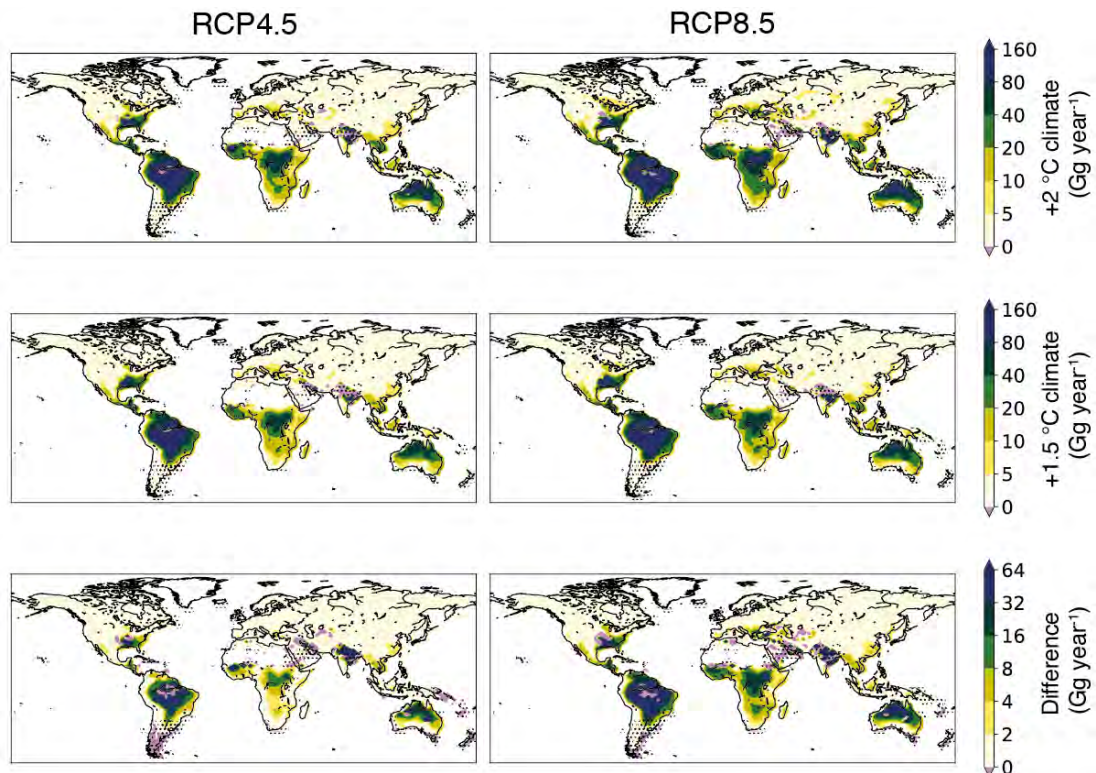
Figure 2.10: 30-year mean isoprene flux change from present-day (1971-2000) for a ΔGMST of 2 °C (top) and 1.5 °C (middle) and the difference between them (bottom). The dotted areas show model disagreement (<80% of models agree with direction of change).

Figure 2.10 shows estimated changes in 30-year average isoprene emissions. The highest increases in isoprene flux are over the Amazon region, eastern USA, parts of India, central Africa, and parts of Austraila. The area showing a decrease in isoprene emissions is relatively small. However, Squire et al. (2014) found that once land use changes were taken into account there was a projected decrease in isoprene emissions from 2000 to 2095 over the Amazon region, India, central Africa, and most of Australia.

Other BVOC emissions affected by temperature change include monoterpenes. To calculate future monoterpene emissions, I used the following equation:

$$\frac{M}{M_S} = e^{\left(\beta(T - T_s)\right)} \tag{2.7}$$

Where M are the monoterpene emissions at temperature T, M_S are the emissions at standard temperature T_S, and β is a constant (0.09 K^{-1}) . By rearranging 2.7 and substituting 2005 ERA-Interim temperatures and MEGAN monoterpene fluxes I estimated monoterpene emissions using present-day and future CMIP5 data:

$$M_{CMIP5} = M_{2005} e^{\left(\beta(T - T_{2005})\right)} \tag{2.8}$$

where M_{2005} and T_{2005} are 2005 monoterpene emissions and 2005 mean temperatures respectively, and T_{CMIP5} are monthly mean daily mean temperatures from CMIP5 models.
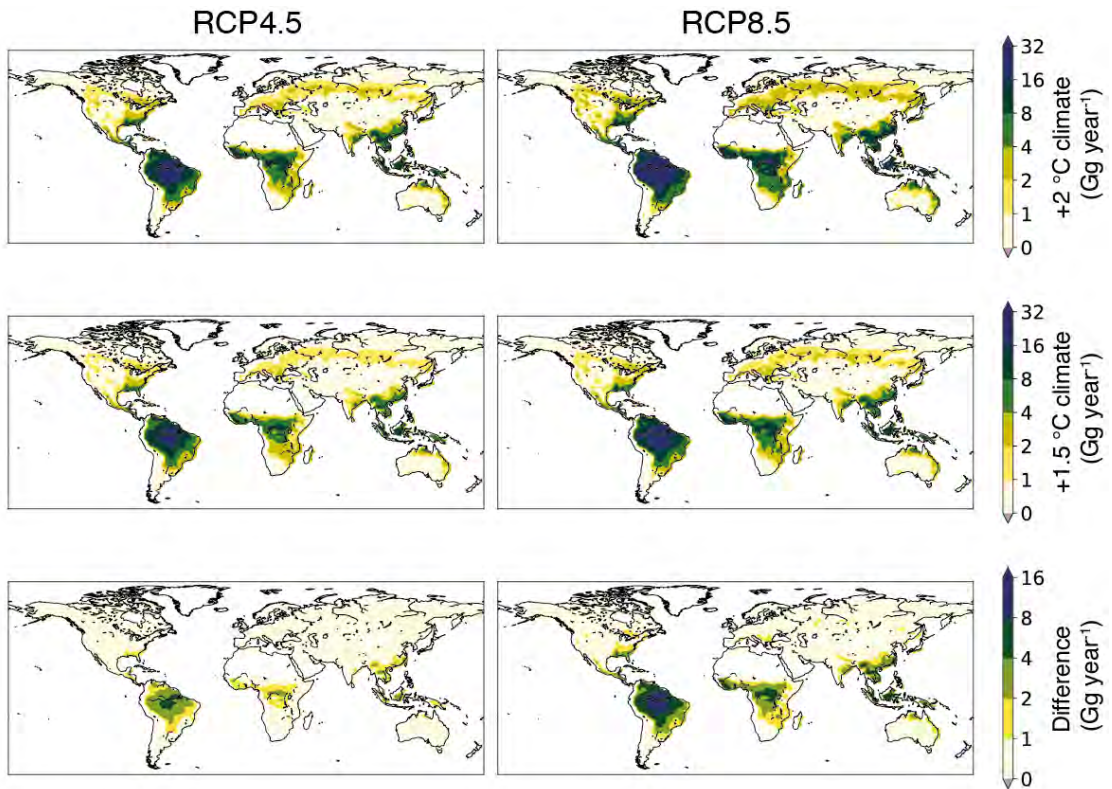
Figure 2.11: 30-year mean monoterpene flux change from present-day (1971-2000) for a ΔGMST of 2 °C (top) and 1.5 °C (middle) and the difference between them (bottom). The dotted areas show model disagreement (<80% of models agree with direction of change).

Figure 2.11 shows the change in estimated 30-year average monoterpene emissions. The spatial correlation coefficient was 0.22 between monoterpene and isoprene emissions. The largest increases in monoterpene and isoprene emissions were in the Amazon region, central Africa, and south-east Asia.

Lightning NO$_x$

The extreme temperatures associated with lightning strikes generate NO$_x$ by the recombination of some dissociated O$_2$ and N$_2$ molecules. These lightning NO$_x$ emissions can influence the production of ozone, particularly in the mid and upper troposphere. The impacts of lightning NO$_x$ on ozone at the surface are typically quite

small (Aghedo et al., 2007; Kaynak et al., 2008) so many studies have neglected its effects on ground-level ozone. However, cloud-to-ground lightning has been shown to increase ozone by around 50% in Taipei, Taiwan (Kar and Liou, 2014) and surface ozone was found at higher concentrations during days with a higher number of lightning flashes over Kolkata, India (Middey and Chaudhuri, 2013). Overall, the impact of lightning NO_x emissions on surface ozone will depend on the local photochemical regime – NO_x titration will occur if the ratio between NO_x and VOCs is sufficiently high. Although anthropogenic fuel combustion emissions have more of an impact over surface ozone, the global mean influence of lightning is greater than that of biomass burning (Murray, 2016). Therefore, I project changes in lightning frequency and NO_x emissions as a function of ΔGMST.

Here, lightning NO_x emissions were calculated as a function of ΔGMST, using CMIP5 output and an emission parameterisation based on ice flux developed by Finney et al. (2014). Using this parameterisation, Finney et al., (2018) projected a decrease in lightning over the tropics with climate change, which is at odds with the general increase in lightning NO_x projected by the ACCMIP models who used a range of different parametrisations, mainly based on cloud-top height (Finney et al., 2016). I used monthly mean specific cloud ice water content (q), updraught mass flux (Φ_{mass}), and fractional cloud cover (c) at 440 hPa to calculate monthly mean ice flux ϕ_{ice}:

$$\phi_{ice} = \frac{q \times \Phi_{mass}}{c}, \qquad (2.9)$$

which was multiplied by constants provided by Finney et al. (2014) to calculate the flash density (fl m^{-2} s^{-1}):

$$f_l = 6.58 \times 10^{-7} \; \phi_{ice} \qquad\qquad (2.10)$$

$$f_o = 9.08 \times 10^{-8} \; \phi_{ice}, \qquad\qquad (2.11)$$

where f_l and f_o are the flash density over land and ocean, respectively.

Figure 2.12 shows the change in flash frequency, estimated using CMIP5 ice flux. Over the tropics, there is a decrease in lightning frequency, and much of the mid-latitudes in the Northern Hemisphere see an increase, though the magnitude of the increase is not as high as the decrease.

Murray (2016) found that the largest differences for present-day annual-mean simulated ozone with and without lightning were around Chile, Namibia, and western China, although these were not the areas with the highest simulated lightning NO_x emissions. Figure 2.12 shows a decrease over most of these areas, which may mean that there is a decrease in average values of surface ozone in these areas.
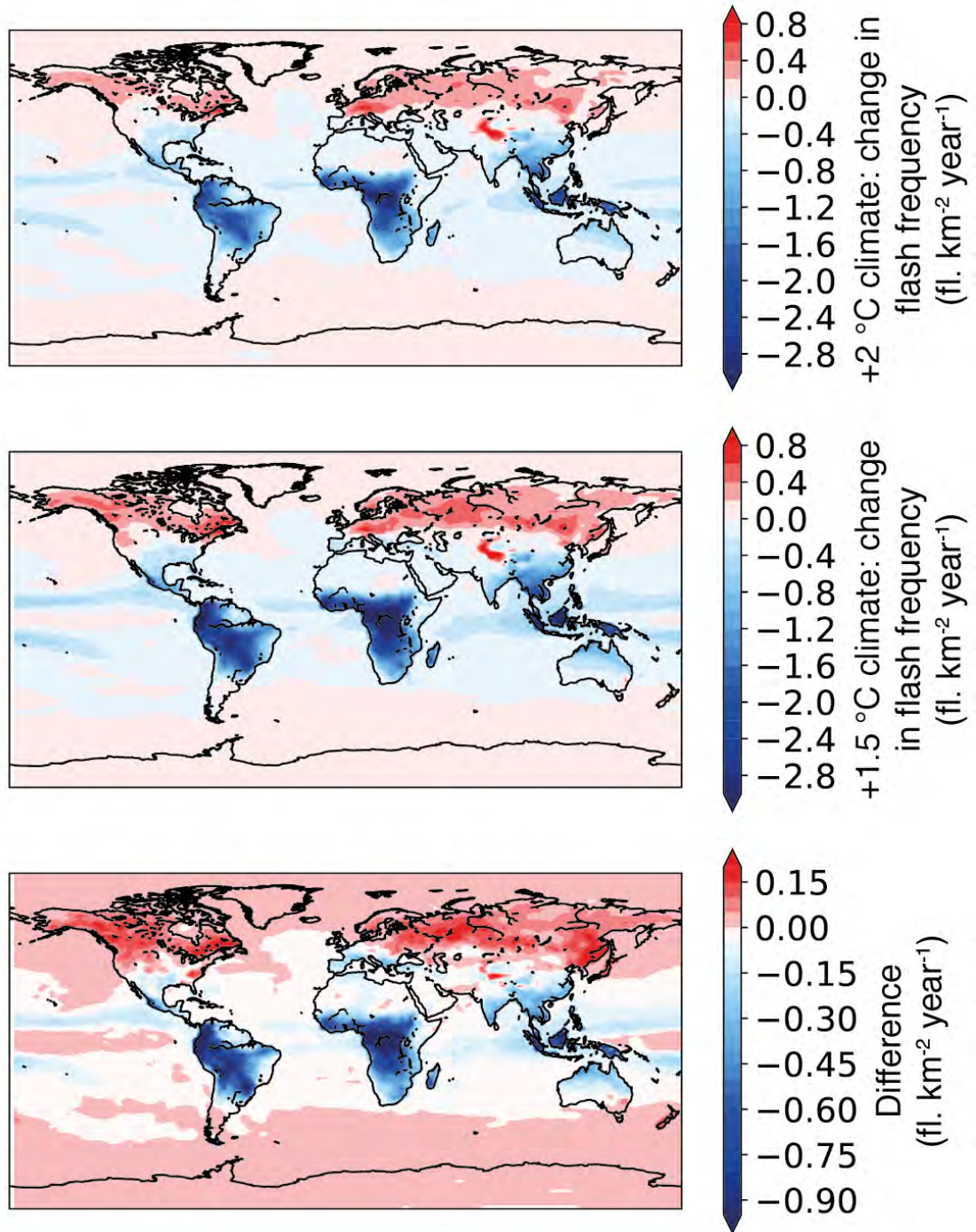
Figure 2.12: Change in estimated lightning flash frequency for a ΔGMST of 2 °C (top) and 1.5 °C (middle), and the difference between the two climates (bottom).
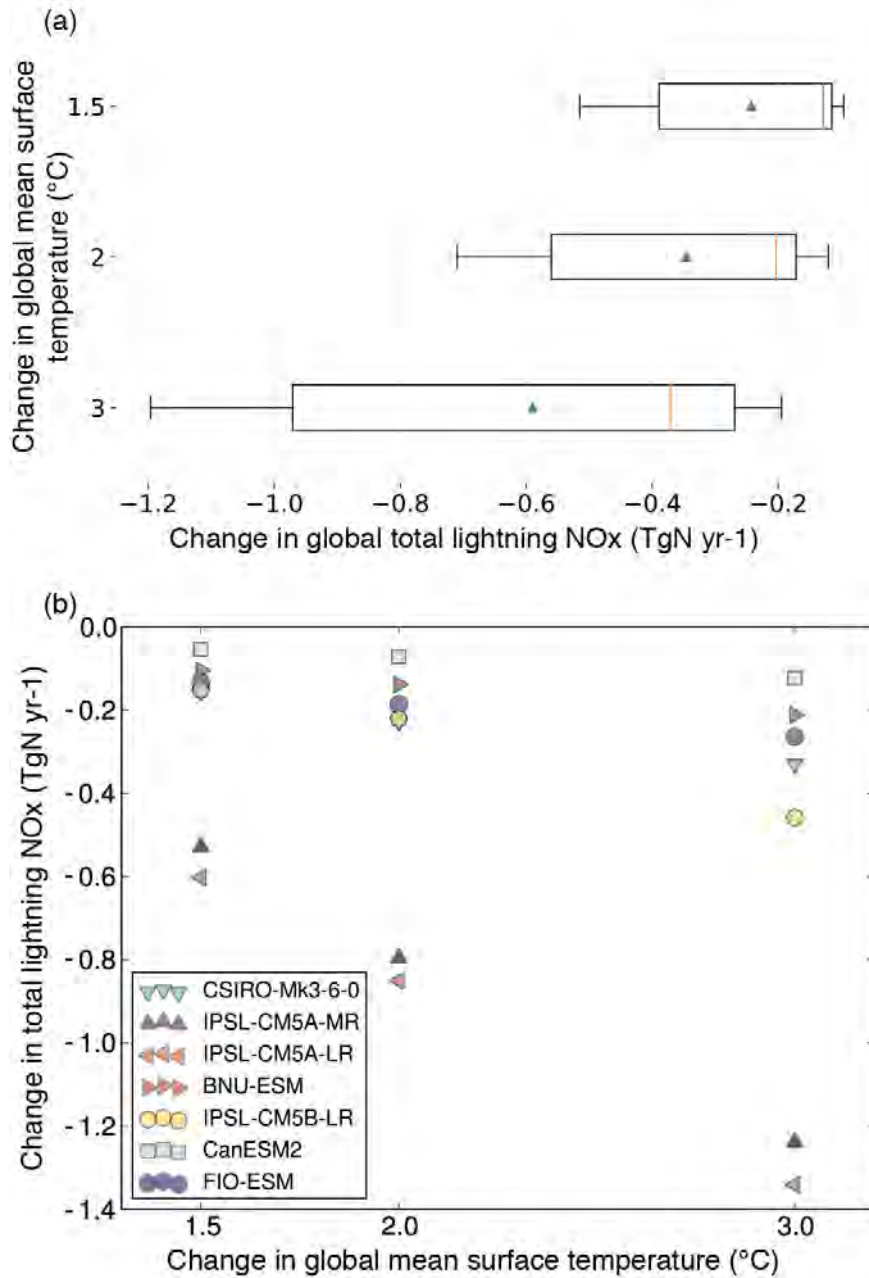
Figure 2.13: (a) The calculated change in global total lightning NOx emissions from present-day (1971 – 2000) as a function of global mean surface temperature, (b) same as (a), but shows each model individually.

Figure 2.13 shows the change in global total NOx emissions from present-day as a function of ΔGMST, calculated from estimating model ice flux using 2.9. The global multi-model mean total NOx decreases with ΔGMST, while the model variability increases. There were only seven CMIP5 models with all the relevant parameter

outputs, and, using their outputs with the Finney et al. (2018) parameterisation they all indicate a decrease in lightning NO_x individually (shown in Figure 2.13 (b)). Lightning mainly contributes to ozone in the free troposphere, where it has a lifetime of months, allowing for hemispheric transport. Lightning also contributes to the formation of PAN, which enables transport of NO_x. For example, in the tropics it contributes 30-80% towards total column PAN concentrations (Fischer et al., 2014). Therefore, a general decrease in lightning NOx emissions should decrease the intercontinental transport of NO_x and ozone.

2.5.3 Daily maximum surface temperature and air quality

While average surface ozone decreases in many regions due to climate change, surface ozone extremes may increase in some regions (i.e., the climate penalty), which will have a detrimental impact on human health.

Higher temperatures are typically associated with higher levels of surface ozone and, in addition to increases in mean temperatures, extreme temperatures are expected to increase in frequency and intensity with ΔGMST (e.g., Nangombe et al., 2018; Wehner et al., 2018). Porter *et al.* (2015) found that 49% of sites studied in the USA show daily maximum temperature as the main meteorological driver of summer ozone using quantile regression. Romer *et al.* (2018) found a slope of 1.7 ± 0.2 ppb $°C^{-1}$ between daily afternoon-average temperature and ozone in Centreville, Alabama. Similarly, Fiore *et al.* (2015) found a linear relationship between July mean daily maximum temperature (mx2t) and July mean daily maximum 8-hour mean (MDA8) ozone Pennsylvania State Clean Air Status and Trends Network (CASTNet) site in Pennsylvania (41° N, 78° W, 378 m). There was also a shift in ozone levels after NO_x emissions controls were introduced in eastern USA in 2002 (Bloomer et al., 2009).

To explore the relationship between surface temperature and ozone extremes, I used ERA-Interim mx2t output and TOAR MDA8 ozone data. I interpolated mx2t and TOAR ozone data onto the same 2° x 2° grid.

Figure 2.14(a) shows the relationship between TOAR ozone and ERA-Interim temperature for the corresponding grid cell to the CASTNet site in Pennsylvania (40° N 78° W). There is a positive trend (3.46 ppb °C^{-1} for 1990-2001 and 1.94 ppb °C^{-1} for 2002-2014). The decrease in slope after emission controls are introduced was found in other areas of the USA by Bloomer et al. (2009). At higher temperatures the 95% confidence intervals (CI) do not overlap, so emission controls made a significant difference to ozone concentrations during warmer summers. Before policy, the relationship between temperature and ozone is more likely to be significant than after policy. Likewise, the correlation coefficient is higher before policy was introduced (r^2 = 0.69 for 1990-2001 and r^2 = 0.43 for 2002-2014).

For comparison, Figure 2.14(b) and (c) show the relationship between TOAR ozone and ERA-interim daily maximum temperature for south-east England (grid cell 52 °N 0 °W) and the Kantō region in Japan (36 °N 140 °E) respectively. There is a positive correlation between temperature and ozone for both areas, but it is much stronger for the grid cell in the UK (r^2 = 0.71) than Japan (r^2 = 0.29). Policies and laws regarding air quality have been introduced in the UK and Japan, with several introduced between 1990 and 2014 (Wakamatsu et al., 2013). In the UK example, MDA8 ozone is generally lower in later years. On the other hand, some of the higher ozone concentration values in (c) are years after additional NO$_x$ emission controls have been introduced in Japan, possibly because the area was VOC-limited, so ozone titration was reducing ozone levels before the controls were introduced.
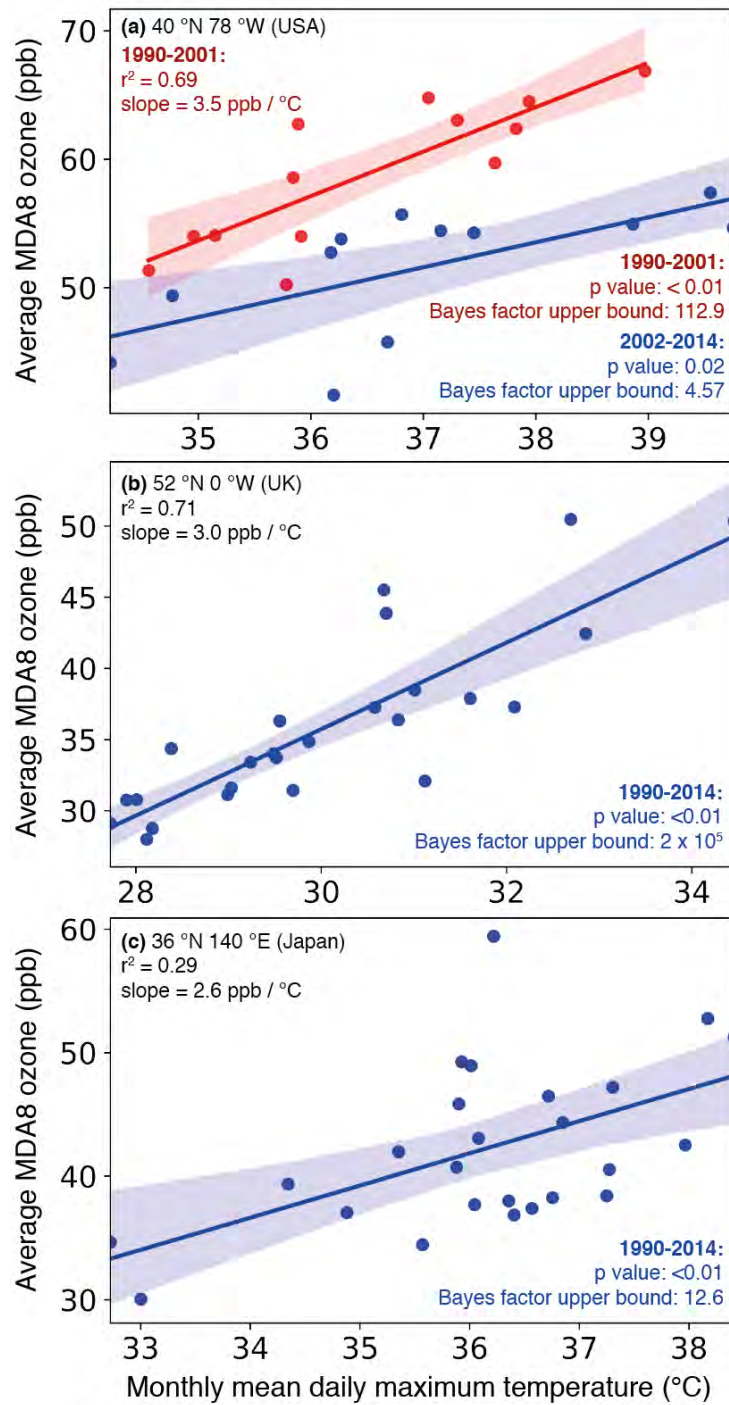
Figure 2.14: Scatter plot between TOAR July-average MDA8 ozone and ERA-Interim July-average daily maximum temperature for (a) 40 °N 78 °W, (b) 52 °N 0 °W, and (c) 36 °N 140 °E grid cells. For the location in the USA (a), the red (top) points show data from 1990-2001 (before extra NO_x emission controls) and the blue (bottom) points show data from 2002-2014. For the locations in the UK (b) and Japan (c), there is just one line showing the line of best fit for 1990-2014. The line and filled area show the ordinary least squares regression line and 95% confidence interval.

Figure 2.15 shows the correlation coefficient between ERA-Interim monthly mean daily maximum temperature and TOAR monthly mean MDA8 ozone for summer (June, July, August). Correlation is highest in most of mainland Europe in July and eastern USA in August. Only a few grid cells had enough data to calculate a correlation coefficient in the Southern Hemisphere for summer (December, January, February).
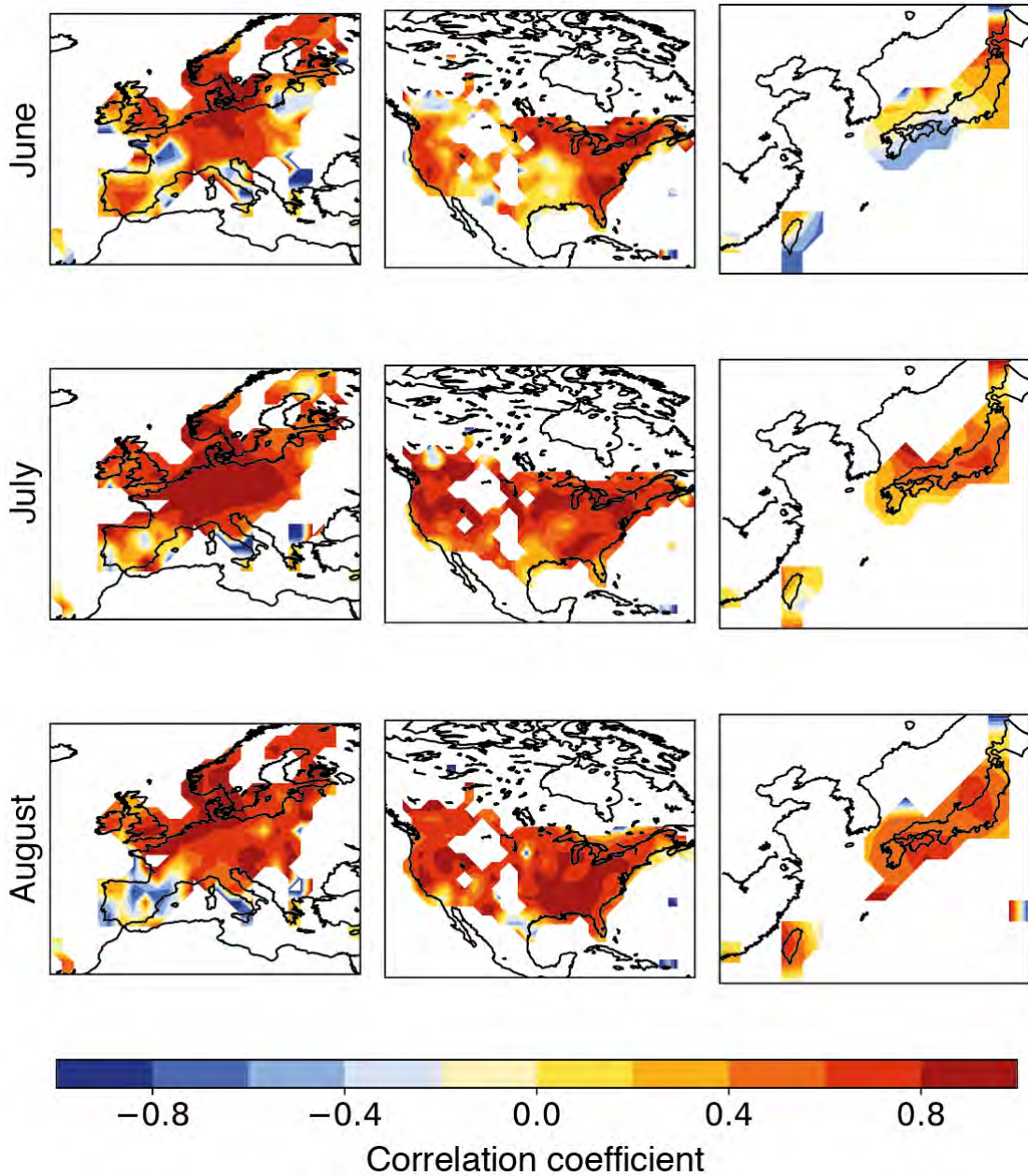
Figure 2.15: The correlation coefficient between ERA-Interim monthly mean daily maximum temperature and TOAR monthly mean MDA8 surface ozone for June, July, and August between 1990 and 2001 for Europe, North America, and East Asia.

Figure 2.15 shows the correlation coefficient between ERA-Interim monthly mean daily maximum temperature and TOAR monthly mean MDA8 ozone for North America and Europe for June, July, and August. The correlation is strongest for Western Europe in July and Eastern USA in August.

Figure 2.16 shows the change in January and July mean daily maximum temperature using CMIP5 RCP8.5 output. There is a larger increase over north Africa and the Middle East than the USA and Europe, but there are no gridded MDA8 ozone TOAR data for those regions. Average daily maximum temperatures in July increase up to around 1.5 °C for a +1.5 °C climate for most of Europe and the USA and there is a difference of up to 0.6 °C between +1.5 and +2 °C climates.
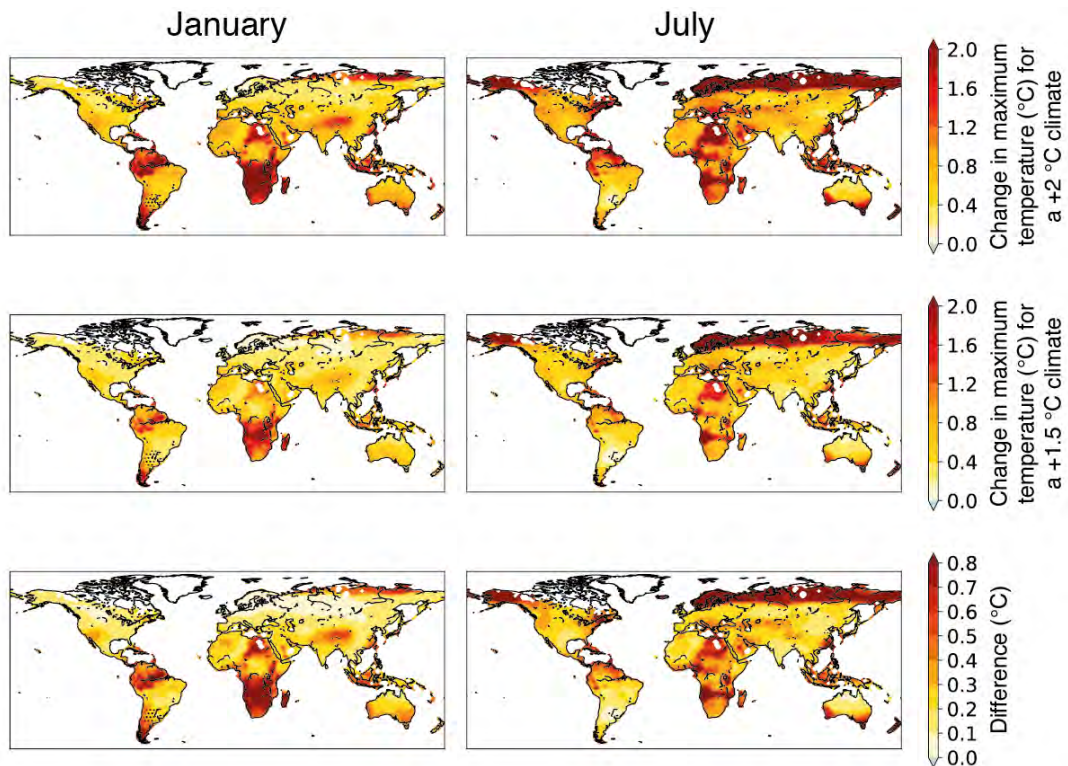
Figure 2.16: 30-year mean January and July averages for daily maximum surface temperature change from present-day (1971-2000) for a ΔGMST of 1.5 °C and 2 °C, and the change in maximum temperature from a 1.5 °C to a 2 °C ΔGMST. The dotted areas show where less than 80% of models agree with the direction of change in the mean surface temperature change.

Thermal decomposition of PAN

A strong contributor to the relationship between surface ozone and temperature is peroxyacetyl nitrate (PAN) (Sillman and Samson, 1995), which is very stable at cold temperatures and can decompose to release NO_x at warmer temperatures, like so:

$$PAN + M \rightarrow CH_3COO_2 + NO_2 + M. \tag{2.12}$$
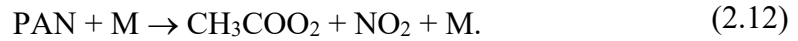
PAN is more stable than ozone and is not soluble in water. It is the main reservoir for nitrogen oxide radicals ($NO_x = NO + NO_2$), contributing to their long-range transport and promoting ozone production in regions away from the source of precursor emissions.

The primary sink of PAN is thermal decomposition, so I estimated the changes in thermal decomposition rate for the warmer climates using CMIP5 RCP8.5 output.

The rate of thermal decomposition for PAN was estimated using the Arrhenius relation:

$$k = A e^{-E_a/RT}, \tag{2.13}$$

where constants A and E_a were assumed to be 16.2 s^{-1} and 112.5 kJ mol^{-1} respectively (Grosjean et al., 1994) and T represents the temperature and I used monthly mean daily maximum temperature at the surface.

Increasing temperatures will lead to a reduction in PAN volume mixing ratio and will affect the long-range transport of NO_2 and may enhance local mixing ratios of PAN, particularly in urban areas, where emissions of NO_x are generally higher.
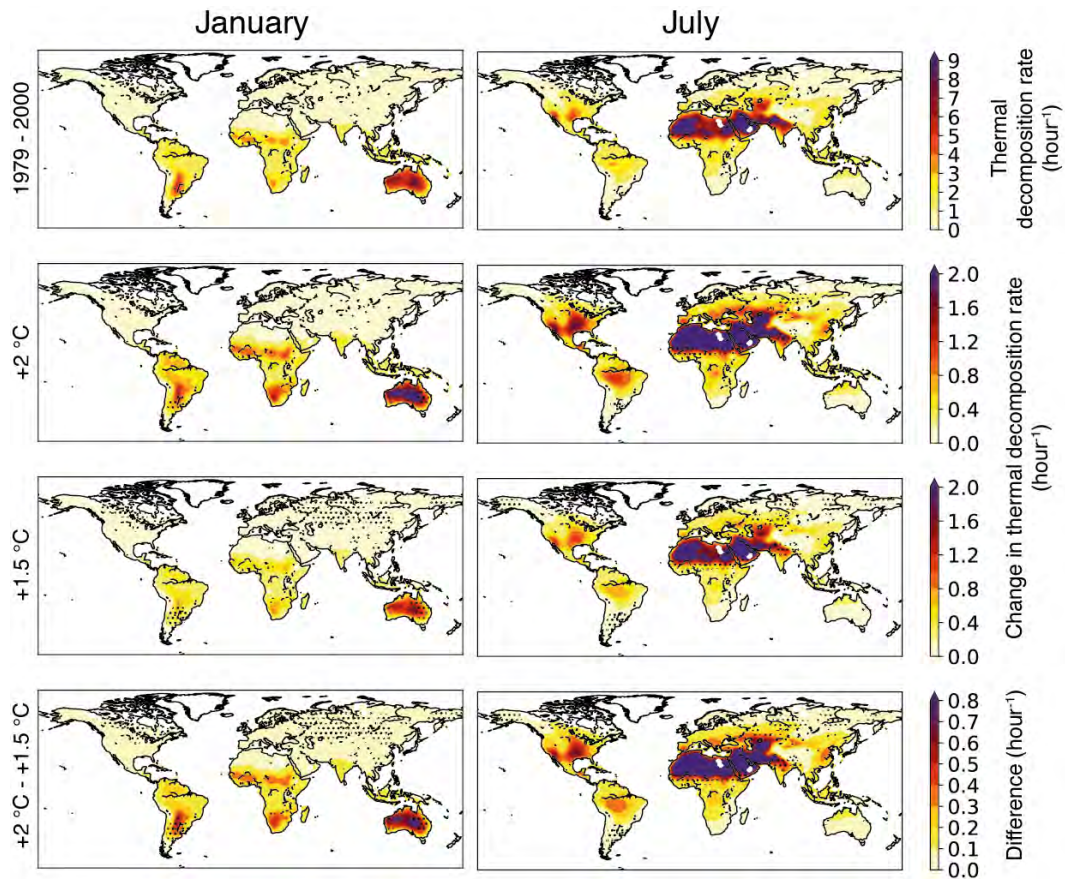
Figure 2.17: The estimated rate of thermal decomposition of PAN at the surface for present-day, the change in thermal decomposition from present-day for +2 °C and 1.5 °C climates, and the difference between them. Calculated using monthly mean daily maximum surface temperatures for January and July.

Figure 2.17 shows the thermal decomposition of PAN for 1979-2000, and changes for +1.5 and +2 °C climates, calculated using CMIP5 daily maximum temperatures. As expected, the thermal decomposition rate is highest in the SH (NH) in January (July), due to its relationship with temperature. In January, the largest increases can be seen over large parts of Australia, which in NO_x-limited conditions may lead to a decrease in PAN and an increase in surface ozone, as was the case in January 2013 in Sydney, Australia (Utembe et al., 2018). In July, the largest increases in decomposition rate are in Northern Africa and the Middle East. Ozone and PAN concentrations over the Persian Gulf region are seasonally anti-correlated so that in summer the short lifetime

of NO_x leads to higher levels of ozone, where summer-time ozone levels in 2006 exceeded air quality guidelines (defined by the EU), though this was not the case when model simulations did not include anthropogenic emissions (Lelieveld et al., 2009). So, one would expect the shorter PAN lifetime in July would lead to elevated levels of ozone in this region, and they would regularly be above recommended guidelines unless anthropogenic emissions are reduced in the future.

Isoprene emissions

Figure 2.10 shows the estimated change in yearly average isoprene emissions. However, using daily mean temperatures does not take the daily cycle of temperature into account, which may mean that isoprene emissions are underestimated over the course of a day (Ashworth 2010). Therefore, I estimate isoprene emissions changes using CMIP5 daily maximum temperature.

Figure 2.18 shows the January and July mean changes in isoprene emissions estimated using daily maximum temperature. Many of the areas that showed an increase in yearly mean isoprene in Figure 2.10 now show a decrease using monthly-mean daily maximum temperatures, including parts of Brazil and Australia, because at very high temperatures isoprene emissions start to decline (Singsaas and Sharkey, 2000; Zimmer et al., 2000). I assumed that isoprene emissions start declining above 39.35 °C because I defined T_{Opt} = 312.5K. Over the USA, estimated isoprene emissions are more than halved for a +2 °C climate compared to a +1.5 °C climate.
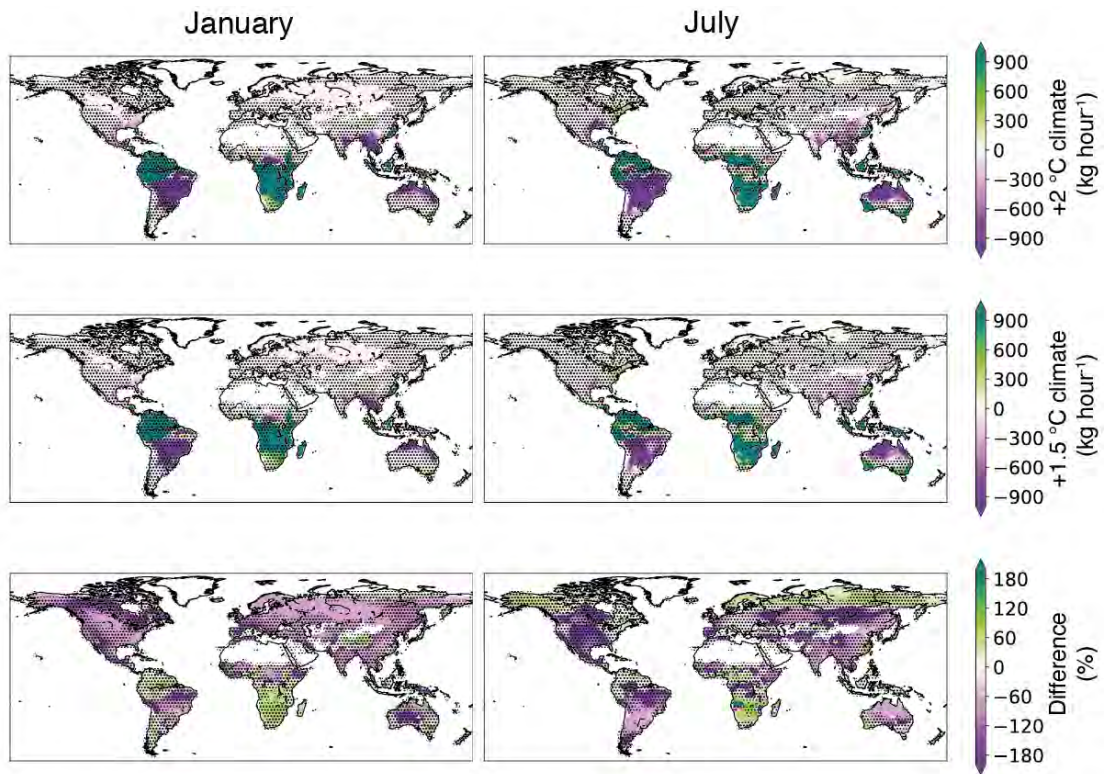
Figure 2.18: Estimated change in isoprene emissions from present-day for +2 °C and 1.5 °C climates, and the difference between them. Calculated using monthly mean daily maximum surface temperatures for January and July.

Dry days

Dry spell duration is expected to increase with ΔGMST in the Mediterranean, North-East Brazil, and Southern Africa; however the simulated response is not robust when considering the sign of change in dry spell duration for the majority of the USA and substantial parts of the rest of the world for +1.5 and +2 °C climates (Hoegh-Guldberg et al., 2018; Schleussner et al., 2016).

Dry conditions affect plant stomata, thus reducing the vegetation sink for ozone, which leads to an increase in ozone. However, chronic exposure to higher levels of ozone can permanently damage plant stomata so that they do not close in response to drought (Mills et al., 2009), resulting in a negative feedback between dry spells and surface

ozone levels. In addition, dry weather reduces the amount of soil water available, which can have an impact on biogenic emissions.

I found that the relationship between total July precipitation and MDA8 ozone was not significant for most of Europe and North America (not shown). Therefore, I calculated the correlation coefficient between monthly mean MDA8 surface ozone and the total number of dry days for June, July, and August, where dry days are defined as days with < 1mm precipitation.

Figure 2.19 shows that there is a positive correlation between ozone and the number of dry spells for most of Europe and North America. However, it is not as strong as the correlation between daily maximum temperature and ozone for the majority of places, as shown in Figure 2.15. The total number of dry days is highly correlated with daily maximum temperature in these regions in summer (Figure 2.20). For December – February, parts of Brazil, Australia, Central and Southern Africa show a high correlation between ERA-Interim daily maximum temperature and the total number of dry days.
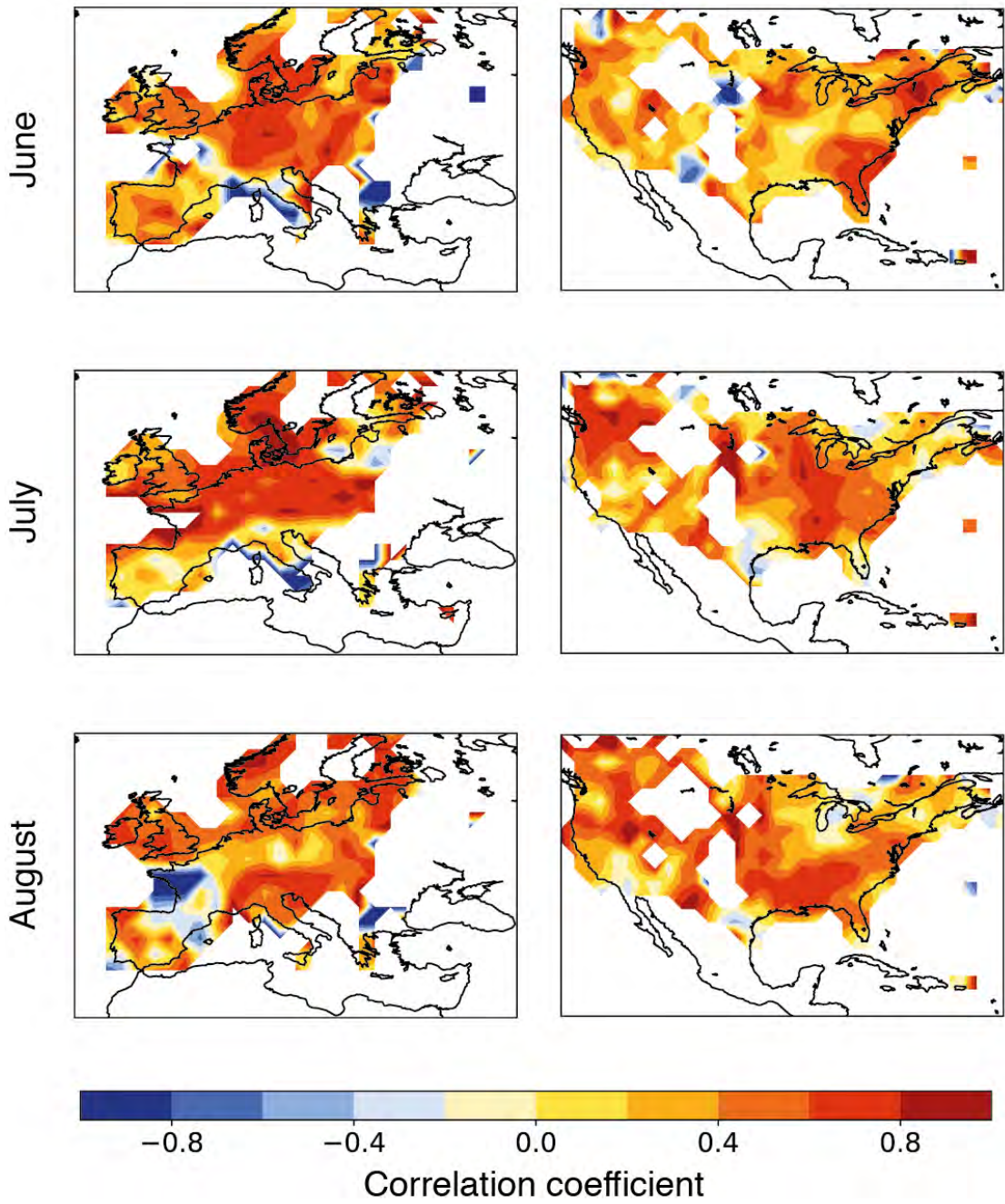
Figure 2.19: The correlation coefficient between the total number of dry days using ERA-Interim reanalysis data and the monthly-average MDA8 ozone for June, July and August 1990 - 2001.
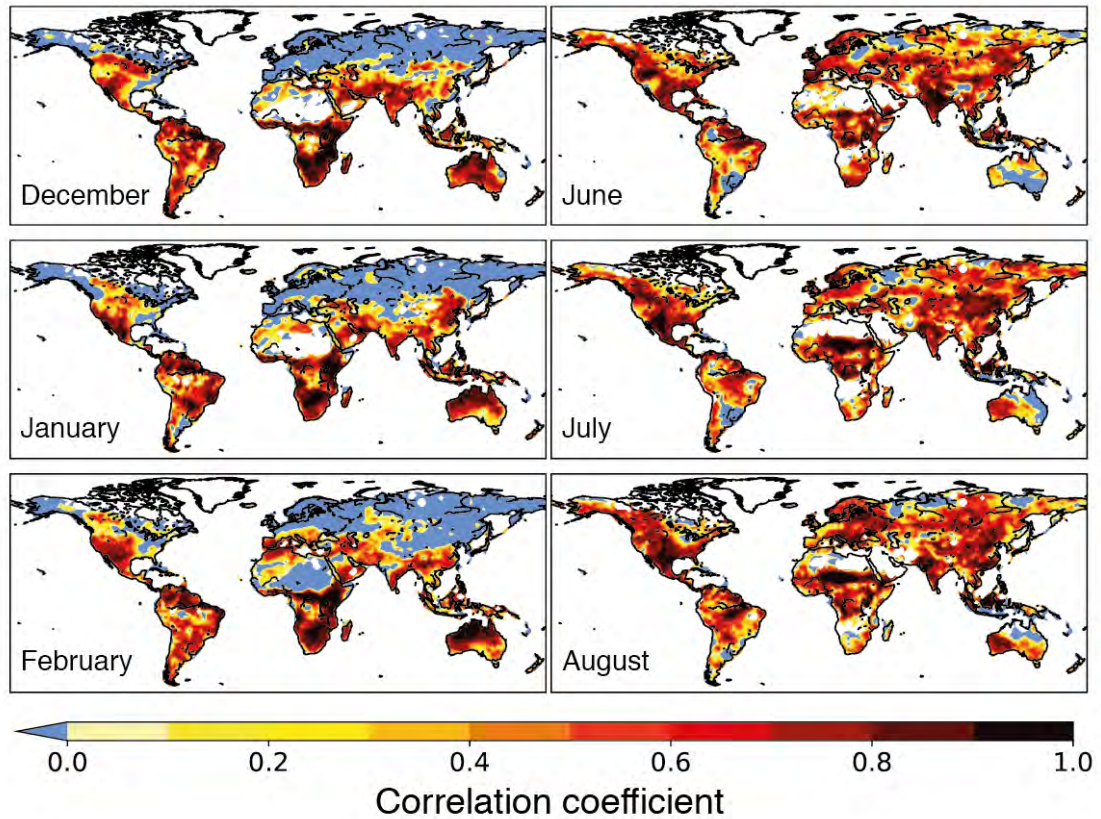
Figure 2.20: The correlation coefficient between the monthly total number of dry days and monthly mean daily maximum surface temperature, where a dry day is defined by total daily precipitation < 1mm.

Air stagnation index (ASI)

The ASI defines a stagnant day as one with less than 1mm total precipitation, surface (10 m) wind speed less than 3.5 ms^{-1}, and mid-tropospheric (500 mb) wind speed as less than 13 ms^{-1} (Horton et al., 2012). Air stagnation is associated with increased levels of air pollution (Fiore et al., 2012; Jacob and Winner, 2009) and by the end of the century the frequency and persistence of stagnation events are expected to increase over western USA, India, and Mexico under RCP8.5 scenario (Horton et al., 2014).

Since air stagnation is commonly associated with elevated levels of surface ozone (Jacob and Winner, 2009), I explore the relationship between monthly mean TOAR

MDA8 ozone and the total number of stagnant days that month using ERA-Interim reanalysis data. Figure 2.21 shows the correlation coefficient between average June, July, and August MDA8 ozone and the total number of stagnant days for that month. Correlation between the number of stagnant days and average MDA8 surface ozone is much lower than the correlation between the average daily maximum temperature and surface ozone. As TOAR data were only available monthly, it was not possible to check whether MDA8 ozone was higher on stagnant days.

Heatwaves and air stagnation are both associated with clear skies and, in Europe, cloud cover is an important indicator of maximum daily temperature, though not necessarily a climate driver (Tang et al., 2012). Less cloud cover results increased short-wave radiation, which affects photochemical processes. Therefore, I looked at the relationship between surface ozone and total cloud cover using monthly mean TOAR MDA8 ozone and ERA-Interim total cloud cover data. Figure 2.22 shows the correlation coefficient between monthly mean MDA8 ozone and monthly mean total cloud cover for June, July, and August. The strongest negative correlation is in western Europe in July and eastern USA in August, the same as surface temperature (Figure 2.15). This similarity between cloud cover and temperature reflects a correlation between temperature and cloudiness in the summer.

Although global cloud feedback is likely positive (Zelinka et al., 2017), cloud cover has declined over some land areas, including over Europe and North America (Mao et al., 2019). Therefore, climate change may mean an increase in ozone in the absence of emission reduction, due to changes in cloudiness. In other areas, for example in western Europe in August, there may be a decrease in ozone with cloudiness. Aerosols also affect the formation and properties of clouds (Ackerman, 2000; Kaufman, 2006).

Therefore, I did not explore CMIP5 projections in cloudiness or incoming radiation: aerosol emissions would change with time and it would be difficult to separate that effect from the effect of global warming.
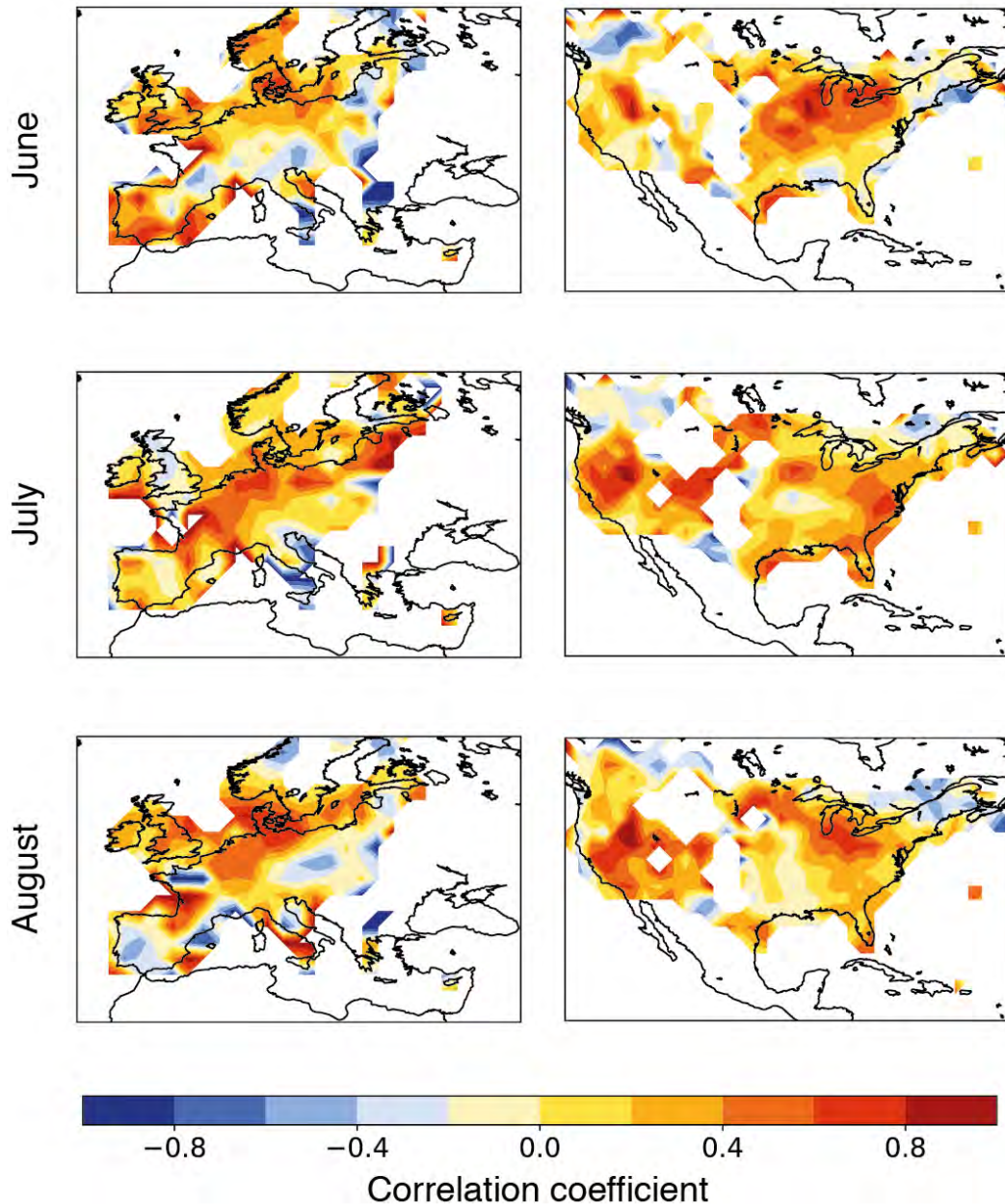
Figure 2.21: The correlation coefficient between the total number of stagnant days and mean MDA8 ozone for June, July and August 1990-2001. Stagnant days are defined by the air stagnation index (daily-mean 10 m wind speed < 3.2 ms^{-1}, daily-mean 500 mb wind speed < 13 ms^{-1}, and total daily precipitation < 1mm).
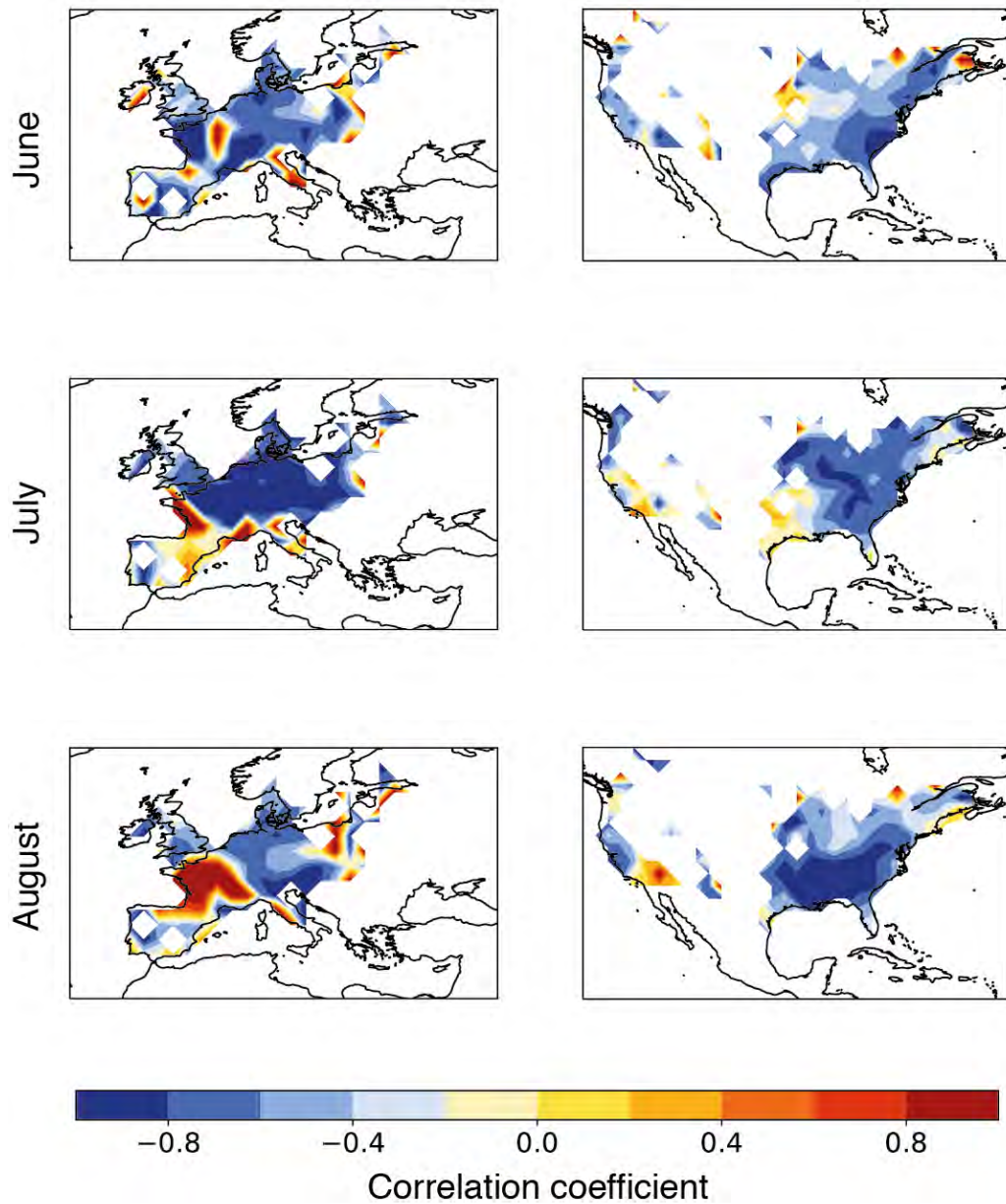
Figure 2.22: The correlation coefficient between the monthly mean total cloud cover (%) and mean MDA8 ozone for June, July and August 1990-2001.

Figure 2.23 shows that the correlation coefficient between maximum surface temperature and the number of stagnant days is above 0.8 for parts of Europe and the USA in July. This is not surprising considering that air stagnation in summer is associated with higher temperatures. Therefore, any correlation between daily

temperatures (or stagnant days) and ozone could be due to the air stagnation (or high temperatures) associated with them.
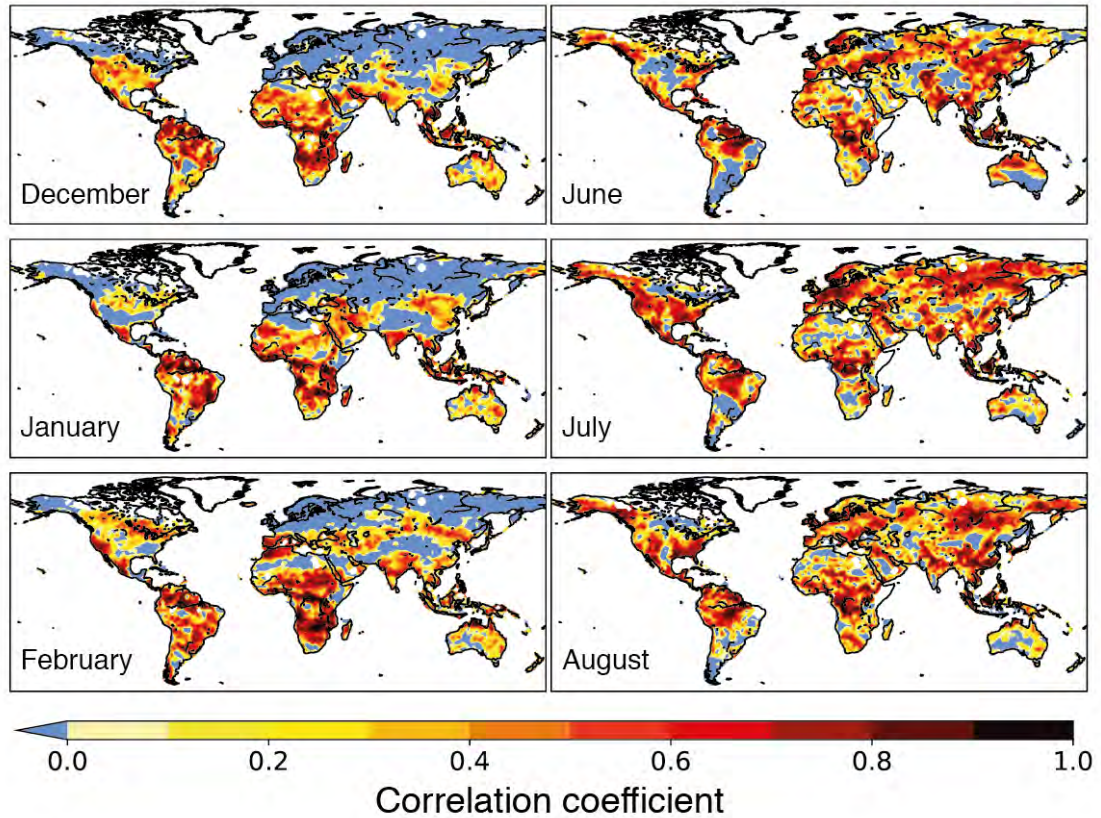
Figure 2.23: The correlation coefficient between the monthly total number of stagnant days and monthly mean daily maximum surface temperature using ERA-Interim reanalysis output. Stagnant days are defined by the air stagnation index (daily-mean 10 m wind speed < 3.2 ms^{-1}, daily-mean 500 mb wind speed < 13 ms^{-1}, and total daily precipitation < 1mm).

2.6 Discussion

There are various studies exploring the meteorological impacts of +1.5 and +2 °C climates (e.g., Barcikowska et al., 2018; Lehner et al., 2017; Wehner et al., 2018), and studies addressing the impacts of climate change on atmospheric chemistry for specific

time periods (e.g., Pommier et al., 2017; Stevenson et al., 2005; Tai et al., 2012). However, there is little research into atmospheric chemistry or air quality as a function of ΔGMST. If policymakers aim for a particular ΔGMST goal, it is necessary for them to know what impact reaching this target will have on air quality so that the appropriate air quality legislation can be applied. Research for a particular time period does not quantify the benefits of choosing a pathway towards a particular ΔGMST goal, which is important for decision makers who may find the negative effects of ambitious mitigation daunting.

Although, it is important for decision makers to have an idea of time-scale when planning adaptation efforts, the ΔGMST is projected to be 0.3-1.7 or 2.6-4.8 °C higher by the end of the century following RCP2.6 and RCP8.5 scenarios respectively, with vast differences between the impacts. So, although a +2 °C climate does differ from another +2 °C climate following a different emissions pathway, the differences in climate between two +2 °C climates at different points in time are likely smaller than a +1 °C climate and a 3.7 °C climate at a similar point in time. It also allows decision-makers to assess the most suitable ΔGMST target by assessing likely risks and achievable routes towards the target. Plus, possible impacts as a function of ΔGMST and pathways towards possible temperature targets may be more useful to communicate to the general public than explaining that climate projections for 2050 are based on four theoretical emission scenarios.

There was a positive correlation between ΔGMST and annual-mean surface ozone over Eastern USA, South Brazil, and Eastern China using ACCMIP output with constant anthropogenic precursor emissions. Stronger positive correlations may mean that these areas have the biggest ozone air quality gains from climate mitigation alone. Modelling

surface ozone in the USA, Garcia-Menendez et al. (2015) found the largest air quality benefits from climate policy were in eastern USA. They also found that the pollution-related health benefits outweighed the associated costs for the USA overall. These findings were a comparison between climates with ΔGMST of 6 °C and <1.5 °C and should be motivation for policy-makers to aim for a +1.5 °C world.

The positive correlation between ΔGMST and ozone could be linked to an increase in biogenic VOC emissions with ΔGMST. I estimated some of the highest increases in annual-mean isoprene and monoterpene emissions in these regions. Wang et al. (2013) also found an increase in annual-mean surface ozone over Eastern China between a 2000 climate and a 2050 climate, though the increase in summer-time mean was much smaller.

Using CMIP5 output, I found that annual-mean surface ozone was lower for both +1.5 °C and +2 °C climates than present-day for most of the globe using both RCP4.5 and RCP8.5 scenarios. However, using RCP8.5 surface ozone was higher for a +2°C climate for many regions, possibly showing that any anthropogenic emission reductions under the RCP8.5 scenario were not enough to stop surface ozone concentrations increasing with ΔGMST and the increase in anthropogenic methane emissions. Unlike other ozone precursor emissions, anthropogenic emissions of methane increase and decrease with the ΔGMST for RCP8.5 and RCP4.5 respectively (shown in the Appendix).

This is similar to findings comparing ozone levels in Europe for a +3 °C and a +2 °C climate: the difference was significant and a +3 °C trajectory would destroy the benefits from emission reduction policies (Fortems-Cheiney et al., 2017). Ozone was higher using the RCP8.5 scenario than the RCP4.5 scenario almost everywhere, and the difference in surface ozone between the two scenarios was generally larger than the

0.5°C difference between the two climates, demonstrating the importance of air quality policy when it comes to surface ozone levels. Other than over India, both RCP8.5 and RCP4.5 show lower surface ozone for +1.5 and +2 °C climates than present day, showing that positive outcomes of policy will not be completely reversed if climate change targets for +2 °C climate are met. This mirrors results in European summer (Watson et al., 2016).

Climate change will also impact air quality extremes as well as annual-mean ozone. I found a strong correlation (correlation coefficient above 0.8) between monthly-mean ERA-Interim daily maximum temperature and TOAR MDA ozone for a large area of mainland Europe in July and Eastern USA in August. Many areas with a larger increase in daily maximum temperature with ΔGMST (e.g., Southern Africa) did not have enough TOAR data to explore the relationship between ozone and temperature. The positive correlation over most of the USA and the estimated decrease in PAN lifetime would imply an increase in summertime surface ozone over Eastern USA. Though, Wu et al. (2008) found little change between a 2000 climate to a 2050 climate, keeping emissions constant over Eastern USA and Schnell et al. (2016) found an increase in the multi-model mean, though there was disagreement in the change in direction between models.

One limitation to the analysis using ACCMIP data was that most ACCMIP models only used a short amount of time to run their simulations to calculate the 2030 and 2100 climatology so the model ozone could depend more on climate variability than anthropogenic climate change (Barnes et al., 2016). Also, GFDL-AM3 and HadGem2 only had output for Em2000Cl2030 and Em2000Cl2100 respectively.

An issue with estimating isoprene and monoterpene emissions using CMIP5 data, was that future emissions were estimated by scaling present-day emissions, which ignores the impacts of climate change on land cover. Temperature change and the increase in the frequency in extreme events may cause shifts in vegetation cover, for example the drying of the Amazonian climate, which will impact biogenic emissions. Sanderson et al. (2003) found that disregarding land cover changes could lead to overestimating global emissions in 2090 by around 39 Tg yr^{-1} ($\sim$ 5% more). This may also mean that I am estimating the largest increases/decreases in the wrong regions.

There is a need for model experiments that consider atmospheric chemistry as a function of ΔGMST. It is not possible to assess the impacts of climate change separately to precursor emissions using CMIP5 experimental output. The half a degree additional warming, prognosis and projected impacts (HAPPI) experiment has proposed a framework for assessing regional and extreme weather changes and their impacts (Mitchell et al., 2017). There is an experiment as part of the Chemistry Climate Model Initiative (CCMI) similar to the ACCMIP climate sensitivity experiments used in this chapter (unlike ACCMIP, the output is a continuous time series), where future greenhouse gas emissions, therefore climate, is based on RCP6.0 emission scenario and emissions of ozone and aerosol precursors set to 1960 emissions (V Eyring et al., 2013; Morgenstern et al., 2017). In future work, CCMI output could be used to assess climate impacts on tropospheric ozone at various ΔGMST, but only five models run this particular simulation (Morgenstern et al., 2017). In addition, this only offers one path towards the +1.5 or +2 °C targets (RCP6.0) so it is not possible to compare differences between emission scenarios.

2.7 Conclusion

This study does not quantify results for decision-makers directly, but it is impetus for further study.

The difference in surface ozone between the RCP8.5 and RCP4.5 scenarios imply that reductions in anthropogenic precursor emissions can reduce the impact of climate change on surface ozone. There is also a strong relationship between high daily maximum temperatures and MDA8 ozone in Europe. Therefore, in the next chapter, I will explore the impact of historical air quality policy on pollution during a heatwave, as well as explore the potential of future emission reductions.

3 Avoided and potential air pollution levels and health impacts: The 2003 European heatwave as an exemplar extreme event

In this chapter, I look at air pollution, including surface ozone, during a specific period of high temperatures and dry conditions in more detail: the European heatwave in 2003. In absence of anthropogenic forcing, the extreme temperatures experienced during this heatwave would occur once every 100 years. When global mean surface temperature (GMST) is 1.5°C above pre-industrial levels (+1.5 °C world) the likelihood of a similar event in a given year would be about 59%, and in a +2 °C world the likelihood would be about 42% (Andrew D King and Karoly, 2017).

Air quality policy plays an important role in future air pollution in a warmer climate. For example, emission controls are expected to have a much greater effect on European air quality than +2 °C climate change (Lacressonnière et al., 2017; Watson et al., 2016).

3.1 Introduction

The 2003 European heatwave was period of record-breaking temperatures caused by a high pressure system over Western Europe. Over 70,000 people died prematurely in Europe during the summer heatwave of 2003 (Robine et al., 2008), driven by both extreme temperatures and the elevated air pollution levels associated with the stagnant atmospheric conditions (Dear et al., 2005; Filleul et al., 2006; Fischer et al., 2004). In

England and Wales, an estimated 21-38% of the total excess deaths in the first two weeks of August were associated with elevated levels of near-surface ozone and PM_{10} (particulate matter < 10µg diameter). By the end of this century, heatwaves over Europe are expected to increase in intensity and duration under a business-as-usual scenario (Meehl and Tebaldi, 2004), and the frequency of stagnation events are expected to increase over Mediterranean Europe (Horton et al., 2014). The abnormally high value of the summer Northern Annular Mode (NAM) index also played a part in the weather conditions during the 2003 heatwave and has shown a significant increasing trend from 1958 to 2002 (Ogi et al., 2005).

Studies have linked the meteorological conditions during the European heatwave in 2003 to elevated levels of surface ozone, a secondary pollutant produced by photochemical reactions involving nitrogen oxides (NO and NO_2, together known as NO_x), carbon monoxide and volatile organic compounds (VOCs). Ozone has a negative health effect on humans and plants (Francis et al., 2011; Landrigan et al., 2018; Monks et al., 2015; Solberg et al., 2008; World Health Organization, 2013). Solberg *et al.*, (2008) found that the feedback between increased temperature and photochemical formation was a significant contributor to ozone in August 2003: a 10 °C increase in temperature led to a 5% increase in peak ozone. The 2003 heatwave had clear skies associated with the stagnant high-pressure system (Francis et al., 2011), affecting ozone formation. The higher temperatures drove higher emissions of the reactive biogenic VOC isoprene (Lee et al., 2006), an ozone precursor. Drought conditions during the heatwave will have caused plants to close their stomata to reduce water loss, reducing the dry deposition ozone sink (Vieno et al., 2010).

Stagnant air conditions also bring low wind speeds and lack of precipitation, meaning that pollutants build up as they are not dispersed or washed away (Jacob and Winner, 2009). Particulate matter (PM) describes a range of pollutants that are also of concern for human health (Cohen et al., 2017; Davidson et al., 2005). PM is described as primary (directly emitted) or secondary (arising from the chemistry of gas phase precursors) and is derived from biogenic and anthropogenic sources. PM is typically classified according to size for regulatory purposes: $PM_{2.5}$ and PM_{10}, where the number denotes the upper limit of the particles' aerodynamic diameter in μm, and ultra-fine particles, which have a diameter less than or equal to 100 nm. Due to the diversity of PM sources, formation, and components, there is typically a weaker relationship between meteorological components and PM concentrations than ozone concentrations (Wise, 2009). Concentrations of PM were elevated during the 2003 heatwave due to the accumulation of particles, chemical formation of secondary organic aerosols, and wildfire emissions (Hodzic et al., 2007).

Such extreme events present a challenge for policy efforts to limit poor air quality, and if pollutant emissions do not change then increases in the frequency and duration of these events could result in more days where air pollution exceeds health limits (the so-called "climate penalty" (Jacob and Winner, 2009)). In this chapter, I propose that historical extreme events provide an excellent test for the effectiveness of air quality policies on the air pollution levels they seek to control. Such events are both a putative "worst case scenario" (the 2003 heatwave was one of the strongest in Europe since 1950 (Russo et al., 2010)) as well as being grounded in lived experience (Hazeleger et al., 2015), unlike using a range of climate model projections.

This sort of approach has been recently used to evaluate and test flood risk management in the UK, using the extreme rainfall from Storm Desmond in December 2015 (Hankin et al., 2017). Vautard et al. (2005) looked at what impact theoretical emergency emission scenarios and planned 2010 emission reductions would have had on surface ozone during the 2003 heatwave. For this study, I used a set of chemistry climate model (CCM) simulations to explore the European air quality levels in the meteorological background of the 2003 European heatwave. I estimated the beneficial impact of air quality policy introduced between 1970 and 2003 by simulating a "world avoided" (pollution without air policy) as well as a base case scenario using 2003 emissions. I also considered two alternative future pollution emission scenarios (using RCP2.6 and RCP8.5 pollutant emissions).

Increases in population, urbanisation and economic activity have driven increases in pollutant concentrations over Europe since the industrial revolution. However, the increases have been mitigated by various policies and changes in the emission factor, which is the average emission rate associated with a given source, relative to units of activity (e.g., there are more cars, but less NO_x emissions per car (Vestreng et al., 2009)). The UK's 1956 Clean Air Act was enacted in response to the "Great Smog of London" in December 1952, which lasted four days and was estimated to have caused 4,000 excess deaths (Jacobson, 2002). Subsequent major policy initiatives were at the international scale, including the first European air quality directive in 1970 (Crippa et al., 2016; Jacobson, 2002) and the 1979 United Nations Convention on Long-Range Transboundary Air Pollution (United Nations Economic Comission for Europe, 1979), covering sulphur dioxide, NO_x, CO and soot (black carbon). Without these and subsequent policies in place, it could be expected that the air pollution during the 2003 heatwave would have been much worse. Indeed, the fact that ozone levels did not reach

extreme values everywhere has been linked to emission decreases through modelling experiments (Vautard et al., 2007, 2005), and that the pollution levels would have been further mitigated if 2010 European legislation had been in place at the time.

Previous studies have explored the long-term consequences of an absence of political action or technological advances on air quality (Archibald et al., 2017; Crippa et al., 2016; Daskalakis et al., 2016; Turnock et al., 2016). Emissions are usually estimated by taking emissions from before policy changes and technological advances and scaling them by human population or activity data (data on the magnitude of a human activity resulting in emissions - e.g., fuel consumption - during a particular time period), These emissions scenarios are sometimes referred to as "world avoided" scenarios. These studies have focussed on long-term impacts of a world avoided scenario, rather than extreme events. Turnock et al. (2016) used 2010 activity data and 1970 emission factors to simulate 2010 European air quality without technological advancements and found that around 80,000 premature deaths were prevented by air quality mitigation measures. Daskalakis et al. (2016) found that the benefit of air quality legislation was clearer when taking the poulation increase into account, rather than just comparing total 1980 and 2010 emission scenarios. Archibald et al. (2017) found that around 519,000 premature mortalities were avoided in 2010 over Europe and USA due to reduced levels of sulphate, ozone, and nitrogen dioxide since 1970 due to technological advances and legislation. Heatwaves are associated with higher levels of air pollutants, so the air quality benefit of these policies should be explored for such extreme events. Moreover, as heatwaves and stagnation events are expected to increase in the future with continued climate change (Beniston, 2004; Christidis et al., 2015), air quality episodes like those in 2003 may also increase. Episodes such as these therefore provide important

benchmarks to test the effectiveness and robustness of planned or potential air quality policies.

In this study, I used the exemplar event of the 2003 heatwave to investigate the air quality for a world avoided scenario as well as future emission scenarios. For the world avoided, I assume that 1970 represents the time before the majority of present-day air quality legislation was introduced, and therefore used estimates of 1970 emissions as the base. To arrive at estimates of 2003 emissions, I scaled up the 1970 emissions with 2003 population, as previous "world avoided" studies (Archibald et al., 2017; Daskalakis et al., 2016), as well as scaling them up with both population and GDP simultaneously, based on the Kaya Identity (Kaya, 1990). For future emission scenarios, I assess the robustness of air pollutant emission reductions using unscaled 2030 emissions and the 2003 heatwave meteorological conditions. Future air quality pollutant emissions are taken from the Representative Concentration Pathways (RCPs), using the aggressive mitigation (RCP2.6 (van Vuuren et al., 2011)) and the "business-as-usual" (RCP8.5 (Riahi et al., 2011)) scenarios. While RCP8.5 scenario is a high greenhouse gas emission scenario, it includes mitigation of air quality pollutant emissions (Lamarque et al., 2011). Both RCP2.6 and RCP8.5 have reduced emissions of air quality pollutants compared to the present-day for Europe, though reduced to different levels and with different spatial distributions. Therefore, I evaluate whether these scenarios are enough to avoid bad air quality during extreme events like the one in 2003 (but with a 2030 population and economy) and the difference between the two scenarios for extremes in Europe. The simulations were conducted with global chemistry-climate models (CCMs), which, while they have comparatively low spatial resolution when compared against regional models, have been demonstrated to capture large-scale air

quality extremes well (Schnell et al., 2014). Stock, Russo and Pyle (2014) found that average ozone production efficiency (net number of ozone molecules produced per number of molecules of NO_x lost) in July over Europe was only ~1% higher using the coarse resolution (~150 km) model than the fine resolution (~40 km) model. Unfortunately, the model resolution means that ozone extremes in urban centres are not estimated, which will affect health impact estimations.

3.2 Methods

3.2.1 Models and emissions

I used two different global CCMs to simulate pollution levels over Europe: The Geophysical Fluid Dynamics Laboratory atmospheric model 3 (GFDL-AM3) and the Community Atmosphere Model with Chemistry (CAMChem). Both models had meteorological conditions nudged with reanalyses in order to replicate 2003 conditions. Global-scale models were used due to availability of tools.

GFDL-AM3 is a CCM with a horizontal resolution of 1° x 1° (~ 111 km x 71 km at 50°N) and 48 vertical levels, extending to 0.01 hPa (Donner et al., 2011; Naik et al., 2013). The model was run from 2001 to 2004 and nudged to reanalysis winds from NCEP (Kalnay et al., 1996). This version of the GFDL-AM3 has been modified from the one used for the Atmospheric Chemistry Model Intercomparison Project (ACCMIP) (Lamarque et al., 2013) to include interactive isoprene emissions and the FAST-J scheme for calculation of photolysis rates (Wild et al., 2000). Reaction rates follow those recommended by Sander et al. (2006) and the formation of sulphate aerosol via oxidation of sulphur dioxide and dimethyl sulphide is fully coupled with gas-phase

chemistry. Interannual variability in ozone deposition velocity is not considered, which could underestimate the reduction in ozone deposition due to drought stress.

CAMChem (Tilmes et al., 2016) is a configuration of the Community Earth System Model (CESM1) (Kay et al., 2015), and has a horizontal resolution of 1.9° latitude x 2.5° longitude (~ 208 km x 178 km at 50°N) and 56 vertical levels, extending to 3 hPa. The model was run from January 2003, performing the simulations using specified dynamics and nudging to analysed air temperatures, winds, surface fluxes and surface pressure from the Modern-Era Retrospective Analysis for Research and Applications (MERRA) reanalysis product (http://gmao.gsfc.nasa.gov/merra/) (Rienecker et al., 2011). Many chemistry-specific parameterizations in the model are based on those in MOZART-4 (Emmons et al., 2009). This model has the advantage of being coupled to a land surface model, so it can simulate the impact of heatwaves on stomatal conductance and, therefore, ozone deposition.

For both CCMs, present-day surface anthropogenic emissions were provided by MACCity (http://ether.ipsl.jussieu.fr/eccad) (Granier et al., 2011) and future emissions were from RCP2.6 (van Vuuren et al., 2011) and RCP8.5 (Riahi et al., 2011). All biogenic, biomass burning, and aircraft emissions remain at 2003 levels, with methane concentrations held fixed at 2003 levels (1755 ppb) to avoid long model spin up times; these were also from the MACCity dataset. Although, ozone formation is strongly affected by biomass emissions, we are focussing on changes in air quality policy rather than land use changes, so they stay constant. In addition, anthropogenic emissions were only changed from the base 2003 levels for Europe (35-81°N, 26°W-40°E) and North America (15°N–55°N, 60–125°W), and between them over the North Atlantic (35°-60°N, 26-60°W) with 2003 emissions outside these regions for every simulation. This

is because of the focus on impacts during a European heatwave and North American emissions have a strong influence on European surface ozone levels using chemical transport models (Fiore et al., 2009).

Table 3.1: Matrix of experiments carried out, showing which emissions scenario was used and if it was scaled by 2003 population and GDP

Experiment	Base emissions	Population	GDP
Control	2003	2003	2003
1970	1970	1970	1970
Em70Pop03	1970	2003	1970
Em70GDP03	1970	2003	2003
RCP2.6	2030 (RCP2.6)	2030 (RCP2.6)	2030 (RCP2.6)
RCP8.5	2030 (RCP8.5)	2030 (RCP8.5)	2030 (RCP8.5)

There were six simulations in total (see Table 3.1), including a control run using 2003 emissions and 2003 meteorology. There were three world avoided emission scenarios, which were based on 1970 emissions: 1) where the 1970 emissions were not scaled, 2) where emissions were scaled with population (i.e., 1970 emissions x 2003 population / 1970 population; hereafter referred to as Em70Pop03), and 3) where the emissions were scaled with population and GDP (in constant 2010 US $; Em70GDP03). Population data for the scaling was provided on a 1° x 1° grid from the History Database of the Global Environment (HYDE) version 3.1 (Klein Goldewijk et al., 2011, 2010), and country-level GDP data were from the World Bank (The World Bank, 2014). To take

into account changes in shipping emissions, they were scaled by total goods unloaded annually at seaports (UNCTADstat, n.d.) for both world avoided scenarios. The emissions were interpolated onto the same grid as the population data, scaled and then interpolated to the appropriate model grid. The scaling for the Em70GDP03 scenario was based on the Kaya identity (Kaya, 1990):

$$E_{2003} = E_{1970} \times \frac{P_{2003}}{P_{1970}} \times \frac{G_{2003}}{G_{1970}}, \tag{3.1}$$

Where E, P, and G are the gridded emissions, gridded population and country-level GDP respectively. Emissions in each grid square was scaled by the population in that grid square and the GDP of the relevant country by using country masks.

Table 3.2: Newly Industrialised Countries' CO_2 emissions per capita and for 1970 and 2003 using data from The World Bank (accessed 21-02-2019). The first column shows CO_2 emissions per capita for 1970, the second shows estimated CO_2 emissions per capita for 2003 by scaling 1970 emissions by GDP, and actual CO_2 emissions per capita in 2003.

Country	1970 CO_2 emissions (metric tonnes per capita)	Scaled by 2003 GDP (estimated metric tonnes per capita)	2003 CO_2 emissions (metric tonnes per capita)
Brazil	0.98	3.51	1.76
China	0.94	13.31	3.52
India	0.35	1.51	0.99
South Africa	6.56	13.54	8.49

To see if this method for estimating emissions was realistic, I assumed other anthropogenic emissions would scale similarly to CO_2 emissions, so I scaled CO_2 emissions per capita and GDP data from newly industrialised countries to see if emissions scaled with GDP between 1970 and 2003. Table 3.2 shows that using 3.1 likely resulted in an overestimation of what emissions would be like without policy in place. On the other hand, emissions per capita increased from 1970 to 2003 so assuming emissions would just simply scale with population would be optimistic.

To evaluate the benefits of future emission scenarios, I used anthropogenic (including shipping) emission projections for RCP2.6 and RCP8.5 for the year 2030. These emissions were not scaled as the emission projections include societal, technological, and behavioural changes, meaning that the population and GDP were both at their projected 2030 levels, with the simulations being as if the 2003 heatwave was occurring with a future population, economy, and policy.

Figure 3.1 compares the total global anthropogenic emissions for the six scenarios using CAMChem. Replacing 2003 emissions by 1970 emissions in the previously defined regions results in lower CO, NO, and NMVOC emissions, though SO_2 emissions became slightly higher so reductions in SO_2 emissions per capita since 1970 have mitigated increases in population since then. For scenarios Em70Pop03 and Em70GDP03 the total global emissions were higher for all species, with GDP making a larger contribution than population to the total emissions. Although, Em70GDP03 is a particularly pessimistic scenario and I would expect 2003 emissions in absence of policy changes would lie in between scenarios Em70Pop03 and Em70GDP03. Future anthropogenic pollutant emissions were reduced for both scenarios compared to the control scenario, and RCP2.6 and RCP8.5 gave similar results. Yet this similarity may

not have been the case if I changed emissions to 2030 emissions globally since RCP8.5 assumes much more modest air quality controls in low income regions (Riahi et al., 2011).
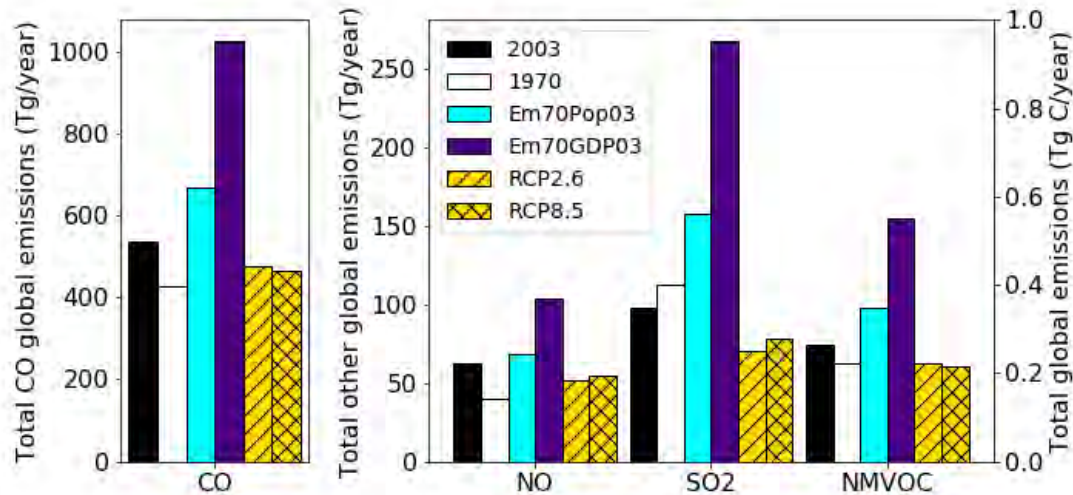
Figure 3.1: Total global anthropogenic emissions for the CAMChem model for 2003 (black); the three "world avoided" scenarios: 1970 emissions (white), 1970 emissions scaled by population (Em70Pop03; cyan), and 1970 emissions scaled by GDP and population (Em70Pop03; violet); and 2030 emission scenarios: "business-as-usual" RCP8.5 scenario (gold hatched) and aggressive mitigation RCP2.6 scenario (gold cross hatched). Emissions outside of Europe, North America, and the North Atlantic Ocean remain at 2003 levels for all experiments.

3.2.2 Estimating excess mortality risk

To give some health context to the simulations, the results were analysed using estimates of the short-term impacts of elevated ozone and $PM_{2.5}$ on human mortality. Estimates of the daily premature mortality E related to ozone or $PM_{2.5}$ for each grid cell were calculated following Ostro et al. (2004)

$$E = y_0 \times AF \times P, \qquad (3.2)$$

where y_0 is the baseline mortality rate at country level, from the World Bank (The World Bank Group, n.d.); P is the gridded population, using the same data as employed for the scaling; and AF is the fraction of deaths attributable to the pollutant concentration, given by (RR – 1) / RR, and where RR is the relative risk for that particular grid square. As relationship between relative risk of mortality and ozone or PM$_{2.5}$ is approximately linear (WHO, 2013a), RR is given by:

$$1 + \beta(x - x_0), \tag{3.3}$$

where the β coefficient depends on pollutant and is the increase in excess mortality with pollutant concentration (see below), x is the concentration of the pollutant, and x_0 is the threshold at which there was no ill effect to human health. For both pollutants, x_0 is set equal to zero because there is little evidence for a minimum concentration that is healthy for humans for either pollutant (Bell et al., 2006; WHO, 2013a). However, I do not assess mortality-risk attributable to ozone concentrations below 20 µg/m^3 (~10 ppb) as recommended by WHO (WHO, 2013a). For ozone, a β value of 0.0029 (95% confidence interval = 0.0014–0.0043) per 10 µg/m^3 was used, and a β value of 0.0123 (95% CI = 0.0045–0.0201) per 10 µg/m^3 was used for PM$_{2.5}$ (WHO, 2013a). The 95% confidence intervals were used in calculating the uncertainty of the mortality risk: the maximum mortality estimation was calculated using the maximum estimated value of ozone (the highest model value after bias correction) and the upper β value in the brackets and the lowest estimation for mortality was calculated using the lower value of ozone and β. It is unlikely that total excess deaths would equal the sum of PM$_{2.5}$- and ozone-attributed premature deaths, so I report excess mortality risk separately for ozone and PM$_{2.5}$ to avoid double-counting mortality. Excess mortality risk per 100,000 people

is calculated for each country and for Europe by dividing the total number of excess deaths by the total population and multiplying the result by 100,000.

For the control and world avoided simulations, mortality risk due to these two components was determined using the 2003 population. For the baseline mortality rate, the average death rate for years 2000, 2001, 2002, 2004, and 2005 was used, using yearly data provided by the World Bank (The World Bank Group, n.d.) and divided by 365 days. The results for an individual country's mortality were normalised per capita, by dividing by the total population for that country (calculated by summing up grid cells included in the country mask). In addition to projecting mortality risk in several countries, I calculated total mortality (mortality risk × population) for 12 European countries (Belgium, Switzerland, Germany, Spain, France, Croatia, Italy, Luxemburg, Netherlands, Portugal, Slovenia, Great Britain) which all experienced a mortality crisis between 3 and 16 August in 2003 (Robine et al., 2008), and were large enough to fill a grid cell for at least one model.

Mortality risk was also calculated for the 2030 RCP2.6 and RCP8.5 scenarios. Projected death rates for the European region in 2030 were from WHO estimates (WHO, 2013b) (9.58 per 1000 population) and the same value was used for both scenarios. Gridded population for 2020 (Center for International Earth Science Information Network - CIESIN - Columbia University, 2016) was used because there are no global gridded population data for 2030. To calculate the total mortality risk for the 12 European countries, I scaled the gridded 2020 population by country-level population projections for 2030 using the B2 and A2r scenarios (International Institute for Applied System Analysis (IIASA), 2009) for RCP2.6 and RCP8.5 respectively, implicitly assuming the same population distribution between 2020 and 2030.

3.3 Evaluating the models

I compared the control scenario for both models to European Monitoring and Evaluation Programme (EMEP) observations of ozone and $PM_{2.5}$ (Tørseth et al., 2012) to evaluate how well the models performed in terms of capturing the magnitude and variability of the pollutant levels during the 2003 heatwave. Each grid cell from the model's base 2003 simulation was compared to the average values for all EMEP stations in that grid cell. Stations with a higher altitude than 3 km above sea level were not considered and the German station DE0008R was removed as it is close to a main road. In total, there are 130 EMEP sites suitable for the ozone evaluation, 21 sites for $PM_{2.5}$ and 27 sites for NO_2. The comparison is presented for the first two weeks of August, when the heatwave took place.

Figure 3.2 presents scatter plots showing the relationship between simulated and observed maximum daily 8-hour mean (MDA8) ozone concentrations, daily mean $PM_{2.5}$ and daily mean NO_2, for all stations and averaged over the heatwave period. For ozone and NO_2, the model results were converted from volume mixing ratio to $\mu g/m^3$ using the simulated surface temperature and pressure. For the two-week period CAMChem generally underestimates $PM_{2.5}$ and GFDL-AM3 generally overestimates NO_2. Table 3.3 shows information about the correlation using all station measurements over the two-week period between simulated and observed MDA8 ozone, $PM_{2.5}$ and NO_2. The relationship between model results and observations is significant for all species according to the p-value, which is much lower than 0.01. For both models, the standard error is higher and the correlation coefficient lower for $PM_{2.5}$ than ozone so the models generally do a better job of simulating ozone than $PM_{2.5}$ during the heatwave, with models generally underestimating $PM_{2.5}$.
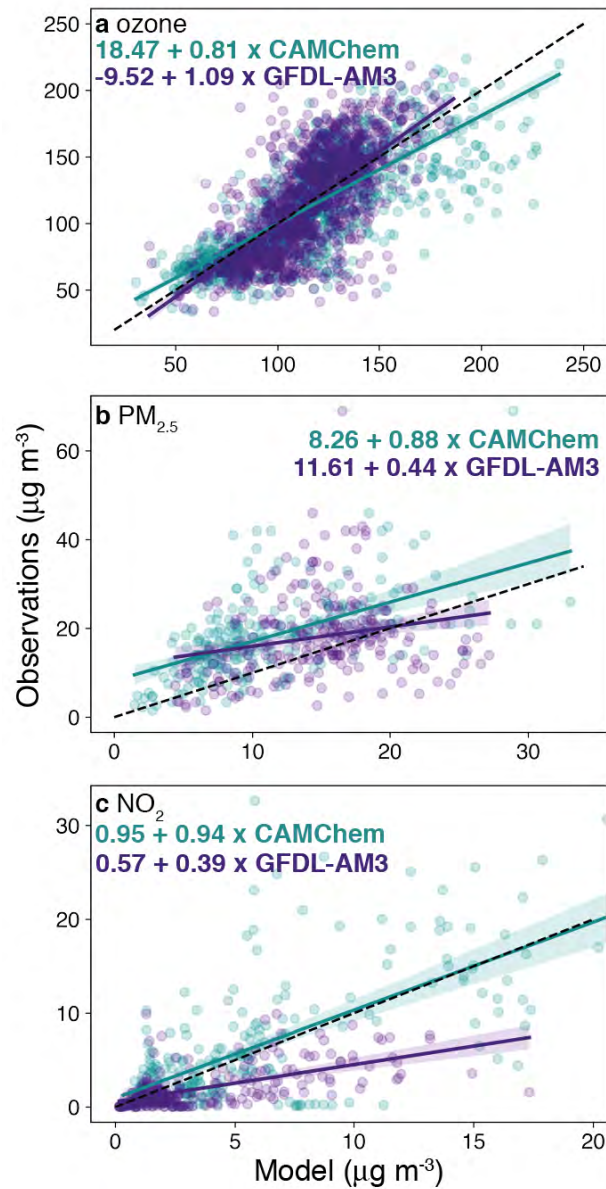
Figure 3.2: Average model grid cell results versus average of all measurement sites' observations in that grid cell during the first fortnight of August for (a) MDA8 ozone, (b) daily mean PM2.5, (c) daily mean NO2. The dashed black line shows where the data would be if the model results were equal to observations. The teal (purple) dashed line shows the linear regression relationship between the CAMChem (GFDL) model and the observations. The intercept and the slope of the lines are written in the bottom-right corner. Confidence interval (95th percentile) shown in lighter shade around the line of best fit.

Table 3.3: Information about the linear regression line of best fit between observation and model data for 1 – 14 August 2003.

Model	CAMChem			GFDL-AM3		
Species	O_3	$PM_{2.5}$	NO_2	O_3	$PM_{2.5}$	NO_2
R value	0.75	0.57	0.66	0.69	0.23	0.60
P value	<0.01	<0.01	<0.01	<0.01	<0.01	<0.01
Standard error ($\mu g/m^3$)	0.02	0.08	0.07	0.03	0.12	0.03

Ozone is mainly underestimated in Switzerland by both models, in Spain and Germany by GFDL-AM3, and in Austria by CAMChem. Similarly, $PM_{2.5}$ is underestimated in Spain and Germany by both models. Underestimation of primary particulates in coarse resolution models could be due to the dilution of peak concentrations. Although the regression between observations and GFDL-AM3 has a low correlation coefficient, I will still use the model because using country averages some values are closer to observations than CAMChem (e.g., Switzerland and Germany).

3.4 Results

3.4.1 Air quality in a World Avoided

Figure 3.3 and Figure 3.4 show model results for the average and maximum MDA8 ozone concentrations respectively during the two-week period for the control scenario and the Em70Pop03 scenario. Both the maximum and average values of MDA8 ozone for the two week period were above WHO air quality guidelines (100 mg/m^3; ~ 51 ppb) (World Health Organization, 2006) for large parts of Europe for both scenarios. CAMChem shows higher fortnight-average concentrations of ozone than GFDL-AM3 for most of Western Europe. Ozone levels are higher for the Em70Pop03 scenario for most of France, with mean MDA8 ozone up to 8% higher.

There is a notable decrease over the UK for both models, with average MDA8 ozone values over 10% and 20% less in some parts of the UK using CAMChem and GFDL-AM3 respectively. This decrease is attributable to ozone titration, as the UK NO_x/VOC ratio was higher for the control scenario than Em70Pop03, whereas the NO_x/VOC ratio remained similar with changes in policy for other regions (see Figure B.1 in the Appendix). As discussed in Section 1.2, a high NO_x/VOC ratio can lead to net destruction of ozone due to higher levels of loss of ozone via reaction with nitrogen oxide. Increases in ozone pollution have been attributed to reductions in emissions of NO_x in previous studies (e.g., Heal et al. (2013), Sicard et al. (2013)). There were decreases in ozone for the Em70Pop03 elsewhere in Europe, (e.g., GFDL-AM3 showed maximum ozone concentrations about 3% lower in Spain), but changes were not as substantial over the UK.
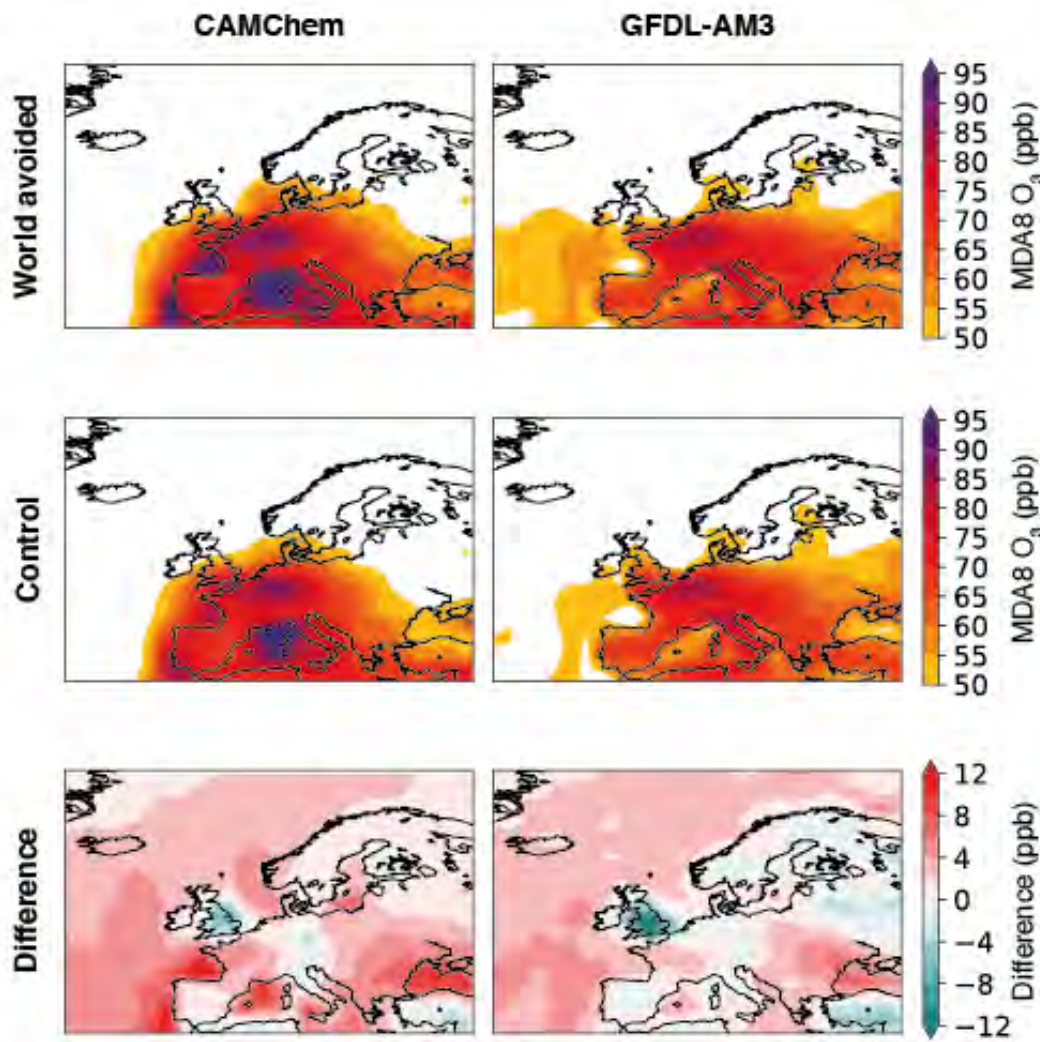
Figure 3.3: The two-week average MDA8 ozone concentration for Em70Pop03 (top) and the control (middle) scenario, and the difference between the two scenarios (bottom). CAMChem results are on the left, GFDL-AM3 are on the right. Note that ozone mixing ratio units are in ppb, and that the European air quality standard for MDA8 ozone of 120 µg/m³ (European Commission, 2018) is ~61 ppb.
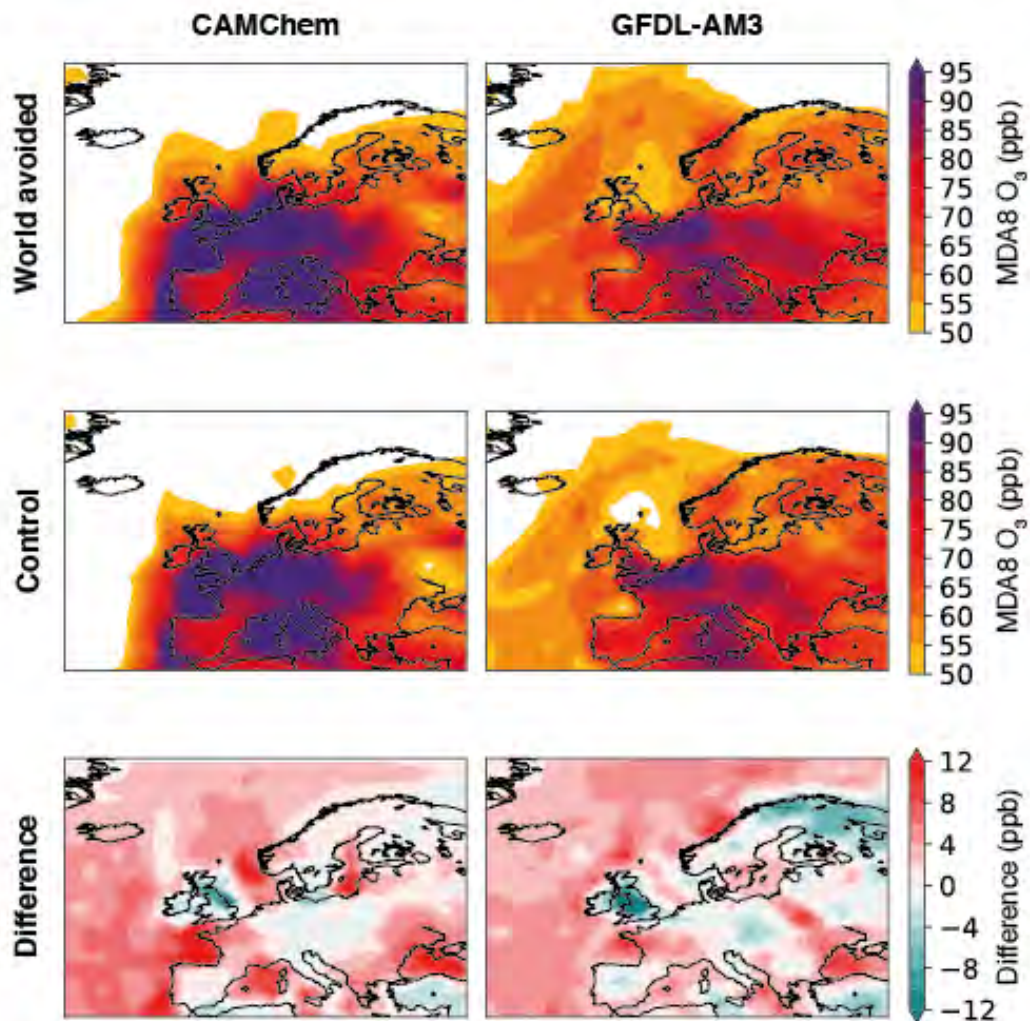
Figure 3.4: The two-week maximum MDA8 ozone concentration for Em70Pop03 (top) and the control (middle) scenario, and the difference between the two scenarios (bottom). CAMChem results are on the left, GFDL-AM3 are on the right.

Figure 3.5 shows the model results for the average daily mean PM$_{2.5}$ for the heatwave period. The Em70Pop03 scenario shows PM$_{2.5}$ levels more than 30 µg/m^3 higher than the control scenario for some regions. Average PM$_{2.5}$ during this period was below the WHO guideline of 25 µg/m^3 (World Health Organization, 2006) for most of Europe for the control scenario. Average PM$_{2.5}$ using Em70Pop03 was more than 50% more than the control scenario for most of Western Europe.
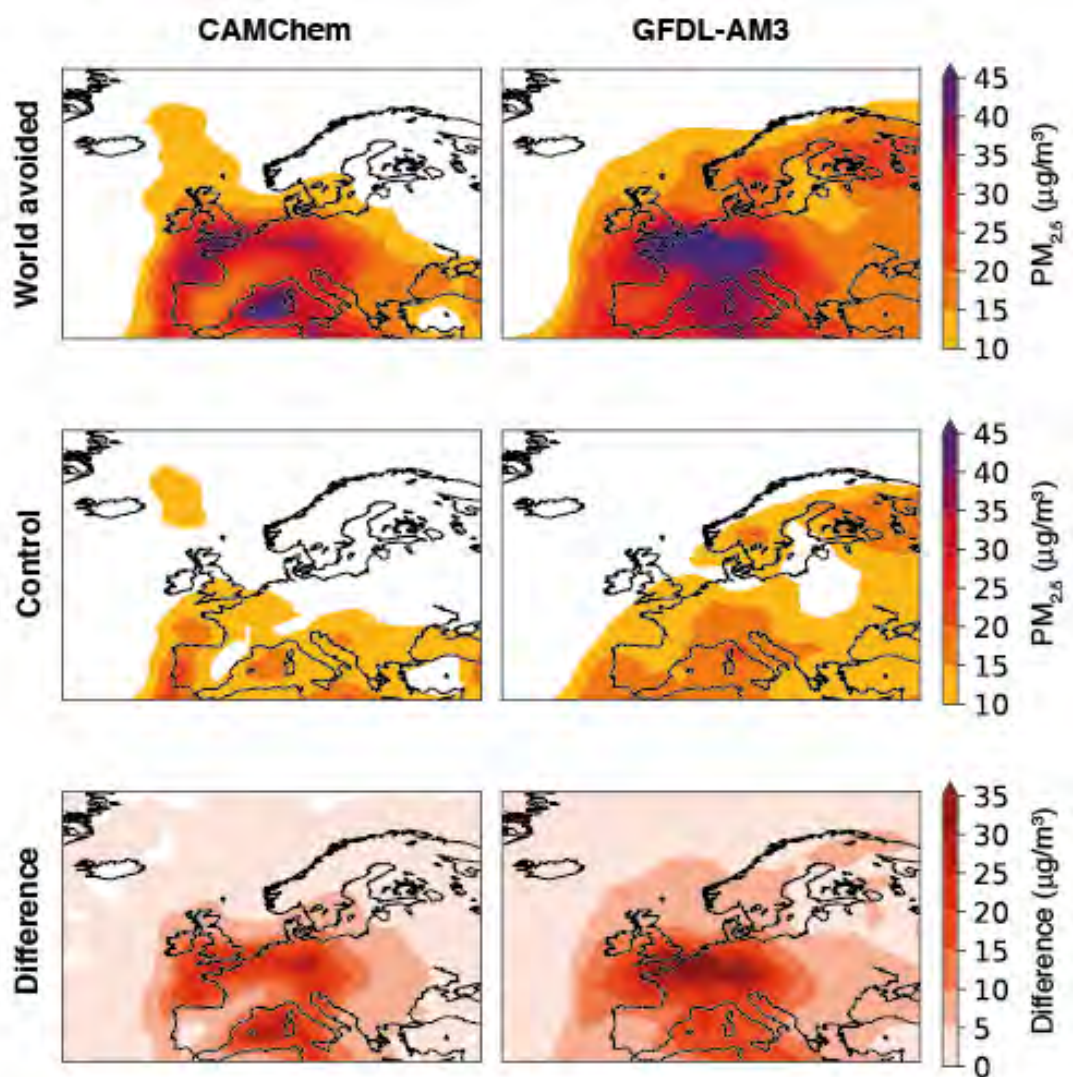
Figure 3.5: The two-week average PM$_{2.5}$ concentration for Em70Pop03 (top) and the control (middle) scenario, and the difference between the two scenarios (bottom). CAMChem results are on the left, GFDL-AM3 are on the right.

Figure 3.6 shows the model results for maximum daily mean PM$_{2.5}$ over the two-week period. For large parts of Europe, PM$_{2.5}$ stayed below WHO guidelines for the control scenario. Although, both models generally underestimated PM$_{2.5}$ for this period so it is possible PM$_{2.5}$ exceeded the guidelines in more regions in reality. Scenario Em70Pop03 shows increases over 40 μg/m^3 compared to the control scenario for large areas of Europe. GFDL-AM3 shows a larger difference between scenarios for the majority of

Western Europe. PM$_{2.5}$ concentrations for Em70Pop03 are more than double that for the control scenario over most of Western Europe using both models. Although, there is less than 50% change over most of the Iberian Peninsula using CAMChem.
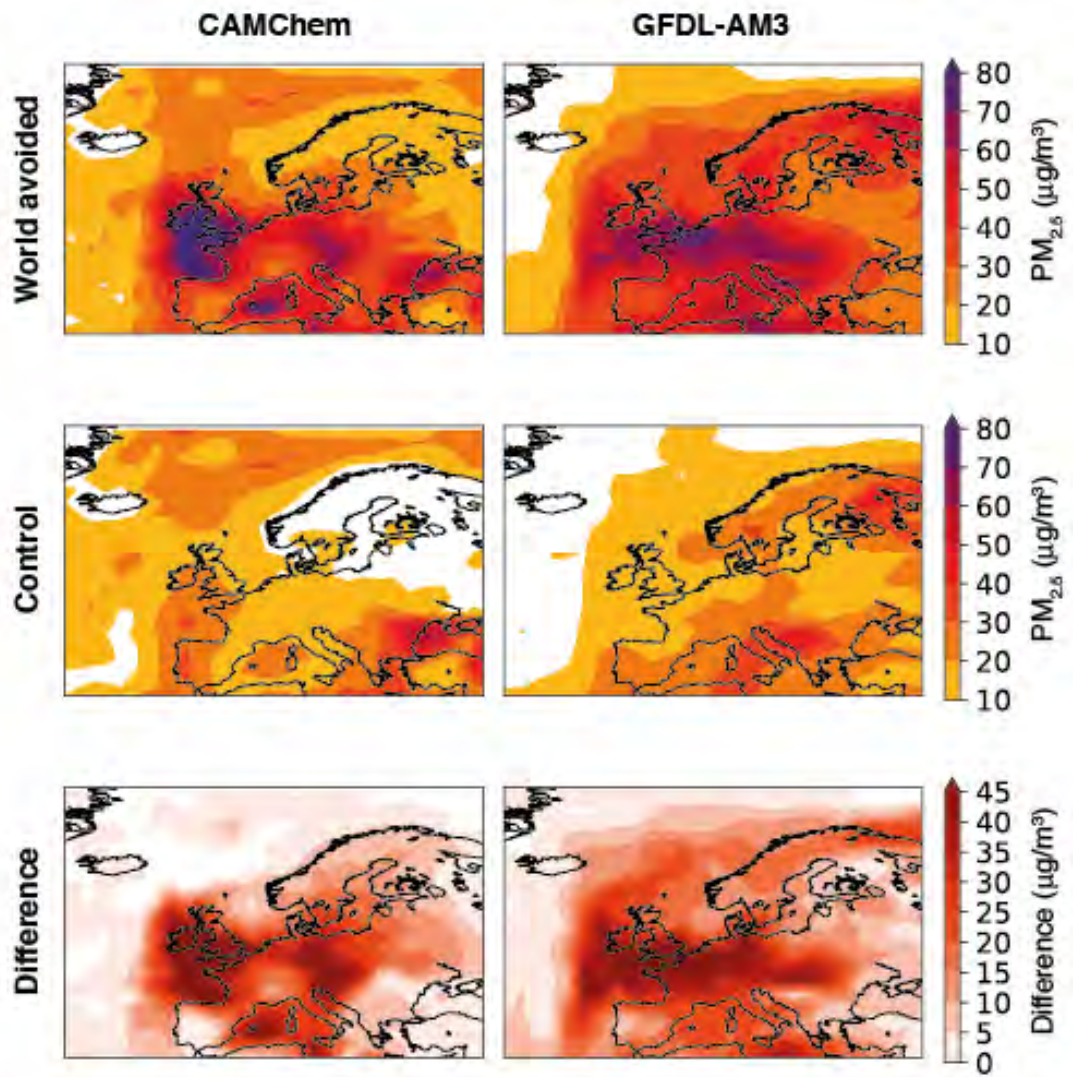
Figure 3.6: The two-week maximum daily mean PM$_{2.5}$ concentration for Em70Pop03 (top) and the control (middle) scenario, and the difference between the two scenarios (bottom). CAMChem results are on the left, GFDL-AM3 are on the right.

Hourly mean NO$_2$ concentrations stayed below 60 ppb for the Em70Pop03 scenario in both models during the two-week period (not shown). This is below the EU guidelines

for hourly mean NO_2 concentration (200 µg/m^3, ~105 ppb), so I limit my discussion to ozone and $PM_{2.5}$ pollution and their health effects.

3.4.2 Air quality using future emission scenarios

Figure 3.7 shows the average MDA8 ozone over the two-week period for the RCP2.6 scenario and the change from the control scenario for both RCP scenarios for both models. Most of Western Europe still exceeds WHO guidelines using the 2030 RCP2.6 emissions scenario. However, compared to the control simulation, there is up to an 8 ppb reduction in average ozone (up to 12% lower ozone) for most of Europe using CAMChem and there is more than a 9 ppb (up to 18%) reduction according to GFDL-AM3. There are similar decreases over Western Europe using RCP8.5, although small increases over parts of Eastern Europe and Russia using CAMChem, reflecting the higher NO and CO emissions in those regions under a business-as-usual scenario.

Figure 3.8 shows the maximum MDA8 ozone concentration and the difference in peak concentrations between RCP scenarios and the control scenario. Maximum MDA8 ozone is lower using both RCP scenarios for the majority of Europe, with some regions seeing a decrease of more than 16 ppb. In contrast to Figure 3.3 and Figure 3.4, the UK sees a reduction in ozone pollution with lower NO_x emissions.
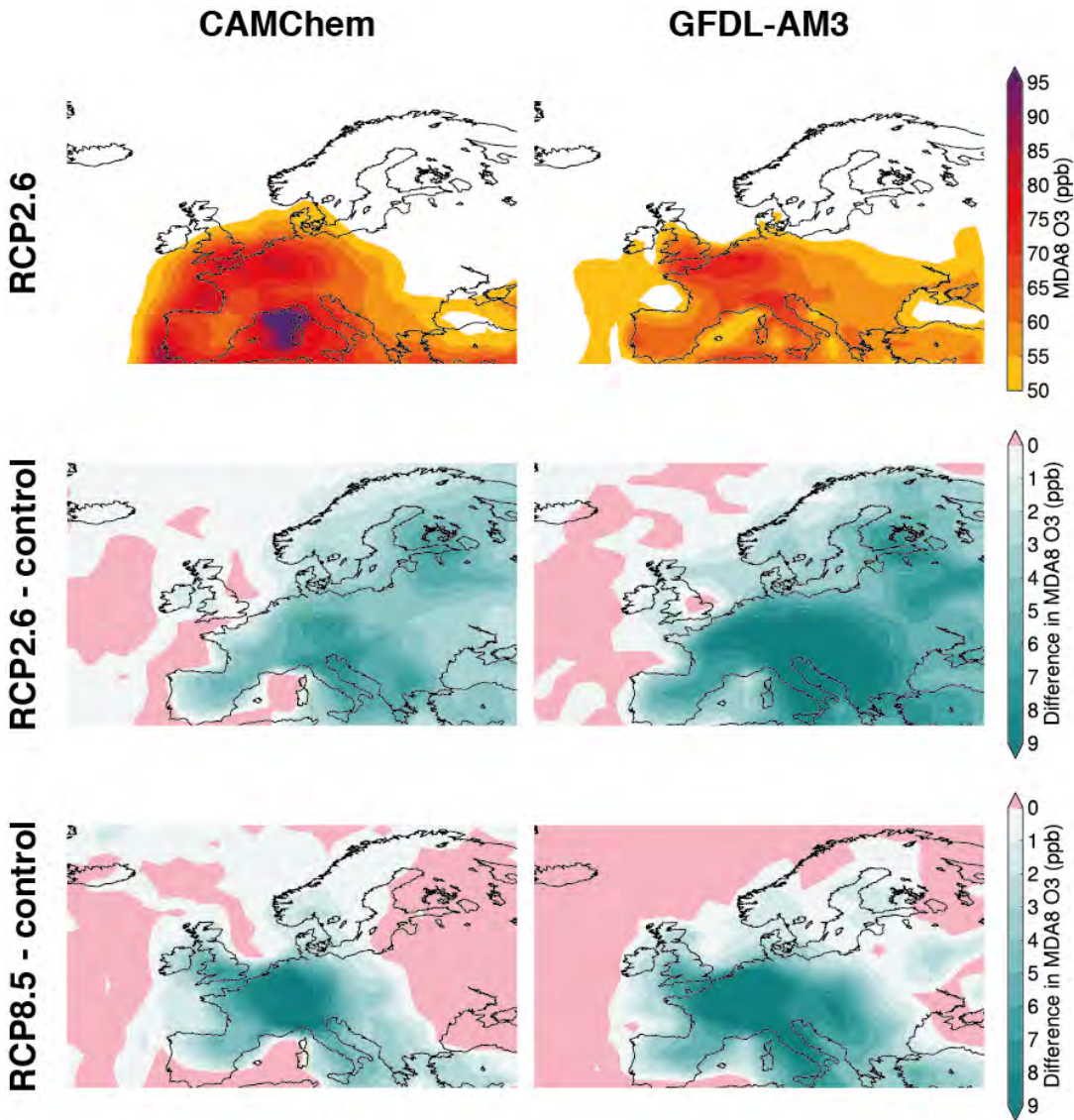
Figure 3.7: Top plot shows the two-week average MDA8 ozone using 2030 emissions from RCP2.6, the middle shows the difference between the RCP2.6 and the control scenario, and the bottom plot shows the difference between the RCP8.5 and the control scenario.
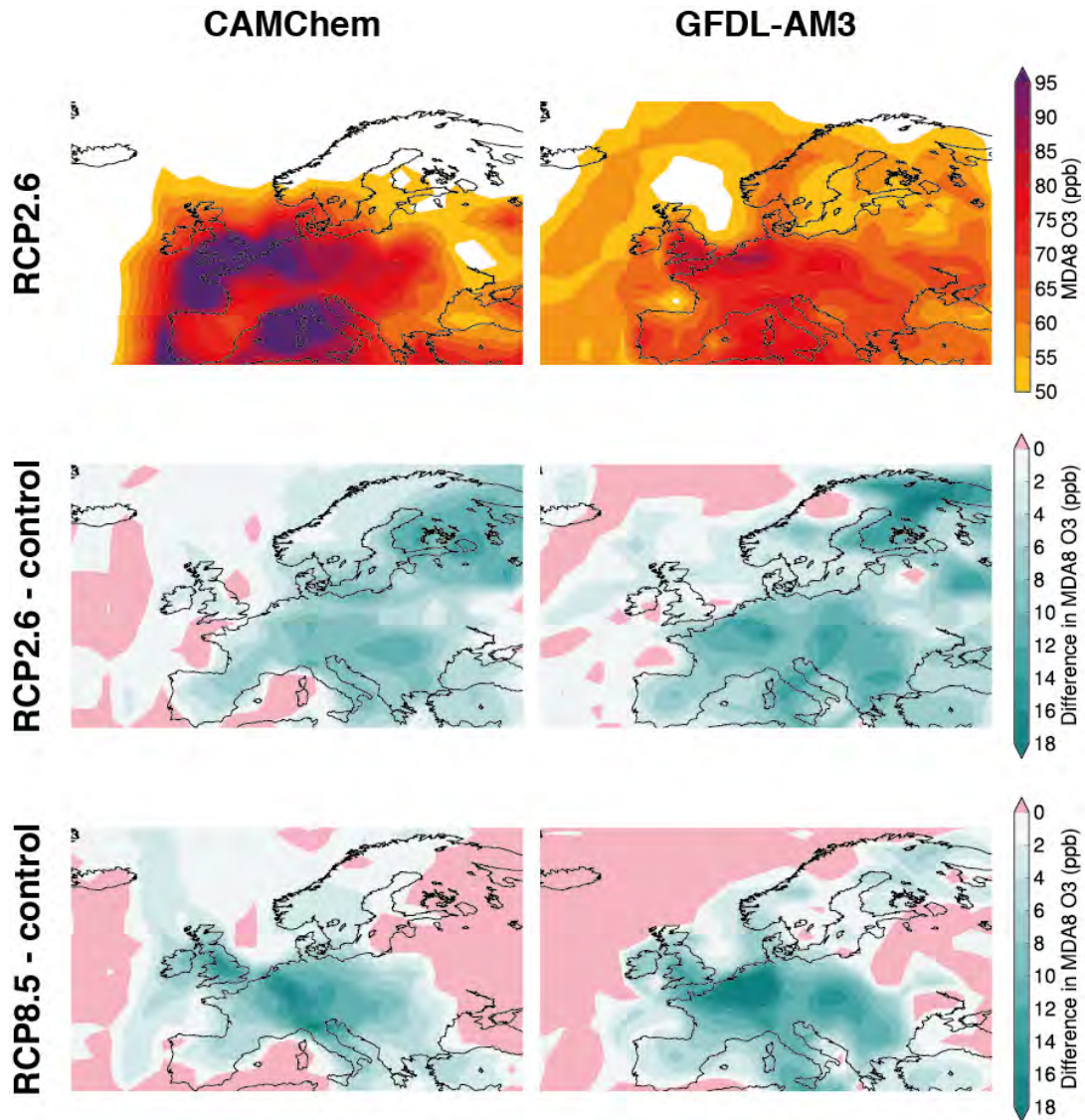
Figure 3.8: Top plot shows the two-week maximum MDA8 ozone using 2030 emissions from RCP2.6, the middle shows the difference between the RCP2.6 and the control scenario, and the bottom plot shows the difference between the RCP8.5 and the control scenario.

Figure 3.9 shows the average daily mean $PM_{2.5}$ levels for the RCP2.6 scenario (top row), and the change from the control scenario for the RCP2.6 and RCP8.5 emission scenarios. The majority of Europe has average $PM_{2.5}$ levels below 15 µg/m^3 for both models for RCP2.6 and RCP8.5 emissions, though levels are between 15 and 20 µg/m^3 lower over Portugal using CAMChem for the future emission scenarios. For CAMChem, $PM_{2.5}$ levels are reduced by up to 7 µg/m^3 over most of the land in Europe

for both emission scenarios. For RCP2.6, there is a 10-40% decrease in $PM_{2.5}$ for most of Europe and for RCP8.5 there is mainly between 10 and 50% reduction. Results for GFDL-AM3 are of similar magnitude: up to 7 µg/m^3 and 20-40% (RCP2.6) and 25-50% (RCP8.5) reductions in average $PM_{2.5}$ for most of Western Europe.
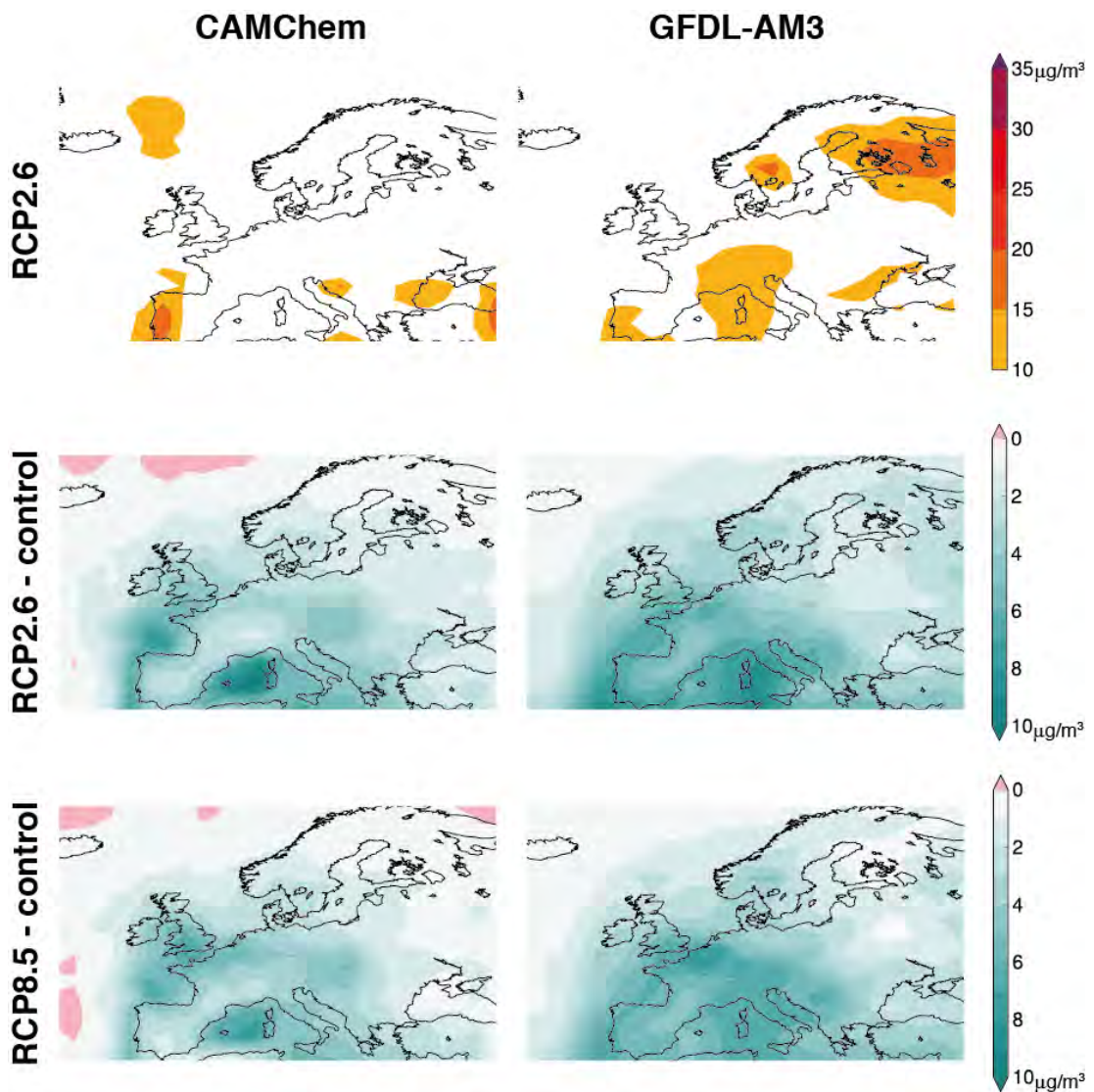
Figure 3.9: Top plot shows the two-week average daily mean $PM_{2.5}$ using 2030 emissions from RCP2.6, the middle shows the difference between the RCP2.6 and the control scenario, and the bottom plot shows the difference between the RCP8.5 and the control scenario.
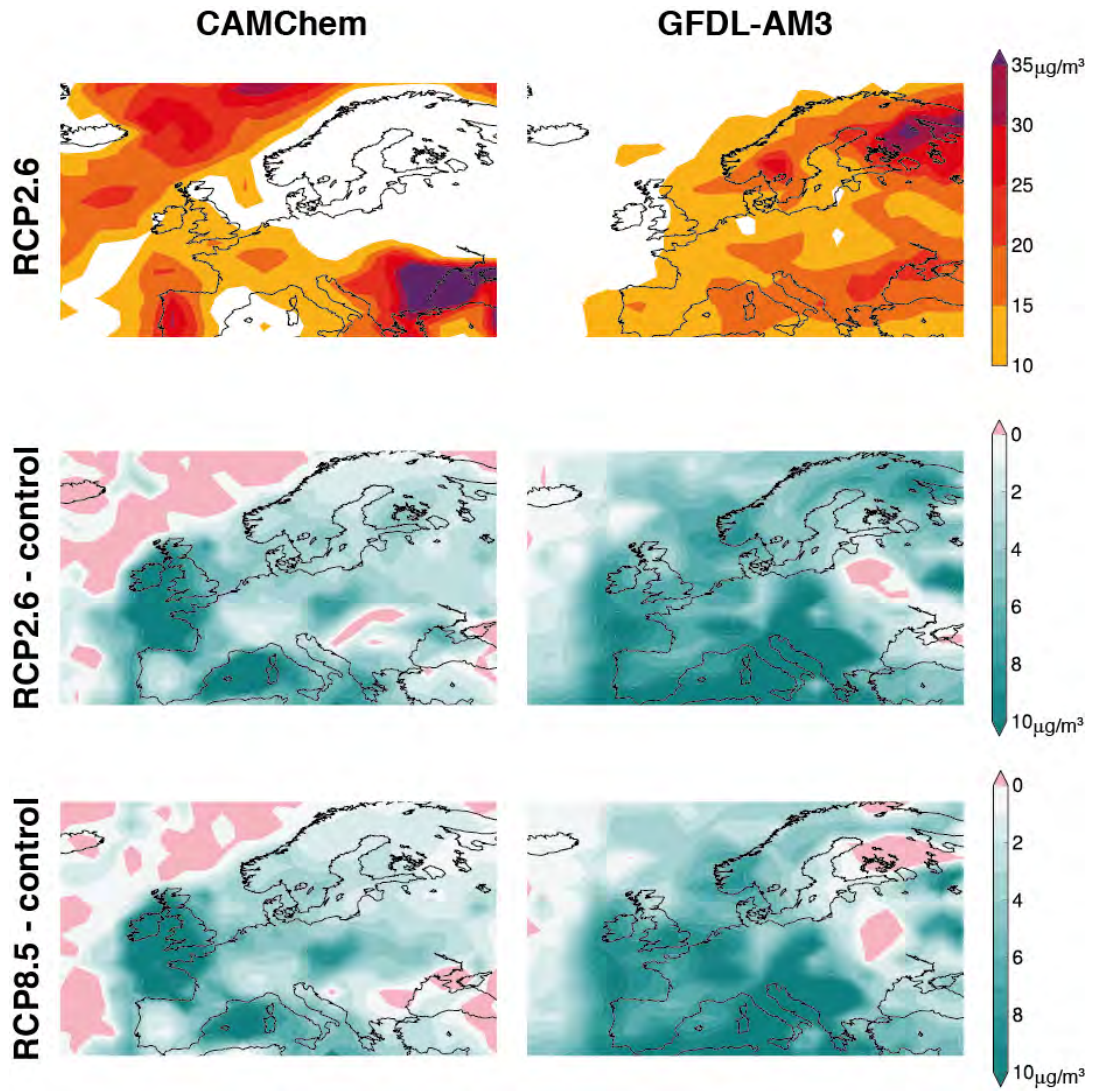
Figure 3.10: Top plot shows the two-week maximum daily mean PM$_{2.5}$ using 2030 emissions from RCP2.6, the middle shows the difference between the RCP2.6 and the control scenario, and the bottom plot shows the difference between the RCP8.5 and the control scenario.

Figure 3.10 shows the two-week maximum daily mean PM$_{2.5}$ levels using the RCP2.6 scenario emissions (top row), and the difference between RCP2.6 and RCP8.5 and the control scenario. Most of mainland Europe stayed below WHO guidelines for the two-week period using both models for the RCP2.6 scenario. PM$_{2.5}$ is lower for the RCP2.6 and RCP8.5 emission scenarios for most of Europe. Both models show a less than 50% reduction for RCP2.6 for most of Europe. For RCP8.5, CAMChem shows more than

50% less PM$_{2.5}$ over parts of the UK and Ireland, and GFDL-AM3 shows more than 50% less PM$_{2.5}$ over parts of the UK and Belgium.

3.4.3 Health impacts

Having considered the scenarios' impacts on pollutant concentrations, we next turn to consider their implications for human health. Figure 3.11 shows the excess short-term mortality risk due to pollutants ozone and PM$_{2.5}$ during the August heatwave for five European countries. Both model results were bias-corrected by applying the appropriate gradient shown in Figure 3.2, an average of these results was taken, and mortality was estimated using 3.2 and 3.3. The uncertainty bars in consider model uncertainty, uncertainty for β coefficient, and the standard deviation for the gradient between the model and observations. Both Em70Pop03 and Em70GDP03 lead to an increase in ozone-related mortality in France and Germany, but lead to a decrease in the UK, Belgium, and the Netherlands. The excess mortality-risk due to ozone was very similar for the control and Em70Pop03 emission scenarios. The change in ozone-related mortality risk in the UK reflects the decrease in ozone over the UK for both models.

The mortality risk attributed to PM$_{2.5}$ for all five countries is approximately double using the Em70GDP03 scenario rather than the control scenario and excess mortality for Em70Pop03 is about halfway in-between. For the control scenario, the PM$_{2.5}$-related mortality risk is less than 1 deaths per 100,000 people for the five countries, with higher mortality risk associated with ozone. For Em70Pop03 the mortality risk is between 1 and 2 excess deaths per 100,000 people and for Em70GDP03 it is around 2 PM$_{2.5}$-related excess deaths per 100,000 people for each country. The mortality risk due to ozone and PM$_{2.5}$ is similar for the Em70Pop03 scenario.
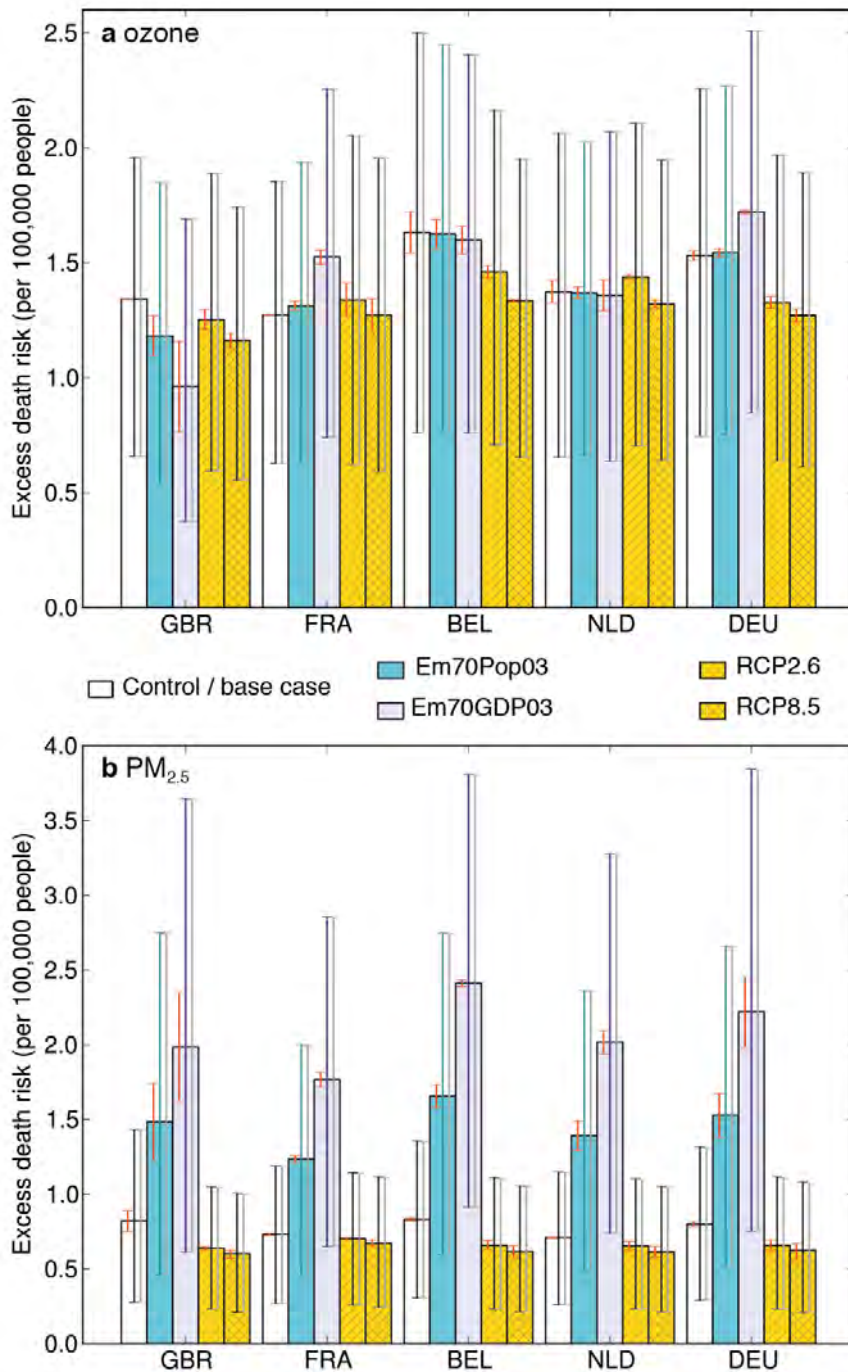
Figure 3.11: Risk of premature mortality in the UK, France, Belgium, the Netherlands, and Germany due to (a) ozone and (b) PM$_{2.5}$ during 1-14 August for the three different scenarios using 2003 population: control (white), Em70Pop03 (teal), Em70GDP03 (violet). Middle uncertainty bars take into account model, bias correction, and relative risk uncertainty. The red uncertainty bar on the left is the uncertainty due to the model and bias correction and the grey uncertainty bar on the right is the uncertainty due to the relative risk 95% confidence interval.

To assess the contribution of model uncertainty and mortality risk uncertainty, I calculated mortality risk with constant model $PM_{2.5}$/ozone and varying RR uncertainty (grey uncertainty bar) as well as varying model ozone/$PM_{2.5}$ uncertainty and constant RR (red uncertainty bar), shown in Figure 3.11. For all scenarios and both pollutants, the magnitude of the grey bar is larger than the magnitude of the red bar on the left and is a similar magnitude to the middle bar which uses both uncertainties. Therefore, the uncertainty for RR contributes more to the overall uncertainty than the difference between the two models and the standard deviation from the line of best fit between models and observations.

By only taking into account uncertainty due to model choice, but ignoring uncertainty due to RR, ozone-related risk of excess deaths would have significantly decreased in the UK, Belgium, and Germany using 2030 anthropogenic precursor emissions. Whereas, pre-2003 air quality policy had already significantly reduced the risk of $PM_{2.5}$-related deaths in all five countries shown in Figure 3.11. Likewise, 2030 emissions would have reduced the risk further, even with a higher 2030 population.

Table 3.4 shows excess-mortality risk for each scenario and pollutant. Mortality for the 1970 scenario was calculated using a 1970 population and death rate, RCP scenario mortality was calculated using 2030 population and death rate projections, and other scenarios used a 2003 population. Total excess mortality risk attributed to ozone pollution for 12 European countries affected by the heatwave using the control scenario was 4793 (2283–7205) deaths, where the range in brackets was calculated using higher and lower values for standard deviation for gradient line between model and observations, model results, and coefficient β. $PM_{2.5}$-related mortality risk was lower than ozone-related mortality risk for this scenario at 2793 (975 – 4762) deaths.

The mortality risk attributed to ozone was 4752 (2235–7221) deaths and 5205 (2411–8019) deaths for Em70Pop03 and Em70GDP03 respectively. So, according to the Em70Pop03 scenario, policy and technology changes may not have had a significant impact on the ozone-attributed deaths during the two-week period. $PM_{2.5}$-attributed mortality risk increased to 4713 (1599 – 8186) deaths using Em70Pop03, which is about 69% more than the control scenario. The mortality risk attributed to $PM_{2.5}$ using the Em70GDP03 scenario was more than double that of the control scenario at 6596 (2248 – 11380) deaths.

Table 3.4: Excess-mortality risk due to ozone and $PM_{2.5}$ for 12 countries in Europe affected by the heatwave in 2003 for different emission scenarios and population

Experiment	Ozone	$PM_{2.5}$
Control	4793 (2283 – 2705)	2793 (975 – 4762)
1970	4597 (2160 – 6993)	4682 (1613 - 8039)
Em70Pop03	4752 (2235 – 7221)	4713 (1599 – 8186)
Em70GDP03	5205 (2411 – 8019)	6596 (2248 – 11,380)
RCP2.6	4576 (2186 – 6856)	2414 (861- 4039)
RCP8.5	4408 (2105 – 6606)	2346 (285 – 3983)

Figure 3.11 and Table 3.4 also show the excess short-term mortality risk for future scenarios RCP2.6 and RCP8.5 in the year 2030. Both scenarios have similar emission reductions over Europe compared to the control and they would reveal similar mortality risk rates to each other for both pollutants in the five countries, with RCP8.5 showing

slightly lower emissions and mortality risk for most European countries. For these scenarios, pollutant-attributed mortality risks are dependent on changes in population and baseline mortality rate as well as changes in emissions. Ozone-related mortality risk total is 4576 (2186 – 6856) deaths for RCP2.6 and 4408 (2105 – 6606) deaths for RCP8.5. $PM_{2.5}$-related mortality risk is about half that of ozone, at 2414 (861–4039) deaths for RCP2.6 and 2346 (825–3983) deaths for RCP8.5. The estimated number of deaths are only slightly lower than that of the control scenario because of further emission reductions and increases in population in 2030.

To test whether or not emission reductions made a significant difference to human mortality due to air pollution during the heatwave, I used a simple statistical test:

$$z = \frac{a - b}{\sqrt{a + b}} \tag{3.4}$$

used by Pocock (2006), where a and b are the number of excess deaths for two different emission scenarios. I compared each scenario to the control scenario and the results and shown in Table 3.5. Values of z above 1.96 and 3.89 correspond to p-values below 0.05 and 0.0001 respectively so anthropogenic emission reductions did make a significant difference to $PM_{2.5}$ levels during the heatwave and further reductions (illustrated by RCP8.5) could have made a significant contribution to ozone levels.

Table 3.5: The results for testing statistical significance between the control scenario and other emission scenarios using 3.4.

Test	z (ozone)	z ($PM_{2.5}$)
Em70Pop03	0.42	22.16

RCP2.6	2.24	5.25
RCP8.5	4.01	6.24

3.5 Discussion

Previous studies have found a beneficial long-term impact of legislation and technology advances on air quality and human health (Archibald et al., 2017; Crippa et al., 2016; Daskalakis et al., 2016; Turnock et al., 2016). In this study, using similar methods to Archibald et al. (2017) and Daskalakis et al. (2016), I looked at the impact of air quality policy on MDA8 ozone and daily mean $PM_{2.5}$ and their potential health impact during an extreme event: namely the 2003 heatwave in Europe. I found that legislation may have increased the number of ozone-attributed excess deaths by about 41, although there may have been 1920 (about 69%) more $PM_{2.5}$-attibuted excess deaths without air quality legislation. Due to reductions in pollutant emissions, both RCP2.6 and RCP8.5 emission scenarios for the year 2030 had lower excess mortality risk for both ozone and $PM_{2.5}$ than the control scenario, despite there being higher population in 2030.

In this study, I propose that scaling 1970 anthropogenic emissions by population would likely underestimate what emissions would be like without policy and technological advances. However, scaling by both GDP and population, gave a very pessimistic view and potentially overestimated them substantially more if they evolved in a similar way to CO_2 emissions in newly industrialised countries can be used as a proxy. Consequently, I estimate world avoided emissions using similar methods to previous

work (Archibald et al., 2017; Daskalakis et al., 2016) – i.e. scaling emissions by population and ignoring changes in GDP.

It is likely that emissions without policy and technological advances may lie somewhere between the two estimates. A more thorough exploration of a world avoided scenario may go back and construct an emission scenario following the implications of each policy or technological advancement. Another way of estimating changes in pollutant emissions would be to use the empirical relationships between urban air pollution and per capita GDP found by (Grossman and Krueger, 1995). They found that the median concentration of heavy particles mostly decreased with income, whereas sulphur dioxide concentration initially increased with income, then decreased, and eventually increased again. Concentration of smoke in cities increased with GDP per capita at first then decreased, this inverted U-shaped relationship was dubbed the 'Environmental Kuznet's Curve' after the relationship between economic growth and income inequality (Kuznets, 1955). However, it may be that the downward slope in pollutant emissions is triggered by environmental policies anyway, as citizens are more concerned by non-economic living conditions as their income rises. If this is the case, a "world avoided" scenario would not have a decrease in emissions because it does not involve policy changes by definition.

Alternatively, as countries get richer, they stop producing pollution-intensive goods and instead import them from countries with less strict environmental laws. If this is the case, then developing countries may not see the same reduction in pollution as income rises.

I acknowledge that the model resolution was too low to project pollutant concentrations and their impacts at the urban scale. Global models, which have low resolution, were

chosen due to the availability of tools. These models tend to overestimate the health impacts of ozone because of the uniformity of ozone concentrations and population density (Punger and West, 2013; Wild and Prather, 2006). In this chapter, the model with lower resolution generally underestimates (overestimates) ozone at higher (lower) concentrations, therefore potentially underestimating the benefits in regions with higher pollution (usually more urban areas). On the other hand, $PM_{2.5}$-related mortality estimates are generally lower with ~100 km resolution than with fine resolution models (Kushta et al., 2018; Punger and West, 2013). Similarly, both models in this chapter have lower estimates for $PM_{2.5}$ than the observations for the majority of grid cells.

Therefore, it would be beneficial to repeat this study with high resolution models to capture some of the smaller scale details. This would mean that the benefits of emission reductions would not be under- or over-estimated.

Similarly to previous studies (e.g., Archibald et al., 2017; Daskalakis et al., 2016), I note that the method for estimating world avoided emissions assumed that emissions are proportional to gridded population, which is not realistic for some sectors. For instance, increases in emissions from energy production would not typically be in the same location as where there was an increase in energy consumption.

Future work aiming to quantify the benefits of air quality policies more robustly will need to explore different scaling methods for different sectors. There are numerous studies on the impact of policy or meteorology on air quality in Europe and the USA, but other regions experience air quality extremes and heatwaves. For instance, the 2007 Asian heatwave impacted countries in East and South Asia. In India, where the Environmental Protection Act of 1986 was passed, around 70% of air pollution in India is due to vehicle emissions so sales in New Delhi are limited to curb further increases

in car sales and cars must comply with exhaust emission standards (Jacobson, 2002)). The 1987 Air pollution Control Law in China was emended in 2000 to aim to reduce sulphur dioxide emissions (Jacobson, 2002). In Japan, the Air Pollution Control Law was enacted in 1968 (Wakamatsu et al., 2013). MACCity (Granier et al., 2011) provided emissions estimates globally and by sector so 1970 transport emissions in India could be scaled by car ownership or 1970 all-sector emissions in South and East Asia could be scaled by population to emulate a world avoided. A CCM could simulate air pollution in Asia with 2007 summer meteorology using various emission scenarios: a base case scenario (2007 emissions), "world avoided" (using scaled 1980 transport emissions), and possible future scenarios (e.g., RCP8.5). The study would assess the impact of policy on air quality during the 2007 Asian heatwave.

Though the mortality risk due to ozone pollution was not reduced overall in the control scenario compared to a world avoided, nearly 2000 $PM_{2.5}$-related excess deaths may have been avoided and maximum $PM_{2.5}$ levels were halved in many regions. For the majority of Europe $PM_{2.5}$ levels remained below WHO guidelines during the two-week period, which could not be said of a world avoided. So, policy measures have had an overall positive effect on air quality during this extreme event. Further emission reductions could lead to further air quality gains, for both ozone and $PM_{2.5}$, as shown by RCP emission scenario results, which may mean there are less deaths overall during an extreme event even if the population has increased.

When making decisions, policy-makers need to consider risk, which depends on the likelihood and the impact of an event. Extreme events, like the heatwave in 2003, may have been "unlikely" in the early 2000s, but they are physically plausible and the impacts are high (Sutton, 2018). Moreover, similar summer temperatures are expected

to be commonplace in Europe by the 2040s, despite summers only expected to be that hot twice every century in the early 2000s (Christidis et al., 2015). Therefore, policy interventions, such as emission reductions, are justifiable when considering the likelihood of similar events.

In terms of impact, the cost of implementing the policy is higher than the savings when only considering avoided mortality during the worst two weeks for mortality of the heatwave. Around 1900 deaths were avoided due to policy interventions, using a statistical value of life of $3.6 million (OECD, 2012), savings are $6840 million. The cost per year of implementing air quality policy in Europe is about $92,000 million (Amann et al., 2017). However, reductions in human mortality for that short period of time do not capture all the benefits of policy intervention. There were other health impacts due to air pollution during the heatwave, where a lack of policy would mean a more people missing work and school, which would have short- and long-term impacts. Furthermore, during the heatwave wheat and maize were the most damaged crops (García-Herrera et al., 2010) and changes in ozone and climate are projected to have a significant impact on future wheat production (Tai and Val Martin, 2017).

3.6   Conclusion

Previous legislation and technological advancements did not make a substantial difference to the total number of ozone-related deaths during the heatwave (and may even have increased them). However, there were about 40% more $PM_{2.5}$-attributed deaths without reductions in air pollution.

Further precursor emission reductions in RCP2.6 and RCP8.5 scenarios prevent ozone- and $PM_{2.5}$-related deaths increasing with the increase in population if a similar heatwave

were to occur in 2030. Future mitigation efforts in RCP2.6 and RCP8.5 leading to reductions of VOC as well as NO_x emissions would mean that ozone would also decrease in areas that had higher ozone in the control scenario than Em70Pop03 and Em70GDP03.

4 A spatially-varying definition of warm days: estimating impacts on populations for 1.5, 2, 3, and 4 °C warmer worlds

In the previous chapter, the impact of a particular heatwave on air quality was investigated. This included estimating the number of pollution-related deaths. Such health effect calculations are typically completed using the same dose-response relationship for each location. For air quality, this relationship will be biased to Europe and North America since most epidemiological studies on air quality and mortality are done in these regions. Therefore, extrapolating health impact calculations globally could be unrealistic, perhaps particularly for developing regions where resilience to impacts may be less. In this chapter, I explore the heath impacts of "warm days", which I define as days where temperatures are above optimum for human health. To address the issue of spatially-varying optimal temperatures, I develop a spatially-varying definition of a warm day based on local temperatures, which could be used to improve risk projections in regions with no data on temperature-related mortality. This analysis is extended with a further framework that puts the health risk in the context of local vulnerability.

4.1   Introduction

Global mean surface temperature (GMST) has seen steady increases over the last several decades, and, in 2016, was almost +1.3 °C above the average GMST for

reference period 1880—1920 (Hansen et al., 2017). At the 2015 Conference of Parties in Paris (COP21), the United Nations Framework Convention on Climate change (UNFCCC) agreed to drive efforts towards limiting GMST to 1.5 °C above pre-industrial temperatures (+1.5 °C) and to stay well below the 2 °C global warming target (UNFCCC, 2015). Even if this GMST target is met, the resultant climate change is still likely to have an impact on ecosystems, agriculture and health (Giannakopoulos et al., 2009; Leemans and Eickhout, 2004; Lewis et al., 2017; Stern, 2007; Weber et al., 2018), and the impacts of a 1.5 °C and a 2 °C ΔGMST differ significantly (Byers et al., 2018; Hoegh-Guldberg et al., 2018; D. Li et al., 2018; Schleussner et al., 2016), so they need to be carefully considered and quantified to inform adaptation or mitigation strategies. These climate impacts and effects will not fall equally on different regions of the globe, due to the spatially-varying nature of both climate change (Joshi et al., 2011; Sutton et al., 2015) and adaptive capacity (Allison et al., 2009; Haddad, 2005). In this chapter I consider the importance of these regional differences for assessing impacts of different GMST targets. I illustrate this by considering the number of people exposed to temperatures that may have an adverse effect on human health, i.e. when the so-called optimum temperature (OT) is exceeded (Bao et al., 2016; Honda et al., 2007). To do this, I exploit a simple but clear statistical relationship apparent from Gasparrini et al. (2015), who have quantified the minimum mortality percentile (MMP) for different locations, giving us a spatially varying definition of what constitutes a "warm day", where a warm day is a day where the mean temperature is above the optimal temperature for human health. The OT is defined as the temperature at which human mortality is lowest (above this temperature there is an increase in human mortality), this temperature corresponds to a percentile – the MMP.

Although there is no universal definition for a warm day or warm spell, they are generally characterized by a day or a number of consecutive days where temperatures are higher than usual, though not usually as intense as heatwaves. While heatwaves are usually defined by seasonally extreme temperatures during the summer period, the term warm spells may be employed during winter months (Sfîcă et al., 2017) or they may be defined by temperatures all year round rather than summer temperatures (Perkins et al., 2012). An increase in duration, intensity and frequency of warm spells and heatwaves is just one consequence of projected anthropogenic climate change (IPCC, 2012; Perkins et al., 2012), leading to multiple impacts on human health and, in particular, with well-defined effects on mortality (Kalkstein and Greene, 1997; Knowlton et al., 2007; McMichael et al., 2006). Other prominent impacts include damages to infrastructure (Kjellstrom et al., 2009; Robson et al., 2010; Rosenzweig et al., 2001; Thornbrugh, 2001) and ecosystems (Arnone et al., 2008; McKechnie and Wolf, 2010; Wernberg et al., 2012). Human exposure to higher temperature can result in premature death, which means that on particularly warm days there may be more deaths than the average expectations for those days (i.e., *excess deaths*). Quantifying these impacts is an important impetus for developing suitable adaptive strategies, such as the heat health watch warning systems. For instance, following 70,000 excess deaths from the 2003 European heatwave (Robine et al., 2008), the French authorities implemented early warning forecast systems which were successful in reducing the deaths in the subsequent 2006 European heatwave (Fouillet et al., 2008; Pascal et al., 2006).

Warm days have been defined by a fixed (e.g., 20 °C) or relative (90th percentile) threshold. Studies on warm spells or weather extremes based on absolute temperature thresholds are usually applied to specific locations because the consequences of different temperatures will vary regionally (Department of Health, 2015; Huynen et al.,

2001; Robinson, 2001; Tan et al., 2007). Percentile-based thresholds are used both in regional (Beniston, 2004; Guo et al., 2017; D. Li et al., 2018; Meehl and Tebaldi, 2004; Murari et al., 2015) and global studies (Perkins et al., 2012; Schleussner et al., 2016). For example, Tomczyk, Piotrowski and Bednorz (2017) defined relatively warm days as a day where the maximum temperature exceeded the annual 95th percentile and a warm spell was defined as five consecutive relatively warm days. Additionally, heatwaves may be defined as the annual "worst" event (e.g., 3 consecutive days with the highest mean average temperature (Meehl and Tebaldi, 2004)) or an event with a particular return value, such as a 7-day heatwave with a 20 year return period (Clark et al., 2010). A different way to define warm day or an extreme event is to tie the definition directly to one of its impacts, such as increases in mortality from high temperatures and high humidity (Mora et al., 2017).

One model for estimating heat-driven mortality is to define a population's OT or 'comfort temperature', which is the temperature at which mortality is lowest (or a temperature range for some locations, considering both low and high temperature-related mortality) (Gosling et al., 2009; Honda et al., 2014; Lowe et al., 2015; McMichael et al., 2008). By definition, there is an increase in heat-related deaths above the OT, and for a given location, the extent of heat-related mortality and the OT are generally dependent on a the local climate (David M. Hondula et al., 2015; Iñiguez et al., 2010; Shi et al., 2015). The percentile of the temperature distribution corresponding to the OT is known as the minimum mortality percentile (MMP). I exploit the MMP in this chapter by using the MPP as the threshold that defines warm days.

Given the projected climate change, the most recent IPCC report stated that it is "virtually certain" that most places will experience more hot and fewer cold extremes

this century (Collins et al., 2013), and previous studies have projected heat-related mortality (Ballester et al., 2011; Honda et al., 2014; Huang et al., 2011; Peng et al., 2011) or human exposure to high temperatures (Z. Liu et al., 2017; Mora et al., 2017) for future time periods (e.g., 2071-2100). In this chapter, I consider changes in human exposure to warm days (by multiplying the number of warm days with human population) for changes in GMST (ΔGMST; e.g., 1.5 °C above pre-industrial temperatures). Even a 1 °C rise in GMST will cause significant regional temperature increases in many countries (Mahlstein et al., 2011) because land masses warm faster than the oceans (Ying, 2012). ΔGMST, as opposed to future time/time period, has been used in multiple studies (Guo et al., 2017; Joshi et al., 2011; Schleussner et al., 2016), and provides a less path dependent and more precise metric for indicating differences in regional climate outcomes than radiative forcing (Tebaldi et al., 2015). Note also that developing countries (concentrated at low latitudes) are expected to experience more frequent temperature extremes earlier and at lower ΔGMST (Harrington et al., 2016; Mahlstein et al., 2011). Impacts in these regions will be particularly severe considering that low income as well as fast climate change outside current bounds is likely to have negative effect on their ability to adapt (Hayden et al., 2011). Additionally, while the relationship between regional mean temperature changes and ΔGMST is often linear (Sutton et al., 2015), this is not the case for the projection of extreme temperature events, the correlation is non-linear (Fischer and Knutti, 2015; Knutti et al., 2016). This highlights the need to use more sophisticated modelling approaches to project the frequency of particularly warm or hot days for different climate targets.

The aims of this chapter are 1) to leverage existing studies to estimate the global distribution of MMP; 2) to quantify the occurrence of future warm days and warm spells for different ΔGMST targets, comparing a constant (81st) percentile definition (as per

Schleussner *et al.* (2016), Tomczyk, Piotrowski and Bednorz (2017) etc.) against my spatially varying definition; and 3) analyse regional exposure and susceptibility to warm days alongside a vulnerability framework (summarised in Figure 4.10(a)), . In Section 4.2, I describe the climate model data and the methodology for assessing ΔGMST. In Section 4.3, I present the statistical model to estimate MMP as a function of location. I project the occurrence of warm days and warm spells as a function of ΔGMST, comparing two thresholds, in Section 4.4 and consider the implications of the results for potential human exposure and vulnerability to warm days in Section 4.5. I conclude with a discussion of the results in Section 4.6 and a conclusion in Section 4.7.

4.2   Climate model data and calculating ΔGMST thresholds

To calculate when models reached ΔGMST thresholds, monthly mean surface temperature output was taken from 29 different global climate models (listed in supplementary Table S1) that took part in phase 5 of the Coupled Model Intercomparison Project (CMIP5) (Taylor et al., 2012b), covering historical (1976-2005; used as a proxy for present-day conditions because that is when CMIP5 historical simulations end) and projected future (2006-2100) changes. I use climate projections from the future emissions scenario with the highest rate of greenhouse gas emissions and warming: the Representative Concentration Pathway (RCP) 8.5 (Riahi et al., 2011). This scenario was chosen as its strong warming means that the climate models cross a range of different ΔGMST thresholds. Additionally, using only one scenario avoids any scenario-dependent climate changes that might occur from the different short-lived climate forcer emission trajectories (van Vuuren et al. 2011), which have been shown to affect regional climate change (Shindell and Faluvegi, 2009; Shindell et al., 2015).

Only one ensemble member (r1i1p1 if available) from each CMIP5 model was included to avoid overweighting my analysis to any particular model. Every model output was fitted to the same 2 x 2° (latitude/longitude) grid, which means that for most models I avoid potential numerical artefacts from increasing the resolution. However, this resolution does not capture certain important sub-grid scale characteristics, such as the urban heat island effect, which will bias the results.

Rather than considering regional climate changes for a given time period, I represent the changes as a function of ΔGMST. The ΔGMST is expressed relative to the pre-industrial period defined as 1850-1900 (e.g., +1.5 °C). However, I derived the ΔGMST levels using a similar method to Schleussner et al. (2016), who utilised a common reference period (1986-2005), which was 0.6 °C warmer than pre-industrial levels. For each model, working forward from 2006, I determined the first simulated 30-year time period during which the time-averaged ΔGMST is equal to or greater than the given ΔGMST outcomes: +1.5, +2, +3 or +4°C, which translates to +0.9, +1.4, +2.4, or +3.4 °C above the reference period. The use of 30-year periods is consistent with the World Meteorological Organization definition of the "climate normal" (WMO, 1989), but differs from the 5-year (Joshi et al., 2011) and 20-year (Schleussner et al., 2016) time-slices used to calculate GMST thresholds in other studies. The projected periods where ΔGMST is 1.5 °C range from 2006-2035 to 2027-2056, which reflects the different transient climate sensitivity in CMIP5 models (IPCC, 2013; Winton et al., 2013). I should note here that some models may reach the 1.5 °C threshold after 1976-2005 and before 2006-2035, which is where historical projections end and future projections begin. The highest ΔGMST representing a +1.5 climate is 1.71 °C (CanESM2). Dates for ΔGMSTs are shown in Supplementary Table S1.

Nicola Wareing - July 2021

4.3 Estimating a spatially-varying human minimum mortality percentile

Previous epidemiological studies have found a range of values for OT for different regions around the world. The World Health Organisation (WHO) and Takahashi et al. (2007) respectively use the 84th and 85th MMP. Their choice in percentiles were based on results from (Honda et al., 2014), which used data from Japan, Europe, and the USA, and (Honda et al., 2007), which used data from Japan. However, Egondi et al. (2015) found that the MMP was closer to the 60th percentile for the urban poor population of Nairobi, Kenya, using daily maximum temperature and mortality data from 2003-2012. Guo et al. (2014) and Gasparrini et al. (2015) found the MMP ranged from the 66th to the 80th percentile and the 60th to the 92nd respectively for each country using daily mean temperature. They found that the average MMP globally using over 300 communities were the 75th and 81st percentiles. I based the percentiles used in this study on results found by Gasparrini *et al.* (2015), despite WHO using results from Honda *et al.* (2007), because their epidemiological study was much larger.

Figure 4.1 shows how the (a) OT and (b) MMP relate to the local climate, defined by the multi-year mean temperature (time periods vary between locations). Local acclimatisation is an important factor when it comes to temperature related mortality, and OT values for a range of studies are generally higher in warmer locations (El-Zein et al., 2004; Gasparrini et al., 2015; McMichael et al., 2008) (as also demonstrated by Figure 4.1(a)). However, when comparing the MMP it is apparent that the average percentiles used by the previous studies mentioned above (75th and 81st) may overestimate the OT in some of the warmest locations ((b)). This could lead to an underestimation in health impacts and the need for adaptation in these areas, if

projections were based on constant percentiles. Both the spatially varying MMP and the 81st percentile overestimate the MMP in most of Spain and some locations in the USA, Canada and Brazil, thus using the 81st percentile could potentially underestimate human health impacts. The 75th percentile underestimates the MMP for most locations so could overestimate the impacts.

For this study, I fitted a cubic relationship between mean temperature and MMP, as indicated by Figure 4.1(b), and extrapolated it to produce a global map of MMP values based on local temperatures. I acknowledge that this is a simplification, and that many other epidemiological and local demographic and socioeconomic factors will ultimately determine the MMP/OT values for a given region (as I discuss in Section 4.4). Nevertheless, Figure 4.1 clearly indicates strong regional variations in OT and MMP, and my aim is to explore the implications of beginning to account for this in future projections, rather than using a constant percentile.

Following Figure 4.1(b), I modelled the relationship between MMP and daily mean temperature using a cubic relationship, using MMP data from Gasparrini et al. (2015) and average daily mean data ($\overline{T}$) from Guo et al. (2014) for each location. I use MMP and daily mean temperature provided by Gasparrini et al. (2015), rather than daily maximum temperature, because they used more locations than Honda *et al.* (2014), who only had data from East Asia, Western Europe, and the USA. The resulting statistical fit is as follows:

$$\text{MMP} = 88.0 - \left(1.3 \times 10^{-3}\right) \overline{T}^{\,3}, \tag{4.1}$$

where average daily mean temperature is in °C. The root-mean-square deviation is 7.65 °C and the r^2 goodness-of-fit measure is 0.63. These values indicate a better fit than the alternatives shown in Table 4.1.
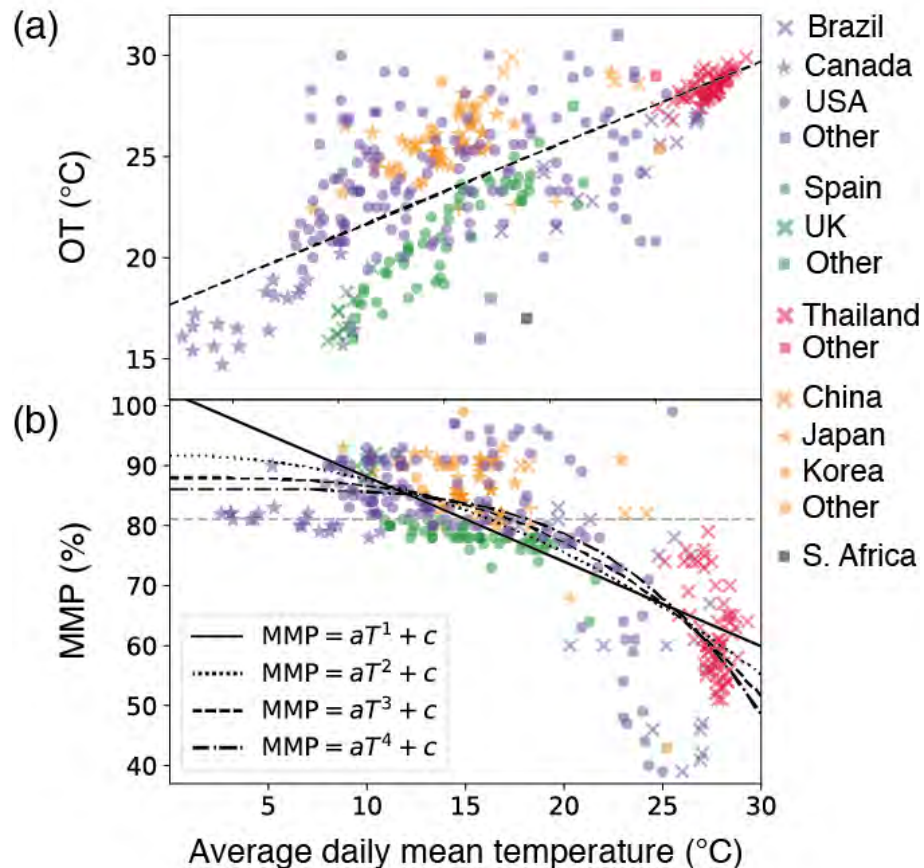
Figure 4.1: (a) The optimal temperature versus the average daily mean temperature, where the colour indicates one of the six regional groupings by the World Health Organisation. Data from the region of the Americas is purple, European region is green, South-East Asia region is red, western Pacific is yellow-orange, and African region is grey. (b) The minimum mortality percentile (MMP) versus average daily mean temperature for each region, where the constant 81st percentile (the average MMP globally found by Gasparrini *et al*. (Gasparrini et al., 2015)) is shown in grey and the estimated MMP as functions of the average daily mean temperature are shown by the black curves.

Figure 4.1 shows optimal temperatures and MMPs grouped by region. Some countries with a higher Human Development Index (HDI) tend to have higher MMP. For

example, MMPs in Japan range from the 80th to 93rd, which has a higher HDI than Spain, which has similar average temperatures and lower MMPs (64th – 81st). However, China, which has a lower HDI than Spain, has higher MMPs. This could be because data were collected for shorter and later time periods than Spain so there has been some more time for adaptation to higher temperatures before the data were taken.

For example, most locations in Spain have an MMP between the 75th and 82nd and they follow the general downward trend ($r^2 = 0.51$). Thailand does see a general decrease in MMP with mean temperature, but data are not highly correlated ($r^2 = 0.21$), with the MMP ranging from 50th to 80th.

Table 4.1: Coefficients and results for regression between average daily mean temperature and minimum mortality percentile.

Model	Intercept (c)	Gradient (a)	R^2	RMSD
$aT + c$	102.2	-1.4	0.55	8.41
$aT^2 + c$	91.7	-4.1×10^{-2}	0.61	7.81
$aT^3 + c$	88.0	1.3×10^{-3}	0.63	7.65
$aT^4 + c$	86.1	-4.6×10^{-5}	0.62	7.73

Figure 4.2 shows maps of OT using present-day (1979-2005) daily mean temperature data from the ERA-Interim reanalysis product (Dee et al., 2011). It compares OT calculated corresponding to the spatially-varying percentile calculated from equation 4.1 (Figure 4.2(a)) against OT determined from a constant 81st percentile, based on the

average MMP from Gasparrini et al. (2015) (Figure 4.2(b)). As would be expected from Figure 4.1, compared to my spatially-varying MMP the 81st percentile estimates a higher (lower) OT in the tropics (mid-latitudes). Some regions where there are the biggest differences between the two estimations of OT do not have any data to validate the statistical model, particularly in Africa, the Middle East, Eastern Europe, and south Asia. I acknowledge that this means that my results should be interpreted with caution, but it does also highlight the need for more research in these regions, although, Fu *et al.* (2018) found that the average MMP for India was the 82nd percentile, which is higher than shown by the results in Figure 4.2 estimated using equation 4.1.
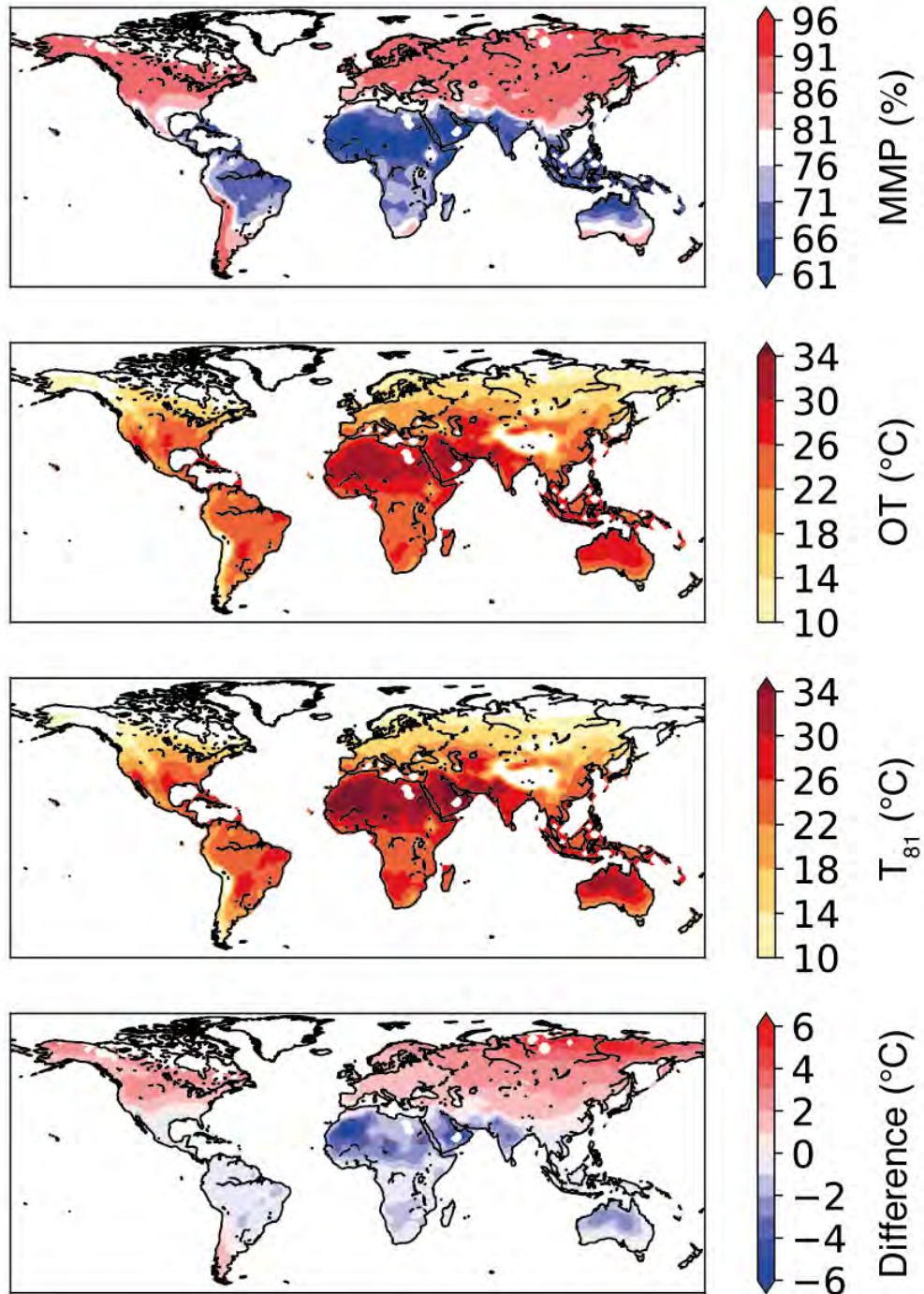
Figure 4.2: The spatially varying minimum mortality percentile (MMP; top). Optimal temperature (OT) calculated using my spatially varying percentile model and the 81st percentile using ERA-Interim daily mean temperature data (1979-2005). The spatially-varying percentile OT minus the 81st percentile OT (bottom). Grid-squares containing zero population are white.

4.4   Projecting changes in warm days and warm spells as a function of ΔGMST

I did not bias correct the 30-year mean ΔGMST from CMIP5 models' because it was calculated relative to each models' pre-industrial GMST. However, as I need to calculate when daily mean temperature was above a specific threshold, the daily mean

CMIP5 data were bias corrected so that they would theoretically have a similar average and standard deviation in daily mean temperature to reality. I used the method recommended by Mahlstein et al. (2015) for index calculations, correcting the simulated 365-day climatology against ERA-Interim reanalysis data (Dee et al., 2011), using the period from 1979-2005 (ignoring any leap days). Briefly, the daily climatologies for each grid point were smoothed using local polynomial regression fitting (LOESS) (Cleveland and Devlin, 1988; Mahlstein et al., 2015), and individual CMIP5 models corrected as function of day and location, depending on the offset between the simulated temperature and that from ERA-Interim.

I used two different thresholds to define a warm day: one being a constant, the 81st percentile, the other, being a spatially varying percentile, calculated by applying the varying MMP model (described in Section 4.3) to each grid cell in each CMIP5 simulation. I found the corresponding OT from that percentile, and any day with a daily mean temperature above the OT was a warm day. A warm spell is defined by three or more consecutive warm days. As I am concerned with human impacts, I disregarded any grid-squares that contained zero population using gridded 2016 population count data from the History Database of the Global Environment (HYDE) (Klein Goldewijk et al., 2011, 2010) – i.e. they are masked white in Figures Figure 4.3-4.8.

Present-day results for the average number of warm days, and warm spell duration using ERA-Interim and CMIP5 data using both threshold definitions are shown in the appendix. I repeat this analysis for future 30-year periods for each global mean surface temperature target. The threshold used to define warm days during the future periods is the OT based on a present-day climate, meaning that I assume no future adaptation to climate change. Dotted areas indicate disagreement between models in Figures 4.3-4.8. I defined model disagreement as where less than 80% of models (24 models) agreed on change in direction from present-day.

Figure 4.3 shows that the change in warm days per year is similar using both MMP threshold definitions, with the biggest increase seen in tropical regions. Most models agree that there is an increase in the number of warm days with increase in ΔGMST. Figure 4.4 shows the average number of warm days per year for the different ΔGMST levels using the two different MMP thresholds. Tropical regions generally have the highest number of warm days using either threshold, with some areas projecting over 300 warm days per year in a +2 °C climate. Unsurprisingly, the spatially varying percentile projects more warm days than the constant percentile in tropical regions because the threshold for warmer regions is lower than 81st percentile (Figure 4.2). By a +4 °C climate, most of Africa experiences warm days for more than half the year. I note again that no African countries were included in the epidemiological results that informed the regression model (Gasparrini et al., 2015). There is some evidence that my model may be conservative in some African countries, for instance, using my model with ERA-Interim reanalysis, I found that the MMP around Nairobi was around the 70th percentile, which is higher than the 60th percentile found by Egondi et al. (2015), meaning that my method may *underestimate* heat-related mortality around Kenya. Though Egondi et al. used daily maximum temperatures for the analysis.
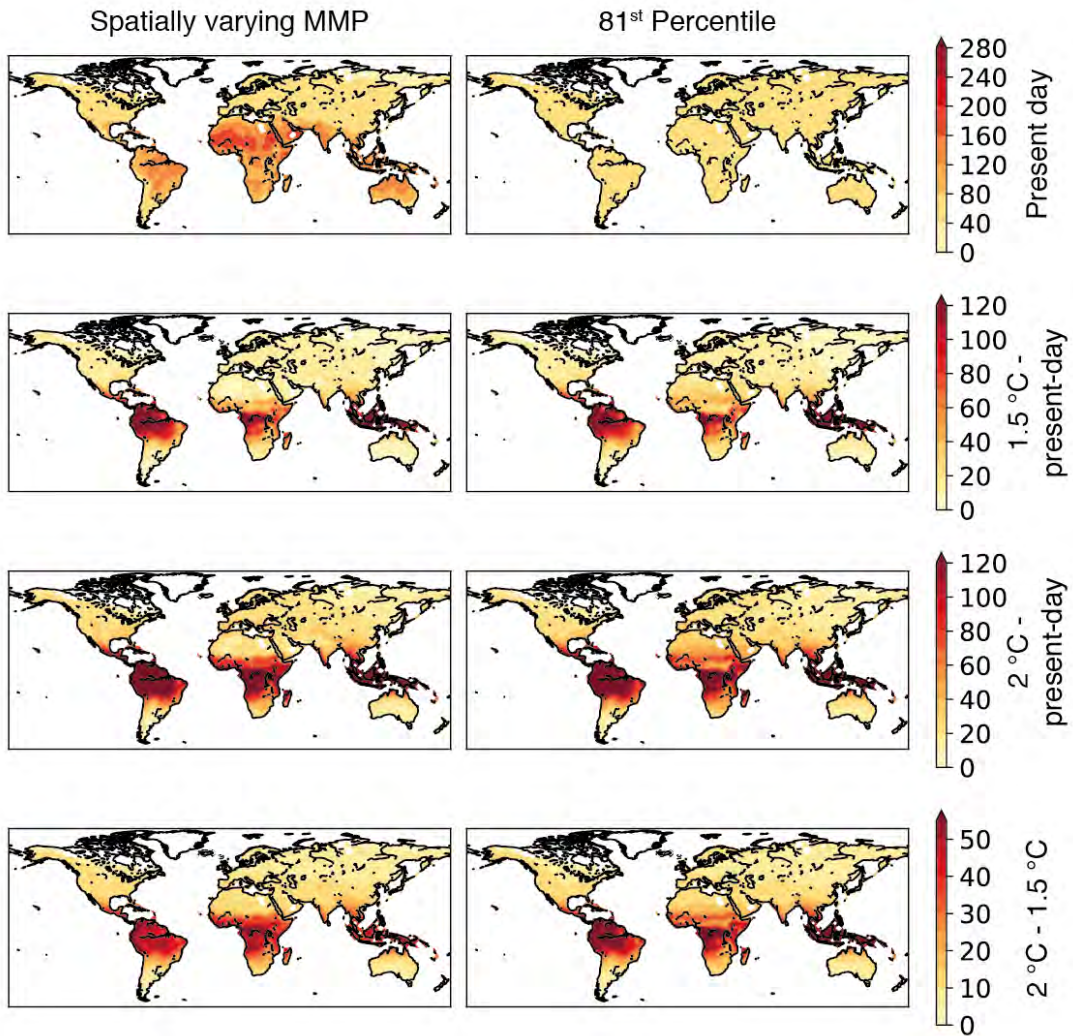
Figure 4.3: Results for the average number of warm days per year for a present-day (1976-2005) climate, change between a 1.5 °C and present-day climate, change between 2 °C and present-day climate, and difference between 2 °C and 1.5 °C climates, using a spatially varying percentile threshold (left) and the constant 81st percentile (right). White areas refer to grid-squares with no population (or negative change), and dots indicate grid cells where there is model disagreement (i.e. less than 80% of models agree with direction of change in sign).
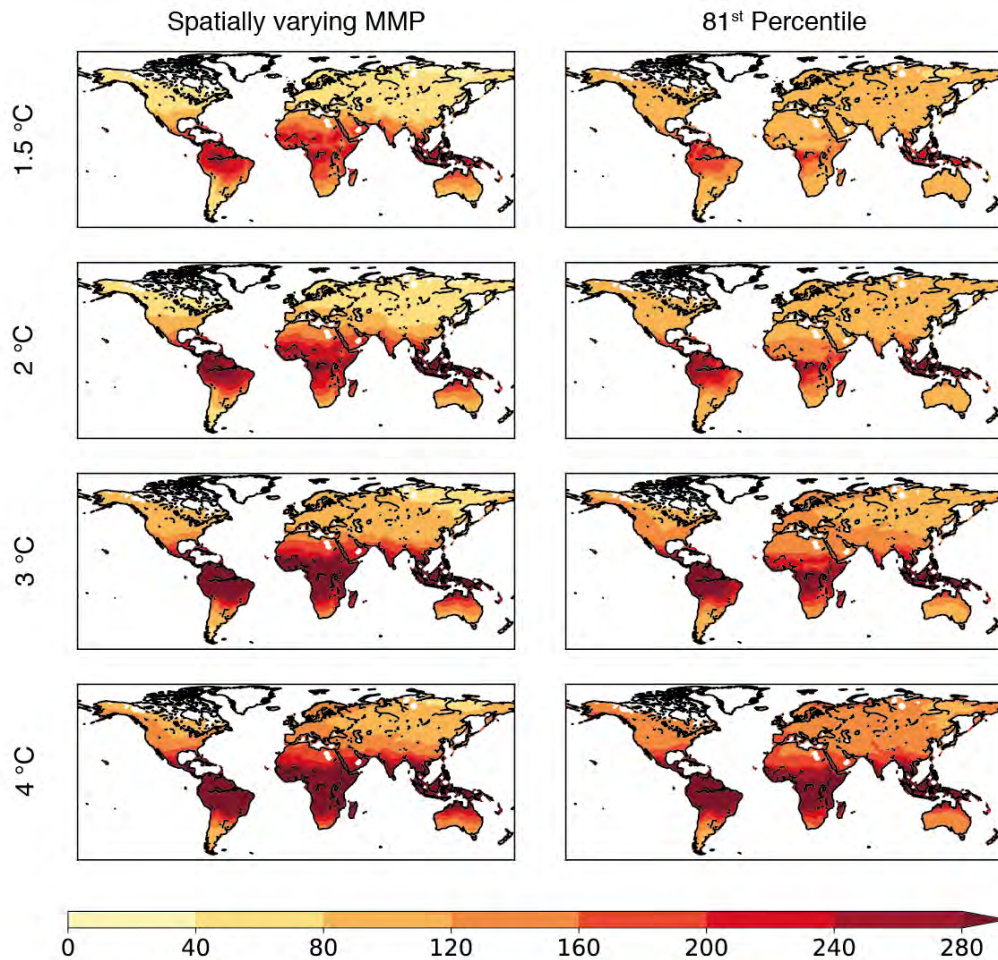
Figure 4.4: Results for the average number of warm days per year for a ΔGMST of 1.5 °C, 2 °C, 3 °C, and 4 °C using a spatially varying percentile threshold (left) and the constant 81st percentile (right). White areas refer to grid-squares with no population as in Figure 4.3, and dots indicate grid cells where there is model disagreement (i.e. less than 80% of models agree with direction of change in warm days).

Figure 4.5 shows the largest increase in the average duration of warm spells in South-East Asia, tropical Africa, and tropical South America (especially the northern Amazon Basin) with the spatially varying percentile showing larger increases in most of these regions. The average duration of a warm spell for present-day was below 10 days for most regions, although the average warm spell defined by the spatially varying MMP was up to 25 days long. In some parts of Central Africa less than 80% models agreed in the change in direction of warm spell duration with ΔGMST. In some parts of Australia,

there was disagreement about the change in direction between a present-day climate and a +1.5 °C climate as well as between +1.5 °C and +2 °C. Figure 4.6 shows that the average duration of warm spells in a +1.5 °C is longest in northern South America and South-East Asia using the spatially varying MMP to define them, and they are longer using this threshold than using the 81st percentile.
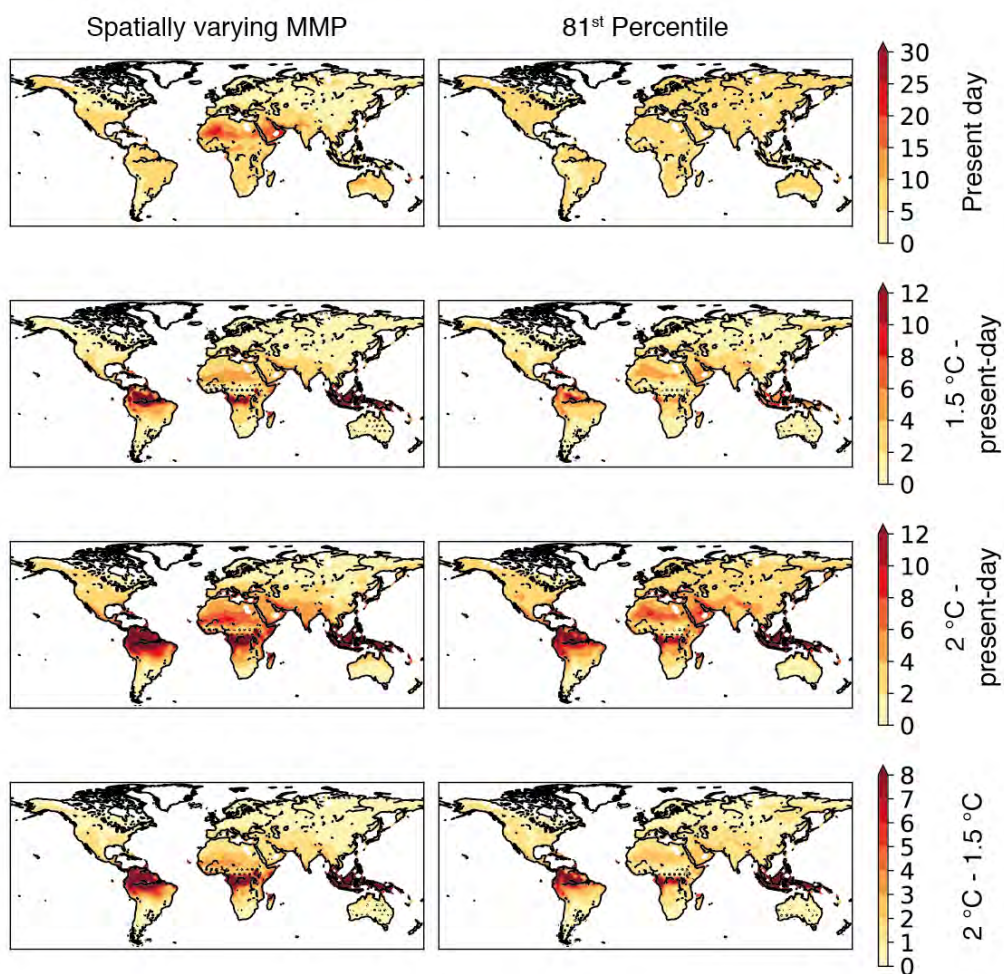
Figure 4.5: Results for the mean duration of a warm spell for a present-day (1976-2005) climate, change between a 1.5 °C and present-day climate, change between 2 °C and present-day climate, and difference between 2 °C and 1.5 °C climates, using a spatially varying percentile threshold (left) and the constant 81st percentile (right). White areas refer to grid-squares with no population (or negative change), and dots indicate grid cells where there is model disagreement (i.e. less than 80% of models agree with direction of change in sign).
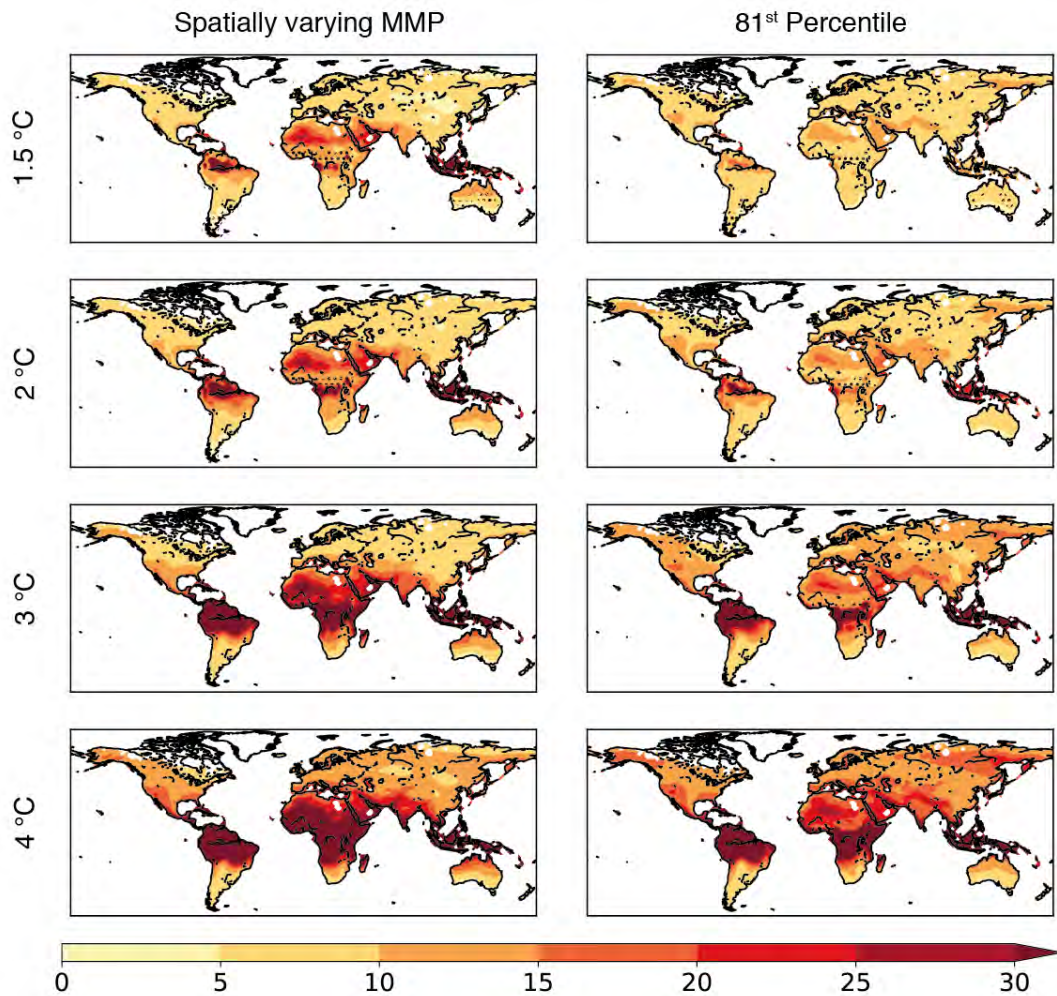
Figure 4.6: Results for the mean duration of warm spells for a ΔGMST of 1.5 °C, 2 °C, 3 °C, and 4 °C using a spatially varying percentile threshold (left) and the constant 81st percentile (right). White areas refer to grid-squares with no population as in Figure 4.3, and dots indicate grid cells where there is model disagreement (i.e. less than 80% of models agree with direction of change in warm days).

Figure 4.7 shows that the maximum duration of a warm spell for present-day is longest in the tropics using the spatially varying percentile. The largest increase in the maximum duration with ΔGMST is in the tropics using both the spatially varying and the 81st percentile. For a +1.5 °C ΔGMST less than 80% models agree that there is an increase in the maximum duration of a warm spell at the mid-latitude regions.

Figure 4.8 shows that the maximum duration of a warm spell is longest in the tropics using both threshold definitions. By +4 °C ΔGMST there is model agreement for most

regions, although there is some disagreement in parts of Australia using the spatially-varying percentile.
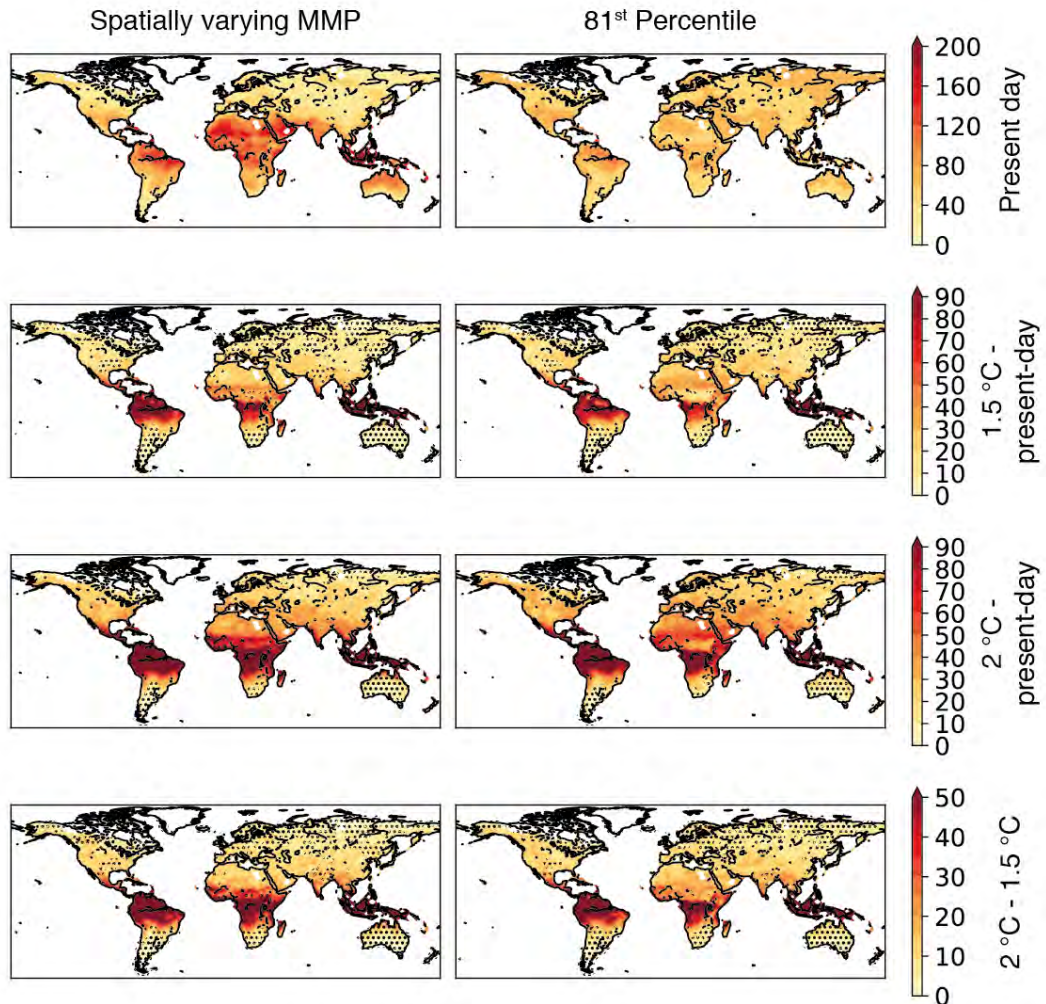
Figure 4.7: Results for the maximum duration of a warm spell for a present-day (1976-2005) climate, change between a 1.5 °C and present-day climate, change between 2 °C and present-day climate, and difference between 2 °C and 1.5 °C climates, using a spatially varying percentile threshold (left) and the constant 81st percentile (right). White areas refer to grid-squares with no population (or negative change), and dots indicate grid cells where there is model disagreement (i.e. more than 80% of models disagree with direction of change in sign).
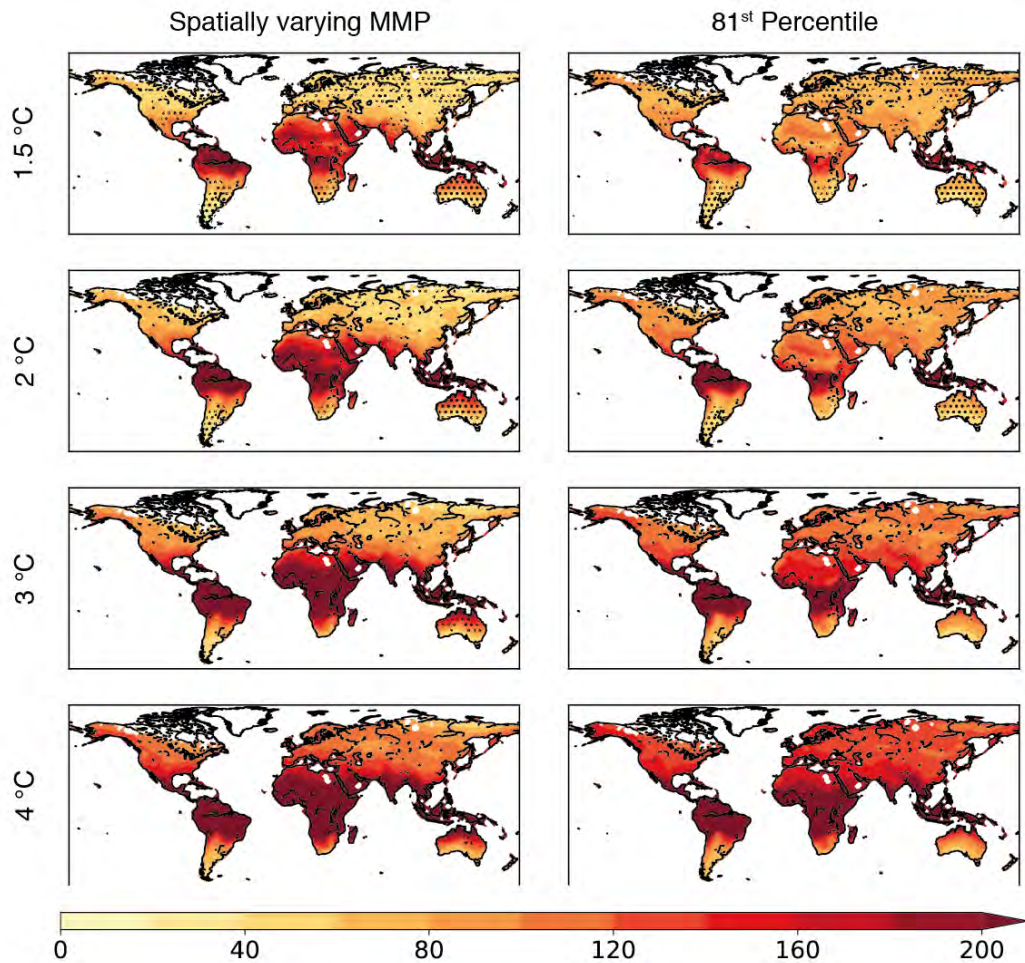
Figure 4.8: Results for the maximum duration of warm spells for a ΔGMST of 1.5 °C, 2 °C, 3 °C, and 4 °C using a spatially varying percentile threshold (left) and the constant 81st percentile (right). White areas refer to grid-squares with no population as in Figure 4.3, and dots indicate grid cells where there is model disagreement (i.e. more than 80% of models disagree with direction of change in warm days).

4.5 Regional exposure and vulnerability to warm days

I compared the potential human exposure to non-optimal temperatures. Exposure to warm days was calculated by multiplying the number of people in each grid cell by the number of warm days per year. Note that exposure in this context does not necessarily mean people are physically being exposed to non-optimal temperatures. The fraction of people literally being exposed to non-optimal temperatures will vary geographically and

is perhaps one of the factors that affect the MMP (e.g., if more people work indoors and have access to air conditioning in that grid cell then the MMP will be higher).

Exposure is used rather than quantifying human mortality because the increase in relative mortality risk as temperature rises will vary regionally (Gosling et al., 2009), and this chapter only considers the threshold at which mortality starts rising. I project exposure of a constant 2016 population (Klein Goldewijk et al., 2011, 2010) to future warm days, similar to the air stagnation exposure index used by Horton et al. (2014) (although they focus on future exposure to the population in the year 2000). I use the same population for each model and ΔGMST so I can explore differences in exposure between models and changes in GMST without population changes affecting the results. This means that policy makers can see the benefits of a lower ΔGMST without increases in population between climate temperature targets exaggerating the differences.

Figure 4.9 shows the future human exposure (people-days) for four different regions, based on the regions used by WHO and the Global Burden of Disease studies (World Health Organization, 2014). "High income North America" (Figure 4.9(a)) shows more exposure using the constant 81st percentile than the spatially varying percentile and exposure using either definition is significantly lower than in South Asia (Figure 4.9(c)) for all ΔGMST levels, despite covering a greater surface area. Tropical Latin America (Figure 4.9(b)) shows more/less exposure than high income North America using the spatially varying/constant percentile. South Asia shows the highest total exposure for all the threshold definitions and ΔGMST targets; although it covers the lowest surface area, it does have more than 1 billion extra people than the other three regions. East Sub-Saharan Africa (Figure 4.9(d)) shows higher exposure and model divergence than the first two regions. Results for other regions are shown in the Appendix.
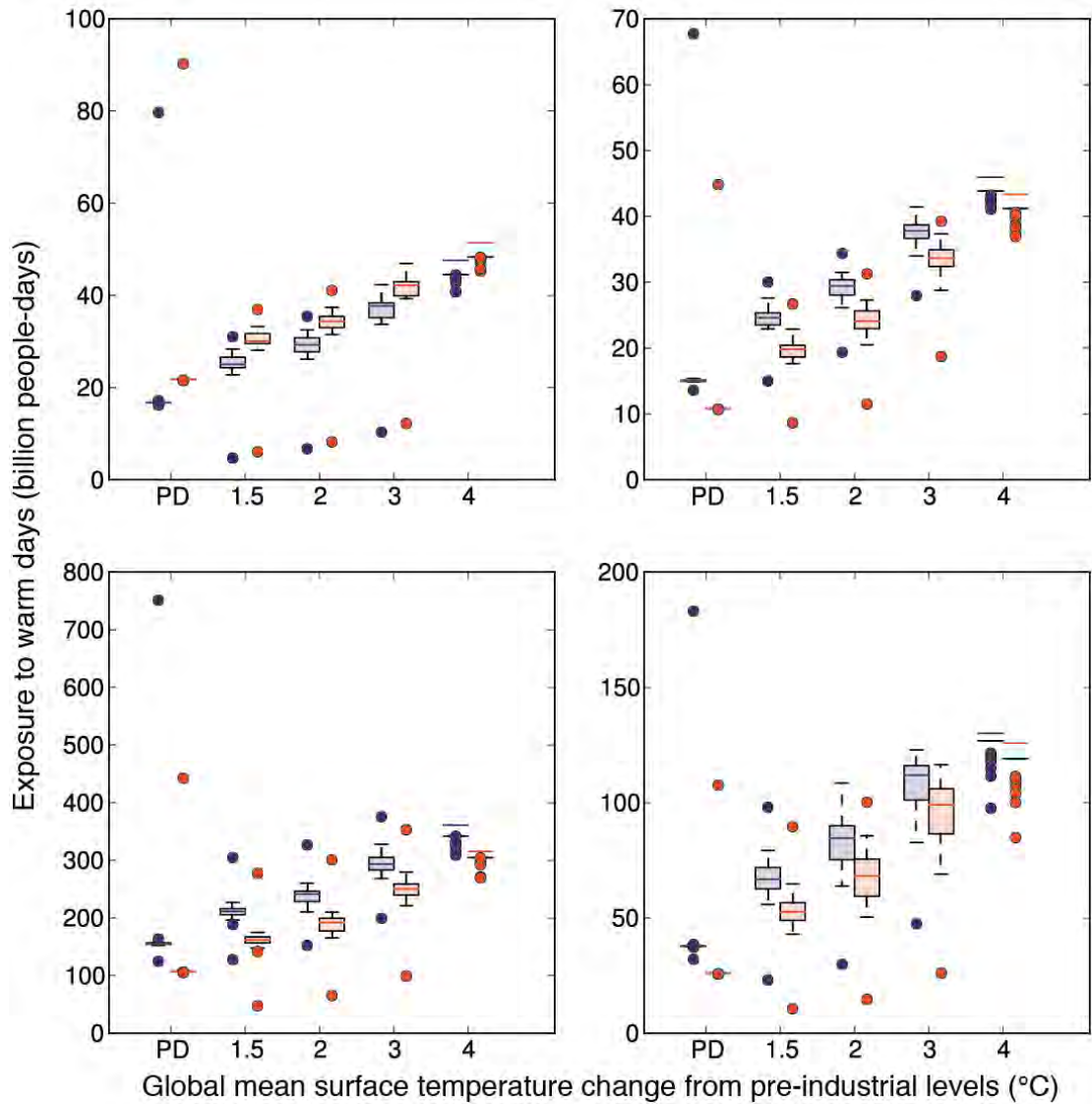
Figure 4.9: Total warm day exposure (warm days multiplied by population count) defined using the spatially varying percentile (purple) and the 81st percentile (orange) thresholds for (a) North America, high income, (b) Latin America, tropical, (c) Asia, south, (d) Sub-Saharan Africa, east. Boxes show the interquartile range of CMIP5 models, whiskers show the most extreme data points within 25%-75% data range, and outliers are data points outside this range. There were only 16 models that reached the 4 °C target.

Higher projected exposure of a population to warm days in the future does not necessarily mean there will be higher impacts, which will depend on a region's ability to alter future exposure to risks or recover from losses related to climate change (i.e. adaptive capacity) (Vincent, 2007). For example, an increase in temperatures may mean

more buildings have air conditioning installed, reducing the exposure to higher temperatures. Therefore, I introduced a vulnerability index, which accounts for a region's exposure, sensitivity, and adaptive captivity to warm days. Since policy decisions are usually made at country-level, I assess how vulnerable countries are to the projected number of warm days, assuming a present-day adaptive capacity. The methods for calculating the exposure, sensitivity, and vulnerability indices were based on methods used by Allison et al. (2009), and are described below. I only calculate exposure and vulnerability for 148 countries, presenting those that are resolved on a 2° x 2° grid.

To calculate the exposure index, I took the population-weighted average number of warm spells over each country and normalised them so that each country had an exposure index between 0 and 1. To normalise the data I used:

$$z_i = \frac{x_i - \min(x)}{\max(x) - \min(x)}$$
(4.2)

where x refers to all the population-weighted average number of warm spells and z_i is the ith country's normalised data.

While there are many factors that make a population more sensitive to higher temperatures than others, such as low education level (Huang et al., 2015; O'Neill et al., 2003), I used the old age dependency ratio. The old age dependency ratio is the number of people over 65 years as a percentage of the working-age population, and several studies have found that the elderly may be the most vulnerable to elevated ambient temperatures (Baccini et al., 2011; Basu and Ostro, 2008; Flynn et al., 2005; Gouveia et al., 2003). I used the projected value for 2025 (the mean year when models reach 1.5 °C) provided by The World Bank Group (The World Bank Group, 2017a).

These data were normalised using the same method as equation 4.2 so each country had a sensitivity index between 0 and 1.

The adaptive capacity of a country refers to its ability to change the exposure to climate change risks. I estimated the adaptive capacity (AC) using 2015 values for health-adjusted life expectancy (HALE) from The World Health Organisation (WHO, 2016) and total GDP for 2010 (I used 2007 values for Syrian Arab Republic) from The World Bank Group (The World Bank Group, 2017b). These values were normalised and averaged together to get an AC, which was then inverted by calculating $(1 - AC)$. From this analysis the USA had the highest AC, therefore had the lowest score, and Sierra Leone had the highest index score because it had the lowest AC.

Figure 4.10 shows that most of the least sensitive countries to warm days (as defined by the old age dependency ratio) were in Africa. However, many of these countries had the lowest ability to adapt (as defined by their HALE and GDP). Likewise, the countries with the highest sensitivity index were generally the ones with the most ability to adapt.

Factors that determine the adaptive capacity and sensitivity of countries may explain the outliers in Figure 4.1 (i.e., cities further away from the MMP = T^3 line). For example, many cities in China and Japan had an MMP above the estimated MMP and both countries have a high capacity to adapt. On the other hand, the MMP of many cities in Canada and Brazil are below the estimated MMP and they have a high capacity to adapt. Canada does have a high sensitivity index (age dependency ratio), so it could be that more focus on preventing heat-related mortality in the elderly population would lead to a higher MMP.

The vulnerability index could be constructed using exposure, sensitivity, and AC in various different ways. Therefore, I calculate the exposure index using two different

methods: 1) an unweighted mean (W1) and 2) a weighted mean, where the AC index was worth half and the exposure and sensitivity indices were worth a quarter (W2) as shown in Figure 4.10(a). An unweighted mean is a more transparent approach, whereas AC having double the weighting is implicit in the IPCC Vulnerability Framework and adapted from a figure by (Johnson and Welch, 2009). Allison et al. (2009) found that the results using both methods were highly correlated (r = 0.96 for the two scenarios determining development and emissions).

Similarly, vulnerability index correlation results between the two threshold definitions is high (W1 r = 0.84 and W2 r = 0.91). Correlation is lower for W1 because the exposure index has more weight than for W2 and the exposure index is the only index affected by the choice of threshold. Therefore, using a spatially varying MMP is less important if adaptive capacity is given a higher weighting as differences between countries is taken into account.
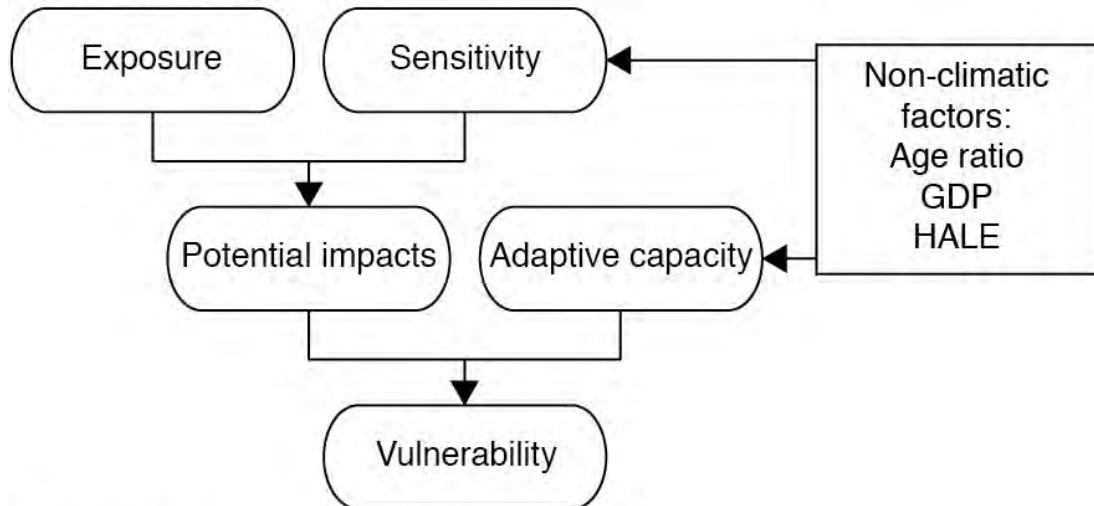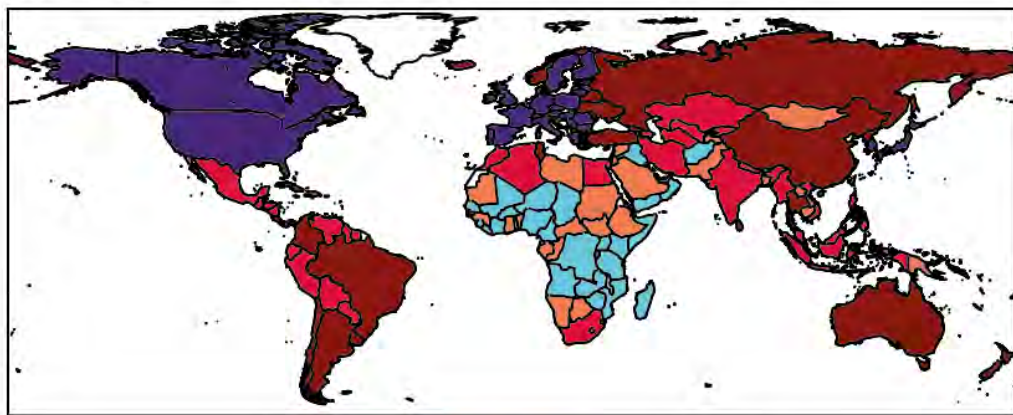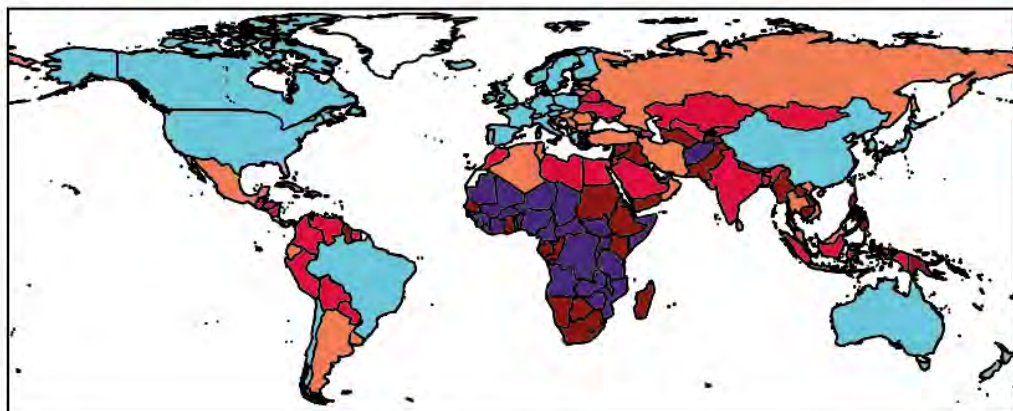
Figure 4.10: (a) Summary of how we quantified vulnerability, based on the IPCC Vulnerability Framework and adapted from a figure by (Johnson and Welch, 2009). Quintiles for each county's (b) sensitivity index, which is defined by a normalised value of elderly population as a percentage of working population and (c) inverted adaptive capacity, defined by an average of normalised HALE and GDP values. Colours represent quintiles, where purple (teal) countries have the highest (lowest) sensitivity index or lowest (highest) ability to adapt. Countries with missing data are white.

Figure 4.11 shows several countries (e.g., Colombia, Democratic Republic of the Congo, Indonesia) had the highest exposure to warm days using both a spatially-varying and constant percentile threshold definition of a warm day. Likewise, some of the cooler countries like Canada had the least exposure to warm days using both threshold definitions. Pakistan and Iraq were in the lowest quintile for exposure using the 81st percentile and in the middle quintile using the spatially varying definition. Neither of these countries were included in the studies by Gasparrini *et al.* (2015) or Honda *et al.* (2014).
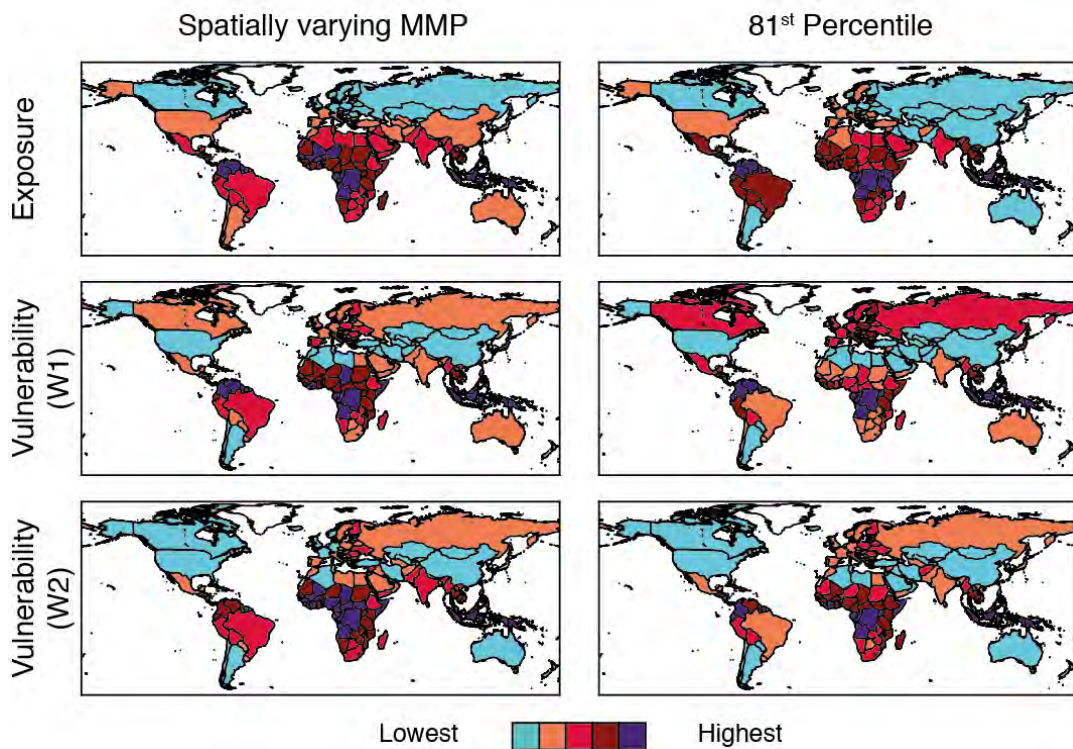
Figure 4.11: The normalised exposure index (top row), defined by the population-weighted mean number of warm days per year; the normalised vulnerability index using the mean of exposure, sensitivity, and AC indices (W1); and the normalised vulnerability index using the weighted mean. Colours represent quintiles, where purple is the highest exposure/vulnerability index and teal represents the lowest exposure/vulnerability. Countries that do not have enough data to calculate the vulnerability index are white.

Several countries (e.g., Democratic Republic of Congo and Indonesia) are in the highest quintile for vulnerability whichever weighting or threshold definition you use, as well as being in the highest quintile for exposure. Whereas the vulnerability index for countries like Japan depend on how much you weight their sensitivity (i.e., aging population ratio) when calculating how vulnerable they are. However, the correlation between the vulnerability indices using the two weighting factors was high (for the spatially varying percentile r = 0.92 and using the 81st percentile as the threshold r = 0.89).

4.6   Discussion

Several studies have assessed future temperature-related mortality using constant percentiles from the daily mean or maximum temperature distribution (Honda et al., 2014; Takahashi et al., 2007; Vardoulakis et al., 2014; World Health Organization, 2014) or they have avoided projecting temperature-related mortality in data-sparse regions altogether (Gasparrini et al., 2017). In this study, I addressed both of these issues by estimating an MMP that varies regionally (between grid squares) based on a statistical relationship between the MMP and the average daily mean temperature. Overall, I find that using a constant percentile to project global exposure to, or mortality from, high temperatures could potentially underestimate health impacts in vulnerable regions, thus underestimating inequalities of climate impacts between countries. While some studies (Gasparrini et al., 2017; Hajat et al., 2014) use region specific MMPs and exposure-response functions based epidemiological studies, it means that there are large areas of the globe with no temperature-related mortality projections. Furthermore, many countries lacking data have warmer climates, which may mean that they have a lower MMP (Figure 4.1(b)): i.e., the mortality associated with higher temperatures starts at a

lower temperature than would be projected with a constant percentile. Additionally, in countries with sufficient mortality and temperature data, Gasparrini *et al.*, (2017) found that tropical countries had the largest increases in temperature-related excess mortality with time under RCP8.5 scenario.

I used a simple regression model to estimate the MMP for each populated grid-square across the globe. It is important to note that I cannot validate my findings for many regions due to the lack of epidemiological studies estimating the MMP, and this underscores the need for additional data in these regions where data is scarce (Campbell-Lendrum et al., 2007). Nevertheless, a simple relationship between average temperature and MMP is evident ((b)), and this study is primarily aimed to illustrate the effect of employing a spatially-varying impact thresholds when quantifying global-scale changes and impacts. Furthermore, my estimates of MMP can be expanded and adapted to suit future studies. For instance, while I define the OT as the temperature at which human mortality increases, future work could estimate temperatures at which hospital admissions increase. However, more heat-related morbidity epidemiological studies outside the USA and Europe with consistent methodology will be required (Ye et al., 2011).

In this study, I only look at changes in daily mean temperature, although there is no single measure of temperature that best predicts human mortality (Barnett et al., 2010). Therefore, future work could use similar regression model methods to estimate OT/MMP using other simple metrics, such as daily maximum temperature. Though, I chose to use daily mean temperature results from Gasparrini *et al.* (2015) because it was a large study that covered 13 different countries. Likewise, future work could take other meteorological conditions, such as relative humidity, into account and use a metric like

'apparent' temperature (Steadman, 1984). Humidity affects latent heat loss via the evaporation of sweat (Hanna and Tait, 2015), which means that it could 'feel' warmer when the relative humidity is high, and could help determine whether a warm spell or heatwave is deadly or not (Mora et al., 2017). More advanced data modelling methods (e.g., Gaussian processes, or machine learning tools) may also provide new insight into the interrelationships of impacts and meteorological conditions.

The spatially-varying MMP model applied a single value to each location and did not account for any differences in economic status, gender, or age distribution of the local population. Therefore, I did not consider future changes in socioeconomic inequality (Curriero et al., 2002; Naughton et al., 2002) or other factors that may affect the MMP.

Likewise, I did not consider how actual exposure to high temperatures (e.g., higher population working outdoors on hot days) varies spatially. Different proportions of the population being outdoors or not having access to air conditioning or drinking water inside their homes may affect MMP and dose-response curves. Ingole et al. (2017) found that the relative risk for heat-related mortality above a particular temperature was higher for those working in farming or manufacturing occupations and those living in poor quality housing. Therefore, the proportion of people working outdoors or living in houses without air conditioning may affect the MMP and dose-response curve. Future studies could explore ways of calculating a geographically-varying dose-response curve that takes into account exposure of a population. However, the mortality data I used for this study only involves the general population for each area and it would be difficult to assess the number of people with outdoor occupations and poor quality housing that mean they are more often exposed to high temperatures.

Additionally, the resolution of the models used in the study meant that I could not account for the urban heat island effect, which may affect future exposure due to the global population living increasingly in urban areas, especially in developing countries (Heilig, 2012).

I made the assumption that there has been no adaptation since the multi-country study by Gasparrini et al. (2015), meaning that I avoid modelling any future acclimatisation or adaptation. Although this is not realistic, and some studies have sought to estimate adaptation to temperature changes, there are significantly fewer studies on adaptation to high temperatures in low-income countries (Berrang-Ford et al., 2011; David M Hondula et al., 2015). In any case, adaptation to warmer temperatures involves complex socioeconomic changes, and projecting future policy and infrastructure is beyond the scope for this study. Therefore, in projecting impacts I assume a worst case scenario, where there is no acclimatisation or adaptation to warmer temperatures and to highlight the need for adaptation, especially in tropical countries, many of which have low capacity to adapt and high exposure to non-optimal temperatures.

In future work, spatially varying MMPs, dose-exposure functions, and adaption functions could be estimated using some of the criteria used to calculate the vulnerability or sensitivity metrics in this study or by Allison et al. (2009). For instance, WHO (2013b) defined 0% adaptation as using an OT that is the MMP of a "present-day" climate, 100% adaptation as using an OT that corresponds to the MMP using a future climate (e.g., +2 °C, 2071-2100), and 50% adaptation as halfway between the two OT values. There could be a spatially-varying or country-level adaptation estimation based on values a regression between changes in OT or MMP over a

particular amount of time and values like HALE and GDP/capita. There is some evidence for a shift in OT over a 23 year period in Japan (Honda et al., 2006)nsiv

In terms of global mean surface temperature changes, I found that under high greenhouse gas emission scenario, RCP8.5, all models used reach a +3 °C climate, and 21 out of 29 models reach +4 °C by the end of the century. There is an increase in the number of warm days and the duration of warm spells with ΔGMST for both threshold definitions, but warm days are more frequent and warm spells are generally longer in tropical countries using the spatially varying percentile. Exposure to detrimental temperatures will be highest in tropical regions, including many low- and middle-income countries, where governments are currently less likely to be investing in pro-active adaptations (Berrang-Ford et al., 2011).

One of the United Nations' Sustainable Development Goals (SDGs) is to reduce inequality within and among countries (UN, 2015). It is clear that some countries are more vulnerable to the impacts of climate change than others. The ideal Shared Socioeconomic Pathway (SSP) for low challenges to mitigation and adaptation is SSP1 – "Sustainability – Taking the Green Road" (Riahi et al., 2017). Policy-makers in high and middle income countries need ensure other countries are not left behind, rather than just focussing on local issues. To achieve climate-resistant development technology, capacity, and resources need to be transferred between developed and least developed economies (Serôa da Motta, 2019). Some countries, like the USA, have a large spread in MMPs at similar mean temperatures, so there needs to be improvements in education and infrastructure in places that have similar climates but worse outcomes within countries too.

4.7   Conclusions

Previous global studies on heat-related mortality assume that a constant percentile-based threshold accounts for regionally-varying tolerances to warm days. I explored the implications of this assumption by comparing the human exposure to non-optimal temperatures using a varying and constant percentile-based threshold, and I found that the distribution of warm days and health impacts differ between threshold definitions. Although, there is a growing body of work that examines regional differences in sensitivity to temperature, there is less work on long-term adaptation to high temperatures in populations outside of Europe and the USA, which includes many countries with lower capacity to adapt to change. For example, in this study, I project that most of the countries with the highest exposure and vulnerability to warm days are in Africa.

There are other communities that commonly use constant thresholds to determine human health impacts, such as global studies on air quality, where thresholds and dose-response relationships are biased towards epidemiological studies on USA and European populations. Therefore, future global studies on air quality or climate impacts should consider ways of estimating differences in susceptibility of populations.

5 Summary and conclusions

This thesis has investigated the impacts of the Paris Agreement temperature goals and air quality policy, and it has contributed to a better understanding of:

1. a) Potential changes in surface ozone and chemistry-relevant physical climate for ΔGMST of 1.5 and 2 °C

2. The role that air quality policy played in air pollution during the European heatwave in 2003 and what impact the heatwave would have on air pollution and human health if it occurred in 2030 (using RCP2.6 and RCP8.5 pollutant emissions)

3. The spatial variation of an optimal temperature for human health and changes in human exposure and vulnerability to temperatures above optimal temperature with ΔGMST

5.1 Summary of chapter conclusions

5.1.1 Chemistry-climate interactions as a function of global mean surface temperature change

Tropospheric ozone is a greenhouse gas and near the surface it can have a detrimental effect on human and plant health. As the surface warms, there is expected to be an increase in air pollution extremes, termed the "climate penalty", which could potentially reduce the benefits of air pollution mitigation policies (Jacob and Winner, 2009).

Chapter 2 presented a study of potential changes in surface ozone and in physical climate that could affect surface ozone.

Keeping anthropogenic precursor emissions constant, there was a positive correlation between GMST and yearly average surface ozone (using ACCMIP models) over eastern USA, Brazil, and South-East China. Regions that see an increase in ozone with increases in GMST, may be the same areas that have the highest air quality gains from climate mitigation without any further air quality policy. Garcia-Menendez et al. (2015) found that limiting ΔGMST to 1.5 °C led to ozone air quality gains over eastern USA. Likewise, a 3.4 W/m^2 emissions pathway led to lower ozone air pollution over eastern China compared to a no mitigation scenario (Xie et al., 2018). The co-benefit of reducing surface ozone pollution could motivate policy makers in these countries to go beyond meeting their Nationally Determined Contribution targets and aim for a ΔGMST of 2 °C. This is without accounting for pollutant emissions that decrease in parallel with greenhouse emissions (e.g., renewable energy technology replacing natural gas). Taking this into account, Vandyck et al. (2018) found that average levels of ozone decrease everywhere by 2050 following a trajectory consistent with a 75% chance of a ΔGMST equal to or less than 2 °C.

Yearly average surface ozone, using CMIP5 output, was lower for +1.5 and +2 °C than present-day for most of the world using both RCP4.5 and RCP8.5. The 0.5 °C difference in GMST generally had a smaller effect on the change in average surface ozone than the emissions scenario, emphasising the importance of anthropogenic emissions. Similarly, in research by Fang et al. (2013), modelled changes in global mortality associated with changes in long-term ozone levels (from 1860 to 2000) were mostly driven by changes in emissions of short-lived air pollutants. In addition, in some regions

there was an increase in ozone for a +2 °C climate, which reflects the difference in anthropogenic emissions of methane, a precursor of ozone, between the two scenarios. For both scenarios, NO_x emissions generally decrease over time, but methane emissions increase for RCP8.5.

Regarding changes in seasonal air quality, there is a positive correlation between monthly-average MDA8 ozone and daily maximum surface temperature for mainland Europe and eastern USA in August. The gridded TOAR dataset is the world's largest collection of homogenous surface ozone observation (Schultz et al., 2017) and trends in TOAR data over time have been explored before (Chang et al., 2017). However, exploring the relationship between surface ozone and monthly mean daily maximum temperature has not been done before with TOAR data.

5.1.2 Avoided and potential air pollution levels and health impacts: The 2003 European heatwave as an exemplar extreme event

Future heatwaves are projected to increase in duration and intensity due to climate change; severe heatwaves, such as the European heatwave in 2003, are expected to become more commonplace (Christidis et al., 2015). In the absence of air quality legislation, the air pollution during the 2003 European heatwave could have been much worse, therefore illustrating the need for air quality policy in a climate with increasing daily maximum temperatures. Avoided $PM_{2.5}$ concentrations during this extreme event were much more drastic than changes in ozone: air quality measures more than halved $PM_{2.5}$ concentrations for most of Western Europe. This illustrates the health benefits of air quality policy during an extreme event, which should be accounted for when considering the costs of infrastructure to reduce emission factors.

There were three methods for estimating world avoided emissions: scaling 1970 emissions by 2003 population and GDP, scaling 1970 emissions only by population, and just using 1970 emissions. Accounting for changes in GDP made a substantial difference in emissions compared to just scaling by population (or not scaling at all). However, if pollutant emissions in a "world avoided" grow in a similar way to CO_2 in Newly Industrialised Countries then scaling with GDP and population, estimates are particularly pessimistic. This scenario where emissions are scaled by GDP and population serves as an extreme "worst case" scenario rather than a realistic one. Therefore, I focus on results from emissions only scaled by population as they are more likely to reflect what could happen in reality without emission controls.

Despite the increase in population in 2030, relative risk of mortality due to both $PM_{2.5}$ and ozone concentrations were lower than the control scenario using RCP2.6 and RCP8.5 2030 emissions. Considering temperatures during the 2003 heatwave will be more common in 2030, this highlights the potential of further emission reductions to policy makers.

5.1.3 A spatially varying definition of warm days: estimating impacts on populations for 1.5, 2, 3, and 4 °C warmer worlds

Changes in surface temperatures with ΔGMST are heterogeneous and the health impacts of these changes will vary between populations. Taking the example of an optimum temperature for human health, above which human mortality starts to increase, it varies between regions and is usually positively correlated with average temperature due to acclimatisation. The optimum temperature is one of the ingredients used to estimate future human mortality due to rises in temperature. Some studies estimate this optimal

temperature using a percentile (minimum mortality percentile; MMP), which is usually based on epidemiological research in various countries, usually those in North America and western Europe. However, there is a lack of studies on temperature-related mortality in Africa, the Middle-East, and south Asia. Some global studies have used the same percentile to quantify heat-related human mortality for each country (World Health Organization, 2014) and others have avoided projecting mortality in countries that lack data (Vicedo-Cabrera et al., 2018).

I find that the MMP decreases with average temperature, rather than being approximately constant globally, so increases in heat-related mortality may start earlier for warmer regions, meaning that differences in exposure to unhealthy temperatures between countries may be underestimated in global projections.

I find that yearly-average temperature explains about 60% of the variance in the MMP for each location in the study by Gasparrini et al. (2015) and this relationship can be used to estimate an MMP for each grid cell when projecting mortality with model temperature projections. This could be helpful to project mortality in regions with fewer mortality and temperature data.

Similar research by Yin et al. (2019) estimated the minimum mortality temperature (or optimum temperature for human health) using the most frequent temperature (this had a higher correlation than annual mean temperature). However, estimating a percentile-based metric may be more helpful than an absolute temperature for projecting human mortality using climate models because it may be less affected by model bias.

Warm days and warm spells are defined using (1) a constant and (2) the spatially varying percentile. The frequency in warm days and duration of warm spells increase

with ΔGMST for most regions using both definitions. The minimum and maximum duration of a warm spell increases for more than 28 days between +1.5 and +2 °C climates for most of the tropics using two different definitions. For a +4 °C world the maximum duration of a warm spell is over 100 days for most of the globe using a constant percentile definition and is over 200 days long for the tropics using either definition.

For a +1.5 °C world, the most vulnerable countries to the increase in warm days (defined by a spatially varying percentile) are in Africa apart from Papua New Guinea, reflecting their high level of exposure and lower capacity to adopt. Using a constant percentile, there were fewer African countries in the top quintile for vulnerability and more in south-east Asia and South America meaning that the need for adaptation in some African countries may be greater than expected if the majority of global projections are using a constant percentile.

5.2 Overall conclusions and limitations

ACCMIP model output only includes times slices for 2000, 2030, and 2100, rather than a continuous simulation from 2000 to 2100. Therefore, it is not possible to compare models when they reach a particular ΔGMST.

There is a positive correlation between the model ΔGMST and the yearly-average surface ozone over eastern USA, Brazil, East China, and North India using constant anthropogenic pollutant emissions. However, there is a negative correlation using CMIP5 model output over eastern USA using RCP4.5 and RCP8.5, showing the potential for pollutant emission reductions to improve air quality despite the negative effect of climate change on surface ozone in the USA. The importance of air quality

policy is also demonstrated by larger increases in ozone for almost everywhere using RCP8.5 compared to RCP4.5.

When investigating the impacts of ΔGMST, I sub-selected CMIP5 models based on their global temperature response. Hence, differences between +1.5 and +2 °C climates may be due to parameter uncertainty rather than the 0.5 °C ΔGMST (James et al., 2017). It also assumes that the impacts of ΔGMST are independent of the path towards the ΔGMST target. One example where path dependency made a difference was when estimating isoprene emissions, CO_2 concentration was dependent on the year when the model reached the ΔGMST target. Higher CO_2 levels also make a difference to temperature extremes (Baker et al., 2018), which would impact surface ozone extremes and heat-related health impacts. If I had more time and space to store processed data, I would look at increases in warm days using RCP2.6 as well as RCP8.5.

In Chapters 2 and 4, I used time periods of 30-years to represent +1.5 and +2 °C worlds, consistent with the World Meteorological Organization (WMO) "climate normal" (WMO, 1989). This method has been used in various studies (Vautard et al., 2014) and others have used a 20-year averaging period . However, the "climate normal" could be defined by another averaging period length or averaging method (e.g., median) (Arguez and Vose, 2011). With more time, I would have found periods corresponding to different ΔGMST using several methods and varying averaging period length and assessed what difference it makes to results. Similarly, with more time and space for data processing I would compare RCP scenarios with the same ΔGMST to assess the impact of pathway. For instance, does a +1.5 °C world look the same at the end of the century for a high mitigation scenario as it would for RCP8.5 with rapid global

warming? Regional change may be sensitive to the rate of warming or be affected by aerosol emissions.

Future heatwaves similar to the European heatwave in 2003 are projected to be more likely as ΔGMST increases and they are associated with poor air quality. Anthropogenic emissions also substantially contributed to air quality during the 2003 heatwave. This indicates the importance of air quality legislation and long-term changes in technology rather than relying on short term measures, such as reduced vehicle usage during the heatwave. "Emergency" emission scenarios may be difficult to implement in some countries and planned emission reductions for 2010 would have been more effective than the 20% reduction in road traffic after the start of the heatwave (Vautard et al., 2005). One limitation to the world avoided estimates is that I scaled all emissions (over land) by gridded population, regardless of sector. Agricultural production of emissions, for instance, will not scale with gridded population. Therefore, benefits of emission reductions may have been overestimated or underestimated in some areas.

I demonstrated that future RCP emission scenarios also improve air quality during a heatwave in Europe meaning that there is still potential to reduce risks during future heatwaves by introducing further legislation despite the growing population.

Estimates of health impacts of climate change may be less reliable in developing countries if the calculations are based on epidemiological studies from wealthier countries. I illustrate this point in chapter 4 by using a spatially varying percentile where heat-related mortality is minimum. However, the spatially varying MMP was based on a simple linear model and only took average daily mean temperature into account. It did not include any African, South Asian, or Middle Eastern countries, although it did have some MMP results from low- and middle- income countries. Also, acclimatisation is

not taken into account as this was for a worst case scenario where developing countries needs were not taken into account.

I conclude in Chapter 3 that emission reductions due to policy and technological advancements reduce the number of premature deaths during an extreme event. In Chapter 4 I find that in the absence of adaptation and mitigation there will be increase in exposure to days where the temperature is above the optimum temperature. These results underline the need for decision-makers to introduce policy that makes it easier to adapt to a changing climate. For example, local government could introduce maximum outdoor and indoor temperatures, above which employers must provide paid leave to workers who would be exposed to these temperatures.

Analysis in Chapter 4 was done with CMIP5 models that were too coarse to consider the urban heat island effect or differences between communities in a region. There will be differences in age, gender, health and socioeconomic status between people within a grid cell, which will affect their exposure to pollution and high temperatures (e.g., they may be more likely to work outdoors) and their tolerance (e.g., a town with a high age ratio may be more vulnerable to high temperatures).

5.2.1 Key points for decision makers

1) Although climate change will increase yearly average surface ozone in some regions, a 0.5 °C difference in ΔGMST (+1.5 vs +2 °C) has less of an impact than the difference between emissions for RCP4.5 and RCP8.5 scenarios.

2) In Europe, air quality policy since 1970 had a beneficial impact on $PM_{2.5}$ during the 2003 heatwave, reducing the risk of pollution related deaths. Unfortunately, levels of surface ozone were higher in some areas than they would have been

without reduction in emissions due to titration. However, with further emission reductions, most of Europe will also see benefits of surface ozone reduction during similar heatwaves. This long-term approach to reducing emissions is especially beneficial for countries that would find it difficult to implement emergency measures.

3) When quantifying the health impacts of climate change globally, the disparity in ability to adapt needs to be taken into account. Many of the areas that have high exposure to health-related impacts and less ability to adapt to climate change (i.e. are more vulnerable to climate change) have contributed least to climate change (Herold et al., 2017). Therefore, as well as taking more responsibility for climate change mitigation, wealthier countries should share adaptation knowledge, expertise, and resources with areas at higher risk. The successes of policy in richer countries, such as reduction in air pollution shown in Chapter 3, should be applied to more vulnerable countries.

5.3 Direction of future work

5.3.1 Future modelling experiments

There is a growing body of research looking at the impacts of +1.5 and +2 °C worlds (Hoegh-Guldberg et al., 2018), however very little of that addresses changes in atmospheric chemistry. This is partly because analysing changes in climate indices as a function of ΔGMST is much more accessible due to the continuous nature of CMIP5 simulations, whereas ACCMIP models only provided historical, 2030, and 2100 time-slice experiments. A multi-model ensemble of chemistry-climate models (CCMs) with chemistry output at different ΔGMST targets (with constant anthropogenic air pollutant

emissions) would improve understanding of the impacts of policy-relevant climate change on air quality. However, it is computationally expensive to run this type of model.

Fortunately, some models as part of the CMIP phase 6 (CMIP6) will be focusing on the feedbacks between climate change and atmospheric chemistry, as part of the CMIP6-endorsed model interdisciplinary project (MIP), Aerosols and Chemistry MIP (AerChemMIP) (Eyring et al., 2016). Aims of AerChemMIP include exploring and how future policies may affect the abundances of near term climate forcers and how anthropogenic emissions affect (Collins et al., 2017). There are variations on the SSP3-7.0 scenario, which is associated with the medium to high end of the range of future forcing pathways for CMIP6 with a relatively high societal vulnerability (O'Neill et al., 2016). Some simulations involve prescribed sea-surface temperatures (SSTs), but different anthropogenic emissions to investigate impacts of climate change on atmospheric chemistry. The reference scenario will see aerosol and ozone precursors evolve as expected with the scenario (ssp370SST), another will have "cleaner" near-term climate forcer emissions (very low ozone precursor emissions due to strict air pollution policies; ssp370SST-lowNTCF), and one will have only lower methane emissions with all other emissions as expected (ssp370SST-lowCH4). Comparison of these scenarios would show you the impact of air quality policy. There are also the equivalent simulations without prescribed SSTs.

To get a sense of the impact of climate change, I would compare the same time-period for ssp370SST-lowNTCF and ssp370-lowNTCF (SSP3-7.0 scenario with low anthropogenic NTCF emissions and associated radiative forcing), as shown in Table 5.1. The same time period for each model will have the same anthropogenic NTCF

emissions, but a different ΔGMST because of the radiative forcing from the NTCF. Therefore, I would find a time period where the ΔGMST is around 0.5 °C lower for the ssp370-lowNTCF scenario and compare surface ozone levels. I would also look at ssp370-lowCH4 (SSP3-7.0 scenario with low anthropogenic methane emissions and associated radiative forcing) for the same time period to see surface ozone at another ΔGSMT.

Table 5.1: Potential experiment to explore the impact of ΔGMST on surface ozone using model simulations from CMIP6

Parameter	Scenarios: ssp370SST-lowNTCF, ssp370-lowNTCF
Time	Same 30-year period
Anthropogenic emissions	Same - low
ΔGMST	Around 0.5 °C difference

It is possible to simulate air pollution using a chemical transport model (CTM) and use the time period when the global climate model (GCM) that drives it reaches a 1.5/2 °C ΔGMST. This has been done to assess the impact of a +2 °C climate and anthropogenic emissions separately on ozone, NO_2, and PM_{10} in Europe (Lacressonnière et al., 2017; Watson et al., 2016). They found that the effect of 2 °C ΔGMST was small compared to the impact of anthropogenic emission reductions. It is good news for policy-makers that a ΔGMST of 2 °C has less of an impact on pollution than future emission reductions. Is this the case outside of Europe?

Lacressonnière et al. (2017) and Watson et al. (2016) focus on annual and seasonal mean pollution. The potential of emission reductions during extreme events typical in a +2°C world versus "present-day" or a +1.5 °C may tell a different story. Using results from global climate models as boundary conditions, numerical weather prediction models can provide high-resolution of high-impact weather in a future climate (Hazeleger et al., 2015). One possible way of comparing the impact of climate change versus emissions scenario on air quality during an extreme event would be to simulate air pollution during projected heatwaves for a present-day and +2 °C climates (finding the worst heatwaves in the same location using the heatwave magnitude index daily (Russo et al., 2010)) using two different emissions scenarios, for example those shown in Table 5.1.

Table 5.2: Possible experiments to assess the impact of climate change and anthropogenic emissions on air quality during an extreme event.

Experiment	Climate that the heatwave occurs in	Emission scenario
Control	2003	2010
Cl2003Em2050	2003	2050 (RCP2.6)
Cl2Em2010	+2 °C	2010
Cl2Em2050	+2 °C	2050 (RCP2.6)

The models used in Chapter 3 were low resolution, which meant that ozone concentrations may be biased due to the nonlinear relationship between ozone

precursors as well as the resolution of the meteorological drivers. It was also not possible to assess urban air quality. In future "world avoided" studies that are focused on extreme events rather than long-term impacts of policy it would be ideal to use models with finer resolution. Markakis et al. (2015) found no significant difference between a 4 km and a 0.5° resolution model for ozone or $PM_{2.5}$ simulations, so it would be helpful to explore the difference in bias between the 0.5°, 1°, and 1.9°x2.5° models. The low resolution models could be downscaled to 0.5° and a weighted mean could be taken from the three models based on performance (e.g., inverse of standard deviation from observation).

5.3.2   Human health impacts

In Chapter 3, premature deaths due to air pollution were estimated using the same relationship for every European country. Although this illustrates the health impacts of air quality legislation, applying the same calculation to regions outside of Europe may underestimate or overestimate the impacts, therefore may underestimate health inequalities between regions. Plus, there are differences in relative risk between places in Europe (Katsouyanni et al., 1997; Vicedo-Cabrera et al., 2020).

Most epidemiological studies on pollution-related mortality are done in Europe and the USA. Therefore, more epidemiological research needs to be done on pollution-related mortality in developing countries to see how relative risk with pollution varies between regions. It is possible that applying exposure-response curves found from studies based in Europe on changes in Africa, for example, may give unrealistic results. However, various barriers exist, such as, access to reliable air quality monitoring and records of morbidity and mortality.

Future human health impact assessments could be improved by developing spatially varying health metrics. For example, There is a reverse significant relationship between the human development index (HDI) and the mortality incidence ratio for lung cancer (Rafiemanesh et al., 2016). Although all the lung cancer in this study may not have been caused by air pollution, I think that it shows potential for future work exploring the relationship between the HDI and exposure-response functions for pollution-related mortality. In Chapter 3, I use the same relative risk for each level of ozone/$PM_{2.5}$ for the whole of Europe. However, Vicedo-Cabrera et al. (2019) found that out of 20 countries, the United Kingdom had the largest relative risk per 10 $\mu g/m^3$ increase in ozone of 0.0035 (95% CI: 1.0024 to 1.0046) and Spain had the lowest of 1.0006 (0.9992 to 1.0019) relative risk per 10 $\mu g/m^3$ increase of ozone. Outside of Europe, mortality risk associated with pollution was higher in South Africa than reported in developing countries (Wichmann and Voyi, 2012).

In Chapter 4, a spatially varying percentile is used to estimate an optimal temperature for human health in regions with no epidemiological studies on temperature-mortality relationships. This MMP varied with average temperature and was based on epidemiological results from various regions. Spatially varying optimum temperatures could be defined using different temperature indices (e.g., daily minimum temperature, heat index) and could be improved by finding other variables they may correlate with, such as GDP per capita and most frequent temperature (as in Yin et al., 2019). Likewise, exposure-response curves (slope between excess mortality and temperature) could be found for regions without observations by using finding how they vary in regions with epidemiological studies. Using more advanced methods, such as machine learning, to find how comfort temperatures and temperature/pollution exposure-mortality/morbidity vary with socioeconomic factors and local climate, could help

estimate appropriate thresholds and dose-response relationships for regions with lack of data.

Future studies could take a more holistic approach to impact assessment and consider multiple environmental stressors. The quantitative risk assessment by the World Health Organization (2014) projected change in mortality related to heat, coastal floods, diarrheal, malaria, dengue and undernutrition using three different economic development scenarios for two different time periods (2030s, 2050s). This approach could be applied to +1.5 and +2 °C climates rather than time periods, to assess the benefits of a lower ΔGMST.

Surface ozone has an adverse effect on agricultural yield (Booker et al., 2009; Mills et al., 2007; Pleijel et al., 2000). Before the mortality crisis in early August 2003, there were excessive temperatures and droughts recorded since June (García-Herrera et al., 2010), potentially exacerbating ozone levels, Chapter 3 could have been extended to include this earlier period and assess the impacts of air quality policy on crop yields.

5.3.3 Informing air quality policy

To simulate a world avoided scenario in Chapter 3, I scaled 1970 emissions with population and GDP, whereas previous studies only took the increase in population into account. The increase in emissions when scaled with GDP as well as population was substantial, which might overestimate what emissions would have been without air quality policy. On the other hand, previous research has used emissions scaled by population for "world avoided" scenarios (Archibald et al., 2017; Daskalakis et al., 2016), but I have found that this may underestimate the theoretical world avoided emissions (Table 3.2). Therefore to avoid underestimating potential gains in air quality

similar studies in the future could consider scaling by another factor that accounts for changes in wealth or production and population, such as gross national income (GNI).

Moreover, I only look at the effect of policy on air quality for one extreme event in Europe. However, the methods used can be applied to other extreme weather events associated with heightened air pollution. For example, there were heatwaves in Mexico and Japan in 2018, Mexico enacted its first air pollution regulations in 1971 and Japan introduced a series of air pollution control laws in 1970 (Jacobson, 2002), thus a similar "world avoided" experiment could be carried out for these events. In addition, using previous heatwaves in developing countries as exemplar events, such as the heatwaves in Pakistan and India in 2015, it may be beneficial for decision-makers to compare the impacts of future RCP emission scenarios during those extreme events as well as changes in average pollutant concentration.

To evaluate chemistry model performance in developing regions during extreme events there will need to be hourly and daily observations of pollutants. Although satellite pollution data is helpful when you are looking at the long-range transport of pollutants, ground level measurements are needed to see what is going on at the surface. Specifically, the TOAR dataset (Schultz et al., 2017) - used in Chapter 2 - had few ozone measurements for Africa, Central and South America, Central and South Asia, and the Middle East. Some providers were concerned about misinterpretation or misuse of the data, or they did not support the TOAR open data policy, and some regions did not have ground-level monitoring stations.

In Africa, only around 6% of children live near reliable, ground-level monitoring stations that provide real-time air quality data, whereas about 72% of children in Europe and North America live near reliable monitoring stations (Rees et al., 2019). There are

around 800,000 estimated premature deaths per year in Africa due to air pollution, with PM$_{2.5}$ causing around two thirds of those deaths (Bauer et al., 2019). There is potential to expand air quality monitoring networks with low-cost sensors, particularly passive sensors (i.e. radiometers and spectrometers), in Sub-Saharan Africa (Amegah, 2018). Likewise, similar low-cost sensors can be used in Central and South America, and Central and South Asia.

European emissions of ozone precursors have a substantial impact on ozone levels in North Africa, with many additional deaths in northern Africa and the Near East attributed to emission from Europe (Duncan et al., 2008). Therefore, European air pollution policy and emission reductions should have a positive effect on African air quality. It would be interesting to apply similar methods shown in Chapter 3 to exploring the impacts of European air quality policy on air pollution in northern Africa during a heatwave. To validate model results there would need to be more ozone observations in northern Africa. One cost-effective option would be to use a cost-effective sensor that uses tungsten trioxide (WO_3) semiconductor (Utembe et al., 2006).

Another option to fill in data gaps in urban areas is to use pollution data from Google Street View cars (Apte et al., 2017), which has much lower temporal resolution so would not be ideal for validating air quality during extreme events. However, it has been used to find long-term relationships between health conditions and air pollutants (Alexeeff et al., 2018) so could be helpful in exploring long term impacts in data-poor regions.

6 References

Ackerman, A.S., 2000. Reduction of Tropical Cloudiness by Soot. Science (80-.). 288, 1042–1047. https://doi.org/10.1126/science.288.5468.1042

Aghedo, A.M., Schultz, M.G., Rast, S., 2007. The influence of African air pollution on regional and global tropospheric ozone. Atmos. Chem. Phys. 7, 1193–1212. https://doi.org/10.5194/acp-7-1193-2007

Alexeeff, S.E., Roy, A., Shan, J., Liu, X., Messier, K., Apte, J.S., Portier, C., Sidney, S., Van Den Eeden, S.K., 2018. High-resolution mapping of traffic related air pollution with Google street view cars and incidence of cardiovascular events within neighborhoods in Oakland, CA. Environ. Heal. 17, 38. https://doi.org/10.1186/s12940-018-0382-1

Allison, E.H., Perry, A.L., Badjeck, M.C., Neil Adger, W., Brown, K., Conway, D., Halls, A.S., Pilling, G.M., Reynolds, J.D., Andrew, N.L., Dulvy, N.K., 2009. Vulnerability of national economies to the impacts of climate change on fisheries. Fish Fish. 10, 173–196. https://doi.org/10.1111/j.1467-2979.2008.00310.x

Amann, M., Holland, M., Maas, R., Vandyck, T., Saveyn, B., 2017. Costs, Benefits and Economic Impacts of the EU Clean Air Strategy and their Implications on Innovation and Competitiveness 1–59.

Amegah, A.K., 2018. Proliferation of low-cost sensors. What prospects for air pollution epidemiologic research in Sub-Saharan Africa? Environ. Pollut. 241, 1132–1137.

https://doi.org/10.1016/j.envpol.2018.06.044

Anderson, G.B., Bell, M.L., 2010. Heat Waves in the United States: Mortality Risk during Heat Waves and Effect Modification by Heat Wave Characteristics in 43 U.S. Communities. Environ. Health Perspect. 119, 210–218. https://doi.org/10.1289/ehp.1002313

Apte, J.S., Marshall, J.D., Cohen, A.J., Brauer, M., 2015. Addressing Global Mortality from Ambient PM 2.5. Environ. Sci. Technol. 49, 8057–8066. https://doi.org/10.1021/acs.est.5b01236

Apte, J.S., Messier, K.P., Gani, S., Brauer, M., Kirchstetter, T.W., Lunden, M.M., Marshall, J.D., Portier, C.J., Vermeulen, R.C.H., Hamburg, S.P., 2017. High-Resolution Air Pollution Mapping with Google Street View Cars: Exploiting Big Data. Environ. Sci. Technol. 51, 6999–7008. https://doi.org/10.1021/acs.est.7b00891

Archibald, A.T., Folberth, G., Wade, D.C., Scott, D., 2017. A world avoided: impacts of changes in anthropogenic emissions on the burden and effects of air pollutants in Europe and North America. Faraday Discuss. 200, 475–500. https://doi.org/10.1039/C7FD00004A

Arguez, A., Vose, R.S., 2011. The Definition of the Standard WMO Climate Normal: The Key to Deriving Alternative Climate Normals. Bull. Am. Meteorol. Soc. 92, 699–704. https://doi.org/10.1175/2010BAMS2955.1

Arneth, A., Miller, P.A., Scholze, M., Hickler, T., Schurgers, G., Smith, B., Prentice, I.C., 2007. CO_2 inhibition of global terrestrial isoprene emissions: Potential implications for atmospheric chemistry. Geophys. Res. Lett. 34, L18813.

https://doi.org/10.1029/2007GL030615

Arnone, J. a, Verburg, P.S.J., Johnson, D.W., Larsen, J.D., Jasoni, R.L., Lucchesi, A.J., Batts, C.M., von Nagy, C., Coulombe, W.G., Schorran, D.E., Buck, P.E., Braswell, B.H., Coleman, J.S., Sherry, R. a, Wallace, L.L., Luo, Y., Schimel, D.S., 2008. Prolonged suppression of ecosystem carbon dioxide uptake after an anomalously warm year. Nature 455, 383–386. https://doi.org/10.1038/nature07296

Asseng, S., Ewert, F., Martre, P., Rötter, R.P., Lobell, D.B., Cammarano, D., Kimball, B.A., Ottman, M.J., Wall, G.W., White, J.W., Reynolds, M.P., Alderman, P.D., Prasad, P.V. V., Aggarwal, P.K., Anothai, J., Basso, B., Biernath, C., Challinor, A.J., De Sanctis, G., Doltra, J., Fereres, E., Garcia-Vila, M., Gayler, S., Hoogenboom, G., Hunt, L.A., Izaurralde, R.C., Jabloun, M., Jones, C.D., Kersebaum, K.C., Koehler, A.-K., Müller, C., Naresh Kumar, S., Nendel, C., O'Leary, G., Olesen, J.E., Palosuo, T., Priesack, E., Eyshi Rezaei, E., Ruane, A.C., Semenov, M.A., Shcherbak, I., Stöckle, C., Stratonovitch, P., Streck, T., Supit, I., Tao, F., Thorburn, P.J., Waha, K., Wang, E., Wallach, D., Wolf, J., Zhao, Z., Zhu, Y., 2015. Rising temperatures reduce global wheat production. Nat. Clim. Chang. 5, 143–147. https://doi.org/10.1038/nclimate2470

Athanassiadou, M., Baker, J., Carruthers, D., Collins, W., Girnary, S., Hassell, D., Hort, M., Johnson, C., Johnson, K., Jones, R., Thomson, D., Trought, N., Witham, C., 2010. An assessment of the impact of climate change on air quality at two UK sites. Atmos. Environ. 44, 1877–1886. https://doi.org/10.1016/j.atmosenv.2010.02.024

Baccini, M., Kosatsky, T., Analitis, A., Anderson, H.R., D'Ovidio, M., Menne, B., Michelozzi, P., Biggeri, A., 2011. Impact of heat on mortality in 15 European

cities: attributable deaths under different weather scenarios. J. Epidemiol. Community Heal. 65, 64–70. https://doi.org/10.1136/jech.2008.085639

Baker, H.S., Millar, R.J., Karoly, D.J., Beyerle, U., Guillod, B.P., Mitchell, D., Shiogama, H., Sparrow, S., Woollings, T., Allen, M.R., 2018. Higher CO2 concentrations increase extreme event risk in a 1.5 °C world. Nat. Clim. Chang. 8, 604–608. https://doi.org/10.1038/s41558-018-0190-1

Ballester, J., Robine, J.-M., Herrmann, F.R., Rodó, X., 2011. Long-term projections and acclimatization scenarios of temperature-related mortality in Europe. Nat. Commun. 2, 358. https://doi.org/10.1038/ncomms1360

Bao, J., Wang, Z., Yu, C., Li, X., 2016. The influence of temperature on mortality and its Lag effect: a study in four Chinese cities with different latitudes. BMC Public Health 16, 375. https://doi.org/10.1186/s12889-016-3031-z

Barcikowska, M.J., Weaver, S.J., Feser, F., Russo, S., Schenk, F., Stone, D.A., Wehner, M.F., Zahn, M., 2018. Euro-Atlantic winter storminess and precipitation extremes under 1.5 °C vs. 2 °C warming scenarios. Earth Syst. Dyn. 9, 679–699. https://doi.org/10.5194/esd-9-679-2018

Barnes, E.A., Fiore, A.M., Horowitz, L.W., 2016. Detection of trends in surface ozone in the presence of climate variability. J. Geophys. Res. Atmos. 121, 6112–6129. https://doi.org/10.1002/2015JD024397

Barnett, A.G., Tong, S., Clements, A.C.A., 2010. What measure of temperature is the best predictor of mortality? Environ. Res. 110, 604–11. https://doi.org/10.1016/j.envres.2010.05.006

Basu, R., Ostro, B.D., 2008. A Multicounty Analysis Identifying the Populations Vulnerable to Mortality Associated with High Ambient Temperature in California. Am. J. Epidemiol. 168, 632–637. https://doi.org/10.1093/aje/kwn170

Bauer, S.E., Im, U., Mezuman, K., Gao, C.Y., 2019. Desert Dust, Industrialization, and Agricultural Fires: Health Impacts of Outdoor Air Pollution in Africa. J. Geophys. Res. Atmos. 124, 4104–4120. https://doi.org/10.1029/2018JD029336

Bell, M.L., Peng, R.D., Dominici, F., 2006. The Exposure–Response Curve for Ozone and Risk of Mortality and the Adequacy of Current Ozone Regulations. Environ. Health Perspect. 114, 532–536. https://doi.org/10.1289/ehp.8816

Beniston, M., 2004. The 2003 heat wave in Europe: A shape of things to come? An analysis based on Swiss climatological data and model simulations. Geophys. Res. Lett. 31, L02202. https://doi.org/10.1029/2003GL018857

Berrang-Ford, L., Ford, J.D., Paterson, J., 2011. Are we adapting to climate change? Glob. Environ. Chang. 21, 25–33. https://doi.org/10.1016/j.gloenvcha.2010.09.012

Bharadwaj, P., Gibson, M., Zivin, J.G., Neilson, C., 2017. Gray Matters: Fetal Pollution Exposure and Human Capital Formation. J. Assoc. Environ. Resour. Econ. 4, 505–542. https://doi.org/10.1086/691591

Black, E., Blackburn, M., Harrison, G., Hoskins, B., Methven, J., 2004. Factors contributing to the summer 2003 European heatwave. Weather 59, 217–223. https://doi.org/10.1256/wea.74.04

Bloomer, B.J., Stehr, J.W., Piety, C. a., Salawitch, R.J., Dickerson, R.R., 2009.

Observed relationships of ozone air pollution with temperature and emissions. Geophys. Res. Lett. 36, L09803. https://doi.org/10.1029/2009GL037308

Booker, F., Muntifering, R., McGrath, M., Burkey, K., Decoteau, D., Fiscus, E., Manning, W., Krupa, S., Chappelka, A., Grantz, D., 2009. The Ozone Component of Global Change: Potential Effects on Agricultural and Horticultural Plant Yield, Product Quality and Interactions with Invasive Species. J. Integr. Plant Biol. 51, 337–351. https://doi.org/10.1111/j.1744-7909.2008.00805.x

Box, G.E.P., Draper, N.R., 1987. Empirical Model-Building and Response Surfaces. Wiley.

Brutel-Vuilmet, C., Ménégoz, M., Krinner, G., 2013. An analysis of present and future seasonal Northern Hemisphere land snow cover simulated by CMIP5 coupled climate models. Cryosph. 7, 67–80. https://doi.org/10.5194/tc-7-67-2013

Byers, E., Gidden, M., Leclère, D., Balkovic, J., Burek, P., Ebi, K., Greve, P., Grey, D., Havlik, P., Hillers, A., Johnson, N., Kahil, T., Krey, V., Langan, S., Nakicenovic, N., Novak, R., Obersteiner, M., Pachauri, S., Palazzo, A., Parkinson, S., Rao, N.D., Rogelj, J., Satoh, Y., Wada, Y., Willaarts, B., Riahi, K., 2018. Global exposure and vulnerability to multi-sector development and climate change hotspots. Environ. Res. Lett. 13, 055012. https://doi.org/10.1088/1748-9326/aabf45

Campbell-Lendrum, D., Woodruff, R., Prüss-Üstün, A., Corvalán, C., 2007. Quantifying the health impact at national and local levels. World Heal. Organ.

Center for International Earth Science Information Network - CIESIN - Columbia University, 2016. Gridded Population of the World, Version 4 (GPWv4): Population Count [WWW Document]. Palisades, NY NASA Socioecon. Data

Appl. Cent. URL http://dx.doi.org/10.7927/H4X63JVC (accessed 8.22.16).

Cess, R.D., Udelhofen, P.M., 2003. Climate change during 1985-1999: Cloud interactions determined from satellite measurements. Geophys. Res. Lett. 30, 19-1-19–4. https://doi.org/10.1029/2002gl016128

Chang, K.L., Petropavlovskikh, I., Cooper, O.R., Schultz, M.G., Wang, T., 2017. Regional trend analysis of surface ozone observations from monitoring networks in eastern North America, Europe and East Asia. Elementa 5, 1–22. https://doi.org/10.1525/elementa.243

Chen, C.-H., Chan, C.-C., Chen, B.-Y., Cheng, T.-J., Leon Guo, Y., 2015. Effects of particulate air pollution and ozone on lung function in non-asthmatic children. Environ. Res. 137, 40–8. https://doi.org/10.1016/j.envres.2014.11.021

Chen, Y., Zhang, Z., Tao, F., 2018. Impacts of climate change and climate extremes on major crops productivity in China at a global warming of 1.5 and 2.0 °C. Earth Syst. Dyn. 9, 543–562. https://doi.org/10.5194/esd-9-543-2018

Cheng, J., Xu, Z., Bambrick, H., Su, H., Tong, S., Hu, W., 2018. Heatwave and elderly mortality: An evaluation of death burden and health costs considering short-term mortality displacement. Environ. Int. 115, 334–342. https://doi.org/10.1016/j.envint.2018.03.041

Christidis, N., Jones, G.S., Stott, P.A., 2015. Dramatically increasing chance of extremely hot summers since the 2003 European heatwave. Nat. Clim. Chang. 5, 46–50. https://doi.org/10.1038/nclimate2468

Clark, R.T., Murphy, J.M., Brown, S.J., 2010. Do global warming targets limit

heatwave risk? Geophys. Res. Lett. 37, n/a-n/a. https://doi.org/10.1029/2010GL043898

Cleveland, W.S., Devlin, S.J., 1988. Locally Weighted Regression: An Approach to Regression Analysis by Local Fitting. J. Am. Stat. Assoc. 83, 596. https://doi.org/10.2307/2289282

Cohen, A.J., Brauer, M., Burnett, R., Anderson, H.R., Frostad, J., Estep, K., Balakrishnan, K., Brunekreef, B., Dandona, L., Dandona, R., Feigin, V., Freedman, G., Hubbell, B., Jobling, A., Kan, H., Knibbs, L., Liu, Y., Martin, R., Morawska, L., Pope, C.A., Shin, H., Straif, K., Shaddick, G., Thomas, M., van Dingenen, R., van Donkelaar, A., Vos, T., Murray, C.J.L., Forouzanfar, M.H., 2017. Estimates and 25-year trends of the global burden of disease attributable to ambient air pollution: an analysis of data from the Global Burden of Diseases Study 2015. Lancet 389, 1907–1918. https://doi.org/10.1016/S0140-6736(17)30505-6

Collins, J.W., Lamarque, J.F., Schulz, M., Boucher, O., Eyring, V., Hegglin, I.M., Maycock, A., Myhre, G., Prather, M., Shindell, D., Smith, J.S., 2017. AerChemMIP: Quantifying the effects of chemistry and aerosols in CMIP6. Geosci. Model Dev. 10, 585–607. https://doi.org/10.5194/gmd-10-585-2017

Collins, M., Knutti, R., Arblaster, J., Dufresne, J.-L., Fichefet, T., Friedlingstein, P., Gao, X., Gutowski, W.J., Johns, T., Krinner, G., Shongwe, M., Tebaldi, C., Weaver, A.J., Wehner, M., 2013. Long-term Climate Change: Projections, Commitments and Irreversibility, in: Stocker, T.F., Qin, D., Plattner, G.-K., Tignor, M., Allen, S.K., Boschung, J., Nauels, A., Xia, Y., Bex, V., Midgley, P.M. (Eds.), Climate Change 2013: The Physical Science Basis. Contribution of

Working Group I to the Fifth Assessment Report of the Intergovernmental Panel on Climate Change. Cambridge University Press, Cambridge, pp. 1029–1136. https://doi.org/10.1017/CBO9781107415324.024

Collins, W.J., 2003. Effect of stratosphere-troposphere exchange on the future tropospheric ozone trend. J. Geophys. Res. 108, 8528. https://doi.org/10.1029/2002JD002617

Coumou, D., Lehmann, J., Beckmann, J., 2015. The weakening summer circulation in the Northern Hemisphere mid-latitudes. Science (80-.). 348, 324–327. https://doi.org/10.1126/science.1261768

Crippa, M., Janssens-Maenhout, G., Dentener, F., Guizzardi, D., Sindelarova, K., Muntean, M., Van Dingenen, R., Granier, C., 2016. Forty years of improvements in European air quality: regional policy-industry interactions with global impacts. Atmos. Chem. Phys. 16, 3825–3841. https://doi.org/10.5194/acp-16-3825-2016

Curriero, F.C., Heiner, K.S., Samet, J.M., Zeger, S.L., Strug, L., Patz, J.A., 2002. Temperature and Mortality in 11 Cities of the Eastern United States. Am. J. Epidemiol. 155, 80–87. https://doi.org/10.1093/aje/155.1.80

Dai, A., Karl, T.R., Sun, B., Trenberth, K.E., 2006. Recent trends in cloudiness over the United States: A tale of monitoring inadequacies. Bull. Am. Meteorol. Soc. 87, 597–606. https://doi.org/10.1175/BAMS-87-5-597

Daskalakis, N., Tsigaridis, K., Myriokefalitakis, S., Fanourgakis, G.S., Kanakidou, M., 2016. Large gain in air quality compared to an alternative anthropogenic emissions scenario. Atmos. Chem. Phys. 16, 9771–9784. https://doi.org/10.5194/acp-16-9771-2016

Davidson, C.I., Phalen, R.F., Solomon, P.A., 2005. Airborne Particulate Matter and Human Health: A Review. Aerosol Sci. Technol. 39, 737–749. https://doi.org/10.1080/02786820500191348

Dawson, J.P., Adams, P.J., Pandis, S.N., 2007. Sensitivity of ozone to summertime climate in the eastern USA: A modeling case study. Atmos. Environ. 41, 1494–1511. https://doi.org/10.1016/j.atmosenv.2006.10.033

Dear, K., Ranmuthugala, G., Kjellstroem, T., Skinner, C., Hanigan, I., 2005. Effects of temperature and ozone on daily mortality during the August 2003 heat wave in France. Arch. Environ. Occup. Health 60, 205–212. https://doi.org/10.3200/AEOH.60.4.205-212

Dee, D.P., Uppala, S.M., Simmons, A.J., Berrisford, P., Poli, P., Kobayashi, S., Andrae, U., Balmaseda, M.A., Balsamo, G., Bauer, P., Bechtold, P., Beljaars, A.C.M., van de Berg, L., Bidlot, J., Bormann, N., Delsol, C., Dragani, R., Fuentes, M., Geer, A.J., Haimberger, L., Healy, S.B., Hersbach, H., Hólm, E. V., Isaksen, L., Kållberg, P., Köhler, M., Matricardi, M., McNally, A.P., Monge-Sanz, B.M., Morcrette, J.-J., Park, B.-K., Peubey, C., de Rosnay, P., Tavolato, C., Thépaut, J.-N., Vitart, F., 2011. The ERA-Interim reanalysis: configuration and performance of the data assimilation system. Q. J. R. Meteorol. Soc. 137, 553–597. https://doi.org/10.1002/qj.828

Department of Health, 2015. Heatwave plan for England: Protecting health and reducing harm from severe heat and heatwaves, Public Health England. London.

Derksen, C., Brown, R., 2012. Spring snow cover extent reductions in the 2008-2012 period exceeding climate model projections. Geophys. Res. Lett. 39.

https://doi.org/10.1029/2012GL053387

Deryng, D., Conway, D., Ramankutty, N., Price, J., Warren, R., al, G.J. et, C, H.D. and R.C. ed H.D. and R., al, E.W.E. et, Müller C, B.A.P.A.W.K. and F.M., Deryng D, S.W.J.B.C.C. and R.N., al, N.G.C. et, Parry M, R.C.I.A.L.M. and F.G., al, L.D.B. et, al, H.E. et, Moriondo M, G.C. and B.M., P, S.M.A. and S., Wahid A, G.S.A.M. and F.M.R., al, G.S.M. et, Teixeira E I, F.G. van V.H.W.C. and E.F., C, K.M.B. ed H.D. and R., Challinor A J, W.T.R.C.P. and S.J.M., D, M.T.D. and J.P., al, van V.D.P. et, al, R.C. et, Monfreda C, R.N. and F.J.A., Portmann F T, S.S. and D.P., al, W.R. et, Meinshausen M, R.S.C.B. and W.T.M.L., A, O.T.J., al, M.G.A. et, al, A.L. et, Sacks W J, D.D.F.J.A. and R.N., Abbott P C, H.C. and T.W.E., C, P.J. and T., al, L.D.B. et, A, A.E.A. and R., al, T.F.N. et, P, L.S., C, K.B.A. ed H.D. and R., Leakey A D B, B.K.A. and A.E.A., al, T.D. et, al, B.S. et, al, E.D.R. et, Neitsch S L, A.J.G.K.J.R. and W.J.R., R, W.J., Penning de Vries F W T, J.D.M. ten B.H.F.M. and B.A., Thuzar M, P.A.B.A.N.A.P.L.M.B.M. and J.K., Modhej A, N.A.E.Y.A.A. and N.G., al, S.J.H.J. et, M, P.J.R. and G., Ferris R, E.R.W.T.R. and H.P., B, W.T.M.L. and R.S.C., Rotmans J, H.M. and D.T.E., al, V.V.D.P. et, Warren R, Y.R.M.S.O.T.J. and de la N.S.S., O, D.J. and P.W., W, P.M. and K.R., A, R.C.W. and W.D., W, R.C., S, G., 2014. Global crop yield response to extreme heat stress under multiple climate change futures. Environ. Res. Lett. 9, 034011. https://doi.org/10.1088/1748-9326/9/3/034011

Donat, M.G., Alexander, L. V., 2012. The shifting probability distribution of global daytime and night-time temperatures. Geophys. Res. Lett. 39. https://doi.org/10.1029/2012GL052459

Donner, L.J., Wyman, B.L., Hemler, R.S., Horowitz, L.W., Ming, Y., Zhao, M., Golaz,

J.-C., Ginoux, P., Lin, S.-J., Schwarzkopf, M.D., Austin, J., Alaka, G., Cooke, W.F., Delworth, T.L., Freidenreich, S.M., Gordon, C.T., Griffies, S.M., Held, I.M., Hurlin, W.J., Klein, S.A., Knutson, T.R., Langenhorst, A.R., Lee, H.-C., Lin, Y., Magi, B.I., Malyshev, S.L., Milly, P.C.D., Naik, V., Nath, M.J., Pincus, R., Ploshay, J.J., Ramaswamy, V., Seman, C.J., Shevliakova, E., Sirutis, J.J., Stern, W.F., Stouffer, R.J., Wilson, R.J., Winton, M., Wittenberg, A.T., Zeng, F., 2011. The Dynamical Core, Physical Parameterizations, and Basic Simulation Characteristics of the Atmospheric Component AM3 of the GFDL Global Coupled Model CM3. J. Clim. 24, 3484–3519. https://doi.org/10.1175/2011JCLI3955.1

Dosio, A., 2017. Projection of temperature and heat waves for Africa with an ensemble of CORDEX Regional Climate Models. Clim. Dyn. 49, 493–519. https://doi.org/10.1007/s00382-016-3355-5

Dosio, A., Fischer, E.M., 2018. Will Half a Degree Make a Difference? Robust Projections of Indices of Mean and Extreme Climate in Europe Under 1.5°C, 2°C, and 3°C Global Warming. Geophys. Res. Lett. 45, 935–944. https://doi.org/10.1002/2017GL076222

Duncan, B.N., West, J.J., Yoshida, Y., Fiore, A.M., Ziemke, J.R., 2008. The influence of European pollution on ozone in the Near East and northern Africa. Atmos. Chem. Phys. 8, 2267–2283. https://doi.org/10.5194/acp-8-2267-2008

Dunne, J.P., Stouffer, R.J., John, J.G., 2013. Reductions in labour capacity from heat stress under climate warming. Nat. Clim. Chang. 3, 563–566. https://doi.org/10.1038/nclimate1827

Egondi, T., Kyobutungi, C., Rocklöv, J., 2015. Temperature Variation and Heat Wave

and Cold Spell Impacts on Years of Life Lost Among the Urban Poor Population of Nairobi, Kenya. Int. J. Environ. Res. Public Health 12, 2735–2748. https://doi.org/10.3390/ijerph120302735

El-Zein, A., Tewtel-Salem, M., Nehme, G., 2004. A time-series analysis of mortality and air temperature in Greater Beirut. Sci. Total Environ. 330, 71–80. https://doi.org/10.1016/j.scitotenv.2004.02.027

Emmons, L.K., Walters, S., Hess, P.G., Lamarque, J.-F., Pfister, G.G., Fillmore, D., Granier, C., Guenther, A., Kinnison, D., Laepple, T., Orlando, J., Tie, X., Tyndall, G., Wiedinmyer, C., Baughcum, S.L., Kloster, S., 2009. Description and evaluation of the Model for Ozone and Related chemical Tracers, version 4 (MOZART-4). Geosci. Model Dev. Discuss. 2, 1157–1213. https://doi.org/10.5194/gmdd-2-1157-2009

European Commission, 2018. Air quality standards [WWW Document]. URL http://ec.europa.eu/environment/air/quality/standards.htm (accessed 6.15.19).

Eyring, V., Arblaster, J.M., Cionni, I., Sedláček, J., Perlwitz, J., Young, P.J., Bekki, S., Bergmann, D., Cameron-Smith, P., Collins, W.J., Faluvegi, G., Gottschaldt, K.-D., Horowitz, L.W., Kinnison, D.E., Lamarque, J.-F., Marsh, D.R., Saint-Martin, D., Shindell, D.T., Sudo, K., Szopa, S., Watanabe, S., 2013. Long-term ozone changes and associated climate impacts in CMIP5 simulations. J. Geophys. Res. Atmos. 118, 5029–5060. https://doi.org/10.1002/jgrd.50316

Eyring, V., Bony, S., Meehl, G.A., Senior, C.A., Stevens, B., Stouffer, R.J., Taylor, K.E., 2016. Overview of the Coupled Model Intercomparison Project Phase 6 (CMIP6) experimental design and organization. Geosci. Model Dev. 9.

https://doi.org/10.5194/gmd-9-1937-2016

Eyring, V, Lamarque, J.-F., Hess, P., Arfeuille, F., Bowman, K., Chipperfield, M.P., Duncan, B., Fiore, A.M., Gettelman, A., Giorgetta, M.A., Granier, C., Hegglin, M., Kinnison, D., Kunze, M., Langematz, U., Luo, B., Martin, R., Matthes, K., Newman, P.A., Peter, T., Robock, A., Ryerson, T., Saiz-Lopez, A., Salawitch, R., Schultz, M., Shepherd, T.G., Shindell, D., Stähelin, J., Tegtmeier, S., Thomason, S., Tilmes, S., Vernier, J.-P., Waugh, D.W., Young, P.J., 2013. Overview of IGAC/SPARC Chemistry-Climate Model Initiative (CCMI) Community Simulations in Support of Upcoming Ozone and Climate Assessments. SPARC Newsl. 48–66.

Fang, Y., Naik, V., Horowitz, L.W., Mauzerall, D.L., 2013. Air pollution and associated human mortality: The role of air pollutant emissions, climate change and methane concentration increases from the preindustrial period to present. Atmos. Chem. Phys. 13, 1377–1394.

Fecht, D., Fischer, P., Fortunato, L., Hoek, G., de Hoogh, K., Marra, M., Kruize, H., Vienneau, D., Beelen, R., Hansell, A., 2015. Associations between air pollution and socioeconomic characteristics, ethnicity and age profile of neighbourhoods in England and the Netherlands. Environ. Pollut. 198, 201–210. https://doi.org/10.1016/j.envpol.2014.12.014

Filleul, L., Cassadou, S., Médina, S., Fabres, P., Lefranc, A., Eilstein, D., Le Tertre, A., Pascal, L., Chardon, B., Blanchard, M., Declercq, C., Jusot, J.-F.F., Prouvost, H., Ledrans, M., 2006. The Relation Between Temperature, Ozone, and Mortality in Nine French Cities During the Heat Wave of 2003. Environ. Health Perspect. 114, 1344–1347. https://doi.org/10.1289/ehp.8328

Fink, A.H., Brücher, T., Krüger, A., Leckebusch, G.C., Pinto, J.G., Ulbrich, U., 2004. The 2003 European summer heatwaves and drought -synoptic diagnosis and impacts. Weather 59, 209–216. https://doi.org/10.1256/wea.73.04

Finney, D.L., Doherty, R.M., Wild, O., Huntrieser, H., Pumphrey, H.C., Blyth, A.M., 2014. Using cloud ice flux to parametrise large-scale lightning. Atmos. Chem. Phys. 14, 12665–12682. https://doi.org/10.5194/acp-14-12665-2014

Finney, D.L., Doherty, R.M., Wild, O., Stevenson, D.S., MacKenzie, I.A., Blyth, A.M., 2018. A projected decrease in lightning under climate change. Nat. Clim. Chang. 8, 210–213. https://doi.org/10.1038/s41558-018-0072-6

Finney, D.L., Doherty, R.M., Wild, O., Young, P.J., Butler, A., 2016. Response of lightning NO x emissions and ozone production to climate change: Insights from the Atmospheric Chemistry and Climate Model Intercomparison Project. Geophys. Res. Lett. 43, 5492–5500. https://doi.org/10.1002/2016GL068825

Fiore, A.M., Dentener, F.J., Wild, O., Cuvelier, C., Schultz, M.G., Hess, P., Textor, C., Schulz, M., Doherty, R.M., Horowitz, L.W., MacKenzie, I.A., Sanderson, M.G., Shindell, D.T., Stevenson, D.S., Szopa, S., Van Dingenen, R., Zeng, G., Atherton, C., Bergmann, D., Bey, I., Carmichael, G., Collins, W.J., Duncan, B.N., Faluvegi, G., Folberth, G., Gauss, M., Gong, S., Hauglustaine, D., Holloway, T., Isaksen, I.S.A., Jacob, D.J., Jonson, J.E., Kaminski, J.W., Keating, T.J., Lupu, A., Marmer, E., Montanaro, V., Park, R.J., Pitari, G., Pringle, K.J., Pyle, J.A., Schroeder, S., Vivanco, M.G., Wind, P., Wojcik, G., Wu, S., Zuber, A., 2009. Multimodel estimates of intercontinental source-receptor relationships for ozone pollution. J. Geophys. Res. 114, D04301. https://doi.org/10.1029/2008JD010816

Fiore, A.M., Naik, V., Leibensperger, E.M., 2015. Air Quality and Climate Connections. J. Air Waste Manage. Assoc. 65, 645–685. https://doi.org/10.1080/10962247.2015.1040526

Fiore, A.M., Naik, V., Spracklen, D. V., Steiner, A., Unger, N., Prather, M., Bergmann, D., Cameron-Smith, P.J., Cionni, I., Collins, W.J., Dalsøren, S., Eyring, V., Folberth, G. a., Ginoux, P., Horowitz, L.W., Josse, B., Lamarque, J.-F., MacKenzie, I. a., Nagashima, T., O'Connor, F.M., Righi, M., Rumbold, S.T., Shindell, D.T., Skeie, R.B., Sudo, K., Szopa, S., Takemura, T., Zeng, G., 2012. Global air quality and climate. Chem. Soc. Rev. 41, 6663–83. https://doi.org/10.1039/c2cs35095e

Fischer, E.M., Knutti, R., 2015. Anthropogenic contribution to global occurrence of heavy-precipitation and high-temperature extremes. Nat. Clim. Chang. 5, 560–564. https://doi.org/10.1038/nclimate2617

Fischer, P.H., Brunekreef, B., Lebret, E., 2004. Air pollution related deaths during the 2003 heat wave in the Netherlands. Atmos. Environ. 38, 1083–1085. https://doi.org/10.1016/j.atmosenv.2003.11.010

Fischer, E. V., Jacob, D.J., Yantosca, R.M., Sulprizio, M.P., Millet, D.B., Mao, J., Paulot, F., Singh, H.B., Roiger, A., Ries, L., Talbot, R.W., Dzepina, K., Pandey Deolal, S., 2014. Atmospheric peroxyacetyl nitrate (PAN): a global budget and source attribution. Atmos. Chem. Phys. 14, 2679–2698. https://doi.org/10.5194/acp-14-2679-2014

Flato, G., Marotzke, J., Abiodun, B., Braconnot, P., Chou, S.C., Collins, W., Cox, P., Driouech, F., Emori, S., Eyring, V., Forest, C., Gleckler, P., Guilyardi, E., Jakob,

C., Kattsov, V., Reason, C., Rummukainen, M., 2014. Evaluation of climate models, in: Intergovernmental Panel on Climate Change (Ed.), Climate Change 2013: The Physical Science Basis. Contribution of Working Group I to the Fifth Assessment Report of the Intergovernmental Panel on Climate Change. Cambridge University Press, Cambridge, pp. 741–866. https://doi.org/10.1017/CBO9781107415324

Flynn, A., McGreevy, C., Mulkerrin, E.C., 2005. Why do older patients die in a heatwave? QJM 98, 227–229. https://doi.org/10.1093/qjmed/hci025

Fortems-Cheiney, A., Foret, G., Siour, G., Vautard, R., Szopa, S., Dufour, G., Colette, A., Lacressonniere, G., Beekmann, M., 2017. A 3 °C global RCP8.5 emission trajectory cancels benefits of European emission reductions on air quality. Nat. Commun. 8, 89. https://doi.org/10.1038/s41467-017-00075-9

Fouillet, A., Rey, G., Wagner, V., Laaidi, K., Empereur-Bissonnet, P., Le Tertre, A., Frayssinet, P., Bessemoulin, P., Laurent, F., De Crouy-Chanel, P., Jougla, E., Hemon, D., 2008. Has the impact of heat waves on mortality changed in France since the European heat wave of summer 2003? A study of the 2006 heat wave. Int. J. Epidemiol. 37, 309–317. https://doi.org/10.1093/ije/dym253

Francis, X.V., Chemel, C., Sokhi, R.S., Norton, E.G., Ricketts, H.M.A., Fisher, B.E.A., 2011. Mechanisms responsible for the build-up of ozone over South East England during the August 2003 heatwave. Atmos. Environ. 45, 6880–6890. https://doi.org/10.1016/J.ATMOSENV.2011.04.035

Fu, S.H., Gasparrini, A., Rodriguez, P.S., Jha, P., 2018. Mortality attributable to hot and cold ambient temperatures in India: a nationally representative case-crossover

study. PLOS Med. 15, e1002619. https://doi.org/10.1371/journal.pmed.1002619

García-Herrera, R., Díaz, J., Trigo, R.M., Luterbacher, J., Fischer, E.M., 2010. A Review of the European Summer Heat Wave of 2003. Crit. Rev. Environ. Sci. Technol. 40, 267–306. https://doi.org/10.1080/10643380802238137

Garcia-Menendez, F., Saari, R.K., Monier, E., Selin, N.E., 2015. U.S. Air Quality and Health Benefits from Avoided Climate Change under Greenhouse Gas Mitigation. Environ. Sci. Technol. 49, 7580–7588. https://doi.org/10.1021/acs.est.5b01324

Gasparrini, A., Guo, Y., Hashizume, M., Lavigne, E., Zanobetti, A., Schwartz, J., Tobias, A., Tong, S., Rocklöv, J., Forsberg, B., Leone, M., De Sario, M., Bell, M.L., Guo, Y.-L.L., Wu, C., Kan, H., Yi, S.-M., de Sousa Zanotti Stagliorio Coelho, M., Saldiva, P.H.N., Honda, Y., Kim, H., Armstrong, B., 2015. Mortality risk attributable to high and low ambient temperature: a multicountry observational study. Lancet 386, 369–375. https://doi.org/10.1016/S0140-6736(14)62114-0

Gasparrini, A., Guo, Y., Sera, F., Vicedo-Cabrera, A.M., Huber, V., Tong, S., de Sousa Zanotti Stagliorio Coelho, M., Nascimento Saldiva, P.H., Lavigne, E., Matus Correa, P., Valdes Ortega, N., Kan, H., Osorio, S., Kyselý, J., Urban, A., Jaakkola, J.J.K., Ryti, N.R.I., Pascal, M., Goodman, P.G., Zeka, A., Michelozzi, P., Scortichini, M., Hashizume, M., Honda, Y., Hurtado-Diaz, M., Cesar Cruz, J., Seposo, X., Kim, H., Tobias, A., Iñiguez, C., Forsberg, B., Åström, D.O., Ragettli, M.S., Guo, Y.L., Wu, C., Zanobetti, A., Schwartz, J., Bell, M.L., Dang, T.N., Van, D. Do, Heaviside, C., Vardoulakis, S., Hajat, S., Haines, A., Armstrong, B., 2017. Projections of temperature-related excess mortality under climate change scenarios. Lancet Planet. Heal. https://doi.org/10.1016/S2542-5196(17)30156-0

Giannakopoulos, C., Le Sager, P., Bindi, M., Moriondo, M., Kostopoulou, E., Goodess, C.M., 2009. Climatic changes and associated impacts in the Mediterranean resulting from a 2 °C global warming. Glob. Planet. Change 68, 209–224. https://doi.org/10.1016/j.gloplacha.2009.06.001

GISSTEMP Team, 2018. GISS Surface Temperature Analysis (GISTEMP) [WWW Document]. NASA Goddard Inst. Sp. Stud. https://doi.org/10.1029/2010RG000345

Gosling, S.N., Lowe, J.A., McGregor, G.R., Pelling, M., Malamud, B.D., 2009. Associations between elevated atmospheric temperature and human mortality: a critical review of the literature. Clim. Change 92, 299–341. https://doi.org/10.1007/s10584-008-9441-x

Gouveia, N., Hajat, S., Armstrong, B., 2003. Socioeconomic differentials in the temperature-mortality relationship in Sao Paulo, Brazil. Int. J. Epidemiol. 32, 390–397. https://doi.org/10.1093/ije/dyg077

Granier, C., Bessagnet, B., Bond, T., D'Angiola, A., van der Gon, H.D., Frost, G.J., Heil, A., Kaiser, J.W., Kinne, S., Klimont, Z., Kloster, S., Lamarque, J.-F., Liousse, C., Masui, T., Meleux, F., Mieville, A., Ohara, T., Raut, J.C., Riahi, K., Schultz, M.G., Smith, S.J., Thompson, A., van Aardenne, J., van der Werf, G.R., van Vuuren, D.P., 2011. Evolution of anthropogenic and biomass burning emissions of air pollutants at global and regional scales during the 1980-2010 period. Clim. Change 109, 163–190. https://doi.org/10.1007/s10584-011-0154-1

Grosjean, D., Grosjean, E., Williams, E.L., 1994. Thermal Decomposition of PAN, PPN and Vinyl-PAN. Air Waste 44, 391–396.

https://doi.org/10.1080/1073161X.1994.10467260

Grossman, G.M., Krueger, A.B., 1995. Economic Growth and the Environment Author (s): Gene M . Grossman and Alan B . Krueger Reviewed work (s): Published by : Oxford University Press. Q. J. Econ. 110, 353–377.

Guenther, a., Karl, T., Harley, P., Wiedinmyer, C., Palmer, P.I., Geron, C., 2006. Estimates of global terrestrial isoprene emissions using MEGAN (Model of Emissions of Gases and Aerosols from Nature). Atmos. Chem. Phys. Discuss. 6, 107–173. https://doi.org/10.5194/acpd-6-107-2006

Guenther, A., Baugh, B., Brasseur, G., Greenberg, J., Harley, P., Klinger, L., Serça, D., Vierling, L., 1999. Isoprene emission estimates and uncertainties for the central African EXPRESSO study domain. J. Geophys. Res. Atmos. 104, 30625–30639. https://doi.org/10.1029/1999JD900391

Guenther, A., Nicholas, C., Fall, R., Klinger, L., Mckay, W. a, Scholes, B., Steinbrecher, R., Tallamraju, R., Taylor, J., Zimmerman, P., 1995. A global model of natural volatile organic compound emissions. J. Geophys. Res. 100, 8873–8892. https://doi.org/10.1029/94JD02950

Guenther, A.B., Jiang, X., Heald, C.L., Sakulyanontvittaya, T., Duhl, T., Emmons, L.K., Wang, X., 2012. The Model of Emissions of Gases and Aerosols from Nature version 2.1 (MEGAN2.1): an extended and updated framework for modeling biogenic emissions. Geosci. Model Dev. 5, 1471–1492. https://doi.org/10.5194/gmd-5-1471-2012

Guo, X., Huang, J., Luo, Y., Zhao, Z., Xu, Y., 2017. Projection of heat waves over China for eight different global warming targets using 12 CMIP5 models. Theor.

Appl. Climatol. 128, 507–522. https://doi.org/10.1007/s00704-015-1718-1

Guo, X., Huang, J., Luo, Y., Zhao, Z., Xu, Y., 2016. Projection of precipitation extremes for eight global warming targets by 17 CMIP5 models. Nat. Hazards 84, 2299–2319. https://doi.org/10.1007/s11069-016-2553-0

Guo, Y., Gasparrini, A., Armstrong, B., Li, S., Tawatsupa, B., Tobias, A., Lavigne, E., de Sousa Zanotti Stagliorio Coelho, M., Leone, M., Pan, X., Tong, S., Tian, L., Kim, H., Hashizume, M., Honda, Y., Guo, Y.-L.L., Wu, C.-F., Punnasiri, K., Yi, S.-M., Michelozzi, P., Saldiva, P.H.N., Williams, G., 2014. Global Variation in the Effects of Ambient Temperature on Mortality: a systematic evaluation. Epidemiology 25, 781–789. https://doi.org/10.1097/EDE.0000000000000165

Haddad, B.M., 2005. Ranking the adaptive capacity of nations to climate change when socio-political goals are explicit. Glob. Environ. Chang. 15, 165–176. https://doi.org/10.1016/j.gloenvcha.2004.10.002

Hajat, S., Vardoulakis, S., Heaviside, C., Eggen, B., 2014. Climate change effects on human health: projections of temperature-related mortality for the UK during the 2020s, 2050s and 2080s. J. Epidemiol. Community Health 68, 641–648. https://doi.org/10.1136/jech-2013-202449

Hankin, B., Lamb, R., Craigen, I., Page, T., Metcalfe, P., Chappell, N., 2017. A whole catchment approach to improve flood resilience in the Eden.

Hanna, E., Tait, P., 2015. Limitations to Thermoregulation and Acclimatization Challenge Human Adaptation to Global Warming. Int. J. Environ. Res. Public Health 12, 8034–8074. https://doi.org/10.3390/ijerph120708034

Hansen, J., Sato, M., Kharecha, P., Von Schuckmann, K., Beerling, D.J., Cao, J., Marcott, S., Masson-Delmotte, V., Prather, M.J., Rohling, E.J., Shakun, J., Smith, P., Lacis, A., Russell, G., Ruedy, R., 2017. Young people's burden: Requirement of negative CO_2 emissions. Earth Syst. Dyn. 8, 577–616. https://doi.org/10.5194/esd-8-577-2017

Hardiman, S.C., Butchart, N., Calvo, N., 2014. The morphology of the Brewer-Dobson circulation and its response to climate change in CMIP5 simulations. Q. J. R. Meteorol. Soc. 140, 1958–1965. https://doi.org/10.1002/qj.2258

Hargreaves, J.C., Annan, J.D., 2014. Can we trust climate models? Wiley Interdiscip. Rev. Clim. Chang. 5, 435–440. https://doi.org/10.1002/wcc.288

Harrington, L.J., Frame, D.J., Fischer, E.M., Hawkins, E., Joshi, M., Jones, C.D., 2016. Poorest countries experience earlier anthropogenic emergence of daily temperature extremes. Environ. Res. Lett. 11, 055007. https://doi.org/10.1088/1748-9326/11/5/055007

Hawkins, E., Sutton, R., 2009. The potential to narrow uncertainty in regional climate predictions. Bull. Am. Meteorol. Soc. 90, 1095–1107. https://doi.org/10.1175/2009BAMS2607.1

Hayden, M.H., Brenkert-Smith, H., Wilhelmi, O. V., 2011. Differential Adaptive Capacity to Extreme Heat: A Phoenix, Arizona, Case Study. Weather. Clim. Soc. 3, 269–280. https://doi.org/10.1175/WCAS-D-11-00010.1

Hazeleger, W., van den Hurk, B.J.J.M., Min, E., van Oldenborgh, G.J., Petersen, A.C., Stainforth, D.A., Vasileiadou, E., Smith, L.A., 2015. Tales of future weather. Nat. Clim. Chang. 5, 107–113. https://doi.org/10.1038/nclimate2450

Heal, M.R., Heaviside, C., Doherty, R.M., Vieno, M., Stevenson, D.S., Vardoulakis, S., 2013. Health burdens of surface ozone in the UK for a range of future scenarios. Environ. Int. 61, 36–44. https://doi.org/10.1016/j.envint.2013.09.010

Heald, C.L., Wilkinson, M.J., Monson, R.K., Alo, C.A., Wang, G., Guenther, A.B., 2009. Response of isoprene emission to ambient CO 2 changes and implications for global budgets. Glob. Chang. Biol. 15, 1127–1140. https://doi.org/10.1111/j.1365-2486.2008.01802.x

Herold, N., Alexander, L., Green, D., Donat, M., 2017. Greater increases in temperature extremes in low versus high income countries. Environ. Res. Lett. 12, 034007. https://doi.org/10.1088/1748-9326/aa5c43

Hodzic, A., Madronich, S., Bohn, B., Massie, S., Menut, L., Wiedinmyer, C., 2007. Wildfire particulate matter in Europe during summer 2003: meso-scale modeling of smoke emissions, transport and radiative effects. Atmos. Chem. Phys. 7, 4043–4064. https://doi.org/10.5194/acp-7-4043-2007

Hoegh-Guldberg, Jacob, O.D., Taylor, M., Bindi, M., Brown, S., Camilloni, I., Diedhiou, A., Djalante, R., Ebi, K.L., Engelbrecht, F., J.Guiot, Hijioka, Y., Mehrotra, S., Payne, A., Seneviratne, S.I., Thomas, A., Warren, R., Zhou, G., 2018. Impacts of 1.5°C of Global Warming on Natural and Human Systems, in: IPCC Special Report on the Impacts of Global Warming of 1.5 ºC above Pre-Industrial Levels and Related Global Greenhouse Gas Emission Pathways, in the Context of Strengthening the Global Response to the Threat of Climate Change, Sustainable Development, A. pp. 175–311.

Honda, Y., Kabuto, M., Ono, M., Uchiyama, I., 2007. Determination of optimum daily

maximum temperature using climate data. Environ. Health Prev. Med. 12, 209–216. https://doi.org/10.1265/ehpm.12.209

Honda, Y., Kondo, M., McGregor, G., Kim, H., Guo, Y.-L., Hijioka, Y., Yoshikawa, M., Oka, K., Takano, S., Hales, S., Kovats, R.S., 2014. Heat-related mortality risk model for climate change impact projection. Environ. Health Prev. Med. 19, 56–63. https://doi.org/10.1007/s12199-013-0354-6

Honda, Y., Ono, M., Kabuto, M., 2006. Do We Adapt to a New Climate as The Globe Warms? Epidemiology 17, S204. https://doi.org/10.1097/00001648-200611001-00519

Hondula, David M, Balling, R.C., Vanos, J.K., Georgescu, M., 2015. Rising Temperatures, Human Health, and the Role of Adaptation. Curr. Clim. Chang. Reports 1–11. https://doi.org/10.1007/s40641-015-0016-4

Hondula, David M., Davis, R.E., Saha, M. V., Wegner, C.R., Veazey, L.M., 2015. Geographic dimensions of heat-related mortality in seven U.S. cities. Environ. Res. 138, 439–452. https://doi.org/10.1016/j.envres.2015.02.033

Horton, D.E., Harshvardhan, Diffenbaugh, N.S., 2012. Response of air stagnation frequency to anthropogenically enhanced radiative forcing. Environ. Res. Lett. 7, 044034. https://doi.org/10.1088/1748-9326/7/4/044034

Horton, D.E., Skinner, C.B., Singh, D., Diffenbaugh, N.S., 2014. Occurrence and persistence of future atmospheric stagnation events. Nat. Clim. Chang. 4, 698–703. https://doi.org/10.1038/nclimate2272

Huang, C., Barnett, A.G., Wang, X., Vaneckova, P., Fitzgerald, G., Tong, S., 2011.

Projecting Future heat-related mortality under climate change scenarios: A systematic review. Environ. Health Perspect. 119, 1681–1690. https://doi.org/10.1289/ehp.1103456

Huang, P., Xie, S.-P., Hu, K., Huang, G., Huang, R., 2013. Patterns of the seasonal response of tropical rainfall to global warming. Nat. Geosci. 6, 357–361. https://doi.org/10.1038/ngeo1792

Huang, Z., Lin, H., Liu, Y., Zhou, M., Liu, T., Xiao, J., Zeng, W., Li, X., Zhang, Y., Ebi, K.L., Tong, S., Ma, W., Wang, L., 2015. Individual-level and community-level effect modifiers of the temperature-mortality relationship in 66 Chinese communities. BMJ Open 5, e009172. https://doi.org/10.1136/bmjopen-2015-009172

Huynen, M.M.T.E., Martens, P., Schram, D., Weijenberg, M.P., Kunst, A.E., 2001. The Impact of Heat Waves and Cold Spells on Mortality Rates in the Dutch Population. Environ. Health Perspect. 109, 463–470. https://doi.org/10.1289/ehp.01109463

Ingole, V., Kovats, S., Schumann, B., Hajat, S., Rocklöv, J., Juvekar, S., Armstrong, B., 2017. Socioenvironmental factors associated with heat and cold-related mortality in Vadu HDSS, western India: a population-based case-crossover study. Int. J. Biometeorol. 61, 1797–1804. https://doi.org/10.1007/s00484-017-1363-8

Iñiguez, C., Ballester, F., Ferrandiz, J., Pérez-Hoyos, S., Sáez, M., López, A., 2010. Relation between Temperature and Mortality in Thirteen Spanish Cities. Int. J. Environ. Res. Public Health 7, 3196–3210. https://doi.org/10.3390/ijerph7083196

International Institute for Applied System Analysis (IIASA), 2009. GGI Scenario Database Ver 2.0 [WWW Document]. URL

http://www.iiasa.ac.at/Research/GGI/DB/ (accessed 3.24.18).

IPCC, 2013. The Physical Science Basis. Contribution of Working Group I to the Fifth Assessment Report of the Intergovernmental Panel on Climate Change. Cambridge University Press, Cambridge. https://doi.org/10.1017/CBO9781107415324

IPCC, 2012. Managing the risks of extreme events and disasters to advance climate change adaptation, A Special Report of Working Groups I and II of the Intergovernmental Panel on Climate Change. Cambridge University Press, Cambridge, UK, and New York, NY, USA.

Isen, A., Rossin-Slater, M., Walker, W.R., 2017. Every Breath You Take—Every Dollar You'll Make: The Long-Term Consequences of the Clean Air Act of 1970. J. Polit. Econ. 125, 848–902. https://doi.org/10.1086/691465

Jacob, D., Kotova, L., Teichmann, C., Sobolowski, S.P., Vautard, R., Donnelly, C., Koutroulis, A.G., Grillakis, M.G., Tsanis, I.K., Damm, A., Sakalli, A., van Vliet, M.T.H., 2018. Climate Impacts in Europe Under +1.5°C Global Warming. Earth's Futur. 6, 264–285. https://doi.org/10.1002/2017EF000710

Jacob, D.J., Winner, D. a., 2009. Effect of climate change on air quality. Atmos. Environ. 43, 51–63. https://doi.org/10.1016/j.atmosenv.2008.09.051

Jacobson, M.Z., 2002. Pollution trends and regulations outside the United States, in: Atmospheric Pollution: History, Science, and Regulation. Cambridge University Press, Cambridge, UK, pp. 225–238.

James, R., Washington, R., Schleussner, C.-F., Rogelj, J., Conway, D., 2017. Characterizing half-a-degree difference: a review of methods for identifying

regional climate responses to global warming targets. Wiley Interdiscip. Rev. Clim. Chang. 8, e457. https://doi.org/10.1002/wcc.457

Jerrett, M., Burnett, R.T., Pope, C.A., Ito, K., Thurston, G., Krewski, D., Shi, Y., Calle, E., Thun, M., 2009. Long-Term Ozone Exposure and Mortality. N. Engl. J. Med. 360, 1085–1095. https://doi.org/10.1056/NEJMoa0803894

Johnson, C.E., Collins, W.J., Stevenson, D.S., Derwent, R.G., 1999. Relative roles of climate and emissions changes on future tropospheric oxidant concentrations. J. Geophys. Res. Atmos. 104, 18631–18645. https://doi.org/10.1029/1999JD900204

Johnson, J.E., Welch, D.J., 2009. Marine Fisheries Management in a Changing Climate: A Review of Vulnerability and Future Options. Rev. Fish. Sci. 18, 106–124. https://doi.org/10.1080/10641260903434557

Joshi, M., Hawkins, E., Sutton, R., Lowe, J., Frame, D., 2011. Projections of when temperature change will exceed 2 °C above pre-industrial levels. Nat. Clim. Chang. 1, 407–412. https://doi.org/10.1038/nclimate1261

Kalkstein, L.S., Greene, J.S., 1997. An evaluation of climate/mortality relationships in large U.S. cities and the possible impacts of a climate change. Environ. Health Perspect. 105, 84–93. https://doi.org/10.1289/ehp.9710584

Kalnay, E., Kanamitsu, M., Kistler, R., Collins, W., Deaven, D., Gandin, L., Iredell, M., Saha, S., White, G., Woollen, J., Zhu, Y., Leetmaa, A., Reynolds, R., Chelliah, M., Ebisuzaki, W., Higgins, W., Janowiak, J., Mo, K.C., Ropelewski, C., Wang, J., Jenne, R., Joseph, D., 1996. The NCEP/NCAR 40-Year Reanalysis Project. Bull. Am. Meteorol. Soc. 77, 437–471. https://doi.org/10.1175/1520-0477(1996)077<0437:TNYRP>2.0.CO;2

Kar, S.K., Liou, Y.A., 2014. Analysis of cloud-to-ground lightning and its relation with surface pollutants over Taipei, Taiwan. Ann. Geophys. 32, 1085–1092. https://doi.org/10.5194/angeo-32-1085-2014

Katragkou, E., Zanis, P., Kioutsioukis, I., Tegoulias, I., Melas, D., Krger, B.C., Coppola, E., 2011. Future climate change impacts on summer surface ozone from regional climate-air quality simulations over Europe. J. Geophys. Res. Atmos. 116, 1–14. https://doi.org/10.1029/2011JD015899

Katsouyanni, K., Touloumi, G., Spix, C., Schwartz, J., Balducci, F., Medina, S., Rossi, G., Wojtyniak, B., Sunyer, J., Bacharova, L., Schouten, J.P., Ponka, A., Anderson, H.R., 1997. Short term effects of ambient sulphur dioxide and particulate matter on mortality in 12 European cities: results from time series data from the APHEA project. BMJ 314, 1658–1658. https://doi.org/10.1136/bmj.314.7095.1658

Kaufman, Y.J., 2006. Smoke and Pollution Aerosol Effect on Cloud Cover. Science (80-.). 313, 655–658. https://doi.org/10.1126/science.1126232

Kay, J.E., Deser, C., Phillips, A., Mai, A., Hannay, C., Strand, G., Arblaster, J.M., Bates, S.C., Danabasoglu, G., Edwards, J., Holland, M., Kushner, P., Lamarque, J.-F., Lawrence, D., Lindsay, K., Middleton, A., Munoz, E., Neale, R., Oleson, K., Polvani, L., Vertenstein, M., 2015. The Community Earth System Model (CESM) Large Ensemble Project: A Community Resource for Studying Climate Change in the Presence of Internal Climate Variability. Bull. Am. Meteorol. Soc. 96, 1333–1349. https://doi.org/10.1175/BAMS-D-13-00255.1

Kaya, Y., 1990. Impact of Carbon Dioxide emission control on GNP growth: Interpretation of proposed scenarios, in: Paper Presented to the IPCC Energy and

Industry Subgroup, Response Strategies Working Group.

Kaynak, B., Hu, Y., Martin, R. V, Russell, A.G., Choi, Y., Wang, Y., 2008. The effect of lightning NOx production on surface ozone in the continental United States. Atmos. Chem. Phys. 8, 5151–5159. https://doi.org/10.5194/acp-8-5151-2008

Kerr, G.H., Waugh, D.W., 2018. Connections between summer air pollution and stagnation. Environ. Res. Lett. 13, 084001. https://doi.org/10.1088/1748-9326/aad2e2

Kim, C.S., Alexis, N.E., Rappold, A.G., Kehrl, H., Hazucha, M.J., Lay, J.C., Schmitt, M.T., Case, M., Devlin, R.B., Peden, D.B., Diaz-Sanchez, D., 2011. Lung Function and Inflammatory Responses in Healthy Young Adults Exposed to 0.06 ppm Ozone for 6.6 Hours. Am. J. Respir. Crit. Care Med. 183, 1215–1221. https://doi.org/10.1164/rccm.201011-1813OC

Kim, M.J., Park, R.J., Ho, C.-H., Woo, J.-H., Choi, K.-C., Song, C.-K., Lee, J.-B., 2015. Future ozone and oxidants change under the RCP scenarios. Atmos. Environ. 101, 103–115. https://doi.org/10.1016/j.atmosenv.2014.11.016

Kim, Y.-M., Zhou, Y., Gao, Y., Fu, J.S., Johnson, B.A., Huang, C., Liu, Y., 2015. Spatially resolved estimation of ozone-related mortality in the United States under two representative concentration pathways (RCPs) and their uncertainty. Clim. Change 128, 71–84. https://doi.org/10.1007/s10584-014-1290-1

King, Andrew D., Karoly, D.J., 2017. Climate extremes in Europe at 1.5 and 2 degrees of global warming. Environ. Res. Lett. 12, 114031. https://doi.org/10.1088/1748-9326/aa8e2c

King, Andrew D, Karoly, D.J., 2017. Climate extremes in Europe at 1.5 and 2 degrees of global warming. Environ. Res. Lett. 12, 114031. https://doi.org/10.1088/1748-9326/aa8e2c

Kirtman, B., Power, S.B., Adedoyin, J.A., Boer, G.J., Bojariu, R., Camilloni, I., Doblas-Reyes, F.J., Fiore, A.M., Kimoto, M., Meehl, G.A., Prather, M., Sarr, A., Schär, C., Sutton, R., van Oldenborgh, G.J., Vecchi, G., Wang, H.-J., 2013. Near-term Climate Change: Projections and Predictability, in: Intergovernmental Panel on Climate Change (Ed.), Climate Change 2013 - The Physical Science Basis. Cambridge University Press, Cambridge, pp. 953–1028. https://doi.org/10.1017/CBO9781107415324.023

Kjellstrom, T., Holmer, I., Lemke, B., 2009. Workplace heat stress, health and productivity – an increasing challenge for low and middle-income countries during climate change. Glob. Health Action 2, 2047. https://doi.org/10.3402/gha.v2i0.2047

Klein Goldewijk, K., Beusen, A., Janssen, P., 2010. Long-term dynamic modeling of global population and built-up area in a spatially explicit way: HYDE 3.1. The Holocene 20, 565–573. https://doi.org/10.1177/0959683609356587

Klein Goldewijk, K., Beusen, A., Van Drecht, G., De Vos, M., 2011. The HYDE 3.1 spatially explicit database of human-induced global land-use change over the past 12,000 years. Glob. Ecol. Biogeogr. 20, 73–86. https://doi.org/10.1111/j.1466-8238.2010.00587.x

Knowlton, K., Lynn, B., Goldberg, R.A., Rosenzweig, C., Hogrefe, C., Rosenthal, J.K., Kinney, P.L., 2007. Projecting Heat-Related Mortality Impacts Under a Changing

Climate in the New York City Region. Am. J. Public Health 97, 2028–2034. https://doi.org/10.2105/AJPH.2006.102947

Knowlton, K., Rotkin-Ellman, M., Geballe, L., Max, W., Solomon, G.M., 2011. Six Climate Change–Related Events In The United States Accounted For About $14 Billion In Lost Lives And Health Costs. Health Aff. 30, 2167–2176. https://doi.org/10.1377/hlthaff.2011.0229

Knutti, R., Masson, D., Gettelman, A., 2013. Climate model genealogy: Generation CMIP5 and how we got there. Geophys. Res. Lett. 40, 1194–1199. https://doi.org/10.1002/grl.50256

Knutti, R., Rogelj, J., Sedláček, J., Fischer, E.M., 2016. A scientific critique of the two-degree climate change target. Nat. Geosci. 9, 13–18. https://doi.org/10.1038/ngeo2595

Kunkel, K.E., Huang, H.C., Liang, X.Z., Lin, J.T., Wuebbles, D., Tao, Z., Williams, A., Caughey, M., Zhu, J., Hayhoe, K., 2008. Sensitivity of future ozone concentrations in the northeast USA to regional climate change. Mitig. Adapt. Strateg. Glob. Chang. 13, 597–606. https://doi.org/10.1007/s11027-007-9137-y

Kushta, J., Pozzer, A., Lelieveld, J., 2018. Uncertainties in estimates of mortality attributable to ambient PM 2.5 in Europe. Environ. Res. Lett. 13, 064029. https://doi.org/10.1088/1748-9326/aabf29

Kuznets, S., 1955. Economic Growth and Income Inequality. Am. Econ. Rev. 45, 1–28.

Lacressonnière, G., Foret, G., Beekmann, M., Siour, G., Engardt, M., Gauss, M., Watson, L., Andersson, C., Colette, A., Josse, B., Marécal, V., Nyiri, A., Vautard,

R., 2016. Impacts of regional climate change on air quality projections and associated uncertainties. Clim. Change 136, 309–324. https://doi.org/10.1007/s10584-016-1619-z

Lacressonnière, G., Watson, L., Gauss, M., Engardt, M., Andersson, C., Beekmann, M., Colette, A., Foret, G., Josse, B., Marécal, V., Nyiri, A., Siour, G., Sobolowski, S., Vautard, R., 2017. Particulate matter air pollution in Europe in a +2 °C warming world. Atmos. Environ. 154, 129–140. https://doi.org/10.1016/j.atmosenv.2017.01.037

Lamarque, J.-F., Kyle, G.P., Meinshausen, M., Riahi, K., Smith, S.J., van Vuuren, D.P., Conley, A.J., Vitt, F., 2011. Global and regional evolution of short-lived radiatively-active gases and aerosols in the Representative Concentration Pathways. Clim. Change 109, 191–212. https://doi.org/10.1007/s10584-011-0155-0

Lamarque, J.-F., Shindell, D.T., Josse, B., Young, P.J., Cionni, I., Eyring, V., Bergmann, D., Cameron-Smith, P., Collins, W.J., Doherty, R.M., Dalsoren, S., Faluvegi, G., Folberth, G., Ghan, S.J., Horowitz, L.W., Lee, Y.H., MacKenzie, I.A., Nagashima, T., Naik, V., Plummer, D., Righi, M., Rumbold, S.T., Schulz, M., Skeie, R.B., Stevenson, D.S., Strode, S., Sudo, K., Szopa, S., Voulgarakis, A., Zeng, G., 2013. The atmospheric chemistry and climate model intercomparison Project (ACCMIP): Overview and description of models, simulations and climate diagnostics. Geosci. Model Dev. 6, 179–206.

Lambert, F.H., Harris, G.R., Collins, M., Murphy, J.M., Sexton, D.M.H., Booth, B.B.B., 2013. Interactions between perturbations to different Earth system components simulated by a fully-coupled climate model. Clim. Dyn. 41, 3055–3072.

https://doi.org/10.1007/s00382-012-1618-3

Landrigan, P.J., Fuller, R., Acosta, N.J.R., Adeyi, O., Arnold, R., Basu, N. (Nil), Baldé, A.B., Bertollini, R., Bose-O'Reilly, S., Boufford, J.I., Breysse, P.N., Chiles, T., Mahidol, C., Coll-Seck, A.M., Cropper, M.L., Fobil, J., Fuster, V., Greenstone, M., Haines, A., Hanrahan, D., Hunter, D., Khare, M., Krupnick, A., Lanphear, B., Lohani, B., Martin, K., Mathiasen, K. V., McTeer, M.A., Murray, C.J.L., Ndahimananjara, J.D., Perera, F., Potočnik, J., Preker, A.S., Ramesh, J., Rockström, J., Salinas, C., Samson, L.D., Sandilya, K., Sly, P.D., Smith, K.R., Steiner, A., Stewart, R.B., Suk, W.A., van Schayck, O.C.P., Yadama, G.N., Yumkella, K., Zhong, M., 2018. The Lancet Commission on pollution and health. Lancet 391, 462–512. https://doi.org/10.1016/S0140-6736(17)32345-0

Lee, H., 2015. Turning the focus to solutions. Science (80-.). 350, 1007. https://doi.org/10.1126/science.aad8954

Lee, J.D., Lewis, A.C., Jacob, M., Hamilton, J.F., Hopkins, J.R., Watson, N.M., Saxton, J.E., Ennis, C., Carpenter, L.J., Carslaw, N., Fleming, Z., Brandy, B.J., Oram, D.E., Penkett, S.A., Jana, S., Norton, E., Rickard, A.R., Whalley, L.K., Heard, D.E., Bloss, W.J., Gravestock, T., Smith, S.C., Stanton, J., Pilling, M.J., Jenkin, M.E., 2006. Ozone photochemistry and elevated isoprene during the UK heatwave of august 2003. Atmos. Environ. 40, 7598–7613. https://doi.org/10.1016/j.atmosenv.2006.06.057

Leemans, R., Eickhout, B., 2004. Another reason for concern: regional and global impacts on ecosystems for different levels of climate change. Glob. Environ. Chang. 14, 219–228. https://doi.org/10.1016/j.gloenvcha.2004.04.009

Lehner, F., Coats, S., Stocker, T.F., Pendergrass, A.G., Sanderson, B.M., Raible, C.C., Smerdon, J.E., 2017. Projected drought risk in 1.5°C and 2°C warmer climates. Geophys. Res. Lett. 44, 7419–7428. https://doi.org/10.1002/2017GL074117

Lelieveld, J., Evans, J.S., Fnais, M., Giannadaki, D., Pozzer, A., 2015. The contribution of outdoor air pollution sources to premature mortality on a global scale. Nature 525, 367–371. https://doi.org/10.1038/nature15371

Lelieveld, J., Hoor, P., Jöckel, P., Pozzer, A., Hadjinicolaou, P., Cammas, J.P., Beirle, S., 2009. Severe ozone air pollution in the Persian Gulf region. Atmos. Chem. Phys. 9, 1393–1406. https://doi.org/10.5194/acp-9-1393-2009

Lewis, S.C., King, A.D., 2017. Evolution of mean, variance and extremes in 21st century temperatures. Weather Clim. Extrem. 15, 1–10. https://doi.org/10.1016/j.wace.2016.11.002

Lewis, S.C., King, A.D., Mitchell, D.M., 2017. Australia's Unprecedented Future Temperature Extremes Under Paris Limits to Warming. Geophys. Res. Lett. 44, 9947–9956. https://doi.org/10.1002/2017GL074612

Li, C., Michel, C., Seland Graff, L., Bethke, I., Zappa, G., Bracegirdle, T.J., Fischer, E., Harvey, B.J., Iversen, T., King, M.P., Krishnan, H., Lierhammer, L., Mitchell, D., Scinocca, J., Shiogama, H., Stone, D.A., Wettstein, J.J., 2018. Midlatitude atmospheric circulation responses under 1.5 and 2.0 °C warming and implications for regional impacts. Earth Syst. Dyn. 9, 359–382. https://doi.org/10.5194/esd-9-359-2018

Li, D., Zhou, T., Zou, L., Zhang, W., Zhang, L., 2018. Extreme High-Temperature Events Over East Asia in 1.5°C and 2°C Warmer Futures: Analysis of NCAR

CESM Low-Warming Experiments. Geophys. Res. Lett. 45, 1541–1550. https://doi.org/10.1002/2017GL076753

Lim, S.S., Vos, T., Flaxman, A.D., Danaei, G., Shibuya, K., Adair-Rohani, H., AlMazroa, M.A., Amann, M., Anderson, H.R., Andrews, K.G., Aryee, M., Atkinson, C., Bacchus, L.J., Bahalim, A.N., Balakrishnan, K., Balmes, J., Barker-Collo, S., Baxter, A., Bell, M.L., Blore, J.D., Blyth, F., Bonner, C., Borges, G., Bourne, R., Boussinesq, M., Brauer, M., Brooks, P., Bruce, N.G., Brunekreef, B., Bryan-Hancock, C., Bucello, C., Buchbinder, R., Bull, F., Burnett, R.T., Byers, T.E., Calabria, B., Carapetis, J., Carnahan, E., Chafe, Z., Charlson, F., Chen, H., Chen, J.S., Cheng, A.T.-A., Child, J.C., Cohen, A., Colson, K.E., Cowie, B.C., Darby, S., Darling, S., Davis, A., Degenhardt, L., Dentener, F., Des Jarlais, D.C., Devries, K., Dherani, M., Ding, E.L., Dorsey, E.R., Driscoll, T., Edmond, K., Ali, S.E., Engell, R.E., Erwin, P.J., Fahimi, S., Falder, G., Farzadfar, F., Ferrari, A., Finucane, M.M., Flaxman, S., Fowkes, F.G.R., Freedman, G., Freeman, M.K., Gakidou, E., Ghosh, S., Giovannucci, E., Gmel, G., Graham, K., Grainger, R., Grant, B., Gunnell, D., Gutierrez, H.R., Hall, W., Hoek, H.W., Hogan, A., Hosgood, H.D., Hoy, D., Hu, H., Hubbell, B.J., Hutchings, S.J., Ibeanusi, S.E., Jacklyn, G.L., Jasrasaria, R., Jonas, J.B., Kan, H., Kanis, J. a., Kassebaum, N., Kawakami, N., Khang, Y.-H., Khatibzadeh, S., Khoo, J.-P., Kok, C., Laden, F., Lalloo, R., Lan, Q., Lathlean, T., Leasher, J.L., Leigh, J., Li, Y., Lin, J.K., Lipshultz, S.E., London, S., Lozano, R., Lu, Y., Mak, J., Malekzadeh, R., Mallinger, L., Marcenes, W., March, L., Marks, R., Martin, R., McGale, P., McGrath, J., Mehta, S., Memish, Z.A., Mensah, G. a., Merriman, T.R., Micha, R., Michaud, C., Mishra, V., Hanafiah, K.M., Mokdad, A. a., Morawska, L., Mozaffarian, D., Murphy, T., Naghavi, M., Neal, B., Nelson, P.K., Nolla, J.M.,

Norman, R., Olives, C., Omer, S.B., Orchard, J., Osborne, R., Ostro, B., Page, A., Pandey, K.D., Parry, C.D., Passmore, E., Patra, J., Pearce, N., Pelizzari, P.M., Petzold, M., Phillips, M.R., Pope, D., Pope, C.A., Powles, J., Rao, M., Razavi, H., Rehfuess, E. a., Rehm, J.T., Ritz, B., Rivara, F.P., Roberts, T., Robinson, C., Rodriguez-Portales, J. a., Romieu, I., Room, R., Rosenfeld, L.C., Roy, A., Rushton, L., Salomon, J. a., Sampson, U., Sanchez-Riera, L., Sanman, E., Sapkota, A., Seedat, S., Shi, P., Shield, K., Shivakoti, R., Singh, G.M., Sleet, D. a., Smith, E., Smith, K.R., Stapelberg, N.J., Steenland, K., Stöckl, H., Stovner, L.J., Straif, K., Straney, L., Thurston, G.D., Tran, J.H., Van Dingenen, R., van Donkelaar, A., Veerman, J.L., Vijayakumar, L., Weintraub, R., Weissman, M.M., White, R. a., Whiteford, H., Wiersma, S.T., Wilkinson, J.D., Williams, H.C., Williams, W., Wilson, N., Woolf, A.D., Yip, P., Zielinski, J.M., Lopez, A.D., Murray, C.J., Ezzati, M., 2012. A comparative risk assessment of burden of disease and injury attributable to 67 risk factors and risk factor clusters in 21 regions, 1990–2010: a systematic analysis for the Global Burden of Disease Study 2010. Lancet 380, 2224–2260. https://doi.org/10.1016/S0140-6736(12)61766-8

Lin, X., Trainer, M., Liu, S.C., 1988. On the Nonlinearity of the Tropospheric Ozone Production. J. Geophys. Res. 93, 879–888. https://doi.org/10.1029/JD093iD12p15879

Liu, W., Sun, F., Lim, W.H., Zhang, J., Wang, H., Shiogama, H., Zhang, Y., 2017. Global meteorological drought and severe drought affected population in 1.5 °C and 2 °C warmer worlds. Earth Syst. Dyn. Discuss. 1–45. https://doi.org/10.5194/esd-2017-85

Liu, Z., Anderson, B., Yan, K., Dong, W., Liao, H., Shi, P., 2017. Global and regional

changes in exposure to extreme heat and the relative contributions of climate and population change. Sci. Rep. 7, 43909. https://doi.org/10.1038/srep43909

Lobell, D.B., Field, C.B., 2007. Global scale climate–crop yield relationships and the impacts of recent warming. Environ. Res. Lett. 2, 014002. https://doi.org/10.1088/1748-9326/2/1/014002

Lowe, R., Ballester, J., Creswick, J., Robine, J.-M., Herrmann, F.R., Rodó, X., 2015. Evaluating the performance of a climate-driven mortality model during heat waves and cold spells in Europe. Int. J. Environ. Res. Public Health 12, 1279–94. https://doi.org/10.3390/ijerph120201279

Ma, J., Xie, S.-P., 2013. Regional Patterns of Sea Surface Temperature Change: A Source of Uncertainty in Future Projections of Precipitation and Atmospheric Circulation*. J. Clim. 26, 2482–2501. https://doi.org/10.1175/JCLI-D-12-00283.1

Mahlstein, I., Knutti, R., Solomon, S., Portmann, R.W., 2011. Early onset of significant local warming in low latitude countries. Environ. Res. Lett. 6, 034009. https://doi.org/10.1088/1748-9326/6/3/034009

Mahlstein, I., Spirig, C., Liniger, M. a, Appenzeller, C., 2015. Estimating daily climatologies for climate indices derived from climate model data and observations. J. Geophys. Res. Atmos. 120, 2808–2818. https://doi.org/10.1002/2014JD022327

Malley, C.S., Henze, D.K., Kuylenstierna, J.C.I., Vallack, H.W., Davila, Y., Anenberg, S.C., Turner, M.C., Ashmore, M.R., 2017. Updated Global Estimates of Respiratory Mortality in Adults ≥30Years of Age Attributable to Long-Term Ozone Exposure. Environ. Health Perspect. 125, 087021.

https://doi.org/10.1289/EHP1390

Mao, K., Yuan, Z., Zuo, Z., Xu, T., Shen, X., Gao, C., 2019. Changes in Global Cloud Cover Based on Remote Sensing Data from 2003 to 2012. Chinese Geogr. Sci. 29, 306–315. https://doi.org/10.1007/s11769-019-1030-6

Markakis, K., Valari, M., Perrussel, O., Sanchez, O., Honore, C., 2015. Climate-forced air-quality modeling at the urban scale: sensitivity to model resolution, emissions and meteorology. Atmos. Chem. Phys. 15, 7703–7723. https://doi.org/10.5194/acp-15-7703-2015

Martins, E.M., Nunesa, A.C.L., Corrêa, S.M., 2015. Understanding ozone concentrations during weekdays and weekends in the urban area of the city of Rio de Janeiro. J. Braz. Chem. Soc. 26, 1967–1975. https://doi.org/10.5935/0103-5053.20150175

Masui, T., Matsumoto, K., Hijioka, Y., Kinoshita, T., Nozawa, T., Ishiwatari, S., Kato, E., Shukla, P.R., Yamagata, Y., Kainuma, M., 2011. An emission pathway for stabilization at 6 Wm−2 radiative forcing. Clim. Change 109, 59–76. https://doi.org/10.1007/s10584-011-0150-5

Mba, W.P., Longandjo, G.-N.T., Moufouma-Okia, W., Bell, J.-P., James, R., Vondou, D.A., Haensler, A., Fotso-Nguemo, T.C., Guenang, G.M., Tchotchou, A.L.D., Kamsu-Tamo, P.H., Takong, R.R., Nikulin, G., Lennard, C.J., Dosio, A., 2018. Consequences of 1.5 °C and 2 °C global warming levels for temperature and precipitation changes over Central Africa. Environ. Res. Lett. 13, 055011. https://doi.org/10.1088/1748-9326/aab048

McDonnell, W.F., Abbey, D.E., Nishino, N., Lebowitz, M.D., 1999. Long-term ambient

ozone concentration and the incidence of asthma in nonsmoking adults: The Ahsmog study. Environ. Res. 80, 110–121. https://doi.org/10.1006/enrs.1998.3894

McGuffie, K., Henderson-Sellers, A., 2005. A history of and introduction to climate models, in: A Climate Modelling Primer. John Wiley & Sons, Ltd, Chichester, UK. https://doi.org/10.1002/0470857617

McKechnie, A.E., Wolf, B.O., 2010. Climate change increases the likelihood of catastrophic avian mortality events during extreme heat waves. Biol. Lett. 6, 253–256. https://doi.org/10.1098/rsbl.2009.0702

McMichael, A.J., Wilkinson, P., Kovats, R.S., Pattenden, S., Hajat, S., Armstrong, B., Vajanapoom, N., Niciu, E.M., Mahomed, H., Kingkeow, C., Kosnik, M., O'Neill, M.S., Romieu, I., Ramirez-Aguilar, M., Barreto, M.L., Gouveia, N., Nikiforov, B., 2008. International study of temperature, heat and urban mortality: the "ISOTHURM" project. Int. J. Epidemiol. 37, 1121–31. https://doi.org/10.1093/ije/dyn086

McMichael, A.J., Woodruff, R.E., Hales, S., 2006. Climate change and human health: present and future risks. Lancet 367, 859–869. https://doi.org/10.1016/S0140-6736(06)68079-3

Meehl, G.A., Tebaldi, C., 2004. More intense, more frequent, and longer lasting heat waves in the 21st century. Science 305, 994–997. https://doi.org/10.1126/science.1098704

Middey, A., Chaudhuri, S., 2013. The reciprocal relation between lightning and pollution and their impact over Kolkata, India. Environ. Sci. Pollut. Res. Int. 20,

3133–9. https://doi.org/10.1007/s11356-012-1219-z

Mills, G., Buse, A., Gimeno, B., Bermejo, V., Holland, M., Emberson, L., Pleijel, H., 2007. A synthesis of AOT40-based response functions and critical levels of ozone for agricultural and horticultural crops. Atmos. Environ. 41, 2630–2643. https://doi.org/10.1016/j.atmosenv.2006.11.016

Mills, Gi., Hayes, F., Wilkinson, S., Davies, W.J., 2009. Chronic exposure to increasing background ozone impairs stomatal functioning in grassland species. Glob. Chang. Biol. 15, 1522–1533. https://doi.org/10.1111/j.1365-2486.2008.01798.x

Mitchell, D., AchutaRao, K., Allen, M., Bethke, I., Beyerle, U., Ciavarella, A., Forster, P.M., Fuglestvedt, J., Gillett, N., Haustein, K., Ingram, W., Iversen, T., Kharin, V., Klingaman, N., Massey, N., Fischer, E., Schleussner, C.-F., Scinocca, J., Seland, Ø., Shiogama, H., Shuckburgh, E., Sparrow, S., Stone, D., Uhe, P., Wallom, D., Wehner, M., Zaaboul, R., 2017. Half a degree additional warming, prognosis and projected impacts (HAPPI): background and experimental design. Geosci. Model Dev. 10, 571–583. https://doi.org/10.5194/gmd-10-571-2017

Monks, P.S., Archibald, A.T., Colette, A., Cooper, O., Coyle, M., Derwent, R., Fowler, D., Granier, C., Law, K.S., Mills, G.E., Stevenson, D.S., Tarasova, O., Thouret, V., von Schneidemesser, E., Sommariva, R., Wild, O., Williams, M.L., 2015. Tropospheric ozone and its precursors from the urban to the global scale from air quality to short-lived climate forcer. Atmos. Chem. Phys. 15, 8889–8973. https://doi.org/10.5194/acp-15-8889-2015

Mora, C., Dousset, B., Caldwell, I.R., Powell, F.E., Geronimo, R.C., Bielecki, C.R., Counsell, C.W.W., Dietrich, B.S., Johnston, E.T., Louis, L. V., Lucas, M.P.,

McKenzie, M.M., Shea, A.G., Tseng, H., Giambelluca, T.W., Leon, L.R., Hawkins, E., Trauernicht, C., 2017. Global risk of deadly heat. Nat. Clim. Chang. 7, 501–506. https://doi.org/10.1038/nclimate3322

Morgenstern, O., Hegglin, M.I., Rozanov, E., O&apos;Connor, F.M., Abraham, N.L., Akiyoshi, H., Archibald, A.T., Bekki, S., Butchart, N., Chipperfield, M.P., Deushi, M., Dhomse, S.S., Garcia, R.R., Hardiman, S.C., Horowitz, L.W., Jöckel, P., Josse, B., Kinnison, D., Lin, M., Mancini, E., Manyin, M.E., Marchand, M., Marécal, V., Michou, M., Oman, L.D., Pitari, G., Plummer, D.A., Revell, L.E., Saint-Martin, D., Schofield, R., Stenke, A., Stone, K., Sudo, K., Tanaka, T.Y., Tilmes, S., Yamashita, Y., Yoshida, K., Zeng, G., 2017. Review of the global models used within phase 1 of the Chemistry–Climate Model Initiative (CCMI). Geosci. Model Dev. 10, 639–671. https://doi.org/10.5194/gmd-10-639-2017

Murari, K.K., Ghosh, S., Patwardhan, A., Daly, E., Salvi, K., 2015. Intensification of future severe heat waves in India and their effect on heat stress and mortality. Reg. Environ. Chang. 15, 569–579. https://doi.org/10.1007/s10113-014-0660-6

Murazaki, K., Hess, P., 2006. How does climate change contribute to surface ozone change over the United States? J. Geophys. Res. Atmos. 111, 1–16. https://doi.org/10.1029/2005JD005873

Murray, L.T., 2016. Lightning NOx and Impacts on Air Quality. Curr. Pollut. Reports 2, 115–133. https://doi.org/10.1007/s40726-016-0031-7

Naik, V., Horowitz, L.W., Fiore, A.M., Ginoux, P., Mao, J., Aghedo, A.M., Levy, H., 2013. Impact of preindustrial to present-day changes in short-lived pollutant emissions on atmospheric composition and climate forcing. J. Geophys. Res.

Atmos. 118, 8086–8110. https://doi.org/10.1002/jgrd.50608

Nangombe, S., Zhou, T., Zhang, W., Wu, B., Hu, S., Zou, L., Li, D., 2018. Record-breaking climate extremes in Africa under stabilized 1.5 °C and 2 °C global warming scenarios. Nat. Clim. Chang. 8, 375–380. https://doi.org/10.1038/s41558-018-0145-6

Naughton, M.P., Henderson, A., Mirabelli, M.C., Kaiser, R., Wilhelm, J.L., Kieszak, S., Rubin, C.H., McGeehin, M.A., 2002. Heat-related mortality during a 1999 heat wave in Chicago. Am. J. Prev. Med. 22, 221–227. https://doi.org/10.1016/S0749-3797(02)00421-X

Newman, P.A., Oman, L.D., Douglass, A.R., Fleming, E.L., Frith, S.M., Hurwitz, M.M., Kawa, S.R., Jackman, C.H., Krotkov, N.A., Nash, E.R., Nielsen, J.E., Pawson, S., Stolarski, R.S., Velders, G.J.M., 2008. What would have happened to the ozone layer if chlorofluorocarbons (CFCs) had not been regulated? Atmos. Chem. Phys. Discuss.

Niemelä, R., Hannula, M., Rautio, S., Reijula, K., Railio, J., 2002. The effect of air temperature on labour productivity in call centres—a case study. Energy Build. 34, 759–764. https://doi.org/http://dx.doi.org/10.1016/S0378-7788(02)00094-4

NOAA NCDC, n.d. Global Land and Ocean Temperature Anomalies [WWW Document]. URL https://www.ncdc.noaa.gov/cag/global/time-series/globe/land_ocean/ann/12/1880-2019.csv (accessed 3.29.20).

Nuvolone, D., Balzi, D., Pepe, P., Chini, M., Scala, D., Giovannini, F., Cipriani, F., Barchielli, A., 2013. Ozone short-term exposure and acute coronary events: A multicities study in Tuscany (Italy). Environ. Res. 126, 17–23.

https://doi.org/10.1016/j.envres.2013.08.002

O'Gorman, P.A., Muller, C.J., 2010. How closely do changes in surface and column water vapor follow Clausius–Clapeyron scaling in climate change simulations? Environ. Res. Lett. 5, 025207. https://doi.org/10.1088/1748-9326/5/2/025207

O'Neill, B.C., Tebaldi, C., van Vuuren, D.P., Eyring, V., Friedlingstein, P., Hurtt, G., Knutti, R., Kriegler, E., Lamarque, J.-F., Lowe, J., Meehl, G.A., Moss, R., Riahi, K., Sanderson, B.M., 2016. The Scenario Model Intercomparison Project (ScenarioMIP) for CMIP6. Geosci. Model Dev. 9, 3461–3482. https://doi.org/10.5194/gmd-9-3461-2016

O'Neill, M.S., Zanobetti, A., Schwartz, J., 2003. Modifiers of the Temperature and Mortality Association in Seven US Cities. Am. J. Epidemiol. 157, 1074–1082. https://doi.org/10.1093/aje/kwg096

OECD, 2012. Mortality Risk Valuation in Environment, Health and Transport Policies, Mortality risk valuation in environment. OECD Publishing, Paris. https://doi.org/10.1787/9789264130807-en

Ogi, M., Yamazaki, K., Tachibana, Y., 2005. The summer northern annular mode and abnormal summer weather in 2003. Geophys. Res. Lett. 32, 1–4. https://doi.org/10.1029/2004GL021528

Ostro, B., Campbell-Lendrum, D., Corvalán, C., Woodward, A., 2004. Outdoor air pollution: Assessing the environmental burden of disease at national and local levels. WHO Environ. Burd. Dis. Ser. No. 5.

Palipane, E., Grotjahn, R., 2018. Future Projections of the Large-Scale Meteorology

Associated with California Heat Waves in CMIP5 Models. J. Geophys. Res. Atmos. https://doi.org/10.1029/2018JD029000

Parker, W.S., 2011. When Climate Models Agree: The Significance of Robust Model Predictions. Philos. Sci. 78, 579–600. https://doi.org/10.1086/661566

Pascal, M., Laaidi, K., Ledrans, M., Baffert, E., Caserio-Schönemann, C., Le Tertre, A., Manach, J., Medina, S., Rudant, J., Empereur-Bissonnet, P., 2006. France's heat health watch warning system. Int. J. Biometeorol. 50, 144–53. https://doi.org/10.1007/s00484-005-0003-x

Pendergrass, A.G., Lehner, F., Sanderson, B.M., Xu, Y., 2015. Does extreme precipitation intensity depend on the emissions scenario? Geophys. Res. Lett. 42, 8767–8774. https://doi.org/10.1002/2015GL065854

Peng, R.D., Bobb, J.F., Tebaldi, C., McDaniel, L., Bell, M.L., Dominici, F., 2011. Toward a quantitative estimate of future heat wave mortality under global climate change. Environ. Health Perspect. 119, 701–706. https://doi.org/10.1289/ehp.1002430

Peñuelas, J., Llusià, J., 2001. The complexity of factors driving volatile organic compound emissions by plants. Biol. Plant. https://doi.org/10.1023/A:1013797129428

Perkins-Kirkpatrick, S.E., Gibson, P.B., 2017. Changes in regional heatwave characteristics as a function of increasing global temperature. Sci. Rep. 7, 12256. https://doi.org/10.1038/s41598-017-12520-2

Perkins, S.E., Alexander, L. V., Nairn, J.R., 2012. Increasing frequency, intensity and

duration of observed global heatwaves and warm spells. Geophys. Res. Lett. 39, L20714. https://doi.org/10.1029/2012GL053361

Pleijel, H., Danielsson, H., Karlsson, G.., Gelang, J., Karlsson, P.., Selldén, G., 2000. An ozone flux–response relationship for wheat. Environ. Pollut. 109, 453–462. https://doi.org/10.1016/S0269-7491(00)00048-8

Pocock, S.J., 2006. The simplest statistical test: how to check for a difference between treatments. BMJ 332, 1256–8. https://doi.org/10.1136/bmj.332.7552.1256

Pommier, M., Fagerli, H., Gauss, M., Simpson, D., Sharma, S., Sinha, V., Ghude, S.D., Landgren, O., Nyiri, A., Wind, P., 2017. Impact of regional climate change and future emission scenarios on surface O3 and PM2.5 over India. Atmos. Chem. Phys. Discuss. 1–41. https://doi.org/10.5194/acp-2017-519

Porter, W.C., Heald, C.L., Cooley, D., Russell, B., 2015. Investigating the observed sensitivities of air-quality extremes to meteorological drivers via quantile regression. Atmos. Chem. Phys. 15, 10349–10366. https://doi.org/10.5194/acp-15-10349-2015

Post, E.S., Grambsch, A., Weaver, C., Morefield, P., Huang, J., Leung, L.Y., Nolte, C.G., Adams, P., Liang, X.Z., Zhu, J.H., Mahoney, H., 2012. Variation in estimated ozone-related health impacts of climate change due to modeling choices and assumptions. Environ. Health Perspect. 120, 1559–1564. https://doi.org/DOI:10.1289/ehp.1104271

Prather, M., Midgley, P., Rowland, F.S., Stolarski, R., 1996. The ozone layer: the road not taken. Nature 381, 551–554. https://doi.org/10.1038/381551a0

Punger, E.M., West, J.J., 2013. The effect of grid resolution on estimates of the burden of ozone and fine particulate matter on premature mortality in the USA. Air Qual. Atmos. Heal. 6, 563–573. https://doi.org/10.1007/s11869-013-0197-8

Rafiemanesh, H., Mehtarpour, M., Khani, F., Hesami, S.M., Shamlou, R., Towhidi, F., Salehiniya, H., Makhsosi, B.R., Moini, A., 2016. Epidemiology, incidence and mortality of lung cancer and their relationship with the development index in the world. J. Thorac. Dis. 8, 1094–1102. https://doi.org/10.21037/jtd.2016.03.91

Rasmussen, D.J., Fiore, A.M., Naik, V., Horowitz, L.W., McGinnis, S.J., Schultz, M.G., 2012. Surface ozone-temperature relationships in the eastern US: A monthly climatology for evaluating chemistry-climate models. Atmos. Environ. 47, 142–153. https://doi.org/10.1016/j.atmosenv.2011.11.021

Rasmussen, D.J., Hu, J., Mahmud, A., Kleeman, M.J., 2013. The Ozone–Climate Penalty: Past, Present, and Future. Environ. Sci. Technol. 47, 14258–14266. https://doi.org/10.1021/es403446m

Rees, N., Wickham, A., Choi, Y., Burdziej, J., Glovinsky, M., Wicks, T., Wang, S., Narasimhan, G., Anthony, D., Chandy, L., 2019. Silent Suffocation in Africa. New York.

Reichler, T., Kim, J., 2008. How Well Do Coupled Models Simulate Today's Climate? Bull. Am. Meteorol. Soc. 89, 303–312. https://doi.org/10.1175/BAMS-89-3-303

Revell, L.E., Tummon, F., Stenke, a., Sukhodolov, T., Coulon, a., Rozanov, E., Garny, H., Grewe, V., Peter, T., 2015. Drivers of the tropospheric ozone budget throughout the 21st century under the medium-high climate scenario RCP 6.0. Atmos. Chem. Phys. 15, 5887–5902. https://doi.org/10.5194/acp-15-5887-2015

Rhines, A., Huybers, P., 2013. Frequent summer temperature extremes reflect changes in the mean, not the variance. Proc. Natl. Acad. Sci. 110, E546–E546. https://doi.org/10.1073/pnas.1218748110

Riahi, K., Grübler, A., Nakicenovic, N., 2007. Scenarios of long-term socio-economic and environmental development under climate stabilization. Technol. Forecast. Soc. Change 74, 887–935. https://doi.org/10.1016/j.techfore.2006.05.026

Riahi, K., Rao, S., Krey, V., Cho, C., Chirkov, V., Fischer, G., Kindermann, G., Nakicenovic, N., Rafaj, P., 2011. RCP 8.5—A scenario of comparatively high greenhouse gas emissions. Clim. Change 109, 33–57. https://doi.org/10.1007/s10584-011-0149-y

Riahi, K., van Vuuren, D.P., Kriegler, E., Edmonds, J., O'Neill, B.C., Fujimori, S., Bauer, N., Calvin, K., Dellink, R., Fricko, O., Lutz, W., Popp, A., Cuaresma, J.C., KC, S., Leimbach, M., Jiang, L., Kram, T., Rao, S., Emmerling, J., Ebi, K., Hasegawa, T., Havlik, P., Humpenöder, F., Da Silva, L.A., Smith, S., Stehfest, E., Bosetti, V., Eom, J., Gernaat, D., Masui, T., Rogelj, J., Strefler, J., Drouet, L., Krey, V., Luderer, G., Harmsen, M., Takahashi, K., Baumstark, L., Doelman, J.C., Kainuma, M., Klimont, Z., Marangoni, G., Lotze-Campen, H., Obersteiner, M., Tabeau, A., Tavoni, M., 2017. The Shared Socioeconomic Pathways and their energy, land use, and greenhouse gas emissions implications: An overview. Glob. Environ. Chang. 42. https://doi.org/10.1016/j.gloenvcha.2016.05.009

Rienecker, M.M., Suarez, M.J., Gelaro, R., Todling, R., Bacmeister, J., Liu, E., Bosilovich, M.G., Schubert, S.D., Takacs, L., Kim, G.-K., Bloom, S., Chen, J., Collins, D., Conaty, A., da Silva, A., Gu, W., Joiner, J., Koster, R.D., Lucchesi, R., Molod, A., Owens, T., Pawson, S., Pegion, P., Redder, C.R., Reichle, R.,

Robertson, F.R., Ruddick, A.G., Sienkiewicz, M., Woollen, J., Rienecker, M.M., Suarez, M.J., Gelaro, R., Todling, R., Julio Bacmeister, Liu, E., Bosilovich, M.G., Schubert, S.D., Takacs, L., Kim, G.-K., Bloom, S., Chen, J., Collins, D., Conaty, A., Silva, A. da, Gu, W., Joiner, J., Koster, R.D., Lucchesi, R., Molod, A., Owens, T., Pawson, S., Pegion, P., Redder, C.R., Reichle, R., Robertson, F.R., Ruddick, A.G., Sienkiewicz, M., Woollen, J., 2011. MERRA: NASA's Modern-Era Retrospective Analysis for Research and Applications. J. Clim. 24, 3624–3648. https://doi.org/10.1175/JCLI-D-11-00015.1

Robine, J.-M., Cheung, S.L.K., Le Roy, S., Van Oyen, H., Griffiths, C., Michel, J.-P., Herrmann, F.R., 2008. Death toll exceeded 70,000 in Europe during the summer of 2003. C. R. Biol. 331, 171–178. https://doi.org/10.1016/j.crvi.2007.12.001

Robinson, P.J., 2001. On the Definition of a Heat Wave. J. Appl. Meteorol. 40, 762–775. https://doi.org/10.1175/1520-0450(2001)040<0762:OTDOAH>2.0.CO;2

Robson, M., Rogula, J., Auffhammer, M., Miller, N., VanDorn, J., 2010. An integrated framework for quantifying and valuing climate change impacts on urban energy and infrastructure: A Chicago case study. J. Great Lakes Res. 36, 94–105. https://doi.org/10.1016/j.jglr.2010.03.011

Romer, P.S., Duffey, K.C., Wooldridge, P.J., Edgerton, E., Baumann, K., Feiner, P.A., Miller, D.O., Brune, W.H., Koss, A.R., de Gouw, J.A., Misztal, P.K., Goldstein, A.H., Cohen, R.C., 2018. Effects of temperature-dependent NOx emissions on continental ozone production. Atmos. Chem. Phys. 18, 2601–2614. https://doi.org/10.5194/acp-18-2601-2018

Rosenzweig, C., Iglesias, A., Yang, X., Epstein, P.R., Chivian, E., 2001. Climate change

and extreme weather events - implications for food production, plant diseases, and pests. Chang. Hum. Heal. 2, 90–104. https://doi.org/10.1097/JOM.0b013e31817d32da

Rougier, J., Sexton, D.M.H., Murphy, J.M., Stainforth, D., 2009. Analyzing the Climate Sensitivity of the HadSM3 Climate Model Using Ensembles from Different but Related Experiments. J. Clim. 22, 3540–3557. https://doi.org/10.1175/2008JCLI2533.1

Russo, S., Dosio, A., Sillmann, J., 2010. Top ten European heatwaves since 1950 and their occurrence in the future. Environ. Res. Lett. 10, 124003. https://doi.org/10.1088/1748-9326/10/12/124003

Sander, S.P., Golden, D.M., Kurylo, M.J., Moortgat, G.K., Wine, P.H., Ravishankara, A.R., Kolb, C.E., Molina, M.J., Finlayson-Pitts, B.J., Huie, R.E., Orkin, V.L., 2006. Chemical kinetics and photochemical data for use in Atmospheric Studies Evaluation Number 15. Eval. 15, JPL Publ. 06–2, Jet Propuls. Lab. 523.

Sanders, N.J., 2012. What Doesn't Kill You Makes You Weaker. J. Hum. Resour. 47, 826–850. https://doi.org/10.3368/jhr.47.3.826

Sanderson, B.M., Xu, Y., Tebaldi, C., Wehner, M., O&apos;Neill, B., Jahn, A., Pendergrass, A.G., Lehner, F., Strand, W.G., Lin, L., Knutti, R., Lamarque, J.-F., 2017. Community Climate Simulations to assess avoided impacts in 1.5 °C and 2 °C futures. Earth Syst. Dyn. Discuss. 1–33. https://doi.org/10.5194/esd-2017-42

Sanderson, M.G., Jones, C.D., Collins, W.J., Johnson, C.E., Derwent, R.G., 2003. Effect of Climate Change on Isoprene Emissions and Surface Ozone Levels. Geophys. Res. Lett. 30, 1936. https://doi.org/10.1029/2003GL017642

Schindlbacher, A., 2004. Effects of soil moisture and temperature on NO, NO 2 , and N 2 O emissions from European forest soils. J. Geophys. Res. 109, D17302. https://doi.org/10.1029/2004JD004590

Schlenker, W., Lobell, D.B., 2010. Robust negative impacts of climate change on African agriculture. Environ. Res. Lett. 5, 014010. https://doi.org/10.1088/1748-9326/5/1/014010

Schleussner, C.-F., Lissner, T.K., Fischer, E.M., Wohland, J., Perrette, M., Golly, A., Rogelj, J., Childers, K., Schewe, J., Frieler, K., Mengel, M., Hare, W., Schaeffer, M., 2016. Differential climate impacts for policy-relevant limits to global warming: the case of 1.5 °C and 2 °C. Earth Syst. Dyn. 7, 327–351. https://doi.org/10.5194/esd-7-327-2016

Schleussner, C.-F., Pfleiderer, P., Fischer, E.M., 2017. In the observational record half a degree matters. Nat. Clim. Chang. 7, 460–462. https://doi.org/10.1038/nclimate3320

Schnell, J.L., Holmes, C.D., Jangam, A., Prather, M.J., 2014. Skill in forecasting extreme ozone pollution episodes with a global atmospheric chemistry model. Atmos. Chem. Phys. 14, 7721–7739. https://doi.org/10.5194/acp-14-7721-2014

Schnell, J.L., Prather, M.J., Josse, B., Naik, V., Horowitz, L.W., Zeng, G., Shindell, D.T., Faluvegi, G., 2016. Effect of climate change on surface ozone over North America, Europe, and East Asia. Geophys. Res. Lett. n/a-n/a. https://doi.org/10.1002/2016GL068060

Schultz, M.G., Schröder, S., Lyapina, O., Cooper, O., Galbally, I., Petropavlovskikh, I., Von Schneidemesser, E., Tanimoto, H., Elshorbany, Y., Naja, M., Seguel, R.,

Dauert, U., Eckhardt, P., Feigenspahn, S., Fiebig, M., Hjellbrekke, A.-G., Hong, Y.-D., Christian Kjeld, P., Koide, H., Lear, G., Tarasick, D., Ueno, M., Wallasch, M., Baumgardner, D., Chuang, M.-T., Gillett, R., Lee, M., Molloy, S., Moolla, R., Wang, T., Sharps, K., Adame, J.A., Ancellet, G., Apadula, F., Artaxo, P., Barlasina, M., Bogucka, M., Bonasoni, P., Chang, L., Colomb, A., Cuevas, E., Cupeiro, M., Degorska, A., Ding, A., Fröhlich, M., Frolova, M., Gadhavi, H., Gheusi, F., Gilge, S., Gonzalez, M.Y., Gros, V., Hamad, S.H., Helmig, D., Henriques, D., Hermansen, O., Holla, R., Huber, J., Im, U., Jaffe, D.A., Komala, N., Kubistin, D., Lam, K.-S., Laurila, T., Lee, H., Levy, I., Mazzoleni, C., Mazzoleni, L., McClure-Begley, A., Mohamad, M., Murovic, M., Navarro-Comas, M., Nicodim, F., Parrish, D., Read, K.A., Reid, N., Ries, L., Saxena, P., Schwab, J.J., Scorgie, Y., Senik, I., Simmonds, P., Sinha, V., Skorokhod, A., Spain, G., Spangl, W., Spoor, R., Springston, S.R., Steer, K., Steinbacher, M., Suharguniyawan, E., Torre, P., Trickl, T., Weili, L., Weller, R., Xu, X., Xue, L., Zhiqiang, M., 2017. Tropospheric Ozone Assessment Report: Database and Metrics Data of Global Surface Ozone Observations. Elem Sci Anth 5, 58. https://doi.org/10.1525/elementa.244

Seppänen, O., Fisk, W.J., Lei, Q.H., 2006. Effect of Temperature on Task Performance in Office Environment. Lawrence Berkeley Natl. Lab. 11.

Serôa da Motta, R. de P., 2019. The sustainable development goals and 1.5 °C climate change. World Rev. Sci. Technol. Sust. Dev. 15, 123–144.

Sfîcă, L., Croitoru, A.-E., Iordache, I., Ciupertea, A.-F., 2017. Synoptic Conditions Generating Heat Waves and Warm Spells in Romania. Atmosphere (Basel). 8, 50. https://doi.org/10.3390/atmos8030050

Sgubin, G., Swingedouw, D., Drijfhout, S., Mary, Y., Bennabi, A., 2017. Abrupt cooling over the North Atlantic in modern climate models. Nat. Commun. 8, 14375. https://doi.org/10.1038/ncomms14375

Shi, L., Kloog, I., Zanobetti, A., Liu, P., Schwartz, J.D., 2015. Impacts of temperature and its variability on mortality in New England. Nat. Clim. Chang. 5, 1–5. https://doi.org/10.1038/nclimate2704

Shindell, D., Faluvegi, G., 2009. Climate response to regional radiative forcing during the twentieth century. Nat. Geosci. 2, 294–300. https://doi.org/10.1038/ngeo473

Shindell, D.T., Faluvegi, G., Rotstayn, L., Milly, G., 2015. Spatial patterns of radiative forcing and surface temperature response. J. Geophys. Res. Atmos. 120, 5385–5403. https://doi.org/10.1002/2014JD022752

Sicard, P., Anav, A., De Marco, A., Paoletti, E., 2017. Projected global ground-level ozone impacts on vegetation under different emission and climate scenarios. Atmos. Chem. Phys. 17, 12177–12196. https://doi.org/10.5194/acp-17-12177-2017

Sicard, P., De Marco, A., Troussier, F., Renou, C., Vas, N., Paoletti, E., 2013. Decrease in surface ozone concentrations at Mediterranean remote sites and increase in the cities. Atmos. Environ. 79, 705–715. https://doi.org/10.1016/j.atmosenv.2013.07.042

Sillman, S., Samson, P.J., 1995. Impact of temperature on oxidant photochemistry in urban, polluted rural and remote environments. J. Geophys. Res. 100, 11497. https://doi.org/10.1029/94JD02146

Singsaas, E.L., Sharkey, T.D., 2000. The effects of high temperature on isoprene synthesis in oak leaves. Plant, Cell Environ. 23, 751–757. https://doi.org/10.1046/j.1365-3040.2000.00582.x

Sitch, S., Cox, P.M., Collins, W.J., Huntingford, C., 2007. Indirect radiative forcing of climate change through ozone effects on the land-carbon sink. Nature 448, 791–794. https://doi.org/10.1038/nature06059

Solberg, S., Hov, Ø., Søvde, A., Isaksen, I.S.A., Coddeville, P., De Backer, H., Forster, C., Orsolini, Y., Uhse, K., 2008. European surface ozone in the extreme summer 2003. J. Geophys. Res. 113, D07307. https://doi.org/10.1029/2007JD009098

Squire, O.J., Archibald, A.T., Abraham, N.L., Beerling, D.J., Hewitt, C.N., Lathière, J., Pike, R.C., Telford, P.J., Pyle, J.A., 2014. Influence of future climate and cropland expansion on isoprene emissions and tropospheric ozone. Atmos. Chem. Phys. 14, 1011–1024. https://doi.org/10.5194/acp-14-1011-2014

Steadman, R.G., 1984. A Universal Scale of Apparent Temperature. J. Clim. Appl. Meteorol. 23, 1674–1687. https://doi.org/10.1175/1520-0450(1984)023<1674:AUSOAT>2.0.CO;2

Stern, N.H., 2007. The Economics of Climate Change: the Stern Review. Cambridge University Press, Cambridge, UK.

Stevenson, D., Doherty, R., Sanderson, M., Johnson, C., Collins, B., Derwent, D., 2005. Impacts of climate change and variability on tropospheric ozone and its precursors. Faraday Discuss. 130, 41. https://doi.org/10.1039/b417412g

Stevenson, D.S., Dentener, F.J., Schultz, M.G., Ellingsen, K., van Noije, T.P.C., Wild,

O., Zeng, G., Amann, M., Atherton, C.S., Bell, N., Bergmann, D.J., Bey, I., Butler, T., Cofala, J., Collins, W.J., Derwent, R.G., Doherty, R.M., Drevet, J., Eskes, H.J., Fiore, A.M., Gauss, M., Hauglustaine, D.A., Horowitz, L.W., Isaksen, I.S.A., Krol, M.C., Lamarque, J.-F., Lawrence, M.G., Montanaro, V., Müller, J.-F., Pitari, G., Prather, M.J., Pyle, J.A., Rast, S., Rodriguez, J.M., Sanderson, M.G., Savage, N.H., Shindell, D.T., Strahan, S.E., Sudo, K., Szopa, S., 2006. Multimodel ensemble simulations of present-day and near-future tropospheric ozone. J. Geophys. Res. 111, D08301. https://doi.org/10.1029/2005JD006338

Stevenson, D.S., Young, P.J., Naik, V., Lamarque, J.-F., Shindell, D.T., Voulgarakis, A., Skeie, R.B., Dalsoren, S.B., Myhre, G., Berntsen, T.K., Folberth, G.A., Rumbold, S.T., Collins, W.J., MacKenzie, I.A., Doherty, R.M., Zeng, G., Van Noije, T.P.C., Strunk, A., Bergmann, D., Cameron-Smith, P., Plummer, D.A., Strode, S.A., Horowitz, L., Lee, Y.H., Szopa, S., Sudo, K., Nagashima, T., Josse, B., Cionni, I., Righi, M., Eyring, V., Conley, A., Bowman, K.W., Wild, O., Archibald, A., 2013. Tropospheric ozone changes, radiative forcing and attribution to emissions in the Atmospheric Chemistry and Climate Model Intercomparison Project (ACCMIP). Atmos. Chem. Phys. 13, 3063–3085.

Stock, Z.S., Russo, M.R., Pyle, J.A., 2014. Representing ozone extremes in European megacities: the importance of resolution in a global chemistry climate model. Atmos. Chem. Phys. 14, 3899–3912. https://doi.org/10.5194/acp-14-3899-2014

Sudo, K., Takahashi, M., Akimoto, H., 2003. Future changes in stratosphere-troposphere exchange and their impacts on future tropospheric ozone simulations. Geophys. Res. Lett. 30. https://doi.org/10.1029/2003GL018526

Sutton, R., Suckling, E., Hawkins, E., 2015. What does global mean temperature tell us

about local climate? Philos. Trans. R. Soc. A Math. Phys. Eng. Sci. 373, 20140426. https://doi.org/10.1098/rsta.2014.0426

Sutton, R.T., 2018. Ideas: a simple proposal to improve the contribution of IPCC WG1 to the assessment and communication of climate change risks. Earth Syst. Dyn. Discuss. 1–3. https://doi.org/10.5194/esd-2018-36

Tai, A.P.K., Mickley, L.J., Jacob, D.J., 2012. Impact of 2000–2050 climate change on fine particulate matter (PM&lt;sub&gt;2.5&lt;/sub&gt;) air quality inferred from a multi-model analysis of meteorological modes. Atmos. Chem. Phys. 12, 11329–11337. https://doi.org/10.5194/acp-12-11329-2012

Tai, A.P.K., Val Martin, M., 2017. Impacts of ozone air pollution and temperature extremes on crop yields: Spatial variability, adaptation and implications for future food security. Atmos. Environ. 169, 11–21. https://doi.org/10.1016/j.atmosenv.2017.09.002

Takahashi, K., Honda, Y., Emori, S., 2007. Assessing Mortality Risk from Heat Stress due to Global Warming. J. Risk Res. 10, 339–354. https://doi.org/10.1080/13669870701217375

Tan, J., Zheng, Y., Song, G., Kalkstein, L.S., Kalkstein, A.J., Tang, X., 2007. Heat wave impacts on mortality in Shanghai, 1998 and 2003. Int. J. Biometeorol. 51, 193–200. https://doi.org/10.1007/s00484-006-0058-3

Tang, Q., Leng, G., Groisman, P.Y., 2012. European Hot Summers Associated with a Reduction of Cloudiness. J. Clim. 25, 3637–3644. https://doi.org/10.1175/JCLI-D-12-00040.1

Taylor, K.E., Stouffer, R.J., Meehl, G.A., 2012a. An Overview of CMIP5 and the Experiment Design. Bull. Am. Meteorol. Soc. 93, 485–498. https://doi.org/10.1175/BAMS-D-11-00094.1

Taylor, K.E., Stouffer, R.J., Meehl, G.A., 2012b. An overview of CMIP5 and the experiment design. Bull. Am. Meteorol. Soc.

Tebaldi, C., O'Neill, B., Lamarque, J.-F., 2015. Sensitivity of regional climate to global temperature and forcing. Environ. Res. Lett. 10, 074001. https://doi.org/10.1088/1748-9326/10/7/074001

The World Bank, 2014. GDP (current US$) [WWW Document]. World Dev. Indic.

The World Bank Group, 2017a. Population Estimates and Projections [WWW Document]. URL https://data.worldbank.org/data-catalog/population-projection-tables (accessed 10.24.17).

The World Bank Group, 2017b. GDP (constant 2010 US$) [WWW Document]. URL https://data.worldbank.org/indicator/NY.GDP.MKTP.KD? (accessed 10.11.17).

The World Bank Group, n.d. Death rate, crude (per 1,000 people) [WWW Document]. URL http://data.worldbank.org/indicator/SP.DYN.CDRT.IN (accessed 8.15.16).

Thomson, A.M., Calvin, K. V., Smith, S.J., Kyle, G.P., Volke, A., Patel, P., Delgado-Arias, S., Bond-Lamberty, B., Wise, M.A., Clarke, L.E., Edmonds, J.A., 2011. RCP4.5: a pathway for stabilization of radiative forcing by 2100. Clim. Change 109, 77–94. https://doi.org/10.1007/s10584-011-0151-4

Thornbrugh, C., 2001. Are America's Cities Ready for the Hot Times Ahead?

Tilmes, S., Lamarque, J.-F., Emmons, L.K., Kinnison, D.E., Marsh, D., Garcia, R.R., Smith, A.K., Neely, R.R., Conley, A., Vitt, F., Val Martin, M., Tanimoto, H., Simpson, I., Blake, D.R., Blake, N., 2016. Representation of the Community Earth System Model (CESM1) CAM4-chem within the Chemistry-Climate Model Initiative (CCMI). Geosci. Model Dev. 9, 1853–1890. https://doi.org/10.5194/gmd-9-1853-2016

Tomczyk, A.M., Piotrowski, P., Bednorz, E., 2017. Warm spells in Northern Europe in relation to atmospheric circulation. Theor. Appl. Climatol. 128, 623–634. https://doi.org/10.1007/s00704-015-1727-0

Tørseth, K., Aas, W., Breivik, K., Fjæraa, A.M., Fiebig, M., Hjellbrekke, A.G., Lund Myhre, C., Solberg, S., Yttri, K.E., 2012. Introduction to the European Monitoring and Evaluation Programme (EMEP) and observed atmospheric composition change during 1972&ndash;2009. Atmos. Chem. Phys. 12, 5447–5481. https://doi.org/10.5194/acp-12-5447-2012

Trenberth, K.E., Dai, A., van der Schrier, G., Jones, P.D., Barichivich, J., Briffa, K.R., Sheffield, J., 2014. Global warming and changes in drought. Nat. Clim. Chang. 4, 17–22. https://doi.org/10.1038/nclimate2067

Trenberth, K.E., Fasullo, J.T., 2012. Climate extremes and climate change: The Russian heat wave and other climate extremes of 2010. J. Geophys. Res. Atmos. 117, n/a-n/a. https://doi.org/10.1029/2012JD018020

Turner, M.C., Jerrett, M., Pope, C.A., Krewski, D., Gapstur, S.M., Diver, W.R., Beckerman, B.S., Marshall, J.D., Su, J., Crouse, D.L., Burnett, R.T., 2016. Long-Term Ozone Exposure and Mortality in a Large Prospective Study. Am. J. Respir.

Crit. Care Med. 193. https://doi.org/10.1164/rccm.201508-1633OC

Turnock, S.T., Butt, E.W., Richardson, T.B., Mann, G.W., Reddington, C.L., Forster, P.M., Haywood, J., Crippa, M., Janssens-Maenhout, G., Johnson, C.E., Bellouin, N., Carslaw, K.S., Spracklen, D. V, 2016. The impact of European legislative and technology measures to reduce air pollutants on air quality, human health and climate. Environ. Res. Lett. 11, 024010. https://doi.org/10.1088/1748-9326/11/2/024010

UN, 2015. Transforming our world: The 2030 agenda for sustainaible development. United Nations 15–18.

UNCTADstat, n.d. World seaborne trade by types of cargo and by group of economies [WWW Document]. United Nations Conf. Trade Dev. URL http://unctadstat.unctad.org/wds/TableViewer/tableView.aspx?ReportId=32363 (accessed 5.10.17).

UNFCCC, 2015. Adoption of the Paris Agreement, in: Conference of the Parties on Its Twenty-First Session. p. 32. https://doi.org/FCCC/CP/2015/L.9

United Nations, 1992. United Nations Framework Convention on Climate Change (UNFCCC). New York.

United Nations Economic Comission for Europe, 1979. 1979 Convention on long-range transboundary air pollution.

Utembe, S., Rayner, P., Silver, J., Guérette, E.-A., Fisher, J., Emmerson, K., Cope, M., Paton-Walsh, C., Griffiths, A., Duc, H., Monk, K., Scorgie, Y., 2018. Hot Summers: Effect of Extreme Temperatures on Ozone in Sydney, Australia.

Atmosphere (Basel). 9, 466. https://doi.org/10.3390/atmos9120466

Utembe, S.R., Hansford, G.M., Sanderson, M.G., Freshwater, R.A., Pratt, K.F.E., Williams, D.E., Cox, R.A., Jones, R.L., 2006. An ozone monitoring instrument based on the tungsten trioxide (WO 3) semiconductor. Sensors Actuators, B Chem. 114, 507–512. https://doi.org/10.1016/j.snb.2005.04.049

van Vuuren, D., Stehfest, E., den Elzen, M., Kram, T., van Vliet, J., Deetman, S., Isaac, M., Klein Goldewijk, K., Hof, A., Mendoza Beltran, A., Oostenrijk, R., van Ruijven, B., 2011. RCP 2.6: exploring the possibility to keep global mean temperature increase below 2°C. Clim. Change 109, 95–116. https://doi.org/10.1007/s10584-011-0152-3

van Vuuren, D.P., Edmonds, J., Kainuma, M., Riahi, K., Thomson, A., Hibbard, K., Hurtt, G.C., Kram, T., Krey, V., Lamarque, J.-F., Masui, T., Meinshausen, M., Nakicenovic, N., Smith, S.J., Rose, S.K., 2011. The representative concentration pathways: an overview. Clim. Change 109, 5–31. https://doi.org/10.1007/s10584-011-0148-z

Vandyck, T., Keramidas, K., Kitous, A., Spadaro, J. V., Van Dingenen, R., Holland, M., Saveyn, B., 2018. Air quality co-benefits for human health and agriculture counterbalance costs to meet Paris Agreement pledges. Nat. Commun. 9, 4939. https://doi.org/10.1038/s41467-018-06885-9

Vardoulakis, S., Dear, K., Hajat, S., Heaviside, C., Eggen, B., McMichael, A.J., 2014. Comparative Assessment of the Effects of Climate Change on Heat- and Cold-Related Mortality in the United Kingdom and Australia. Environ. Health Perspect. 122, 1285–1292. https://doi.org/10.1289/ehp.1307524

Vautard, R., Beekmann, M., Desplat, J., Hodzic, A., Morel, S., 2007. Air quality in Europe during the summer of 2003 as a prototype of air quality in a warmer climate. Comptes Rendus Geosci. 339, 747–763. https://doi.org/10.1016/j.crte.2007.08.003

Vautard, R., Gobiet, A., Sobolowski, S., Kjellström, E., Stegehuis, A., Watkiss, P., Mendlik, T., Landgren, O., Nikulin, G., Teichmann, C., Jacob, D., 2014. The European climate under a 2 °C global warming. Environ. Res. Lett. 9, 034006. https://doi.org/10.1088/1748-9326/9/3/034006

Vautard, R., Honoré, C., Beekmann, M., Rouil, L., 2005. Simulation of ozone during the August 2003 heat wave and emission control scenarios. Atmos. Environ. 39, 2957–2967. https://doi.org/10.1016/j.atmosenv.2005.01.039

Vestreng, V., Ntziachristos, L., Semb, A., Reis, S., Isaksen, I.S.A., Tarrasón, L., 2009. Evolution of NO$_x$ emissions in Europe with focus on road transport control measures. Atmos. Chem. Phys. 9, 1503–1520. https://doi.org/10.5194/acp-9-1503-2009

Vicedo-Cabrera, A.M., Guo, Y., Sera, F., Huber, V., Schleussner, C.-F., Mitchell, D., Tong, S., Coelho, M. de S.Z.S., Saldiva, P.H.N., Lavigne, E., Correa, P.M., Ortega, N.V., Kan, H., Osorio, S., Kyselý, J., Urban, A., Jaakkola, J.J.K., Ryti, N.R.I., Pascal, M., Goodman, P.G., Zeka, A., Michelozzi, P., Scortichini, M., Hashizume, M., Honda, Y., Hurtado-Diaz, M., Cruz, J., Seposo, X., Kim, H., Tobias, A., Íñiguez, C., Forsberg, B., Åström, D.O., Ragettli, M.S., Röösli, M., Guo, Y.L., Wu, C., Zanobetti, A., Schwartz, J., Bell, M.L., Dang, T.N., Do Van, D., Heaviside, C., Vardoulakis, S., Hajat, S., Haines, A., Armstrong, B., Ebi, K.L., Gasparrini, A., 2018. Temperature-related mortality impacts under and beyond

Paris Agreement climate change scenarios. Clim. Change 150, 391–402. https://doi.org/10.1007/s10584-018-2274-3

Vicedo-Cabrera, A.M., Sera, F., Liu, C., Armstrong, B., Milojevic, A., Guo, Y., Tong, S., Lavigne, E., Kyselý, J., Urban, A., Orru, H., Indermitte, E., Pascal, M., Huber, V., Schneider, A., Katsouyanni, K., Samoli, E., Stafoggia, M., Scortichini, M., Hashizume, M., Honda, Y., Ng, C.F.S., Hurtado-Diaz, M., Cruz, J., Silva, S., Madureira, J., Scovronick, N., Garland, R.M., Kim, H., Tobias, A., Íñiguez, C., Forsberg, B., Åström, C., Ragettli, M.S., Röösli, M., Guo, Y.-L.L., Chen, B.-Y., Zanobetti, A., Schwartz, J., Bell, M.L., Kan, H., Gasparrini, A., 2020. Short term association between ozone and mortality: global two stage time series study in 406 locations in 20 countries. BMJ m108. https://doi.org/10.1136/bmj.m108

Vieno, M., Dore, A.J., Stevenson, D.S., Doherty, R.M., Heal, M.R., Reis, S., Hallsworth, S., Tarrason, L., Wind, P., Fowler, D., Simpson, D., Sutton, M.A., 2010. Modelling surface ozone during the 2003 heat-wave in the UK. Atmos. Chem. Phys. 10, 7963–7978. https://doi.org/10.5194/acp-10-7963-2010

Vincent, K., 2007. Uncertainty in adaptive capacity and the importance of scale. Glob. Environ. Chang. https://doi.org/10.1016/j.gloenvcha.2006.11.009

Wakamatsu, S., Morikawa, T., Ito, A., 2013. Air Pollution Trends in Japan between 1970 and 2012 and Impact of Urban Air Pollution Countermeasures. Asian J. Atmos. Environ. 7, 177–190. https://doi.org/10.5572/ajae.2013.7.4.177

Wang, J.X.L., Angell, J.K., 1999. Air Stagnation Climatology for the United States. NOAA Tech. Rep.

Wang, M., Overland, J.E., 2012. A sea ice free summer Arctic within 30 years: An

update from CMIP5 models. Geophys. Res. Lett. 39. https://doi.org/10.1029/2012GL052868

Wang, Y., Shen, L., Wu, S., Mickley, L., He, J., Hao, J., 2013. Sensitivity of surface ozone over China to 2000–2050 global changes of climate and emissions. Atmos. Environ. 75, 374–382. https://doi.org/10.1016/j.atmosenv.2013.04.045

Watson, L., Lacressonnière, G., Gauss, M., Engardt, M., Andersson, C., Josse, B., Marécal, V., Nyiri, A., Sobolowski, S., Siour, G., Szopa, S., Vautard, R., 2016. Impact of emissions and +2 °C climate change upon future ozone and nitrogen dioxide over Europe. Atmos. Environ. 142, 271–285. https://doi.org/10.1016/j.atmosenv.2016.07.051

Weber, T., Haensler, A., Rechid, D., Pfeifer, S., Eggert, B., Jacob, D., 2018. Analyzing Regional Climate Change in Africa in a 1.5, 2, and 3°C Global Warming World. Earth's Futur. 6, 643–655. https://doi.org/10.1002/2017EF000714

Wehner, M., Stone, D., Mitchell, D., Shiogama, H., Fischer, E., Graff, L.S., Kharin, V. V., Lierhammer, L., Sanderson, B., Krishnan, H., 2018. Changes in extremely hot days under stabilized 1.5 and 2.0 °C global warming scenarios as simulated by the HAPPI multi-model ensemble. Earth Syst. Dyn. 9, 299–311. https://doi.org/10.5194/esd-9-299-2018

Wernberg, T., Smale, D.A., Tuya, F., Thomsen, M.S., Langlois, T.J., de Bettignies, T., Bennett, S., Rousseaux, C.S., 2012. An extreme climatic event alters marine ecosystem structure in a global biodiversity hotspot. Nat. Clim. Chang. 3, 78–82. https://doi.org/10.1038/nclimate1627

Whan, K., Zscheischler, J., Orth, R., Shongwe, M., Rahimi, M., Asare, E.O.,

Seneviratne, S.I., 2015. Impact of soil moisture on extreme maximum temperatures in Europe. Weather Clim. Extrem. 9, 57–67. https://doi.org/10.1016/j.wace.2015.05.001

WHO, 2016. Healthy life expectancy (HALE) Data by country [WWW Document]. Mortal. Glob. Heal. Estim. URL http://apps.who.int/gho/data/node.main.HALE?lang=en (accessed 10.9.17).

WHO, 2013a. Health risks of air pollution in Europe – HRAPIE project. Recommendations for concentration–response functions for cost–benefit analysis of particulate matter, ozone and nitrogen dioxide [WWW Document]. URL http://www.euro.who.int/en/health-topics/environment-and-health/air-quality/publications/2013/health-risks-of-air-pollution-in-europe-hrapie-project.-recommendations-for-concentrationresponse-functions-for-costbenefit-analysis-of-particulate-matter,-ozone (accessed 1.5.18).

WHO, 2013b. Projections of mortality and causes of death, 2015 and 2030 [WWW Document]. URL http://www.who.int/healthinfo/global_burden_disease/projections/en/ (accessed 3.22.18).

Wichmann, J., Voyi, K., 2012. Ambient air pollution exposure and respiratory, cardiovascular and cerebrovascular mortality in Cape Town, South Africa: 2001-2006. Int. J. Environ. Res. Public Health 9, 3978–4016. https://doi.org/10.3390/ijerph9113978

Wild, O., Prather, M.J., 2006. Global tropospheric ozone modeling: Quantifying errors due to grid resolution. J. Geophys. Res. Atmos. 111.

Wild, O., Zhu, X., Prather, M.J., 2000. Fast-J: Accurate Simulation of In- and Below-Cloud Photolysis in Tropospheric Chemical Models. J. Atmos. Chem. 37, 245–282. https://doi.org/10.1023/A:1006415919030

Williams, E.J., Fehsenfeld, F.C., 1991. Measurement of soil nitrogen oxide emissions at three North American ecosystems. J. Geophys. Res. 96, 1033. https://doi.org/10.1029/90JD01903

Winton, M., Adcroft, A., Griffies, S.M., Hallberg, R.W., Horowitz, L.W., Stouffer, R.J., 2013. Influence of Ocean and Atmosphere Components on Simulated Climate Sensitivities. J. Clim. 26, 231–245. https://doi.org/10.1175/JCLI-D-12-00121.1

Wise, E.K., 2009. Climate-based sensitivity of air quality to climate change scenarios for the southwestern United States. Int. J. Climatol. 29, 87–97. https://doi.org/10.1002/joc.1713

WMO, 1989. Calculation of monthly and annual 30-year standard normals. World Meterological Organisation, Geneva.

World Health Organization, 2014. Quantitative risk assessment of the effects of climate change on selected causes of death, 2030s and 2050s. World Health Organization.

World Health Organization, 2013. Review of evidence on health aspects of air pollution – REVIHAAP Project. World Heal. Organ.

World Health Organization, 2006. WHO Air quality guidelines for particulate matter, ozone, nitrogen dioxide and sulfur dioxide: global update 2005: summary of risk assessment. Geneva World Heal. Organ. 1–22. https://doi.org/10.1016/0004-6981(88)90109-6

Wu, S., Mickley, L.J., Jacob, D.J., Rind, D., Streets, D.G., 2008. Effects of 2000-2050 changes in climate and emissions on global tropospheric ozone and the policy-relevant background surface ozone in the United States. J. Geophys. Res. Atmos. 113. https://doi.org/10.1029/2007JD009639

Xie, Y., Dai, H., Xu, X., Fujimori, S., Hasegawa, T., Yi, K., Masui, T., Kurata, G., 2018. Co-benefits of climate mitigation on air quality and human health in Asian countries. Environ. Int. 119, 309–318. https://doi.org/10.1016/j.envint.2018.07.008

Ye, X., Wolff, R., Yu, W., Vaneckova, P., Pan, X., Tong, S., 2011. Ambient Temperature and Morbidity: A Review of Epidemiological Evidence. Environ. Health Perspect. 120, 19–28. https://doi.org/10.1289/ehp.1003198

Yin, Q., Wang, J., Ren, Z., Li, J., Guo, Y., 2019. Mapping the increased minimum mortality temperatures in the context of global climate change. Nat. Commun. 10, 1–8. https://doi.org/10.1038/s41467-019-12663-y

Ying, Z., 2012. Projections of 2.0°C Warming over the Globe and China under RCP4.5. Atmos. Ocean. Sci. Lett. 5, 514–520.

Yokohata, T., Annan, J.D., Collins, M., Jackson, C.S., Shiogama, H., Watanabe, M., Emori, S., Yoshimori, M., Abe, M., Webb, M.J., Hargreaves, J.C., 2013. Reliability and importance of structural diversity of climate model ensembles. Clim. Dyn. 41, 2745–2763.

Young, P.J., Archibald, A.T., Bowman, K.W., Lamarque, J.-F., Naik, V., Stevenson, D.S., Tilmes, S., Voulgarakis, A., Wild, O., Bergmann, D., Cameron-Smith, P., Cionni, I., Collins, W.J., Dalsøren, S.B., Doherty, R.M., Eyring, V., Faluvegi, G.,

Horowitz, L.W., Josse, B., Lee, Y.H., MacKenzie, I.A., Nagashima, T., Plummer, D.A., Righi, M., Rumbold, S.T., Skeie, R.B., Shindell, D.T., Strode, S.A., Sudo, K., Szopa, S., Zeng, G., 2013. Pre-industrial to end 21st century projections of tropospheric ozone from the Atmospheric Chemistry and Climate Model Intercomparison Project (ACCMIP). Atmos. Chem. Phys. 13, 2063–2090. https://doi.org/10.5194/acp-13-2063-2013

Young, P.J., Arneth, A., Schurgers, G., Zeng, G., Pyle, J.A., 2009. The CO_2 inhibition of terrestrial isoprene emission significantly affects future ozone projections. Atmos. Chem. Phys. 9, 2793–2803. https://doi.org/10.5194/acp-9-2793-2009

Young, P.J., Naik, V., Fiore, A.M., Gaudel, A., Guo, J., Lin, M.Y., Neu, J.L., Parrish, D.D., Rieder, H.E., Schnell, J.L., Tilmes, S., Wild, O., Zhang, L., Ziemke, J.R., Brandt, J., Delcloo, A., Doherty, R.M., Geels, C., Hegglin, M.I., Hu, L., Im, U., Kumar, R., Luhar, A., Murray, L., Plummer, D., Rodriguez, J., Saiz-Lopez, A., Schultz, M.G., Woodhouse, M.T., Zeng, G., 2018. Tropospheric Ozone Assessment Report: Assessment of global-scale model performance for global and regional ozone distributions, variability, and trends. Elem Sci Anth 6, 10. https://doi.org/10.1525/elementa.265

Zander, K.K., Botzen, W.J.W., Oppermann, E., Kjellstrom, T., Garnett, S.T., 2015. Heat stress causes substantial labour productivity loss in Australia. Nat. Clim. Chang. 5, 647–651. https://doi.org/10.1038/nclimate2623

Zelazowski, P., Malhi, Y., Huntingford, C., Sitch, S., Fisher, J.B., 2011. Changes in the potential distribution of humid tropical forests on a warmer planet. Philos. Trans. R. Soc. A Math. Phys. Eng. Sci. 369, 137–160. https://doi.org/10.1098/rsta.2010.0238

Zelinka, M.D., Randall, D.A., Webb, M.J., Klein, S.A., 2017. Clearing clouds of uncertainty. Nat. Clim. Chang. 7, 674–678. https://doi.org/10.1038/nclimate3402

Zimmer, W., Brüggemann, N., Emeis, S., Giersch, C., Lehning, A., Steinbrecher, R., Schnitzler, J., 2000. Process-based modelling of isoprene emission by oak leaves. Plant. Cell Environ. 23, 585–595. https://doi.org/10.1046/j.1365-3040.2000.00578.x

Zittis, G., Hadjinicolaou, P., Fnais, M., Lelieveld, J., 2016. Projected changes in heat wave characteristics in the eastern Mediterranean and the Middle East. Reg. Environ. Chang. 16, 1863–1876. https://doi.org/10.1007/s10113-014-0753-2

Zivin, J.G., Neidell, M., 2012. The Impact of Pollution on Worker Productivity. Am. Econ. Rev. 102, 3652–3673. https://doi.org/10.1257/aer.102.7.3652

Zu, K., Liu, X., Shi, L., Tao, G., Loftus, C.T., Lange, S., Goodman, J.E., 2017. Concentration-response of short-term ozone exposure and hospital admissions for asthma in Texas. Environ. Int. 104, 139–145. https://doi.org/10.1016/j.envint.2017.04.006

Appendix A: Atmospheric changes that will affect tropospheric ozone above the surface

A.1 Zonal mean temperature

Just as surface temperature change is not spatially homogenous, rate of temperature change varies at different heights. As temperatures decrease in the troposphere, they increase in the stratosphere as reflected in Figure A.1. The largest increases are in the tropical upper troposphere and at the surface, as shown by previous research (Stevenson et al., 2005). Figure A.2 shows the standard deviation between models when using a common time period versus a common ΔGMST. There is greater model uncertainty using ΔGMST in the stratosphere because the emissions of (stratospheric) ozone depleting substances changes with time, rather than surface temperatures, which in turn affects ozone hole recovery and stratospheric temperatures.
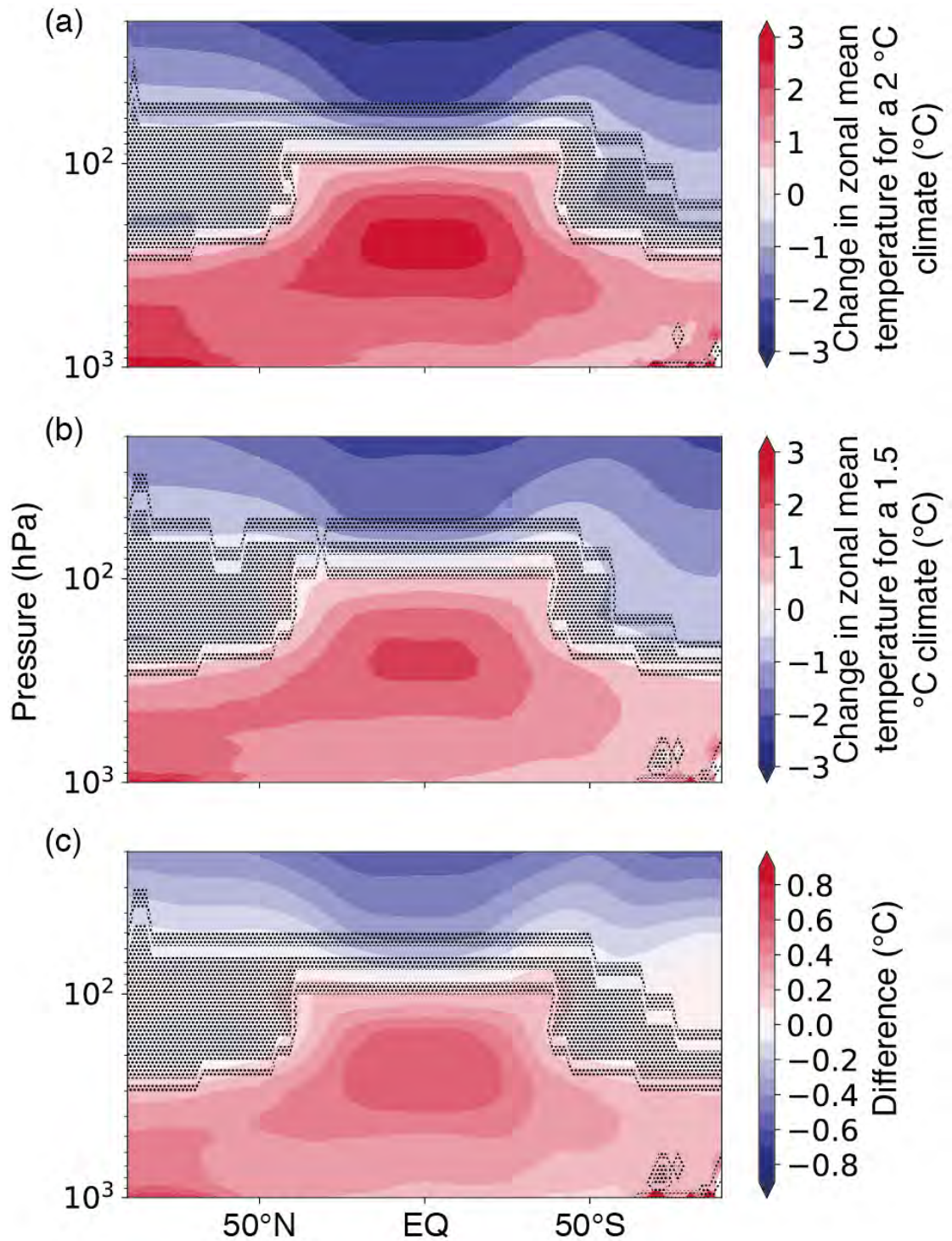
Figure A.1: Zonal mean temperature change from present-day for (a) a 2 °C climate and (b) a 1.5 °C climate, and (c) the difference (a) – (c). The dotted areas show where the standard deviation between models is greater than the multi-model mean.
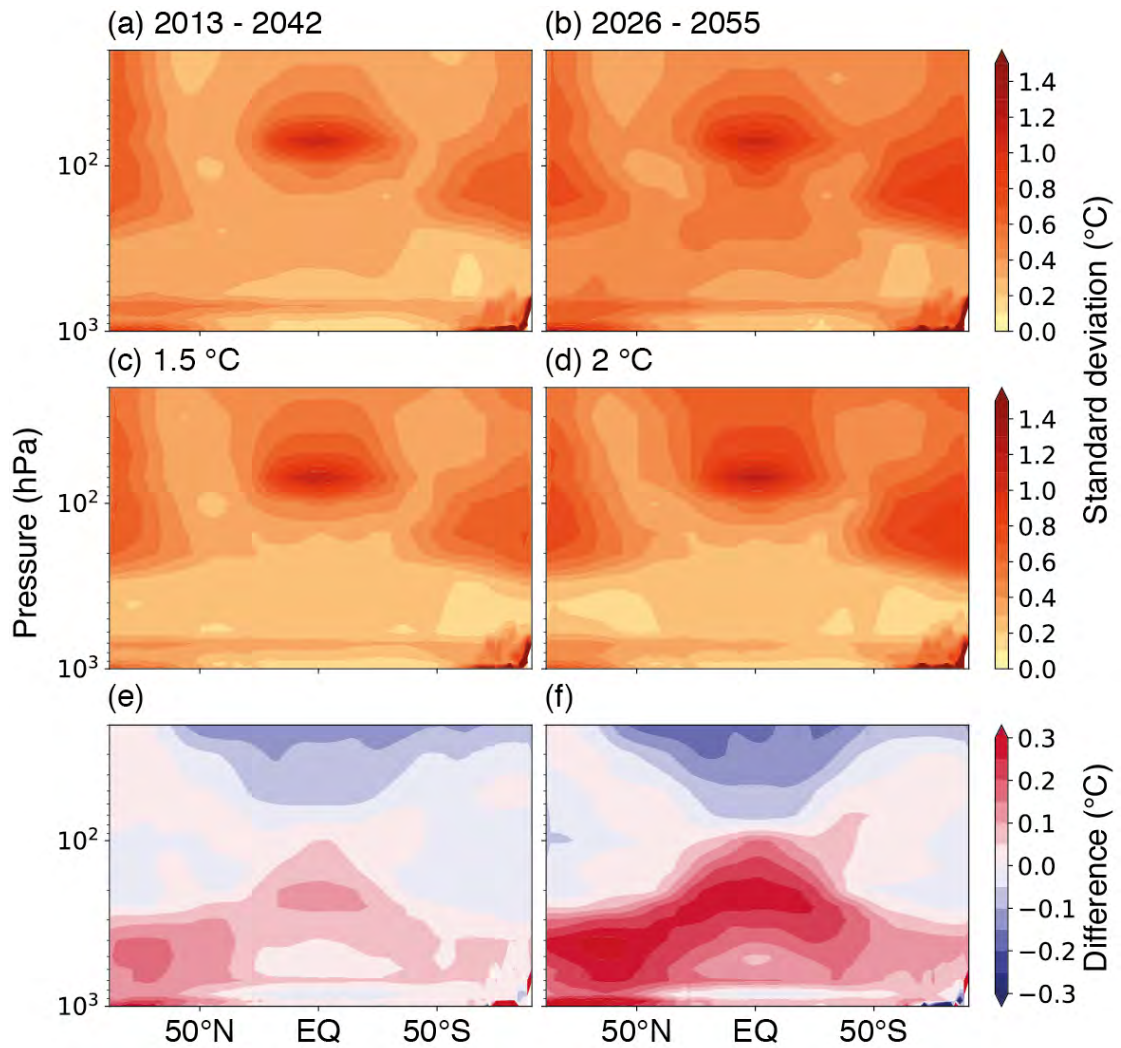
Figure A.2: The standard deviation between models for zonal mean temperature for dates: (a) 2013 – 2042 and (b) 2026 – 2055 and for global mean temperature change: (c) 1.5 and (d) 2 °C. The differences (a) - (c) and (b) – (d) are shown by (e) and (f) respectively.

A.2 Anthropogenic emissions

Anthropogenic emissions vary by country, year, and emissions scenario. Table A.1 shows the global mean anthropogenic methane emissions for RCP4.5 and RCP8.5. I found average methane emissions for the 30-year period when the ΔGMST was 1.5 and 2 °C for each model then calculated the multi-model mean. Methane emissions for RCP8.5 is 284 ppb (15.6%) and 673 ppb (37.3%) higher than RCP4.5 for ΔGMST 1.5

and 2 °C respectively. Table A.2 shows that there is a decrease in methane emissions with GMST and time, whereas there is an increase for RCP8.5.

Table A.1: Multi-model mean global anthropogenic methane emissions (without shipping, aviation, and biomass burning) when each model reaches 1.5 or 2 °C ΔGMST for RCP4.5 and RCP8.5.

Scenario	ΔGMST (°C)	Global methane (ppb)
RCP4.5	1.5	1821
	2.0	1804
RCP8.5	1.5	2105
	2.0	2477

Table A.2: Multi-model mean increase in global mean methane concentrations (ppb) from a +1.5 °C to a +2 °C climate for RCP4.5 and RCP8.5.

Scenario	Mean change (ppb)	Percent change (%)
RCP4.5	-17	-0.9
RCP8.5	372	17.5

Figure A.3 shows methane and NO_x emission projections, downloaded from the RCP database (IIASA, 2009), for all sectors. China, India, and the USA show methane emissions increasing and then peaking towards the end of the century for the RCP8.5

scenario, whereas they mainly slowly decrease for the RCP4.5 scenario. Methane emissions from Brazil and Algeria are much lower than the other countries and emissions are very similar for both scenarios in Algeria.
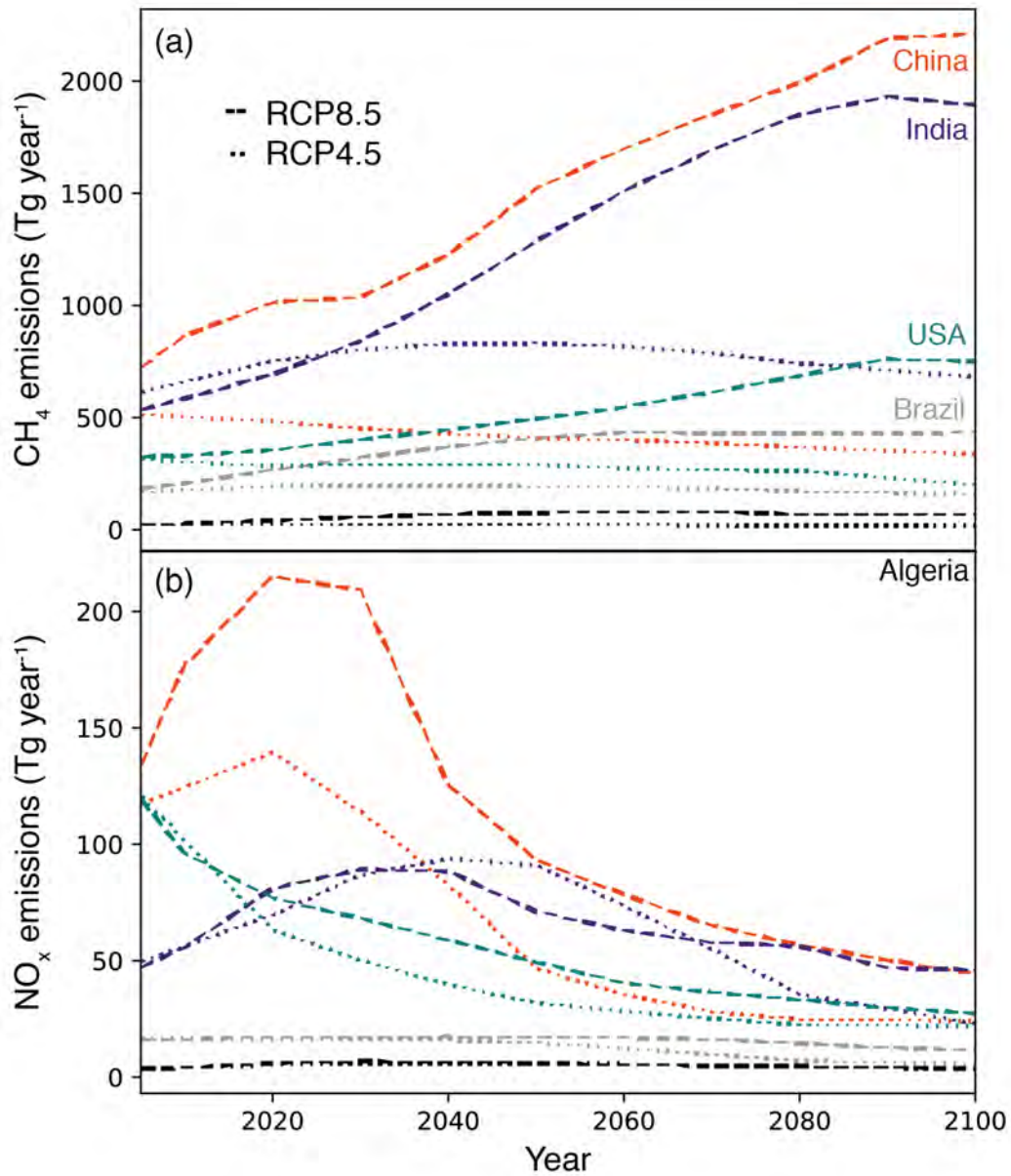

Figure A.3: Total anthropogenic (a) methane and (b) NOx emission projections per year for China (orange-red), India (purple), USA (teal), Brazil (grey), and Algeria (black). RCP45 data is shown by a dotted line, and RCP8.5 is shown by a dashed line.

NO_x emissions decrease for China, and USA for both scenarios, but they decrease faster for RCP4.5. India has higher NO_x emissions for the RCP4.5 scenario during the mid-century, but by the end of the century RCP4.5 emissions are lower. Emissions show less dramatic changes over Algeria and Brazil, with both scenarios showing quite similar emissions.

Appendix B: Emissions scenarios and air quality during the 2003 European heat wave

B.1 Comparison for emission scenarios used for the European 2003 heat wave experiment

Figure B.1 shows the NO_x ratio for five European countries for CAMChem model, which was calculated by using a country mask and dividing the total NO_x emissions by total NMVOC emissions. The NOx ratio for Em70GDP03 is over 75% more than the 2003 NO_x ratio over the UK. The other countries also show a higher NOx ratio for Em70GDP03, however it is not as substantial as the change in the UK and the NOx ratio is lower for the control scenario for the other countries.

Figure B.2 shows the difference between CO emissions for the control scenario and the "world avoided" and future emission scenarios for August. Both models show higher anthropogenic emissions of CO over Europe for "world avoided" scenarios than the 2003 control scenario, with higher emission differences over Western Europe. There was generally a decrease in emissions for RCP scenarios using both models, however there was an increase over Paris for RCP2.6 using CAMChem emissions. Most of Western Europe showed a larger decrease in emissions for RCP8.5 than RCP2.6.

Figure B.3 shows the spatial difference between the control scenario and the other scenario's NO emissions. The largest difference between 1970 and 2003 NO emissions was over the UK, where 1970 emissions were much higher. There were some decreases

in NO over Europe using unscaled 1970 and population scaled emission scenarios, however after scaling by GDP and population the "world avoided" NO emissions see an increase everywhere over Europe. Both RCP scenarios show a decrease in NO emissions over most of Europe for both models.
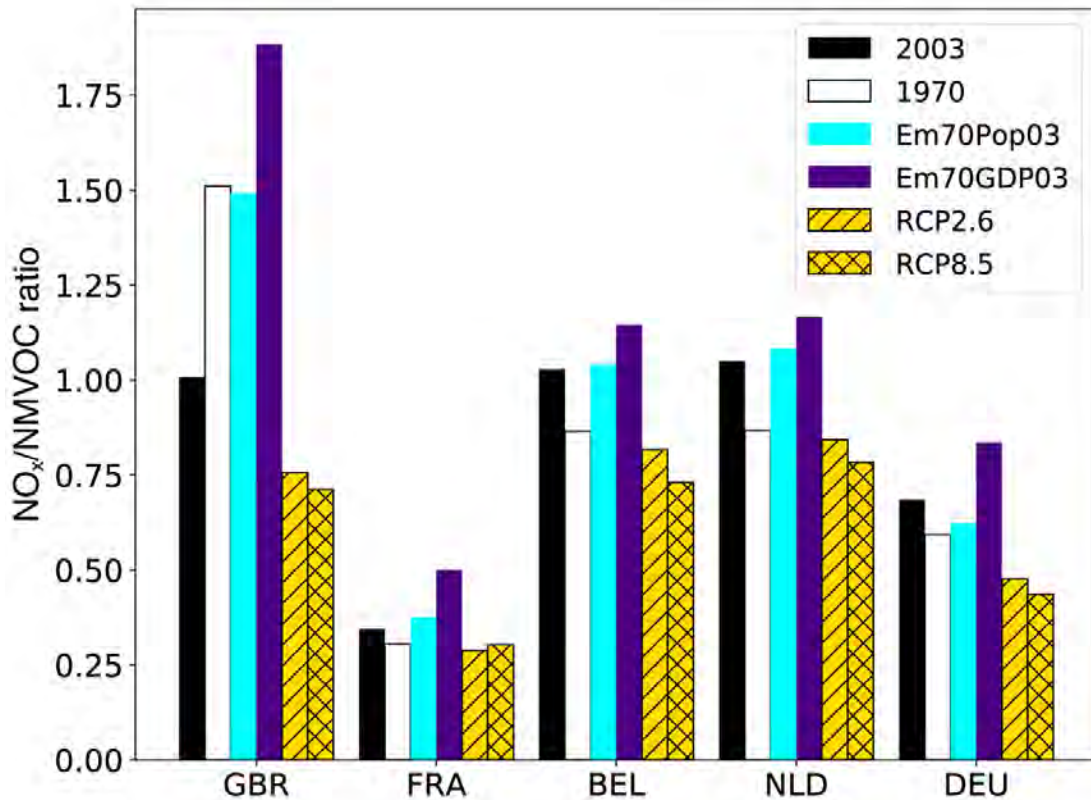

Figure B.1: NOx ratio for the UK, France, Belgium, Netherlands, and Germany for the CAMChem model emissions. The control, unscaled 1970, 1970 scaled by population, 1970 scaled by population and GDP, RCP2.6, and RCP8.5 emissions shown by black, white, cyan, purple, gold hatched, and gold crossed respectively.

Figure B.4 shows the difference between different scenario SO_2 emissions and 2003 SO_2 emissions. Using 1970 and population-scaled 1970 SO2 emissions, the largest increase was over the UK. Though SO2 emissions were less in 1970 than 2003 over some regions, such as Spain, once scaled by GDP there were increases all over Europe.

The majority of SO$_2$ emissions were less over Europe in 2030 using both RCP scenarios, though reductions are more significant in places using the RCP8.5 scenario.

Shipping emissions were lower in 1970 than 2003 for CO, NO, and SO2 for both models. 1970 shipping emissions scaled by the number of ships were higher than 2003 emissions for each species, but the difference wasn't as high as the changes in anthropogenic emissions on land. Both 2030 scenarios show an increase in shipping emissions from 2003.
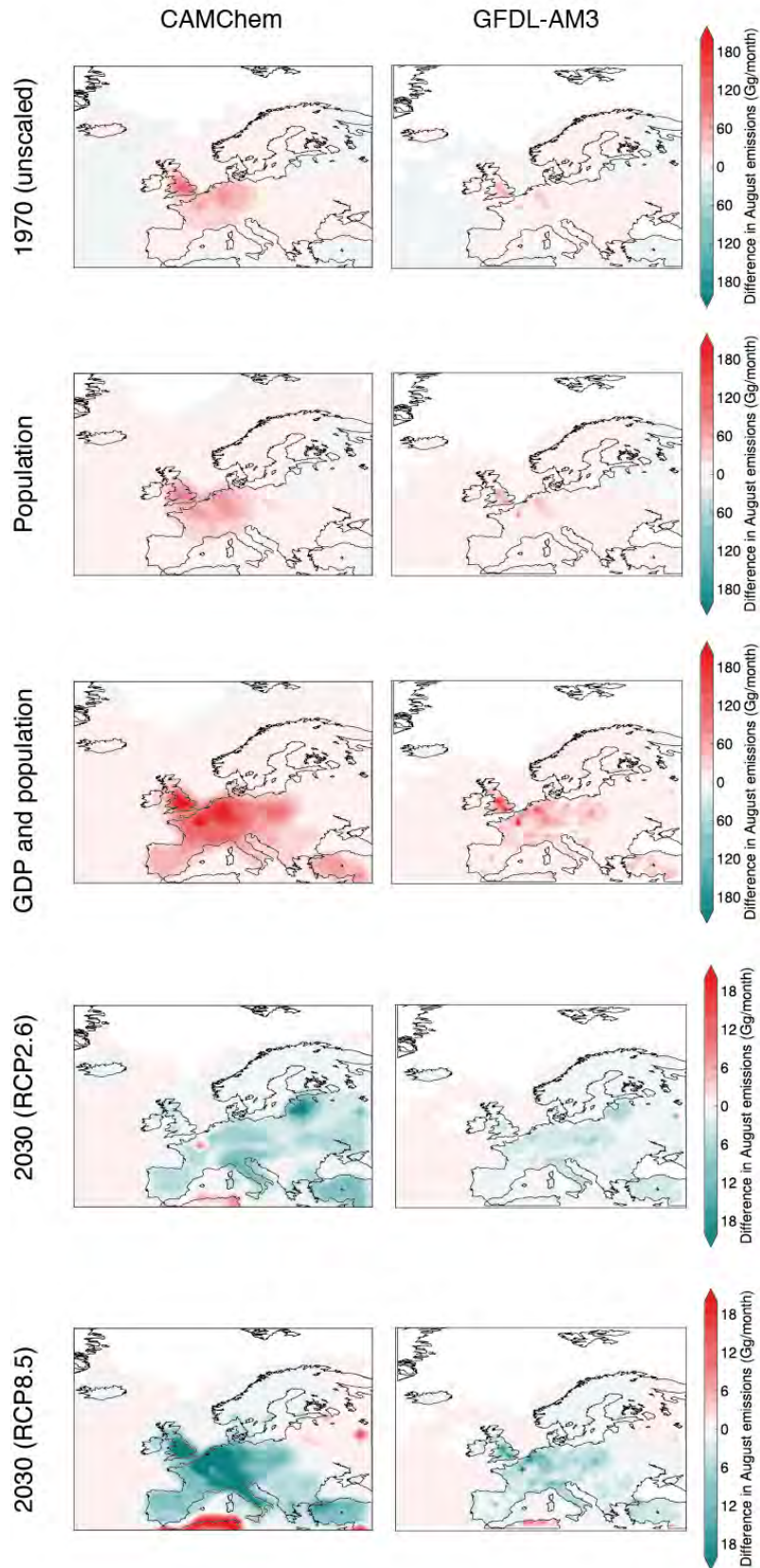
Figure B.2: Difference betwEen total CO emissions in August scenario (rows) and baseline 2003 control scenario for CAMChem (left) and GFDL-AM3 (right). An increase in emissions is shown in red and a decrease is shown in teal.
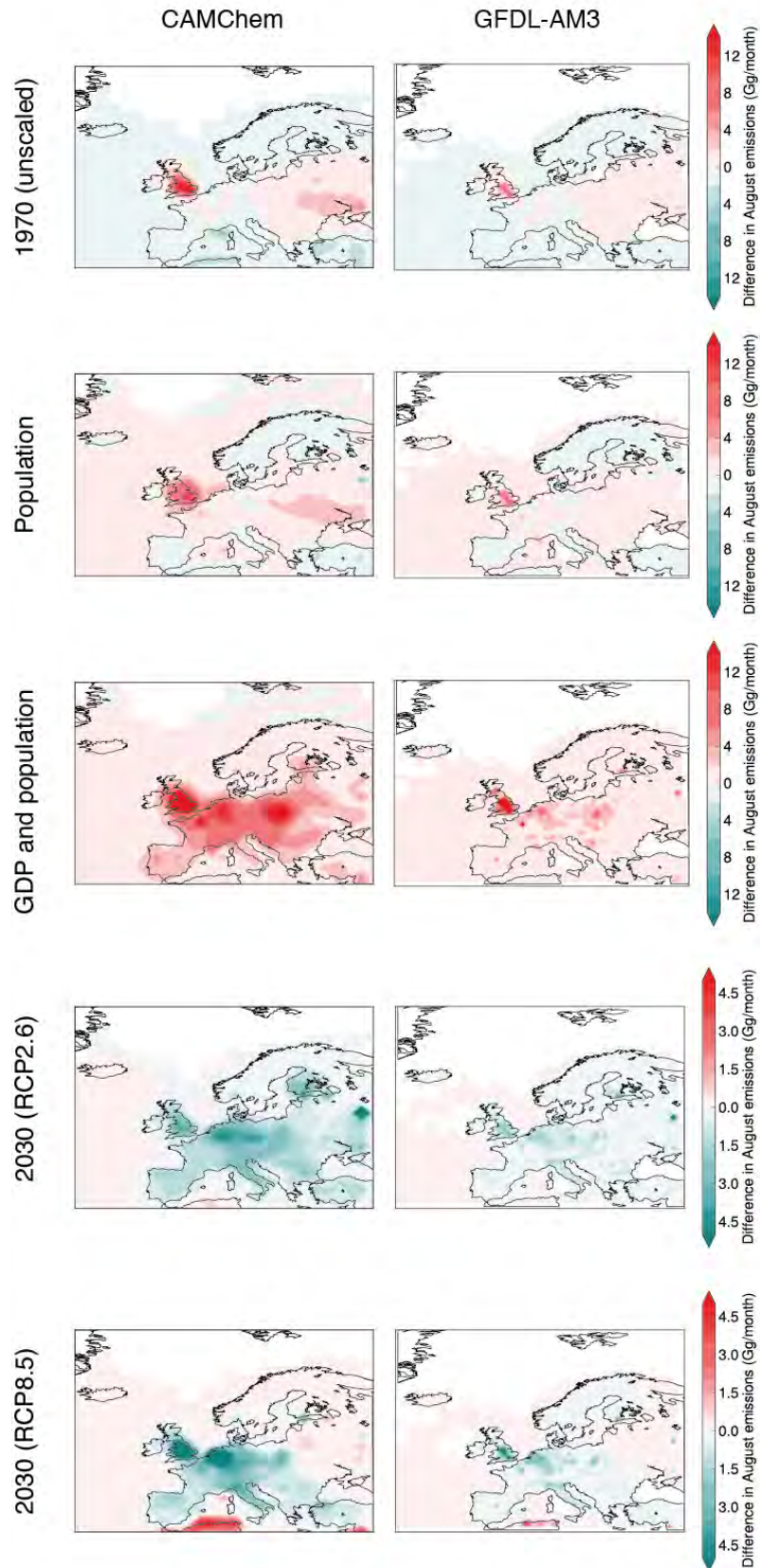
Figure B.3: Difference between total NO emissions in August scenario (rows) and baseline 2003 control scenario for CAMChem (left) and GFDL-AM3 (right). An increase in emissions is shown in red and a decrease is shown in teal.
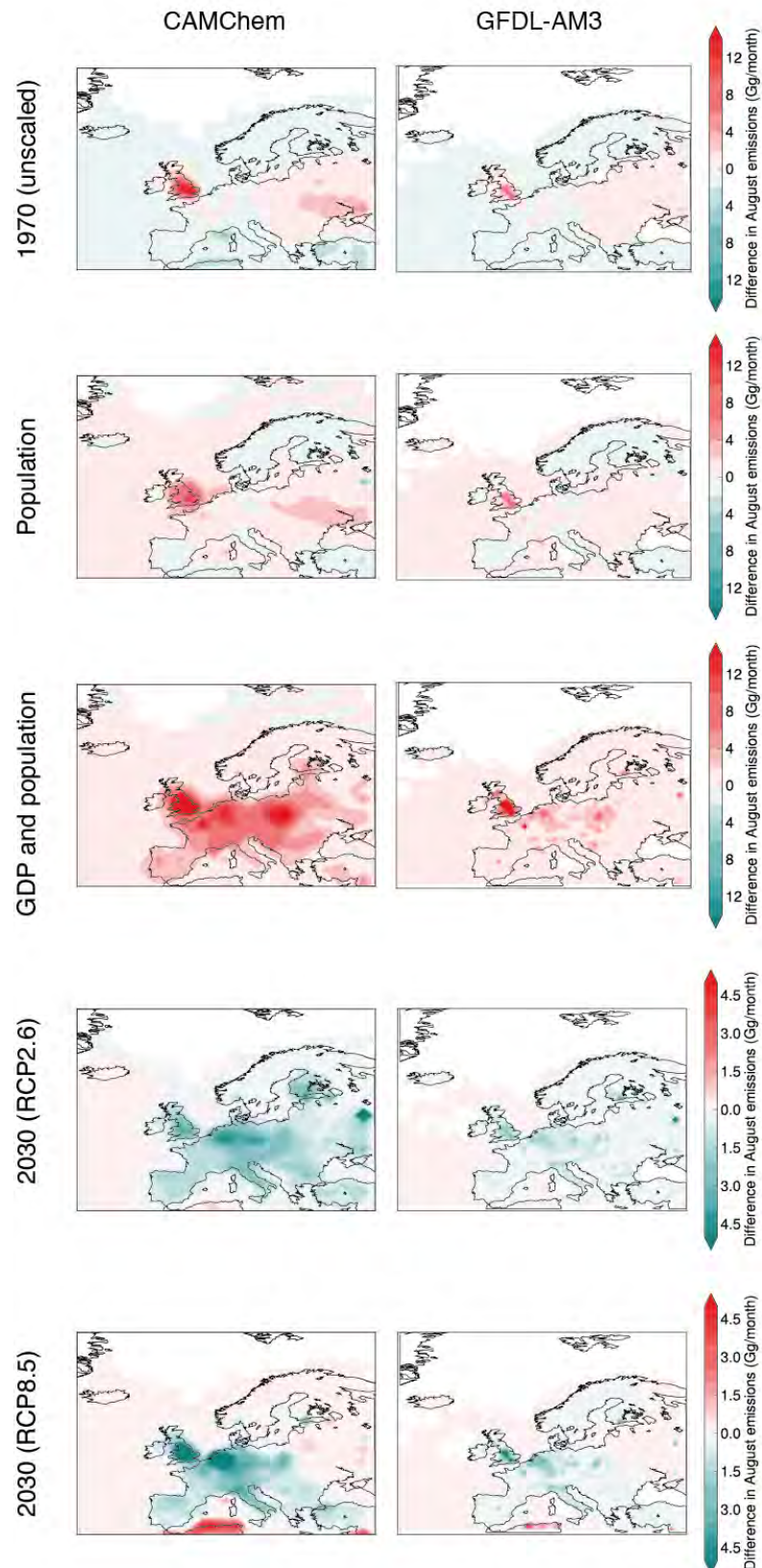
Figure B.4: Difference between total SO_2 emissions in August scenario (rows) and baseline 2003 control scenario for CAMChem (left) and GFDL-AM3 (right). An increase in emissions is shown in red and a decrease is shown in teal.

B.2 Temporal comparison between control scenario and observations during 2003 heatwave
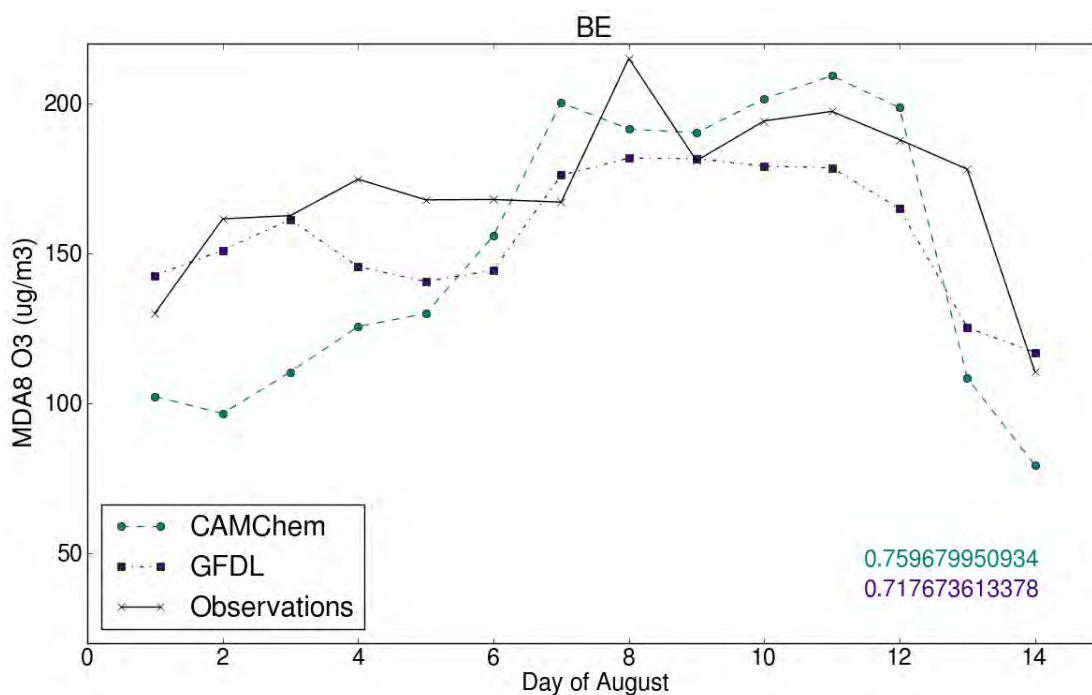

Figure B.5: Maximum daily 8-hour mean ozone for the first fortnight of August. Observations (black crosses) were averaged over 4 EMEP sites in Belgium and models CAMChem (teal circles) and GFDL-AM3 (purple squares) were averaged using a Belgium country-mask. Numbers in the bottom-right corner show the correlation coefficient between CAMChem model results and observations (top/teal), and GFDL-AM3 model results and observations (bottom/purple).

Figures B.5-8 show the maximum daily 8-hour mean (MDA8) O_3 during the first two weeks of August at country-level for observations and models. Observations were the average of all sites in that country and models were the average of all grid squares in that country. CAMChem had a higher correlation with measurements than GFDL-AM3

for MDA8 O₃ and GFDL-AM3 largely underestimated ozone. However, both models

showed elevated levels of ozone at the start of August.
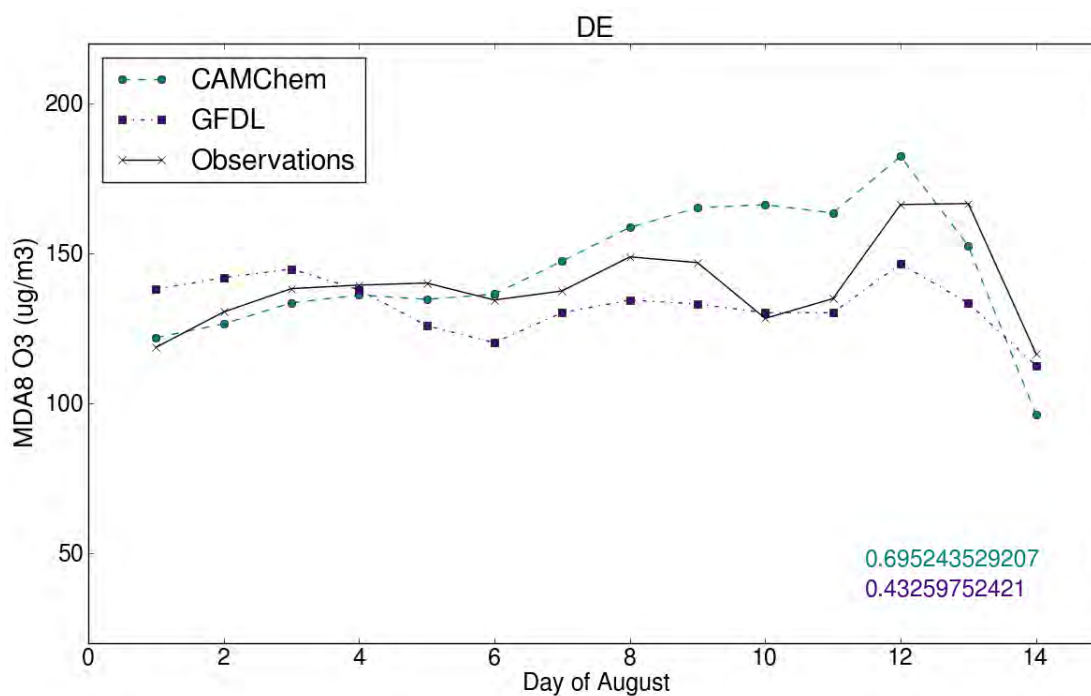
Figure B.6: Maximum daily 8-hour mean ozone for the first fortnight of August. Observations (black crosses) were averaged over 17 EMEP sites in Germany and models CAMChem (teal circles) and GFDL-AM3 (purple squares) were averaged using a Germany country-mask. Numbers in the bottom-right corner show the correlation coefficient between CAMChem model results and observations (top/teal), and GFDL-AM3 model results and observations (bottom/purple).
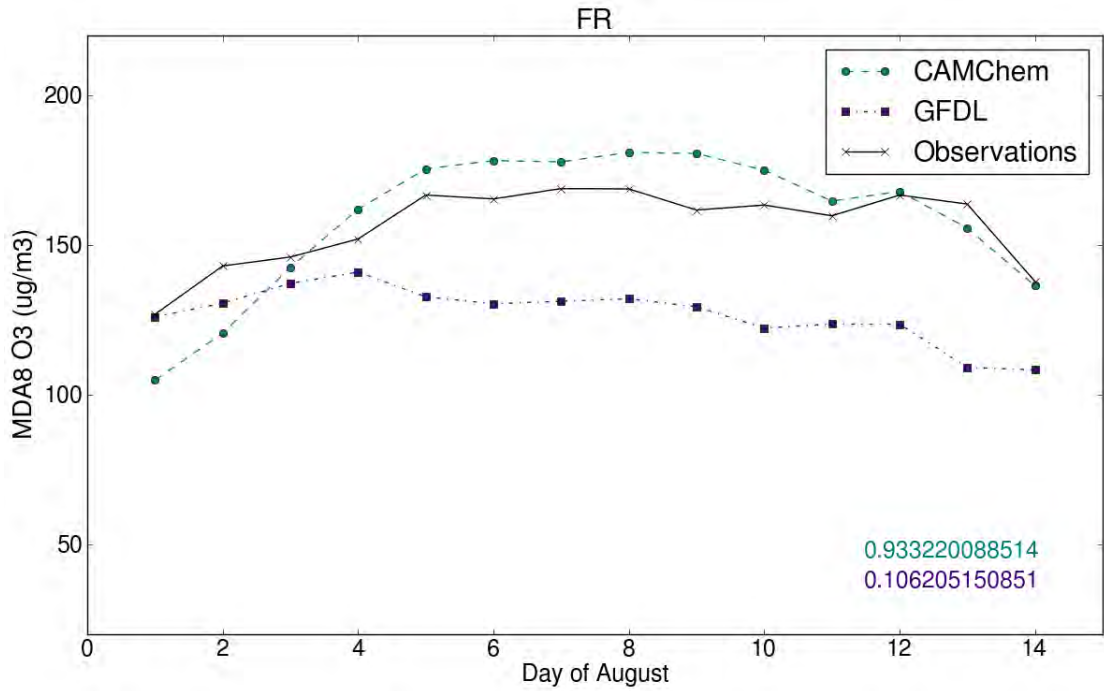
Figure B.7: Maximum daily 8-hour mean ozone for the first fortnight of August. Observations (black crosses) were averaged over 7 EMEP sites in France and models CAMChem (teal circles) and GFDL-AM3 (purple squares) were averaged using a France country-mask. Numbers in the bottom-right corner show the correlation coefficient between CAMChem model results and observations (top/teal), and GFDL-AM3 model results and observations (bottom/purple).
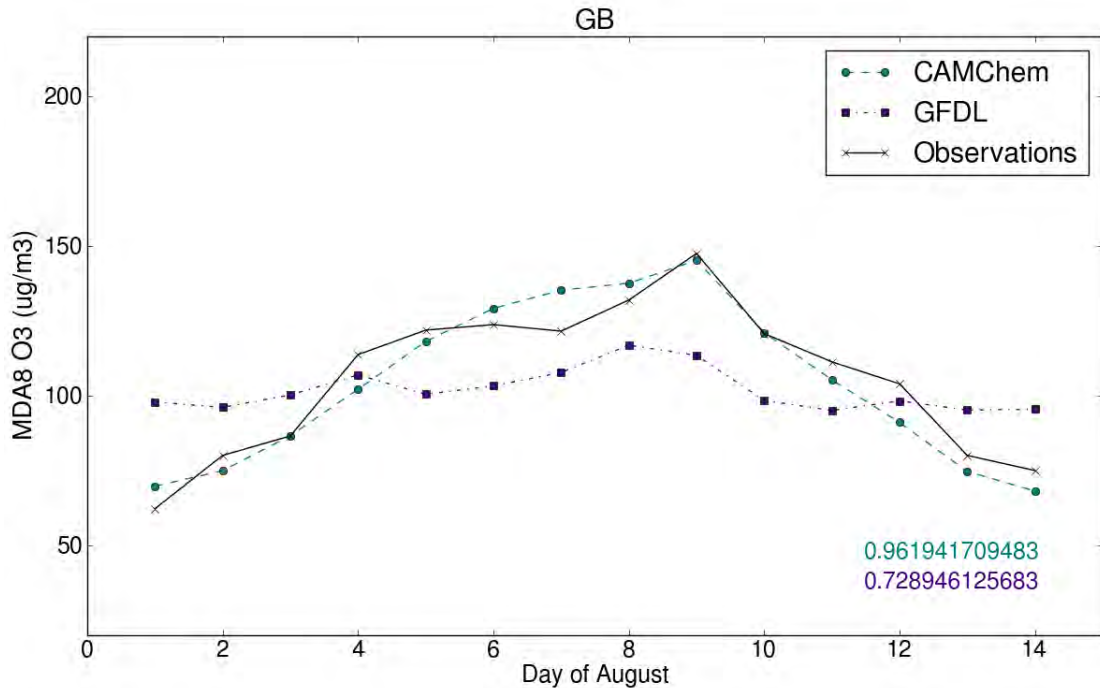
Figure B.8: Maximum daily 8-hour mean ozone for the first fortnight of August. Observations (black crosses) were averaged over 17 EMEP sites in the UK and models CAMChem (teal circles) and GFDL-AM3 (purple squares) were averaged using a UK country-mask. Numbers in the bottom-right corner show the correlation coefficient between CAMChem model results and observations (top/teal), and GFDL-AM3 model results and observations (bottom/purple).

Figures B9-12 show country-level daily mean PM$_{2.5}$ for models and observations and Figure B.11 shows daily mean PM$_{2.5}$ for one site and it's closest grid square for each model (there was only one measurement site for PM$_{2.5}$ in the UK). The correlation coefficient was much lower between CAMChem and observations for PM2.5, and it was slightly negative for both models and observations for Switzerland. GFDL-AM3 results were generally much closer to observations, especially for Switzerland, and both models tended to underestimate PM$_{2.5}$.
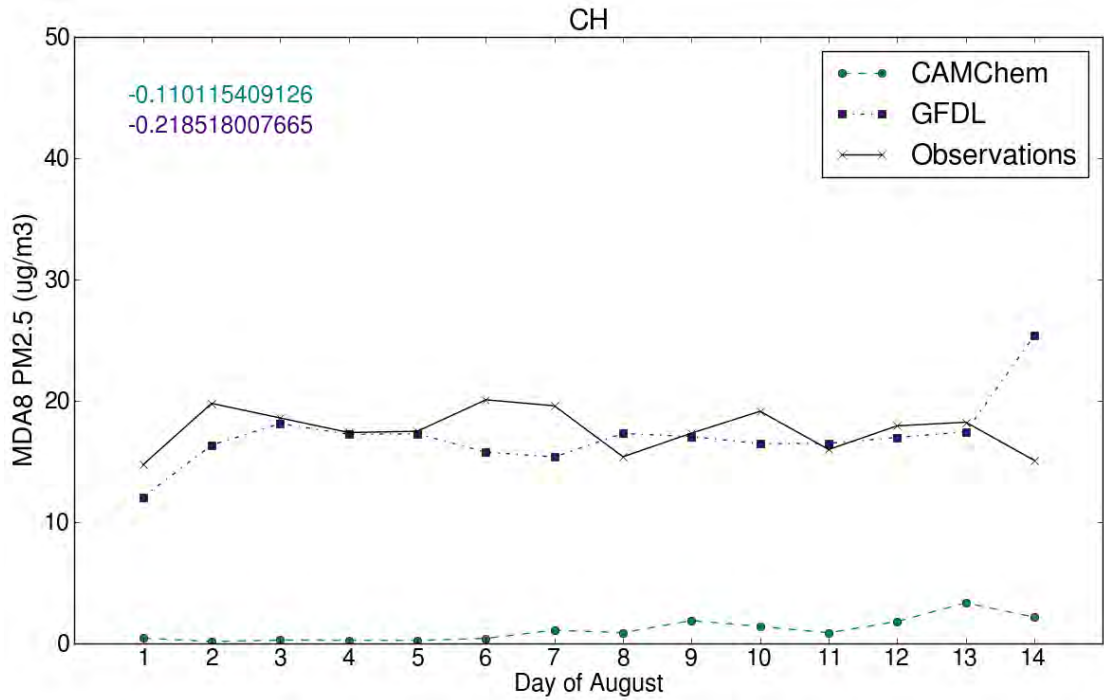
Figure B.9: Daily mean PM2.5 for the first fortnight of August. Observations (black crosses) were averaged over 2 EMEP sites in Switzerland and models CAMChem (teal circles) and GFDL-AM3 (purple squares) were averaged using a Switzerland country-mask. Numbers in the top-left corner show the correlation coefficient between CAMChem model results and observations (top/teal), and GFDL-AM3 model results and observations (bottom/purple).
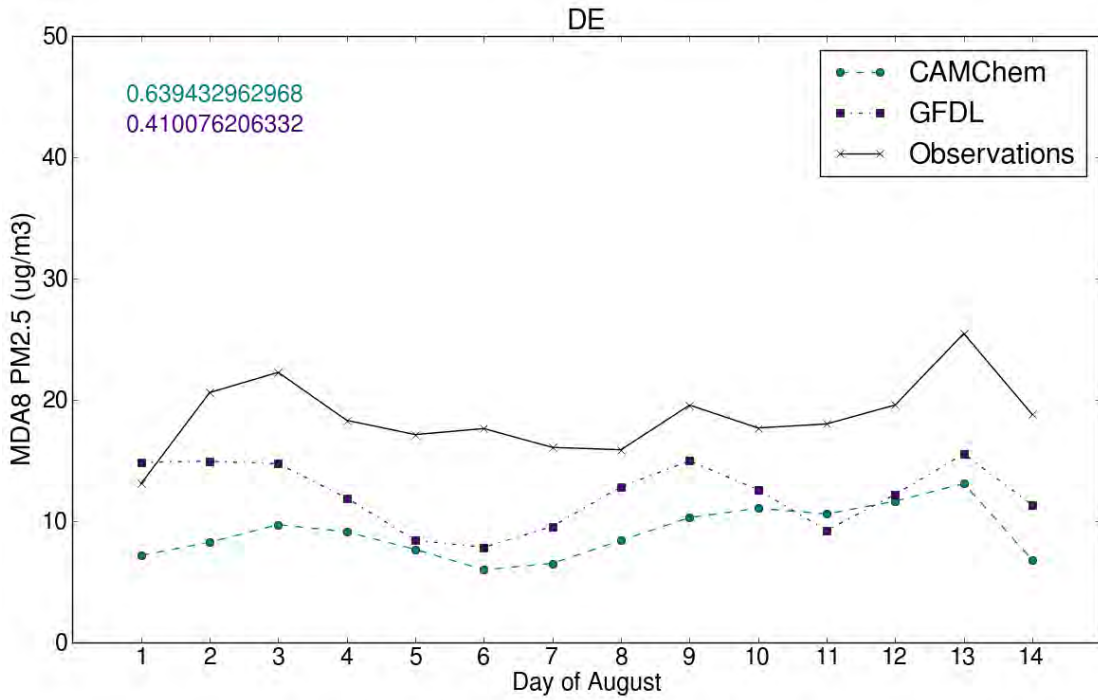
Figure B.10: Daily mean PM2.5 for the first fortnight of August. Observations (black crosses) were averaged over 3 EMEP sites in Germany and models CAMChem (teal circles) and GFDL-AM3 (purple squares) were averaged using a Germany country-mask. Numbers in the top-left corner show the correlation coefficient between CAMChem model results and observations (top/teal), and GFDL-AM3 model results and observations (bottom/purple).
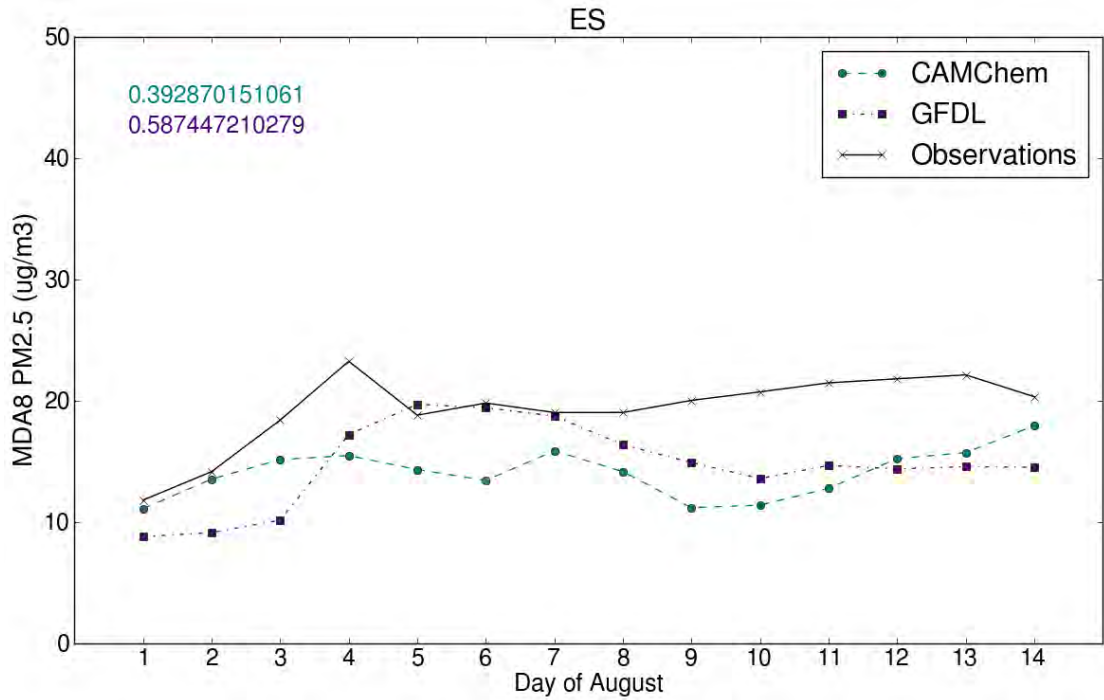
Figure B.11: Daily mean PM$_{2.5}$ for the first fortnight of August. Observations (black crosses) were averaged over 10 EMEP sites in Spain and models CAMChem (teal circles) and GFDL-AM3 (purple squares) were averaged using a Spain country-mask. Numbers in the top-left corner show the correlation coefficient between CAMChem model results and observations (top/teal), and GFDL-AM3 model results and observations (bottom/purple).
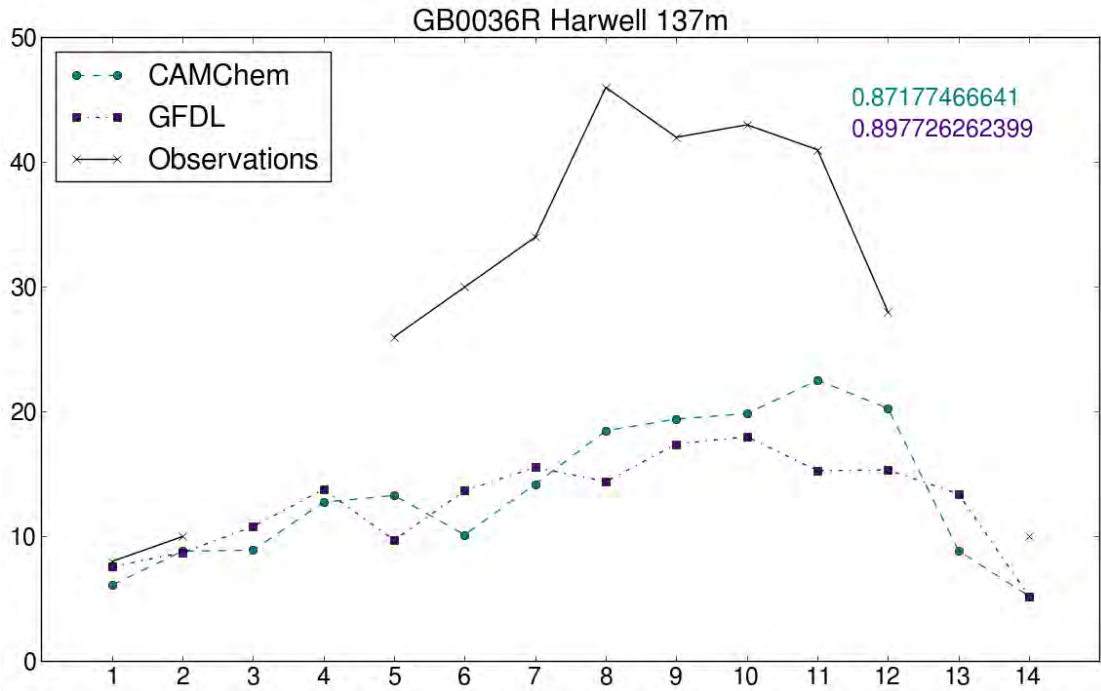
Figure B.12: Daily mean PM2.5 for the first fortnight of August. Observations (black crosses) were from one EMEP site in the UK (Harwell) and model results for CAMChem (teal circles) and GFDL-AM3 (purple squares) were from the corresponding grid square. Station code, name, and altitude of the site are shown at the top of the figure. Numbers in the top-right corner show the correlation coefficient between CAMChem model results and observations (top/teal), and GFDL-AM3 model results and observations (bottom/purple).

Appendix C: Optimum temperature and warm spells

C.1 Climate model data and calculating ∆GMST thresholds

The times when the CMIP5 models reaches each ∆GMST used in this study are listed in Table S1: the earliest possible time period is 2006 – 2035 because this is when future RCP8.5 simulation runs begin. This means that the climate I use to represent a +1.5 °C climate may actually be closer to 2 °C above pre-industrial levels. Although, the earliest the climate exceeds a +2 °C climate is 2014 – 2043 (BNU-ESM). The highest ∆GMST representing the +1.5 °C climate is 1.71 °C (CanESM2) and the mean ∆GMST is 1.55 °C, which means that that the multi-model mean may underestimate the differences between a +1.5 °C and +2 °C climate, therefore downplay the advantages of a +1.5 °C climate.

The latest possible time period is 2071 - 2100 because only future projections from 2006 to 2100 are considered. 13 models do not reach a ∆GMST of 4 °C by the end of the century using this method and GFDL-CM3 was the first model to reach +4 °C climate in 2051 - 2080.

Table C.1: Corresponding 30-year periods when CMIP5 models reach a given ∆GMST.

Model	1.5 °C	2.0 °C	3.0 °C	4.0 °C

ACCESS1-0	2013 – 2042	2025 - 2054	2046 – 2075	2066 – 2095
ACCESS1-3	2016 – 2045	2041 - 2070	2046 – 2075	2067 – 2096
bcc-csm1-1	2006 – 2035	2023 – 2052	2046 – 2075	2070 – 2099
bcc-csm1-1-m	2006 – 2035	2016 - 2045	2046 – 2075	n/a
BNU-ESM	2006 – 2035	2009 - 2038	2031 – 2060	2050 – 2079
CanESM2	2006 – 2035	2012 - 2041	2035 – 2064	2054 – 2083
CCSM4	2006 – 2035	2016 – 2045	2043 – 2072	2063 – 2092
CESM1-BGC	2006 – 2035	2019 – 2048	2045 – 2074	2067 – 2096
CESM1-CAM5	2013 – 2042	2015 – 2044	2043 – 2072	2063 – 2092
CMCC-CM	2014 – 2043	2027 – 2056	2047 – 2076	2064 – 2093
CMCC-CMS	2016 – 2045	2027 – 2056	2047 – 2076	2063 – 2092
CSIRO-Mk3-6-0	2018 – 2047	2030 – 2059	2050 – 2079	2068 – 2097
EC-EARTH	2006 – 2035	2021 – 2050	2046 – 2075	2068 – 2097
GFDL-CM3	2009 – 2038	2021 – 2050	2041 – 2070	2057 – 2086
GFDL-ESM2G	2023 – 2052	2040 – 2069	2066 – 2095	n/a
GFDL-ESM2M	2020 – 2049	2037 – 2066	2067 – 2096	n/a
HadGEM2-CC	2010 – 2039	2026 – 2055	2043 – 2072	2060 – 2089

HadGEM2-ES	2010 – 2039	2022 – 2051	2041 – 2070	2058 – 2087
inmcm4	2029 – 2058	2044 – 2073	2070 – 2099	n/a
IPSL-CM5A-LR	2006 – 2035	2013 – 2042	2034 – 2063	2052 – 2081
IPSL-CM5A-MR	2006 – 2035	2016 – 2045	2036 – 2065	2053 – 2082
IPSL-CM5B-LR	2008 – 2037	2023 – 2052	2048 – 2077	n/a
MIROC5	2019 – 2048	2034 – 2063	2058 - 2087	n/a
MIROC-ESM	2006 – 2035	2016 - 2045	2038 - 2067	2055 – 2084
MIROC-ESM-CHEM	2006 – 2035	2016 - 2045	2036 - 2065	2053 – 2082
MPI-ESM-LR	2006 – 2035	2021 - 2050	2046 – 2075	2066 – 2095
MPI-ESM-MR	2007 – 2036	2024 – 2053	2046 – 2075	2068 – 2097
MRI-CGCM3	2026 – 2055	2038 – 2067	2061 – 2090	n/a
NorESM1-M	2019 – 2048	2034 – 2063	2059 - 2088	n/a

C.2 Estimating a spatially-varying optimum temperature for human health

Only locations where the average daily mean temperature and minimum mortality percentile (MMP) were provided were used to generate the simple regression model – shown by black circles in Figure C.1(a). The dates for MMP calculated by Gasparrini

et al. (2015) and average daily mean temperature provided by Guo et al. (2016) were the same for Australia (3 cities), Brazil (18 cities), Canada (20 census metropolitan areas and 1 city), South Korea (7 cities), Spain (51 capital cities), Taiwan (3 cities), Thailand (62 provinces), UK (9 regions), and USA (135 cities). Data for the six cities in China was provided for different dates. The average daily mean temperatures in Japan were for 1972 – 2012, whereas the MMP was for 1985 – 2012.

Data from other locations on Figure C.1(a) (orange squares and cyan pentagon) were from before the year 2000 and was collected for less than 5 years. For example, the study by El-Zein et al. (2004) took place between 1997 and 1999. However, results from these studies do not include an MMP so are not used after Figure 1a in the main text.

There are many possible reasons for warmer regions having a lower MMP than cooler countries, including socioeconomic ones. Another possible explanation is that they have less variation in temperature (shown in Figure C.1(b)), which may affect the temperature change between neighbouring days. Lin et al. (2013) found that if there was a temperature decrease between neighbouring days then it had a protective effect on non-accidental mortality.
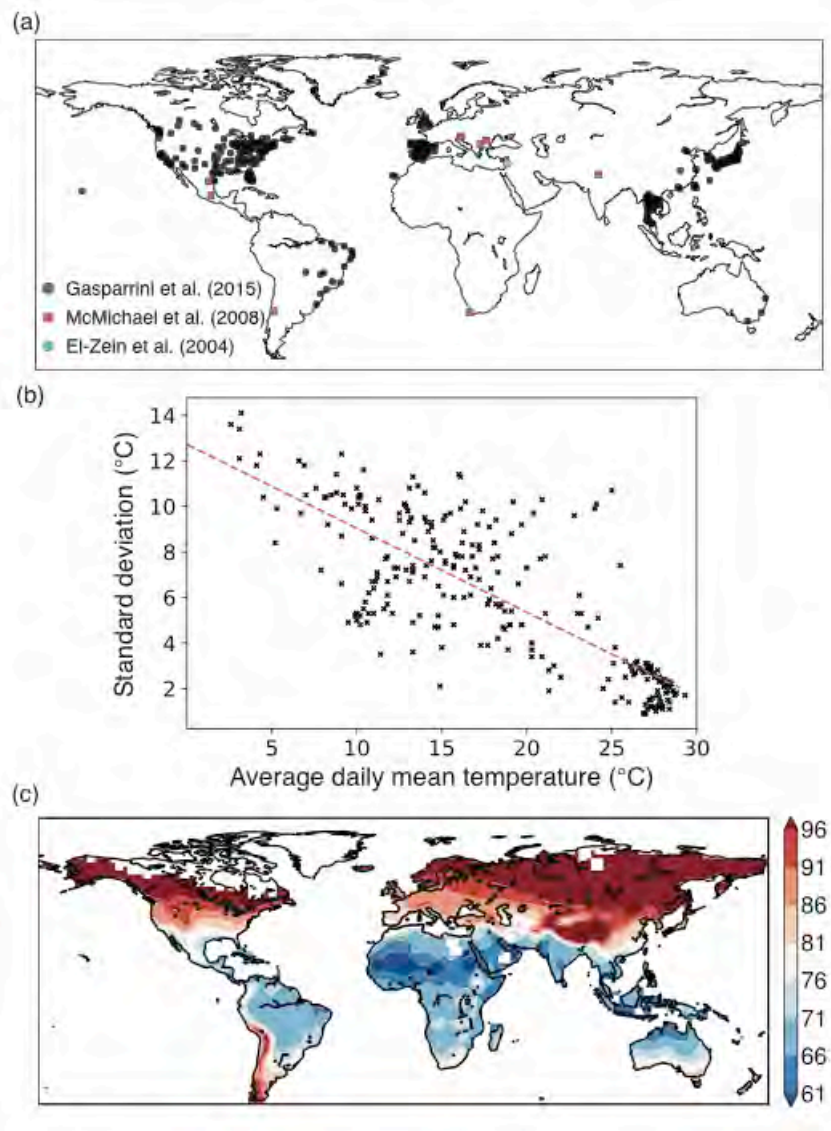
Figure C.1: (a) The locations of all the places used in the study. The grey circles show the places where OT, MMP, and average daily mean temperature were provided by (Gasparrini et al., 2015), therefore allowing us to estimate an MMP for each grid square using my model described in Section 4.3. Orange squares and the cyan pentagon show epidemiological studies that only reported OT and average daily mean temperature (El-Zein et al., 2004; McMichael et al., 2008), which provided information for Figure 1a in the main text. (b) Standard deviation in daily mean temperature as a function of mean temperature (c) The MMP results using the regression model described in Section 4.3. Grid-squares where there is no population are white.

Some countries do not have a similar MMP, even some locations with similar average temperatures have very different MMPs. For instance, places in the USA seem to follow the general pattern (the lower the average temperature, the lower the MMP), but

Honolulu, Hawaii has the highest temperature and highest MMP, making it an obvious outlier. Figure C.2 shows the line of best fit using all data (dashed) vs data from the USA (dotted) and locations with higher temperatures in the USA appear to be worse off than other places with high average temperatures. The line of best fit using only data from the USA is as follows:

$$MMP = 87.8 - \left(1.4 \times 10^{-7}\right) \overline{T}^6, \tag{C.1}$$

where average daily mean temperature is in °C. The root-mean-square deviation is 7.56 °C and the r^2 goodness-of-fit measure is 0.55.

Figure C.2 shows the results if you cluster the data using k-means clustering algorithm. There appears to be two clusters of locations with similar average temperatures, but MMPs are diverging. Differences could be due to access to education and healthcare, which means policy makers need to consider inequalities between states and smaller areas.

Figure C.2: The mean temperature versus the minimum mortality perentile for the USA. The dashed and dotted lines are the lines of best fit using data from all countries and data just from USA locations respectively. The colours represent different clusters of data using k-means clustering and the black circles are the centre of each cluster.

## C.3 Comparison between CMIP5 and ERA-interim present-day results
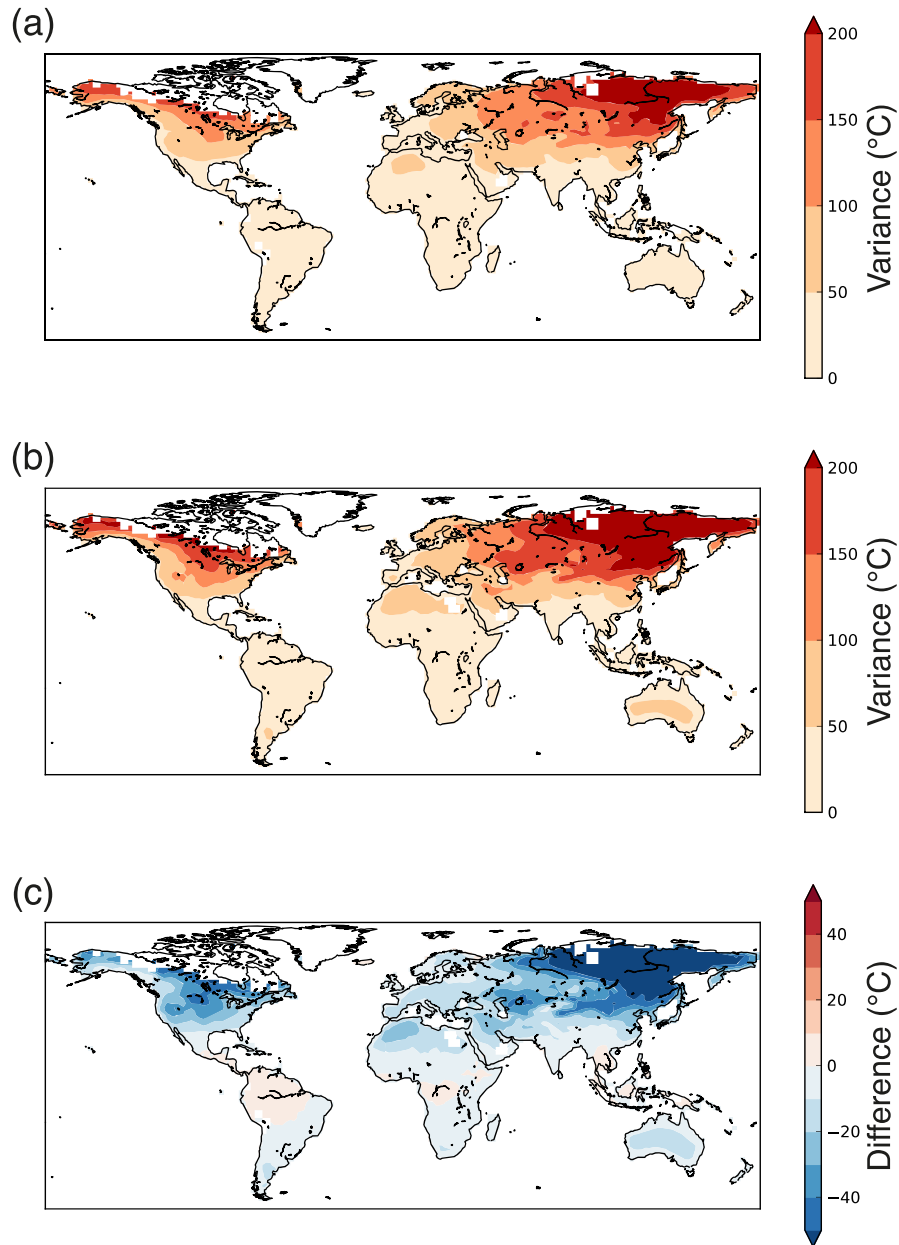
Figure C.3: A comparison between (a) the multi-model mean of the variance in the daily mean temperature (1976-2005) and (b) the ERA-Interim variance in the daily mean temperature (1979-2008). (c) The difference between the CMIP5 multi-model mean and the ERA-Interim variance ranged from -136 °C^2 to 9 °C^2. For the most grid squares the difference between ERA-Interim and multi-model variance was less than the standard deviation between each model's daily mean temperature variance.

After bias correcting the CMIP5 data, I compared the results from 'model-world' and 'reality' by calculating the average number of warm days per year, the mean duration of a warm spell, and the maximum duration of a warm spell for a present-day climate for the bias-corrected CMIP5 model (1976-2005) and ERA-Interim (1979-2008) data. The variance of the multi-model mean bias-corrected CMIP5 models is generally lower than the ERA-Interim data (Figure C.3C3). The smaller variability in temperatures may mean that the models do not reach as high temperatures as ERA-Interim, and not reach climate extremes as often. The difference in the number of warm days is established in Figures S3 and S4, where the number of warm days per year is lower for most regions using the multi-model mean. There is generally less than eight days difference between the multi-model mean and ERA-Interim number of days.

Figure C.6 shows that the average warm spell (using a spatially varying percentile) is longest in western North Africa and the Middle East using both CMIP5 and ERA-Interim data, though the multi-model mean does underestimate the duration. The multi-model mean generally overestimates the duration in the Americas, Southeast Asia, and Australasia. There is less spatial variability using the 81st percentile (Figure C.7). While the average warm spell duration (using the 81st percentile) is underestimated by the multi-model mean over India and parts of the Middle East, it is generally overestimated in the Americas.

Predictably, there are larger differences between the ERA-Interim and the multi-model mean for the maximum duration of a warm spell for many regions (Figure C.8 and Figure C.9). Figure C.8 shows that the maximum warm spell duration is highest in West Africa and west Asia using the spatially varying percentile threshold, though the model generally underestimated maximum length in these regions and overestimated over most of the Americas and Australia. Using the 81st percentile to define the maximum

warm spell duration, the model overestimated over most of the Americas, Africa, and

Australia. There was much less spatial variation in warm spells using this threshold.
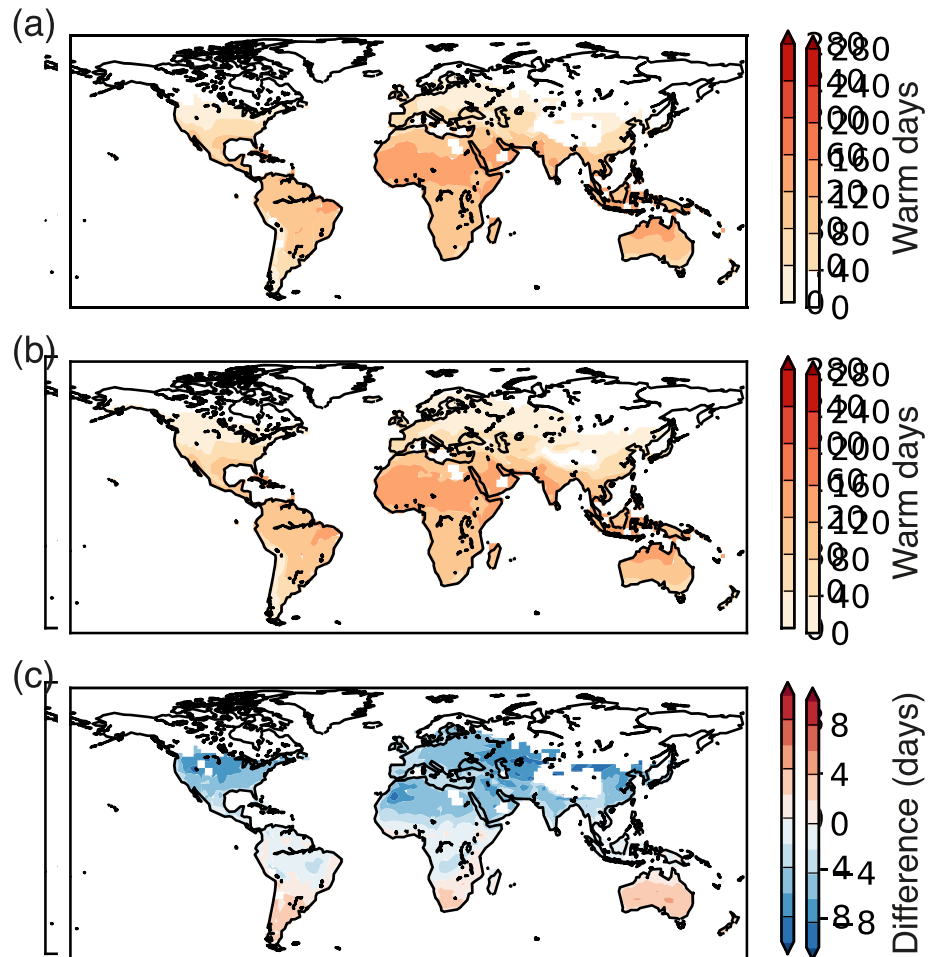
Figure C.4: Average number of warm days (defined by a spatially varying percentile threshold) per year for (a) present-day CMIP5 multi-model mean and (b) present-day ERA-Interim, and (c) the difference in days between them. To show model agreement, grid-squares where the standard deviation between models is greater than the multi-model mean are masked to white.
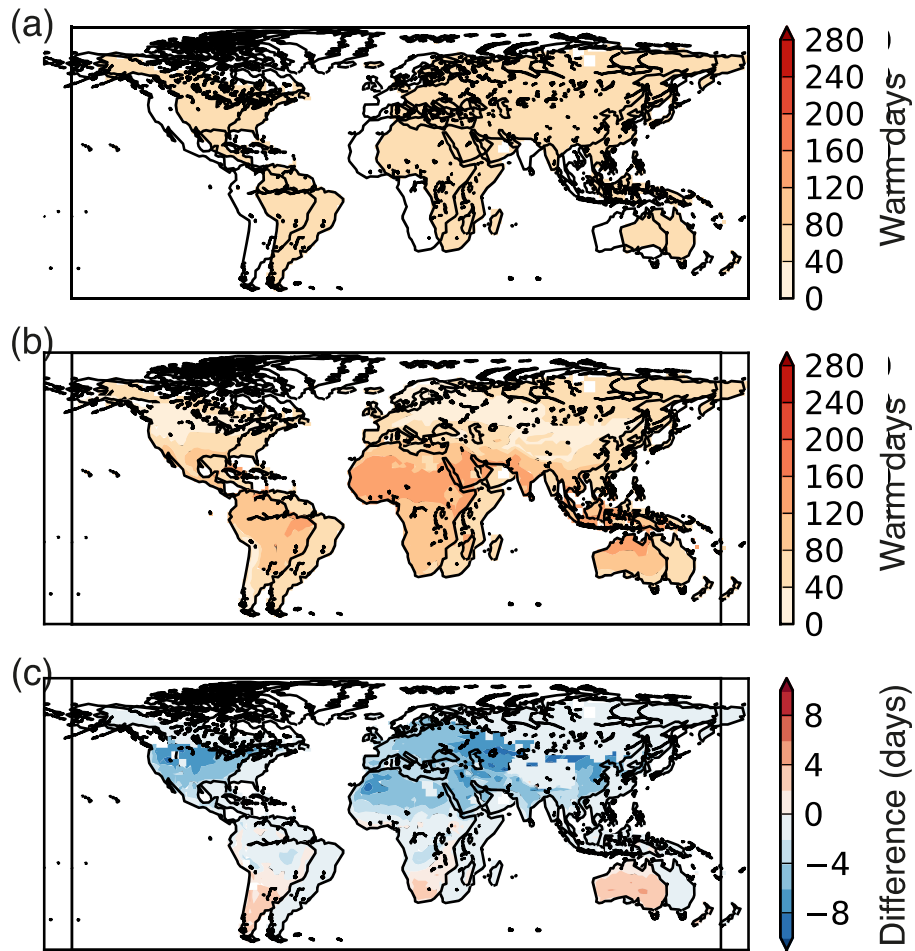
Figure C.5: Average number of warm days (defined by the constant 81st percentile threshold) per year for (a) present-day CMIP5 multi-model mean and (b) present-day ERA-Interim, and (c) the difference in days between them. To show model agreement, grid-squares where the standard deviation between models is greater than the multi-model mean are masked to white.
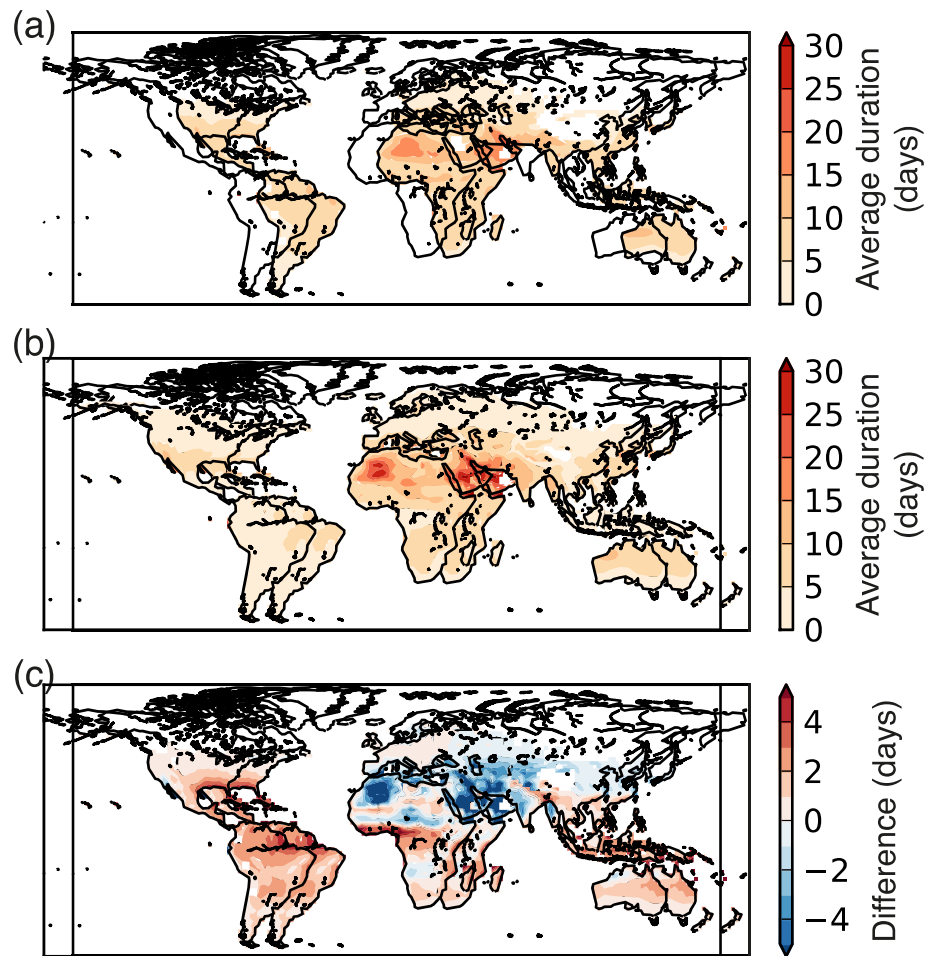
Figure C.6: Average duration (in days) of warm spells defined by more than two consecutive days above OT defined by the spatially varying percentile for (a) CMIP5 multi-model mean and (b) ERA-Interim, and (c) the difference between the two values. Grid-squares where the standard deviation between models is greater than the multi-model mean are masked white.
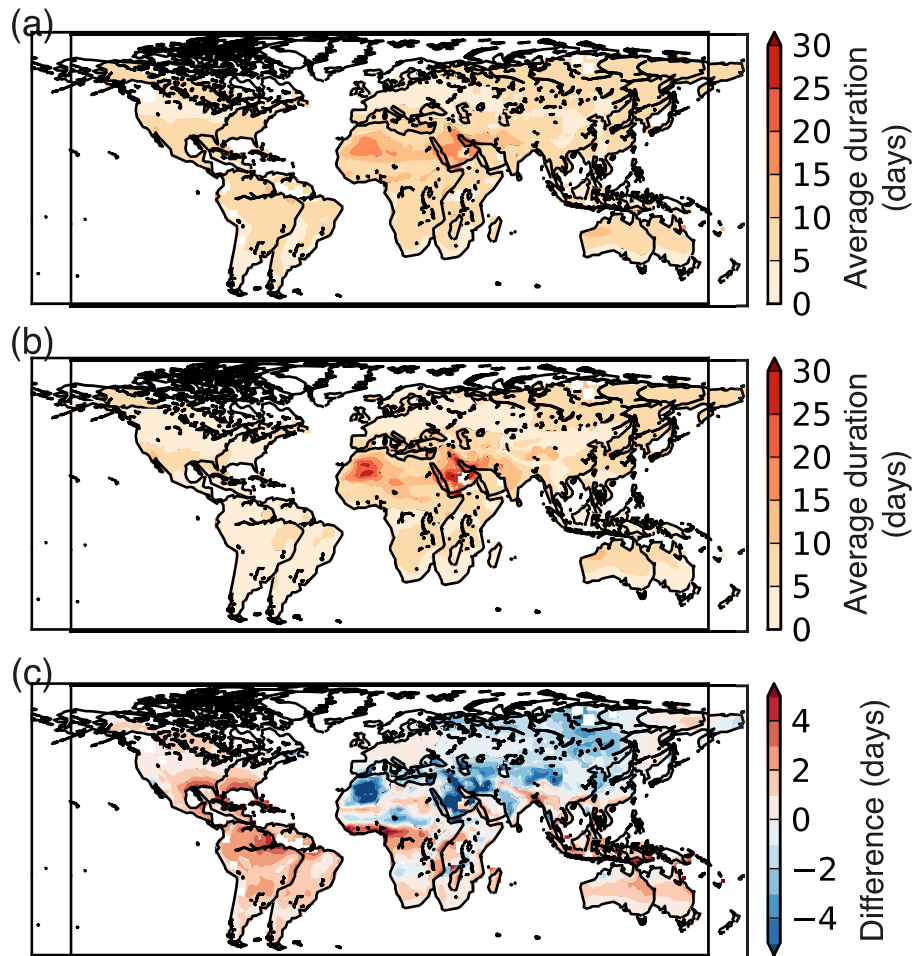
Figure C.7: Average duration (in days) of warm spells defined by more than two consecutive days above the 81st percentile temperature for (a) CMIP5 multi-model mean and (b) ERA-Interim, and (c) the difference between the two values. Grid-squares where the standard deviation between models is greater than the multi-model mean are masked white.
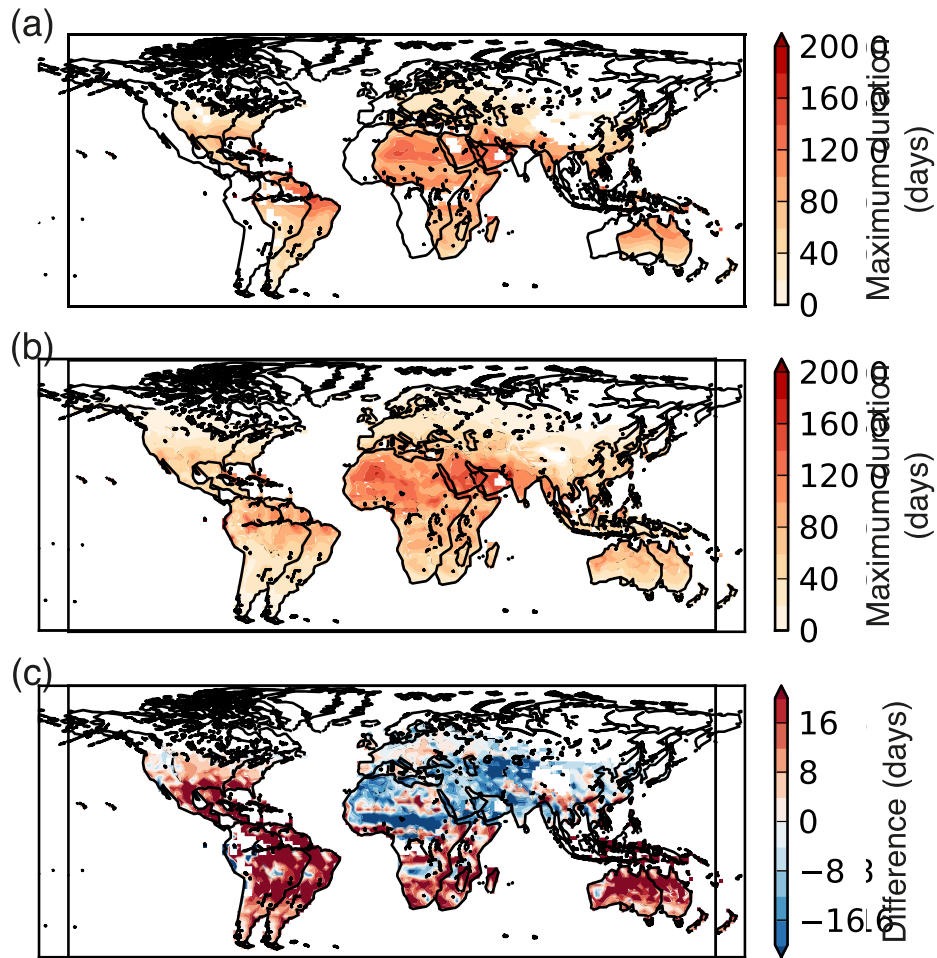
Figure C.8: Maximum duration (in days) of warm spells defined by more than two consecutive days above the spatially varying percentile temperature for (a) CMIP5 multi-model mean and (b) ERA-Interim, and (c) the difference between the two values. Grid-squares where the standard deviation between models is greater than the multi-model mean are masked white.
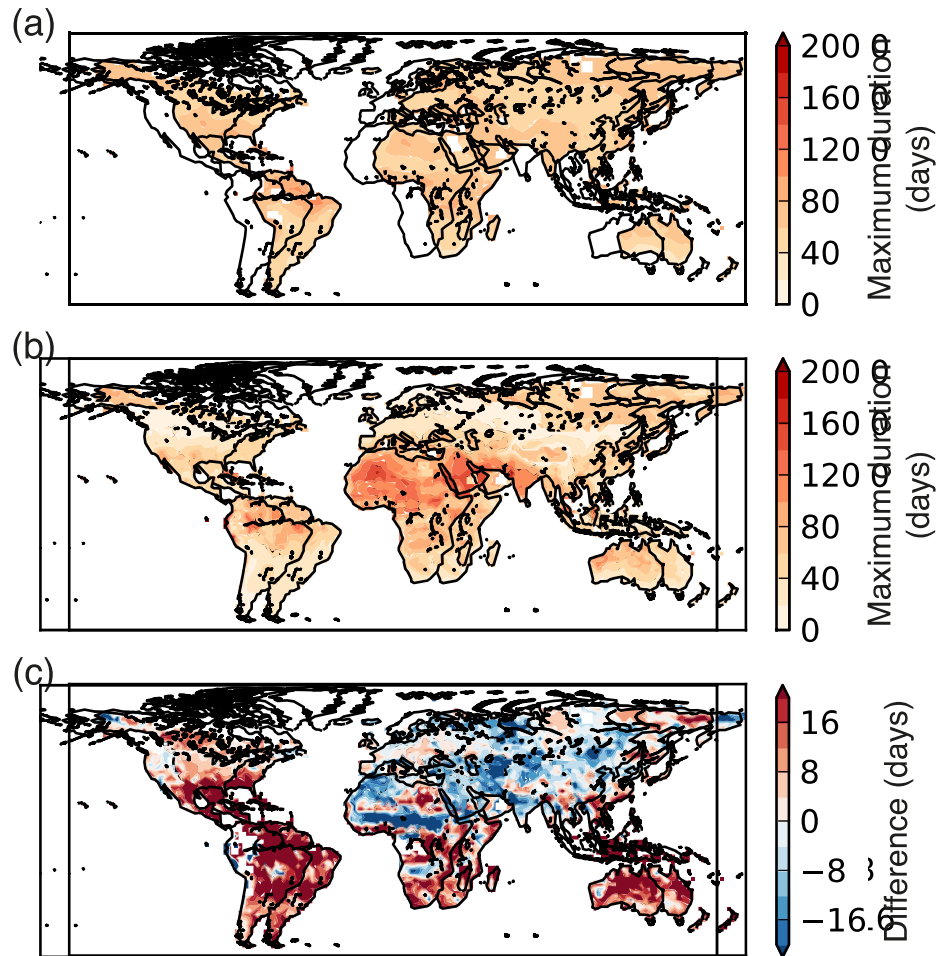
Figure C.9: Maximum duration (in days) of warm spells defined by more than two consecutive days above the constant 81st percentile temperature for (a) CMIP5 multi-model mean and (b) ERA-Interim, and (c) the difference between the two values. Grid-squares where the standard deviation between models is greater than the multi-model mean are masked white.

C.4 Warm days and human exposure as a function of ΔGMST

European politicians and their advisors had previously chosen a 2 °C global warming limit, however smaller low-lying island states would cease to exist by that temperature, therefore there was agreement at the Paris Agreement to aim for 1.5 °C (Lewis, 2016). There are less impact studies at 1.5 °C than at 2 °C, and I compare the number of warm days and duration of warm spells between the two climates in Figure C.10.
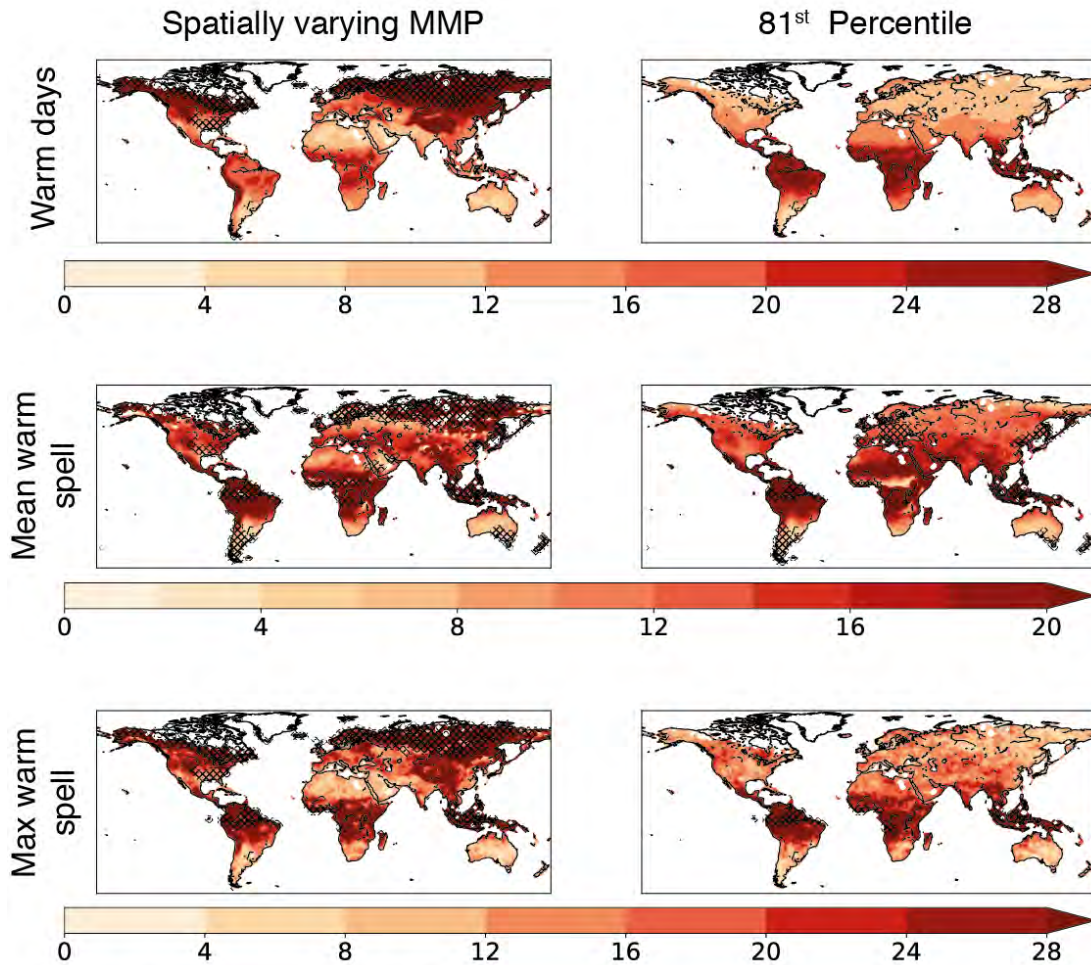
Figure C.10: The percentage increase in the (top) average number of warm days per year, (middle) average duration of a warm spell, and (bottom) maximum duration of a warm spell from a +1.5 °C to a +2 °C climate using the spatially varying percentile threshold (left) and the constant 81st percentile threshold (right). Hatching where the standard deviation between models is more than the multi-model mean.

Using the constant 81st percentile, the greatest percentage difference between the number of warm days in +1.5 °C and +2 °C climates is in the tropics, up to around 35% in some grid squares. Whereas, I project that some temperate regions have a larger percentage increase in warm days than tropical regions (e.g. the number of warm days have a higher relative increase in Colorado than Indonesia) using the spatially varying percentile.

Figure C.11 shows that there is an increase in the multi-model median exposure to warm days with ΔGMST for all regions using both thresholds.


Global mean surface temperature change above pre-industral levels (°C)
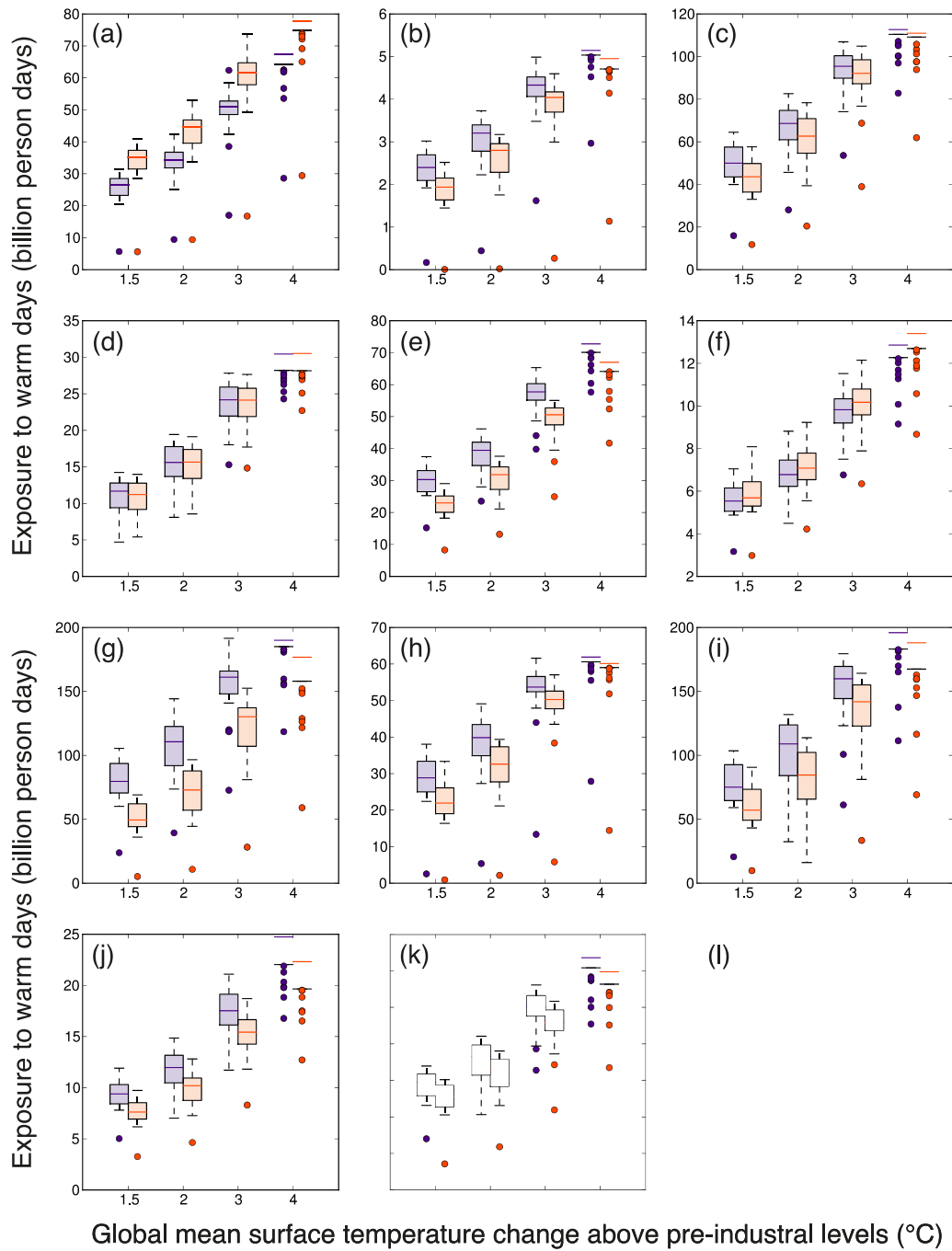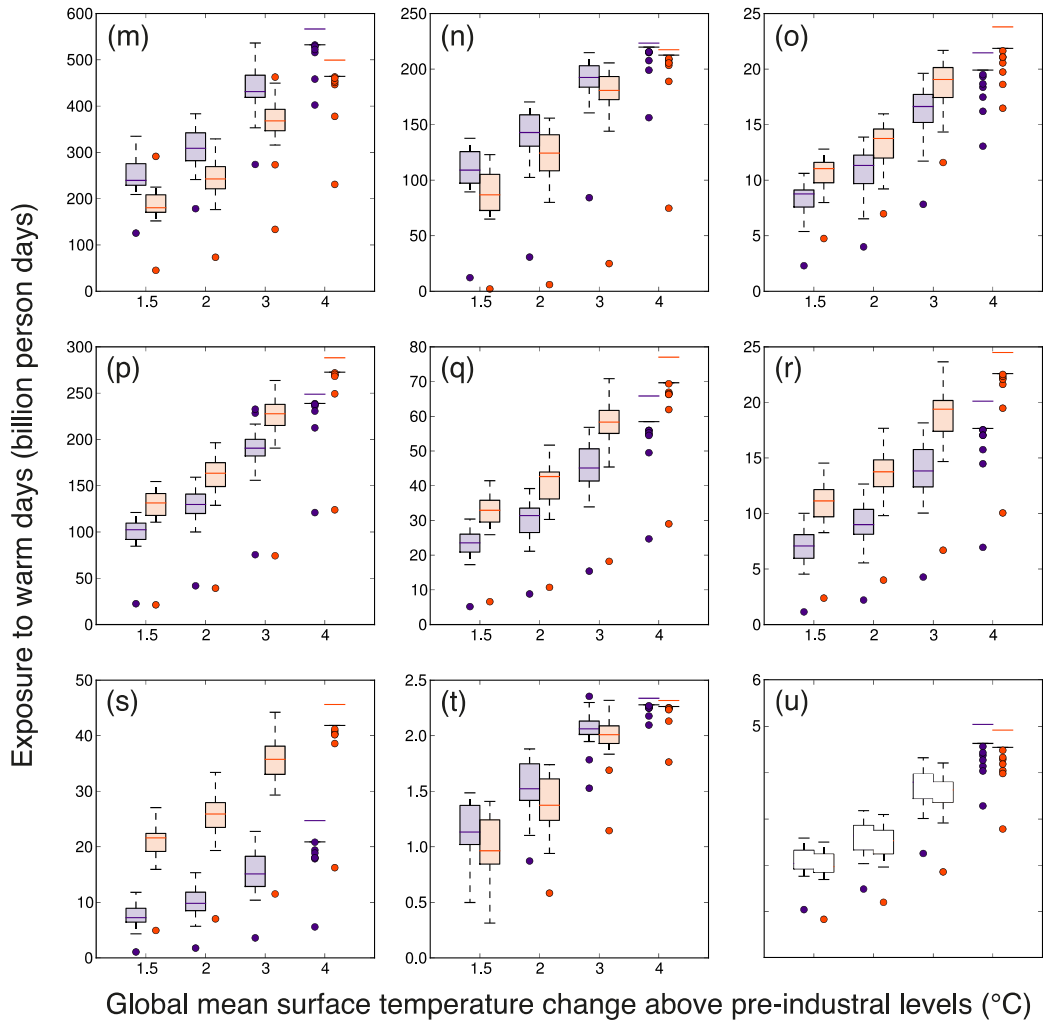
Figure C.11: Total population count multiplied by the number of warm days per year for regions (a) North America, high income, (b) Caribbean, (c) Latin America, central, (d) Latin America, Andean, (e) Latin America, tropical, (f) Latin America, south, (g) Sub-Saharan Africa, west, (h) Sub-Saharan Africa, central, (i) Sub-Saharan Africa, east, (j) Sub-Saharan Africa, south, (k) North Africa/Middle East, (l) Asia, central, (m) Asia, south, (n) Asia, south-east, (o) Asia Pacific, high income, (p) Asia, east, (q) Europe, west, (r) Europe, central, (s) Europe, east, (t) Oceania, (u) Australasia

C.5 Regional definitions

Countries that are too small to be seen on a 2 ° latitude x 2 ° longitude grid square have not been included.

North America, high income

United States America; Canada

Caribbean

Antigua and Barbuda; Bahamas; Barbados; Cuba; Dominica; Dominican Republic; Grenada; Guadeloupe; Haiti; Jamaica; Puerto Rico; Saint Lucia; Saint Vincent and the Grenadines; Suriname; Trinidad and Tobago

Latin America, central

Colombia; Costa Rica; El Salvador; Guatemala; Honduras; Mexico; Nicaragua; Panama; Venezuela

Latin America, Andean

Bolivia (Plurinational State of); Ecuador; Peru

Latin America, tropical

Brazil; Paraguay

Latin America, south

Argentina; Chile; Uruguay

Sub-Saharan Africa, west

Benin; Burkina Faso; Cameroon; Cape Verde; Chad; Cote d'Ivoire; Gambia; Ghana; Guinea; Guinea-Bissau; Liberia; Mali; Mauritania; Niger; Nigeria; Sao Tome and Principe; Sierra Leone; Togo

Sub-Saharan Africa, east

Burundi; Comoros; Djibouti; Eritrea; Ethiopia; Kenya; Madagascar; Malawi; Mozambique; Rwanda; Somalia; Sudan; United Republic of Tanzania; Zambia

Sub-Saharan Africa, central

Angola; Central African Republic; Congo; Democratic Republic of the Congo; Equatorial Guinea; Gabon

Sub-Saharan Africa, south

Botswana; Lesotho; Namibia; South Africa; Swaziland; Zimbabwe

North Africa/Middle East

Algeria; Bahrain; Egypt; Iran (Islamic Republic of); Iraq; Jordan; Kuwait; Lebanon; Libyan Arab Jamahiriya; Morocco; Occupied Palestinian territory; Oman; Qatar; Saudi Arabia; Syrian Arab Republic; Tunisia; Turkey; United Arab Emirates; Yemen

Asia, central

Armenia; Azerbaijan; Georgia; Kazakhstan; Kyrgyzstan; Mongolia; Tajikistan; Turkmenistan; Uzbekistan

Asia, south

Afghanistan; Bangladesh; Bhutan; India; Nepal; Pakistan

Asia, south-east

Cambodia, Indonesia; Lao People's Democratic Republic; Malaysia; Maldives; Mauritius; Myanmar; Philippines; Seychelles; Sri Lanka; Thailand; Timor-Leste; Viet Nam

Asia, east

China; China, Hong Kong Special Administrative Region; China, Province of Taiwan; Democratic People's Republic of Korea

Europe, west

Austria; Belgium; Cyprus; Denmark; Finland; France; Germany; Greece; Iceland; Ireland; Israel; Italy; Luxembourg; Malta; Netherlands; Norway; Portugal; Spain; Sweden; Switzerland; United Kingdom of Great Britain and Northern Ireland

Europe, central

Albania; Bosnia and Herzegovina; Bulgaria; Croatia; Czech Republic; Hungary; Montenegro; Poland; Romania; Serbia; Slovakia; Slovenia; The Former Yugoslav Republic of Macedonia

Europe, east

Belarus; Estonia; Latvia; Lithuania; Republic of Moldova; Russian Federation; Ukraine

Oceania

American Samoa; Fiji; Kiribati; Papua New Guinea; Samoa; Solomon Islands; Tonga; Vanuatu

Australasia

Australia; New Zealand

El-Zein, A., Tewtel-Salem, M., Nehme, G., 2004. A time-series analysis of mortality and air temperature in Greater Beirut. Sci. Total Environ. 330, 71–80. https://doi.org/10.1016/j.scitotenv.2004.02.027

Gasparrini, A., Guo, Y., Hashizume, M., Lavigne, E., Zanobetti, A., Schwartz, J., Tobias, A., Tong, S., Rocklöv, J., Forsberg, B., Leone, M., De Sario, M., Bell, M.L., Guo, Y.-L.L., Wu, C., Kan, H., Yi, S.-M., de Sousa Zanotti Stagliorio Coelho, M., Saldiva, P.H.N., Honda, Y., Kim, H., Armstrong, B., 2015. Mortality risk attributable to high and low ambient temperature: a multicountry observational study. Lancet 386, 369–375. https://doi.org/10.1016/S0140-6736(14)62114-0

Guo, Y., Gasparrini, A., Armstrong, B.G., Tawatsupa, B., Tobias, A., Lavigne, E., Coelho, M. de S.Z.S., Pan, X., Kim, H., Hashizume, M., Honda, Y., Guo, Y.L., Wu, C.-F., Zanobetti, A., Schwartz, J.D., Bell, M.L., Overcenco, A., Punnasiri, K., Li, S., Tian, L., Saldiva, P., Williams, G., Tong, S., 2016. Temperature Variability and Mortality: A Multi-Country Study. Environ. Health Perspect. 124. https://doi.org/10.1289/EHP149

IIASA, 2009. RCP database [WWW Document]. Int. Inst. Appl. Syst. Anal. URL http://www.iiasa.ac.at/web-apps/tnt/RcpDb (accessed 11.20.20).

Kolp, P., Riahi, K., 2009. RCP database [WWW Document]. URL http://www.iiasa.ac.at/web-apps/tnt/RcpDb (accessed 5.16.21).

Lewis, S.L., 2016. The Paris Agreement has solved a troubling problem. Nature 532, 283–283. https://doi.org/10.1038/532283a

Lin, H., Zhang, Y., Xu, Y., Xu, X., Liu, T., Luo, Y., Xiao, J., Wu, W., Ma, W., 2013.

Temperature Changes between Neighboring Days and Mortality in Summer: A Distributed Lag Non-Linear Time Series Analysis. PLoS One 8, e66403. https://doi.org/10.1371/journal.pone.0066403

McMichael, A.J., Wilkinson, P., Kovats, R.S., Pattenden, S., Hajat, S., Armstrong, B., Vajanapoom, N., Niciu, E.M., Mahomed, H., Kingkeow, C., Kosnik, M., O'Neill, M.S., Romieu, I., Ramirez-Aguilar, M., Barreto, M.L., Gouveia, N., Nikiforov, B., 2008. International study of temperature, heat and urban mortality: the "ISOTHURM" project. Int. J. Epidemiol. 37, 1121–31. https://doi.org/10.1093/ije/dyn086

Stevenson, D., Doherty, R., Sanderson, M., Johnson, C., Collins, B., Derwent, D., 2005. Impacts of climate change and variability on tropospheric ozone and its precursors. Faraday Discuss. 130, 41. https://doi.org/10.1039/b417412g